A Comparative Study of the Biological and Molecular Properties of Mesenchymal Stem Cells Isolated from Bone Marrow and the Olfactory System

Steven Andrew Johnstone BSc$_{(Hons)}$ M$_{Res}$

Thesis submitted in fulfilment of the requirements for the degree of Doctor of Philosophy

College of Medical, Veterinary, and Life Sciences

Institute of Infection, Immunity, and Inflammation

University of Glasgow

September 2014

"You can achieve whatever you want in life, you just have to want it enough"

Anne Johnstone – Circa, my childhood

Abstract

Neurodegenerative conditions such as Multiple Sclerosis (MS) and spinal cord injury (SCI) affect hundreds of thousands of people each year worldwide, and numerous cell transplant-based therapeutic strategies are being investigated to aid in the repair and regeneration of the central nervous system. Of particular interest are mesenchymal stem cells (MSCs), due to their differentiation potential, their immunomodulatory effects, and their ability to stimulate various biological properties due to the substantial variety of growth factors, chemokines, and other signalling molecules secreted by these cells. MSCs taken from the bone marrow (BM-MSCs) have demonstrated significant reparative potential in animal models of both MS and SCI. The question I address throughout this thesis however, is whether MSCs from another niche; the olfactory mucosa (OM-MSCs), are a preferable or at least alternative candidate for such therapies, compared to BM-MSCs, and if they are, why are they?

Previous studies have shown that OM-MSCs can be purified and grown from human olfactory mucosa and when incubated with rat glial/neuronal co-cultures are capable of increasing axonal myelination, an effect not elicited by BM-MSCs. This potentially has great therapeutic benefit for a range of neurodegenerative conditions, as a significant part of the regenerative process involves replacing the protective myelin membrane which ensheaths axons.

A comparative study of the two types of MSCs shows a number of similarities, including the expression of the same panel of MSC markers, a 64% homology in miRNA expression, an ability to differentiate towards bone and fat, and a propensity for bone formation when cultured on osteogenic nanotographies.

This thesis also outlines a number of differences between each phenotype which suggest that OM-MSCs could even be a preferred alternative, especially in neuroregenerative therapies. OM-MSCs were shown to express

significantly more Nestin than BM-MSCs, and to proliferate at a significantly higher rate, two observations which may be related. This increased proliferation would have enormous benefit for their use, as BM-MSCs are mitotically quite slow, and any MSC-based therapies would require very large numbers of cells. Twenty six different miRNA were shown to be differentially expressed between BM-MSCs and OM-MSCs. Three of these; miR-140-5p, miR-146a-5p, and miR-335-5p were linked to three important biological functions; myelination, cell survival, and cell proliferation respectively. These three biological functions, importantly, are ones which were observed as being behavioural differences between OM-MSCs and BM-MSCs. OM-MSCs were also shown to secrete significantly more of the pro-myelinating chemokine, CXCL12, which was confirmed as being regulated by the microRNA, miR-140-5p. This offered a potential mechanism for the pro-myelinating effect of OM-MSCs, and also opens up new research potential for investigating therapeutic targets to regulate myelination.

The data presented in this thesis shows many similarities between BM-MSCs and OM-MSCs, but it also highlights some profound differences which suggest that either they originate from a different lineage entirely, or that the cellular niche that they reside in does indeed affect the differentiation and behaviour of mesenchymal stem cells.

Author's Declaration

I declare that, except where referenced to others, this thesis is the product of my work, and has not been submitted for any other degree at the University of Glasgow, or any other institute.

Signature:_____

Printed name: STEVEN ANDREW JOHNSTONE

Acknowledgements

First of all, a huge thanks from the bottom of my heart to my supervisor Sue Barnett, not just for giving me this opportunity in the first place, but for all of your help, guidance, and tolerance. It's been a rollercoaster but one I'll never forget. The next big thanks has to go to my lovely friend and favourite workmate ever, Susan Lindsay. You're positive energy and selfless nature are a credit to us all, thank you so much for everything you've done for me. Thirdly to my other ray of sunshine, Katie Chapple, you brighten up even the dreichest of days with your infectious happiness. It's been a pleasure sitting next to you. Thanks to everyone that I've worked with over the years, from the early days of Jen and Peter, right through to Paul, Daniel, Tiia, "the Mikes", and all in the Dalby group, especially Matt and Carol-Anne, without whom I wouldn't have a chapter 4. Thanks mum for absolutely everything. You gave me the confidence, ability, and opportunity to get where I am now, and all of your sacrifices will motivate me for the rest of my life. And finally to my beautiful wife Julia, you're love and loyalty, your belief in me, and all of your help behind the scenes has allowed me to achieve great things, although my greatest achievement has been marrying you. This thesis is dedicated to you, as it wouldn't even exist without you x

Table of Contents

List of Figures

List of Tables

Abbreviations

ABCAM	Antibodies and Cell Adhesion Molecules
ADE	Acute Disseminated Encephalomyelitis
AFE	Agilent Feature Extraction
AFM	Atomic Force Microscopy
AHL	Acute Haemorrhagic Leukoencephalitis
ALDH1L1	10-formyltetrahydrofolate dehydrogenase
ALS	Amyotrophic Lateral Sclerosis
AMD	Age-Related Macular Degeneration
ANOVA	Analysis of Variance
BDNF	Brain-Derived Neurotrophic Factor
BM	Bone Marrow
BM271-MSC	CD271 Selected Bone Marrow-Derived Mesenchymal Stem Cell
BM-MSC	Bone Marrow-Derived Mesenchymal Stem Cell
BMP	Bone Morphogenic Protein
BMPR	Bone Morphogenic Protein Receptor
CCL	C-C Motif Chemokine
CD	Cluster of Differentiation
CDCP1	CUB Domain Containing Protein 1
cDNA	Complementary DNA
CFU-F	Colony Forming Unit Fibroblast
cm	Centimeter
CM	Conditioned Media
cm^2	Square Centimeter
CNS	Central Nervous System
CPU	Central Processing Unit
CSF	Cerebral Spinal Fluid
CTACK	Cutaneous T-Cell-Attracting Chemokine
CXCL	Chemokine Ligand
CXCR	Chemokine Receptor
DAPI	4’,6-diamidino-2-phenylindole, dihydrochloride

ddH2O	Double Distilled Water
DE	Differentially Expressed
DM-	Differentiation Media Without Insulin
DM+	Differentiation Media With Insulin
DMEM	Delbecco's Modified Eagles Medium
DMSO	Dimethyl Sulphoxide
DNSQ	Disordered Near Square
EAE	Experimental Autoimmune Encephalomyelitis
ECL	Enhanced Chemiluminescence
ECM	Extracellular Matrix
ECS	Embryonic Stem Cell
EDTA	Ethylinediaminetetraacetic acid
EE	Equivalently Expressed
EGF	Endothelial Growth Factor
ENT	Ear Nose and Throat
EtOH	Ethanol
FACS	Fluorescent Activated Cell Sorting
FBS	Foetal Bovine Serum
FDA	Food and Drug Administration
FGF	Fibroblast Growth Factor
g	Gravitational Force
GAPDH	Glyceraldehyde 3-phosphate dehydrogenase
GBC	Globose Basal Cell
G-CSF	Granulocyte- Colony Stimulated Factor
GD	Disialganglioside 2
gDNA	Genomic DNA
GDNF	Glia-Derived Neurotrophic Factor
GFAP	Glial Fibrillary Acidic Protein
GLUT4	Glucose Transporter 4
GM-CSF	Granulocyte and Macrophage-Colony Stimulated Factor
HBC	Horizontal Basal Cell
HBSS	Hank's Balanced Salt Solution

HDAC	Histone Deacetylase
Hg	Mercury
HGF	Hepatocyte Growth Factor
HLA	Human Leukocyte Antigen
HO1	Haem Oxygenase 1
hr	Hour
HS	Horse Serum
HSC	Haematopoietic Stem Cell
IBMX	3-isobutyl-1-methylxanthine
ICAM-1	Intracellular Adhesion Molecule-1
IDO	Indolamine 2,3-dioxygenase
IDT	Integrated DNA Technologies
IFNγ	Interferon Gamma
Ig	Immunoglobulin
Il	Interleukin
iPSC	Induced Pluripotent Stem Cell
IR	Immunoreactivity
LIF	Leukaemia Inhibitory Factor
LP	Lamina Propria
LSGS	Low Serum Growth Supplement
MAP2	Microtubule-Associated Protein 2
MBP	Myelin Basic Protein
MCAM	Melanoma Cell Adhesion Molecule
MCP	Monocyte Chemoattractant Protein
MeOH	Methanol
min	Minute
MIP	Macrophage Inflammatory Protein
miRNA	Micro Ribonucleic Acid
mL	Millilitre
mm	Millimeter
mM	Millimolar
MOG	Myelin Oligodendrocyte Glycoprotein
MRI	Magnetic Resonance Imaging

mRNA	Messenger Ribonucleic Acid
MS	Multiple Sclerosis
MSC	Mesenchymal Stem Cell
NGF	Neural growth Factor
NK	Natural Killer
nM	Nanomolar
$nmol^{-1}$	Nanomolar
NSC	Neural Stem Cell
NTR	Neurotrophic Receptor
^{o}C	Degrees Centigrade
OCN	Osteocalcin
OE	Olfactory Epithelium
OEC	Olfactory Ensheathing Cell
OI	Osteo Imperfecta
OM	Olfactory Mucosa
OM-MSC	Olfactory Mucosa-Derived Mesenchyaml Stem Cell
OPC	Oligodendrocyte Precursor Cell
OPN	Osteopontin
ORN	Olfactory Receptor Neuron
OS	Olfactory System
PBS	Phosphate Buffered Saline
PCA	Principle Component Analysis
PCL	Polycaprolactone
PDGF-AA	Platelet-Derived Growth Factor-AA
PFA	Paraformaldehyde
pFDR	False Discovery Rate
PLL	Poly-L-Lysine
PLP	Proteolipid Protein
PNS	Peripheral Nervous System
QC	Quality Control
RANTES	Regulated on Activation, Normal T Cell Expressed and Secreted
rhGGF2	Recombinant Glial Growth Factor 2

RISC	miRNA-Induced Silencing Complex
RT	Room Temperature
RT-qPCR	Real Time Quantitative Polymerase Chain Reaction
s	Second
SC	Schwann Cell
Sca	Ataxin-1
SCF	Stem Cell Factor
SCFR	Stem Cell Growth Factor Receptor
SCI	Spinal Cord Injury
SCID	Severe Combined Immunodeficiency
SD	Sprague Dawley
SDF	Stromal-Derived Factor
SMA	Smooth Muscle Actin
SMD	Starsgard's Macular Dystrophy
SOP	Standard Operating Procedure
SP1	Specificity Protein 1
TARC	Thymus and Activation Regulated Chemokine
TGF	Transforming Growth Factor
Thy-1	Thymocyte Differentaition Antigen-1
TNF	Tumour Necrosis Factor
TOST	Two One-Sided Test
TPO	Thrombopoietin
TRAIL	TNF-Related Apoptosis-Inducing Ligand
TSLP	Thymic Stromal Lymphopoietin
Tuj-1	Beta-III Tubulin
UV	Ultra Violet
VCAM-1	Vascular Cell Adhesion Molecule-1
VEGF	Vascular Endothelial Growth Factor
VLA-4	Very Late Antigen 4
µL	Microliter
µM	Micromolar
µm2	Square Micrometer

Introduction:

1. General Introduction

1.1. Mesenchymal Stem Cells (MSCs)

Mesenchymal stem cells are a uniquely dynamic and multi-faceted eukaryotic cell with huge potential importance in the field of regenerative medicine. Not only are they essential for the development of the human body, and the support and constant regulation of a number of niches throughout, they have been implicated in a number of regenerative therapies which will be discussed in due course.

MSCs from different niches are thought to carry out separate important roles, and some have been shown to stimulate biological mechanisms that MSCs from other niches do not. The basis of this thesis stems from the discovery by Lindsay *et al*. (1) that MSCs from the olfactory system have the ability to promote axonal myelination whereas MSCs from the bone marrow do not. Throughout this thesis I will compare and contrast the identity and behaviour of both MSC phenotypes to try and understand some of the underlying mechanisms behind their behavioural differences.

This project incorporates cell biology, materials biochemistry, and neuroscience, and, as will be fully explained within the context of this thesis, has potential therapeutic implications in fields of research such as Multiple Sclerosis (MS), Spinal Cord Injury (SCI), and orthopaedics.

1.1.1. A Brief History of Stem Cells

As a result of chemical warfare and the use of atomic weaponry during world war 2, post-war cancer rates soared, leading to a huge drive towards biomedical research, and in particular regenerative medicine (2-4). This lead to Jean Dausset identifying the human leukocyte antigen (HLA), allowing the first successful bone marrow transplant in 1958 (5), and the discovery in 1961 of the haematopoietic stem cell (HSC) by Till and McCulloch (6). In 1968, Tavassoli and Crosby discovered a connection between bone marrow and osteogenesis (7, 8), and further studies by Friedenstein in the late 1960's and 1970's associated these findings with a

another distinct but minor population of stem cells which resides in the bone marrow; a stromal cell which forms bone (9, 10). Further work by Friedenstein *et al.* identified these cells as having a fibroblastic morphology, an adherent capability to plastic surfaces allowing *in vitro* expansion, and a colony forming behaviour which lead to them being termed colony forming unit fibroblasts (CFU-Fs) (11). It was then shown that *in vivo* transplantation of these cells could result in the formation of cells from the other mesenchymal lineages; cartilage, fat, and connective tissue (7), resulting in the common term that is used today; mesenchymal stem cells (MSCs), which was coined by Caplan in 1991 (12).

To date, the only officially used stem cell therapy across the world is the bone marrow transplant. A well established and fully viable therapy for blood related disorders such as leukaemias (13), lymphomas (14), and severe aplastic anaemia (15), as well as immunological disorders such as severe combined immunodeficiency (SCID) (16), and leukocyte adhesion deficiency (17), the bone marrow transplant has saved millions of lives since its genesis in 1958, with over 1,800 patients requiring a bone marrow transplant every year in the UK alone (494). There are a number of human clinical trials involving embryonic stem cells (ESCs) and induced pluripotent stem cells (iPSCs) as therapies for diseases such as Parkinson's (PD) (495), Stargardt's macular dystrophy (SMD) (496), and age-related macular degeneration (AMD) (497). However, due to the ethical issues surrounding ESCs and the autologous potential of MSCs, MSCs are considered by many to be much better alternatives as therapeutic targets, and are currently being studied and trialled across the globe for a wide range of disorders which will be discussed in more detail in section 1.3.

1.1.2. Origins of MSCs

All human life starts when sperms meets ovum, and within 4-5 days of conception dramatic changes have occurred, transforming the fertilised ova (zygote) into a structure called a blastocyst (Figure 1.1). The blastocyst is a simple vesicle consisting of a single layer outer shell of

totipotent stem cells called the trophectoderm, from which ~20 embryonic stem cells are derived and form in an inner compartment of the blastocyst called the inner cell mass, surrounded by a fluid filled cavity called the blastocoel. The embryonic stem cells grow and transform into a tissue called the epiblast from which each of the three germ layers are formed; the ectoderm, mesoderm, and endoderm. Once the three germ layers have begun to form, the whole structure is referred to as the gastrula. The outer layer of the gastrula will eventually form the male or female primordial germ cells, whilst the three germ layers continue to develop into all of the remaining cells which make up the human body (Figure 1.2).

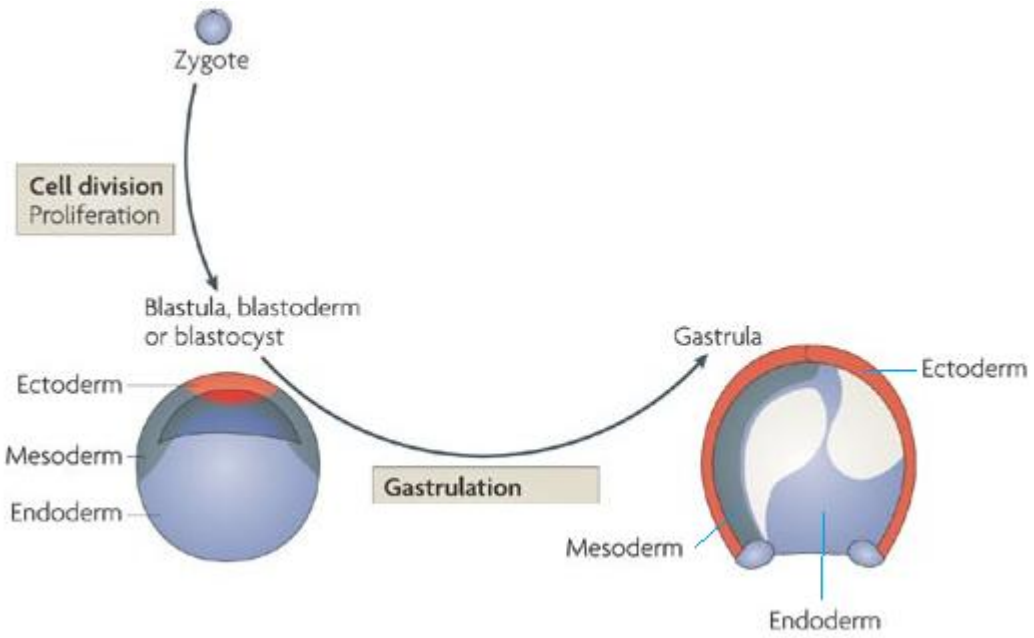

Figure 1.1: Schematic diagram of the first stages of embryogenesis, starting from the zygote through to the blastocyst, and finally the gastrula. The embryonic stem cells in the blastocyst's inner cell mass of the blstocyst differentiate into the epiblast of the late blastocyst, and finally into the three germ lines which start to form at the gastrula; the ectoderm, mesoderm, and endoderm. Diagram modified from Chen *et al.* (2009) (498).

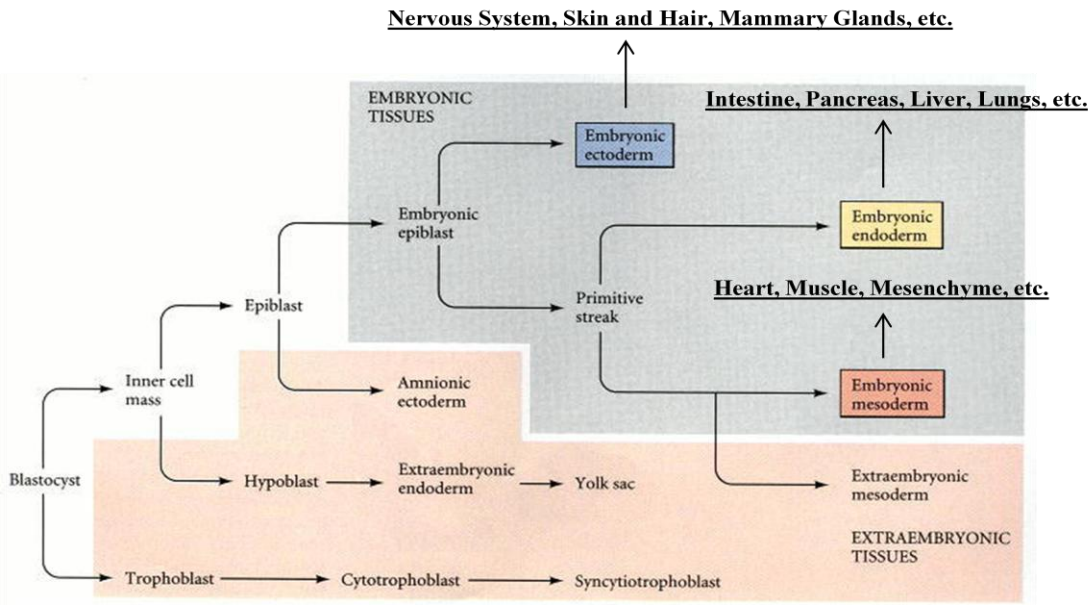

Figure 1.2: Schematic diagram outlining the cells involved in each stage of embryogenesis, starting from the blastocyst shown in figure 1.1. The trophectoderm (outer shell) forms the primordial germ cells (cytotrophoblasts, syncytiotrophoblasts, and intermediate trophoblasts), whereas the three germ layers; ectoderm, mesoderm, and endoderm provide all the other cell types throughout the body. Diagram modified from Gilbert's Developmental Biology, 6th Edition (499).

1.1.2.1. The Ectoderm

The ectoderm, the outermost of the three germ layers, situated between the mesoderm and the trophectoderm (18), is influenced by numerous secreted factors such as nestin, noggin, and Sox2 to differentiate towards cells of the central and peripheral nervous systems, tooth enamel, keratinous structures such as nails and hair, the anus, sweat glands, and various epithelial structures such as the linings of the mouth and nasal cavities (19) (Figures 1.2 and 1.3). The word ectoderm comes from the Greek words for "outside" (ektos), and "skin" (derma), and the ectoderm itself consists of 2 parts; the surface or external ectoderm, and the neuroectoderm which consists of the neural crest and the neural tube (20). Figure 1.3, taken from Rojo *et al.* (21) shows the lineages of a number of surface ectodermal-derived cell populations.

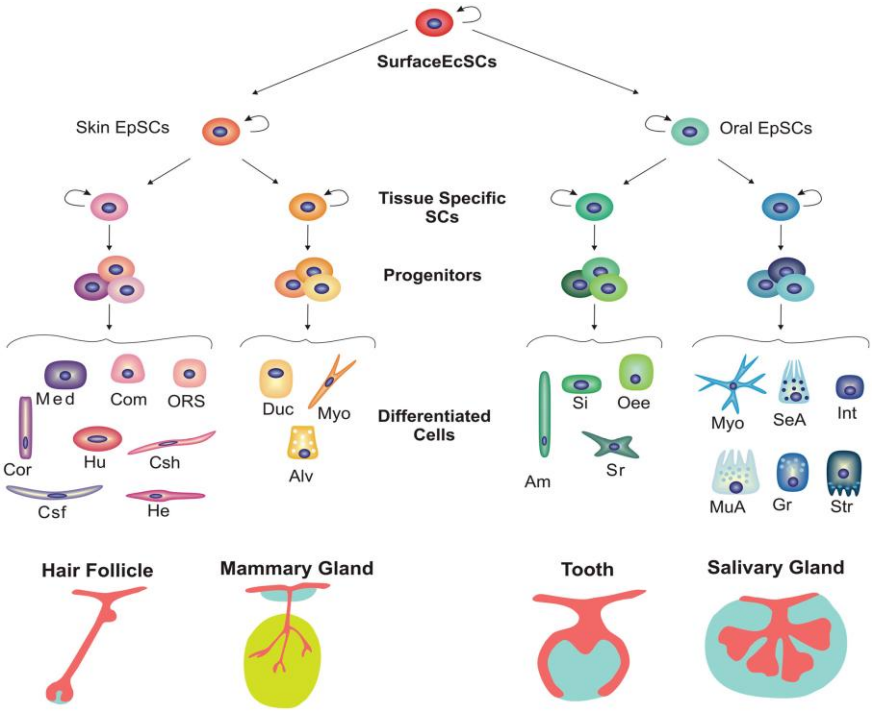

Figure 1.3: Schematic diagram representing some of the surface ectodermal lineage cell types. Surface ectodermal stem cells (SurfaceEcSCs) branch off into either skin or oral lineages and differentiate towards numerous cells which form hair and nails, mammary glands, teeth, salivary and sweat gland, and mucous membranes such as the nasal and oral cavities, and the anus. Diagram taken from Rojo et al. (21).

The neuroectoderm is also divided into two sub-sections; the neural crest and the neural tube which form between the non-neural (surface) ectoderm and the mesoderm when the epidermis converges on itself to form neural folds (22). The neural folds conjoin forming the neural tube, cells from the top of the neural tube where the fold joins transform from epithelial cells to mesenchymal cells, and the epidermis re-forms to create a neuro/mesenchymal niche called the neural crest (Figure 1.4) (499). Neural crest cells then migrate to form more mesenchymal peripheral tissues such as face cartilage, heart septum, and adrenal medulla, as well as the peripheral nervous system. Cells created in the neural tube go on to form all of the cells and components of the central nervous system.

Abbreviation	Cell Name
Alv	Alveolar cell
Am	Ameloblast
Com	Companion layer
Cor	Cortex
Csf	Cuticle of the hair shaft
Csh	Cuticle of the hair sheath
Duc	Duct cell
EcSCs	Ectodermal stem cell
EpSCs	Epithelial stem cell
Gr	Granular duct cell
He	Henley's inner root sheath layer
Hu	Huxley's inner rot sheath layer
Int	Intercalated duct cell
Med	Medulla
Myo	Myoepithelial cell
MuA	Mucous acinus
Oee	Outer enamel epithelium
ORS	Outer root sheath
SeA	Serous acinus
Si	Stratum intermedium cell
Sr	Satellite reticulum
Str	Striated duct cell

Table 1.1: Table of full cell names depicted by abbreviations in figure 1.3 taken from Rojo et al. (21).

Figure 1.5 shows a range of tissues associated with both the neural crest and neural tube.

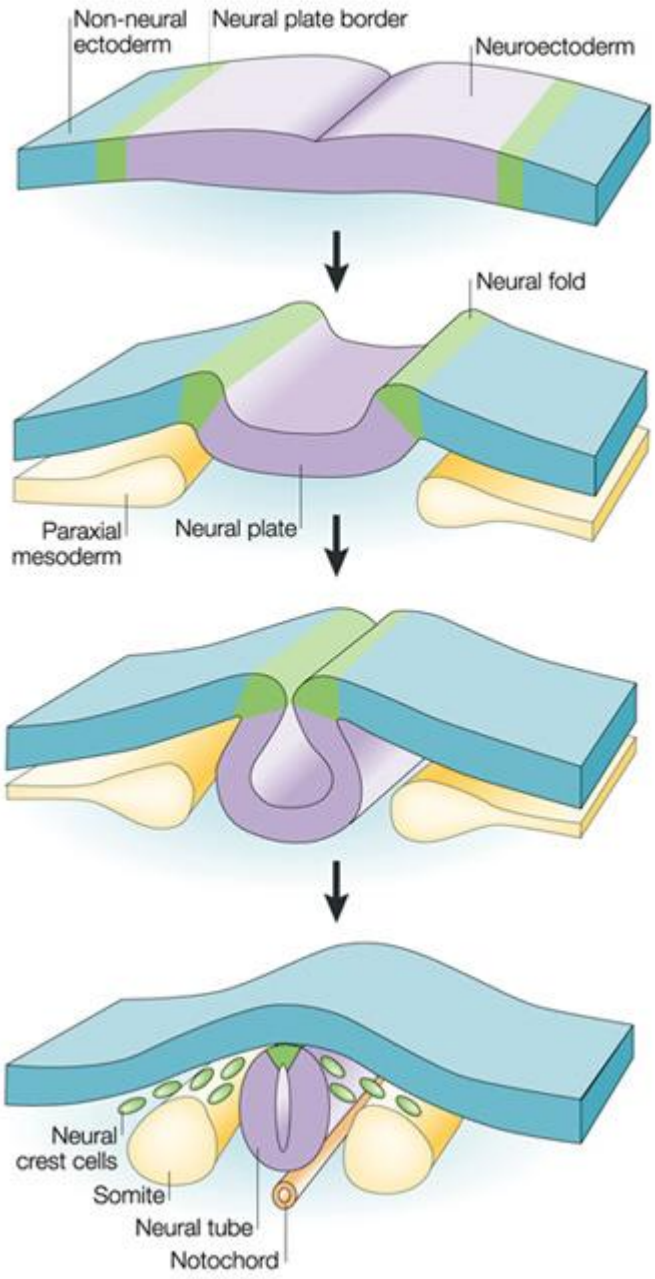

Figure 1.4: Schematic diagram depicting the formation of the neural crest and neural tube. Taken from Bronner-Fraser *et al*. (2003) (500).

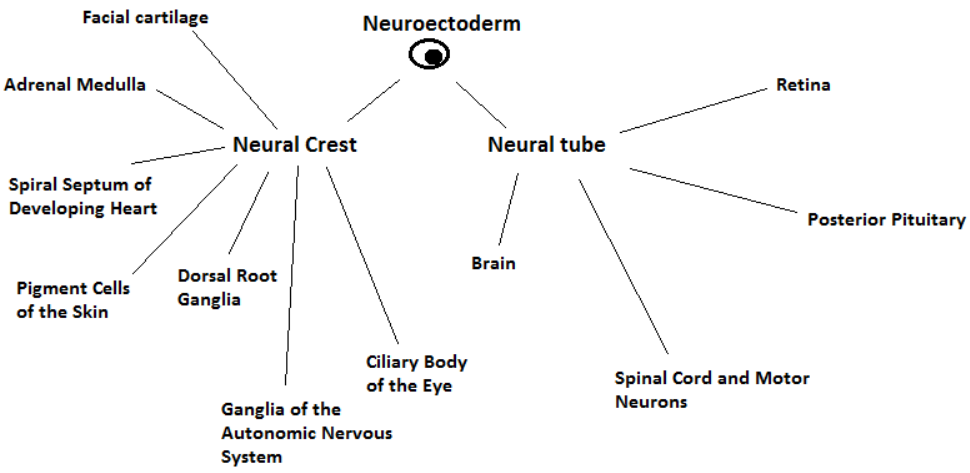

Figure 1.5: Spider diagram depicting the lineages and resultant tissue types of neural crest and neural tube-derived cells.

1.1.2.2. The Endoderm

The endoderm is the innermost of the three germ layers, situated between the mesoderm and the blastocoel, and is responsible for the genesis of the internal organs of the body (except the heart) such as the gut, liver, lungs etc. (23). Figure 1.6 outlines a schematic of endodermally-derived tissues (23).

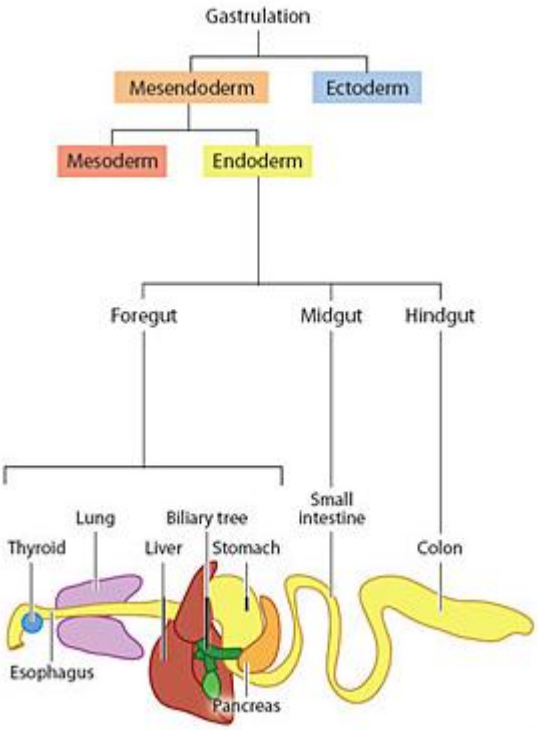

Figure 1.6: Schematic diagram taken from Zorn and Mills (23) depicting the lineage of organogenesis occurring in the endodermal layer.

1.1.2.3. The Mesoderm

The central of the three germ layers, the mesoderm, is responsible for the genesis of the medial parts of the body; the bones, connective tissue, muscles, blood, and also the heart and gonads (24). This is the most important germ layer as far as this thesis is concerned, as it is the germ layer from which mesenchymal stem cells are derived. Figure 1.7 outlines the separate lineages which are derived from the mesodermal layer, and highlights the two distinct stem cell populations mentioned previously which are resident in bone marrow tissue; the haematopoietic stem cells and the mesenchymal stem cells. The mesenchymal stem cells produced by the mesoderm are completely distinct from the neuroepithelial/mesenchymal cells which are derived from the neural crest. As previously mentioned, those cells form only certain ectodermally-derived mesenchymal tissue such as face cartilage, whereas mesenchymal stem cells are responsible for the production of all other mesenchymal tissue throughout the body; bone, fat, and cartilage, as well as smooth, skeletal, and cardiac muscle (25, 26).

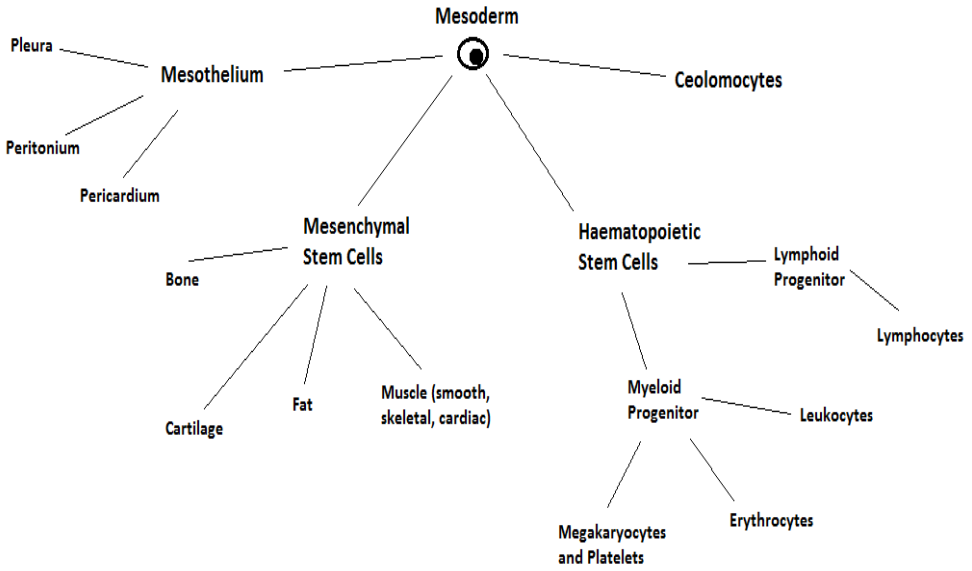

Figure 1.7: Spider diagram depicting the lineages and resultant tissue types of mesodermally-derived cells.

1.1.3. Niche

Niche in biology is much the same as in normal aetiology. It refers to a particular environment within the body where a specific cell might reside. Cell function is optimised by the microenvironment provided by the niche; this is particularly the case for some stem cells. Each niche is different, containing different cells, and a different biochemical environment, different stiffness's, and different roughness's, all to optimise the function and survival of the cells within that niche. With MSCs however, they have been found to be resident in a number of separate and biologically distinct niches, whilst still maintaining their MSC phenotype (27). MSCs are classically linked to the bone marrow (28, 29), but they have since been isolated from a number of other niches such as adipose tissue (30), corneal stroma (31), Wharton's jelly of the umbilical cord (32), tooth pulp (33), amniotic fluid (34), and the olfactory mucosa (1, 35, 36). Although these studies have all identified each niche-derived MSC as true MSCs, very little has been done to compare MSCs from these different niches to identify any differential function, behaviour, gene expression, factor secretion, or effect on separate biological systems. The two niches that are most important throughout this study are the bone marrow and the olfactory mucosa, which will be discussed in more length.

1.1.4. MSC Morphology, Detection, and Function

1.1.4.1. Morphology

When first discovered in the 1960's, MSCs were termed colony forming unit fibroblasts (11) due to their fibroblast-like morphology. This similar morphology however is as far as the similarities between the two cell types go. Fibroblasts don't share the same differentiation capabilities, nor do they have the same cell surface markers (37, 38). Like fibroblasts though, MSCs have small cell bodies with large nuclei and multiple processes, and

can often be mistaken for fibroblasts when studying them under phase microscopy.

1.1.4.2. Detection

MSCs express a number of cell surface markers and intracellular proteins which define them as MSCs. Each MSC phenotype may not express each marker, but there are a number of "classic" MSC markers which are expressed by all MSCs and not fibroblasts. Some of these are CD90, CD105, CD166, and CD271. A list of widely used MSC markers can be found in Table 1.2.

BMPR-1A (ALK-3)	CD44	CD73 (SH3/4)(5'-nucleotidase)	CD166 (ALCAM)	Nestin
BMPR-1B (ALM-6)	CD45	CD90 (Thy-1)	CD271	Sca-1 (Ly6)
BMPR-2	CD51 (Integrin alpha V)	CD105 (SH2) (Endoglin)	CDCP1	SCFR (c-kit)
n-Cadherin	CD54 (ICAM-1)	CD106 (VCAM-1)	Fibronectin	Stro-1
CD29 (Integrin beta)	CD71	CD146 (MCAM)	GD2	Vimentin

Table 1.2: List of MSC-associated cell surface markers and intracellular proteins used to identify MSCs (501).

MSCs have a number of identifiable traits, one being their ability to adhere to plastic surfaces (12). These adherent cells can then be analysed for any number of these MSC markers by immunocytochemistry, flow cytometry, or RT-qPCR. Once the presence of these markers has been established, the cells can be further identified by inducing them to differentiate towards bone and fat. If, under these conditions, their morphology, MSC marker expression, and ability to form bone and fat has been established, then the identity of the MSC can be conclusively validated.

1.1.4.3. Function

MSCs play a number of important roles throughout the body, roles which may differ depending on the location of the particular MSC, but regardless of the MSC's niche, their defining biological capabilities are the same. MSCs are like mini biochemical factories, secreting vast amounts of chemical modulators which regulate many different biological functions, as follows:

1.1.4.3.1. Differentiation

Their primary function is to differentiate towards cells from lineages pertaining to the mesenchyme; bone, fat, cartilage, connective tissue, and muscle (39, 40). This is true of all MSCs. Figure 1.8 outlines each cell lineage which originates from MSCs.

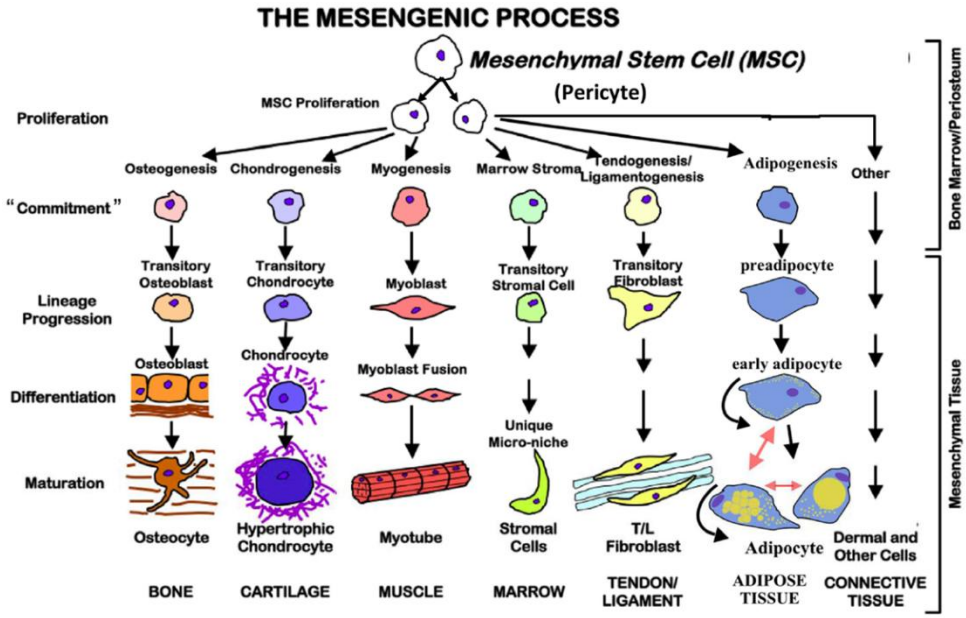

Figure 1.8: Schematic diagram representing each cellular lineage which can originate from a parent MSC. Image taken from DiMarino *et al*. (40).

This differentiation can be induced using factor rich media which determine the fate of MSC by triggering various signalling pathways (41, 42), and also by triggering similar pathways using non-media solutions such as substrate topographies and matrix stiffness's (43-46). A full list of

universally recognised induction media used throughout this study can be found in materials and methods Table 2.10, and the subject of substrate topographies will be further discussed in section 1.3.3.1.

1.1.4.3.2. Immunosuppression

Although the exact mechanisms of immunosuppression induced by MSCs aren't fully understood, it is thought that a number of adhesion molecules and contact-mediated immunosuppressive soluble factors are involved. Cell-cell contact seems crucial in the production of the required soluble factors, either from the MSC's themselves or from the target cells upon contact initiation by the MSC's. For example, Augello *et al* (47) showed that T cell proliferation can be suppressed by the release of the inhibitory molecule PD1, and also nitric oxide (inhibits T cell activation) and indoleamine 2,3-dioxygenase (IDO) (reduces Tryptophan levels essential for lymphocyte proliferation) have been shown to be released by MSC's only after contact with target cells initiates the release of IFNγ (48). Possibly as a self-regulatory mechanism, IFNγ releasing T_H cells are themselves inhibited by MSC-derived IDO, which can also work in conjunction with other cytokines such as prostaglandins to inhibit the activity of natural killer (NK) cells (49). A number of other factors such as TNF, Il-1α or Il-1β (stimulate chemokine production by MSC's), transforming growth factor-β1 (TGFβ1), hepatocyte growth factor (HGF), Il-10, pGe2, haem oxygenase-1 (HO1), and Il-6 are also prevalent in MSC-mediated immunosuppression (50).

1.1.4.3.3. Migration

Administration of stem cells to the host for therapeutic purposes is clearly very important. *In situ* administration is of course the preferred means but is not always possible, either due to the dangerous or inaccessible location of the injury site, such as the CNS, or due to the systemic nature of the injury as is the case with multiple sclerosis. Fortunately MSC's are able to locate and migrate to the area(s) of damage when administered intravenously (51), where they can then maintain repair and restore

function (52). This migration is possible due to MSC's ability to traverse blood vessels via surface adhesion molecules, and to elicit a mechanism of "rolling" dependant on p-selectin and vascular cell-adhesion molecule 1 (VCAM-1) (53). This migration is the result of the detection of chemokines from the site of injury, picked up by the MSC's cell surface receptors (54), and the release of enzymes which allow endothelial degradation and movement across blood vessels (55).

1.1.4.3.4. The "Bystander" Effect

This refers to the MSC's ability to passively or transiently help in a situation of trauma or injury, for example by suppressing immunity or activating endogenous reparative cell populations.

This effect was first witnessed during a skin graft experiment on non-human primates where an *in situ* injection of MSC's prolonged the survival of the graft (56). This was the first of many such bystander effects observed, from the inhibition of pathogenic antibodies (55) to the neuroprotective effect of their releasing anti-inflammatory, anti-apoptotic, and trophic factors (57), the ability of MSC's to transdifferentiate into neuronal cells (58) (Figure 1.9), and their propensity to guide differentiation of neural progenitors towards an oligodendrocytic fate (58).

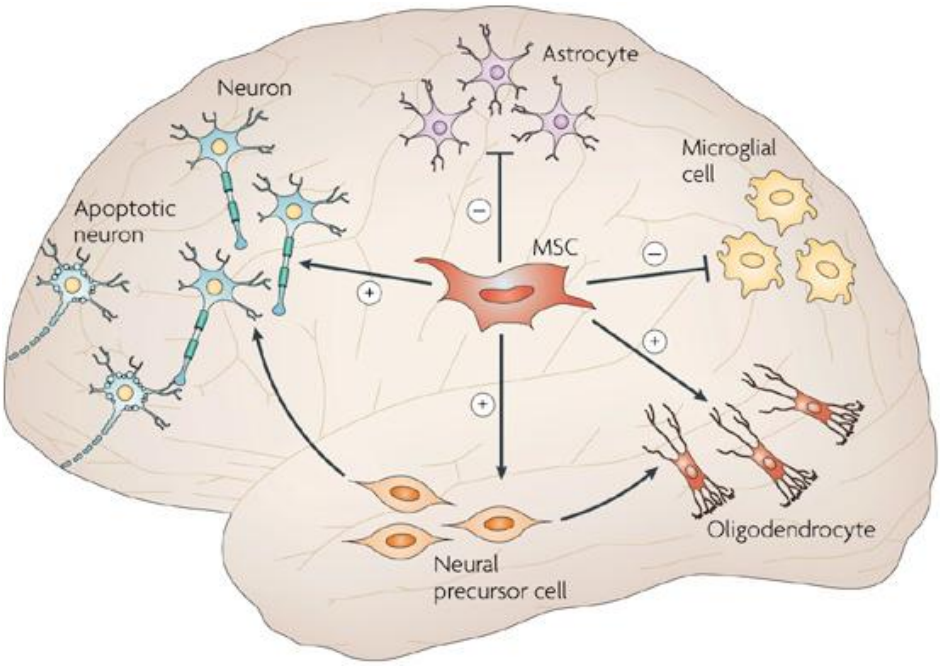

Figure 1.9: The bystander effects and transdifferentiation potential of MSC's in the CNS. MSC's anti-inflammatory capacity can protect microglial cells, their anti-apoptotic effects can increase the proliferation of neuroprotective astrocytes, their trophic factors can influence the differentiation of neural precursor cells, as well as generating neurons and neural precursor cells by transdifferentiation. Image taken from Ruster *et al*. (51).

In short, MSC's are multipotent self-renewing cells, with not only the capacity to differentiate into different mesenchymal cell types, but potentially also some cells from other germ layers, as well as having an immunoprotective effect, an ability to migrate to the site of injury after systemic delivery, and also the ability to influence the genesis of and protection of other neuroprotective cells in the CNS.

1.2. The Central Nervous System (CNS)

The CNS is the core functional compartment of the human body, which takes all information from external and internal stimuli, and translates this into the movement, function, and regulation of each and every cell in the body. It is the computer of the body, and without any of its constituent

parts, the body would cease to function. It consists of the brain, the spinal column, the optic system, and the olfactory bulb of the olfactory system (59, 60), each comprising of a number of different cell types. The Brain and spinal cord can be divided into two distinct areas, the white matter and gray matter (59). The optic and olfactory systems are essentially extensions of the brain, and thus don't comprise of white and gray matter, but they are still considered part of the CNS due to their proximity and connection to the brain (59, 60). The CNS consists predominantly of neurons and glial cells, which work in tandem with each other but have very unique functions.

1.2.1. Cells of the CNS

1.2.1.1. The Neuron

The neuron is a large cell consisting of 3 major parts; the Soma (cell body), the Axon, and the Dendrites (synaptic terminals) (Figure 1.10) (502). Neurons are the wiring of the human body. They transmit messages from distal sensory parts of the body to central localised areas requiring an action to that message, as well as maintaining bodily function by relaying all kinds of messages from within. Neurons carry action potentials generated in the cell's membrane down the axon which is covered by a lipid rich protein membrane called myelin. This myelin sheath acts as insulation, and protects both the signal and the axon itself, much like flex that covers a normal electrical cable. When the action potential reaches the axon terminus, vesicles of signalling molecules called neurotransmitters are formed and secreted across junctions called synapses to be accepted by receptors on the synaptic terminals. These signals are then transported to neighbouring cells via the telodendria (Figure 1.11) (503).

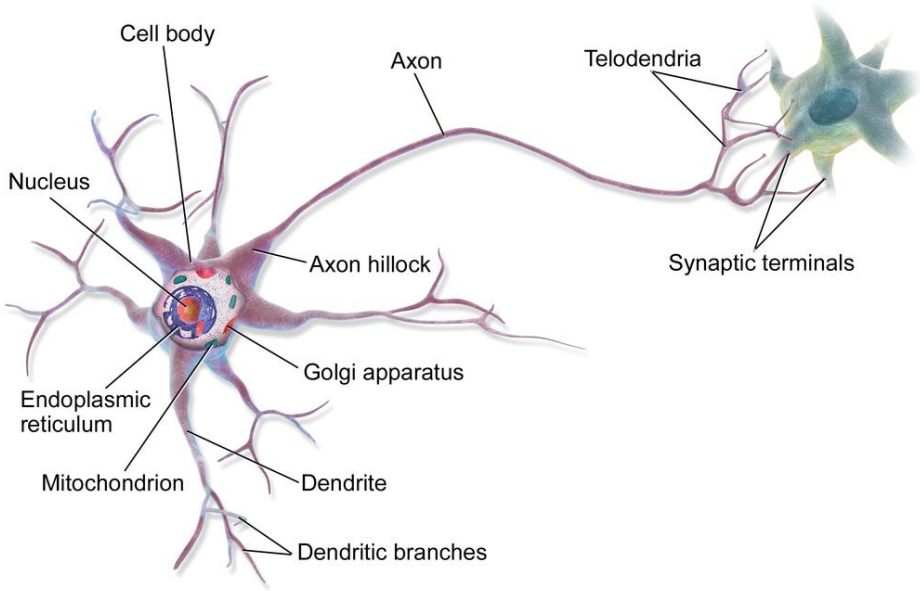

Figure 1.10: Diagram depicting the different sections of the neuron. The cell body contains the nucleus and is responsible for signal production, the axon guides the action potential towards the axon terminus where the signal is transmitted via signalling molecules called neurotransmitters into the synaptic terminals (dendrites) from which the signals are transmitted to neighbouring cells. Image from Wikimedia Commons (502).

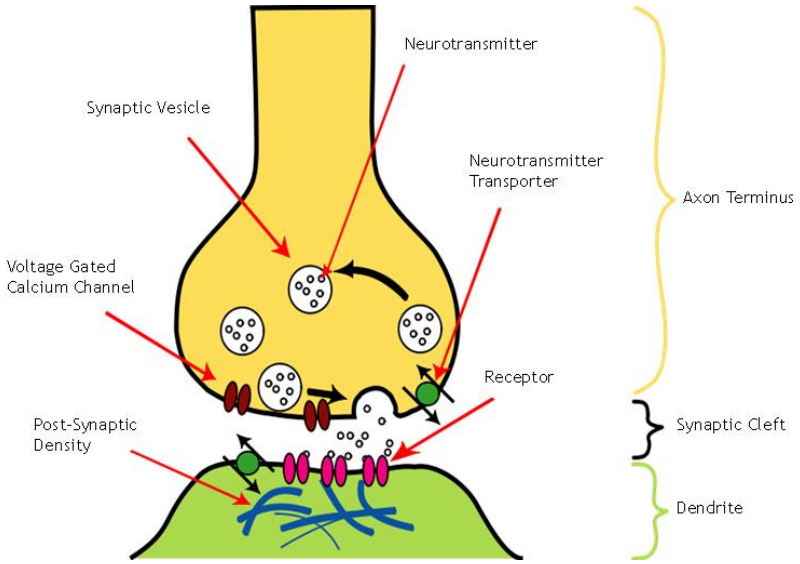

Figure 1.11: Diagram depicting the signal transduction of a neuron via neurotransmitter secretion from axon to dendrite. Image modified from Wikimedia Commons (503).

1.2.1.2. Glia

Glia (from the greek word for "glue") refer to the cells of the nervous system, both PNS and CNS, who act as support cells by way of scaffold/tissue structure, supplying nutrients, production of protective membranes, and recycling dead cells (61-63). CNS glia consist of Microglia, Astrocytes, Oligodendrocytes, Ependymal cells, and Radial glia:

1.2.1.3. Microglia

Microglia are the macrophages of the CNS. The soldiers and scavengers, which phagocytose any xenoparticles and apoptotic debris. Unlike other glial cells which are derived from the ectoderm, adult microglia are derived from haematopoietic stem cells from the mesodermal lineage after injury or disease (64). They are stellate (star shaped) with numerous processes extending from their cell body (Figure 1.12) with which they are constantly touching and assessing the local environment in the search for sub-optimal conditions (61-63). They can be isolated from CNS cultures by their cell surface markers; CD11b, CD45, ED-1, and CD200.

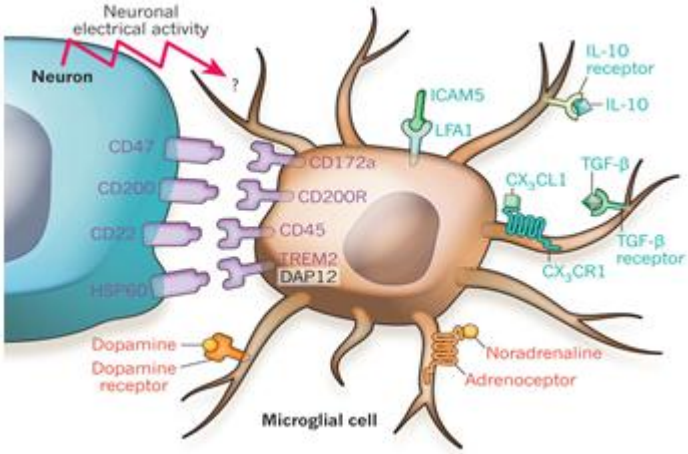

Figure 1.12: Diagram depicting a microglial cell, including its stellate shape, neuronal interaction, and some of its cell surface markers. Image taken from Ransohoff *et al.* (65).

1.2.1.4. Astrocytes

Astrocytes are the most abundant cells in the CNS (66). It is still under debate exactly how abundant they are compared to neurons, but it is generally accepted that they make up the bulk of the stromal tissue in the CNS. As well as providing the architecture for the CNS, astrocytes play other crucial roles, particularly regarding formation of the glial scar post injury (67-70). Astrocytes exist in a continuum of states ranging between reactive and non-reactive (71). Post insult or injury to the CNS, astrocytes become reactive, changing their morphology to extend more processes, and upregulating production of numerous proteins such as Glial Fibrillary Acidic Protein (GFAP), Nestin, and Vimentin (72-74). These reactive astrocytes then form a glial scar, protecting the site of injury from further damage (65-75). Like microglia, astrocytes are also stellate (Figure 1.13), and can be isolated by any of their numerous cell surface markers and intracellular proteins such as GFAP, ALDH1L1, and S100-β (75).

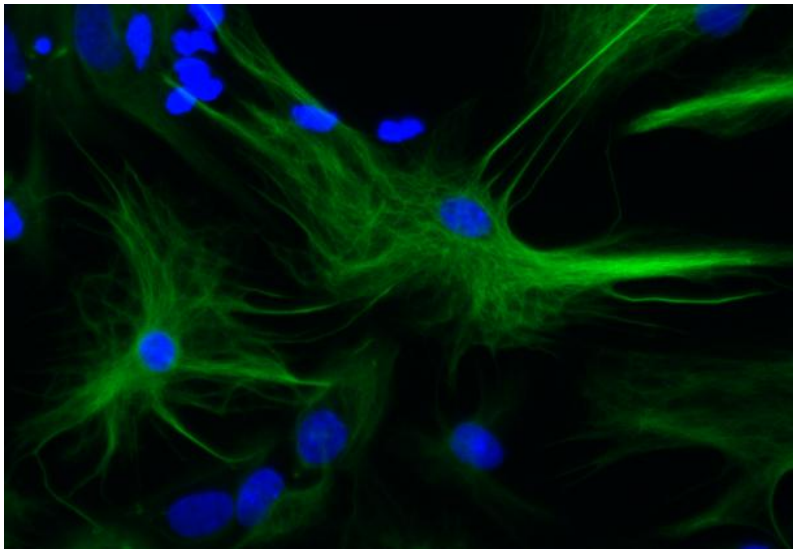

Figure 1.13: Fluorescent image of astrocytes showing positive reactivity to GFAP (Green). Image kindly donated by Daniel McElroy.

1.2.1.5. Oligodendrocytes

Derived from oligodendrocyte precursor cells (OPCs), Oligodendrocytes are the myelinating cells of the CNS (76). Their multiple processes allow them

to interact with multiple axons at once, ensheathing each axon with approximately 1 μm of myelin (76). It is thought that oligodendrocyte myelination is regulated by pro-myelinating factors secreted by astrocytes (70, 77, 78). Ioannidou *et al*. demonstrated with *in vivo* imaging techniques that the processes of each oligodendrocyte are constantly extending and retracting, wrapping strands of myelin round the axon in a corkscrew type manner, before spreading out along the axon to form a sheath (79, 80). Oligodendrocytes are the final CNS phenotype to be formed during embryogenesis, and can be identified during each stage of their development by a number of different cell surface markers outlined in Figure 1.14 (76).

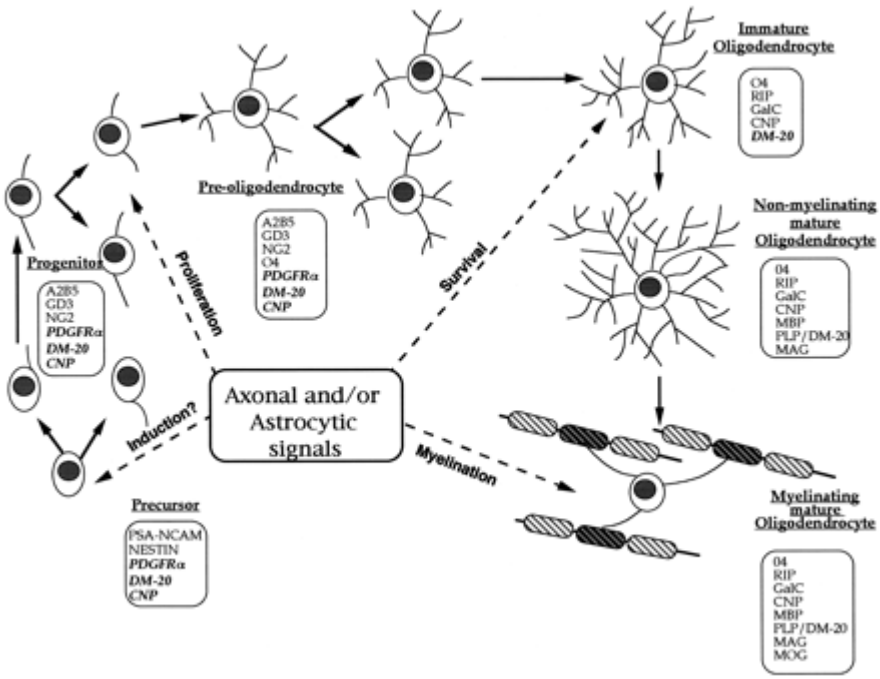

Figure 1.14: Schematic diagram depicting the different stages of oligodendrogenesis, and the cell surface markers which are expressed by the cells at each stage. Image was taken from Baumann *et al*. (76).

1.2.1.6. Ependymal Cells

Ependymal cells are epithelia-like cells which line the central part of the spinal column, and also the ventricular system of the CNS (81). They are covered in a layer of immotile cilia which circulates cerebral spinal fluid

(CSF) that the cells themselves help to produce as part of the choroid plexus (81, 82).

1.2.1.7. Radial Glia

Radial glia have two primary roles in the CNS. During development, radial glia can serve as primitive progenitors to neurons, astrocytes, oligodendrocytes, and ependymal cells (83). They're also utilised by developing neurons as scaffolds, helping to maintain the architecture of the CNS (83-85).

1.2.2. White Matter and Gray Matter

1.2.2.1. White Matter

Making up the majority of the inner brain, and the external parts of the spinal cord, the white matter is predominantly comprised of glia and myelinated axons (86). White matter is responsible for the signal transduction and message relay from the cognitive parts of the CNS to the rest of the body (86). It is essentially the network of electrical circuits which connect the mainframe (brain) to the rest of the system (body). It is white, mainly due to the lipid rich myelin which protects each axon (86), and as an individual gets older, more and more white matter is lost without being regenerated, leading to increasingly impaired cognitive function over time (87). In demyelinating conditions such as multiple sclerosis (MS), the axon's protective myelin sheath is attacked by the body's immune system, and large parts of white matter are degraded and die off (88, 89). Other conditions which effect the white matter include degenerative conditions such as Alzheimer's, during which solid amyloid plaques form over time and disrupt the signalling capabilities of the axons, eventually leading to their degradation and loss of white matter (90, 91). White matter injuries separate to these neurodegenerative conditions, are more likely to be reversible, as the damaged axon is still attached to a healthy cell body and can still be repaired by endogenous glia populations (92, 93). Figure 1.15 shows the white matter and gray matter areas of the CNS.

1.2.2.2. Gray Matter

If the white matter is to be thought of as the electrical circuits extending from the central processing unit (CPU), the gray matter is the CPU itself. It consists mainly of glia and neuronal cell bodies, and is the cognitive part of the CNS where all the signals and messages are processed and generated to be passed through the white matter and into the body (94). Gray matter is located predominantly at the external areas of the brain and in the central regions of the spinal cord, although in the brain, gray matter diffuses with white matter in areas such as the basal ganglia and brain stem nucleus (94). Chronic neurophysiological conditions like Alzheimer's also affect gray matter due to the build-up of plaques denying any repair potential (95). In addition smoking has been heavily linked with increased gray matter degradation (96).

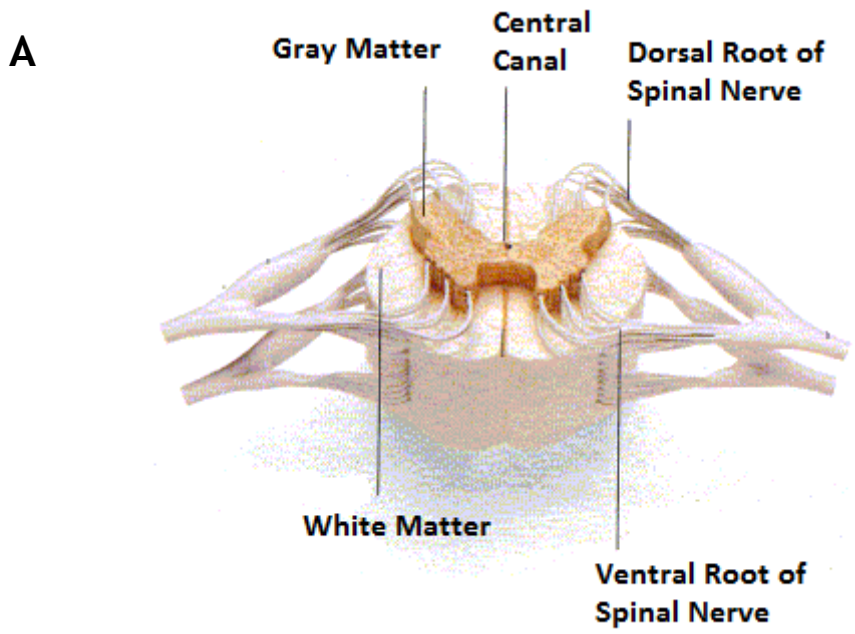

B

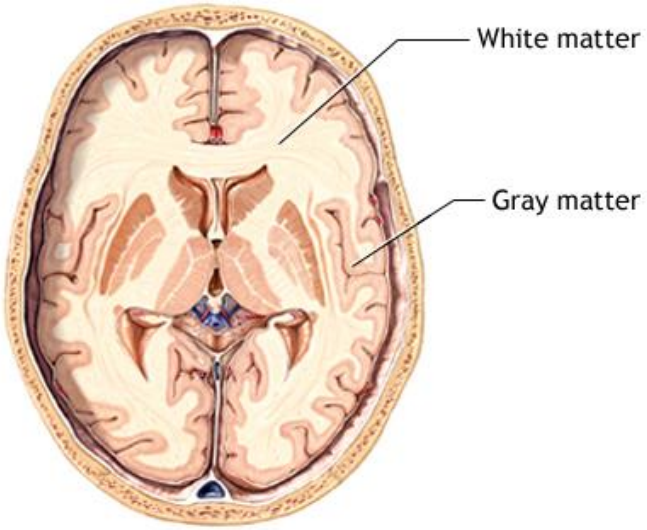

Figure 1.15: Examples of white matter and gray matter in spinal cord (A) and the human brain (B). Images modified from Wikimedia Commons (A) (504) and the National Institute of Health (B) (505).

1.2.3. CNS Injury

As just touched upon, the CNS can be damaged by a number of autoimmune disorders, age-related conditions, and of course from physical trauma caused by accident or injury. Each can be debilitating, degenerative, and even fatal, and although there are a number of treatments available, to date there are no cures for any CNS related conditions, with current therapies focusing mainly on treating secondary symptoms and slowing any disease progression (97). There are many reasons as to why the CNS is so difficult to repair. It is a very complex and sensitive structure which is very susceptible to secondary damage and thus difficult to operate on. Diseases of the CNS are often multifactorial, involving multiple pathologies and affecting multiple cellular phenotypes. The CNS also has its own repair mechanisms which can impair any potential regeneration (98).

1.2.3.1. Autoimmune disorders of the CNS

An autoimmune disorder is one where the body's immune system malfunctions and starts attacking certain parts of the body. There are a number of autoimmune disorders which affect the CNS such as Diffuse myelinoclastic sclerosis (99), Acute haemorrhagic leukoencephalitis (AHL) (100), Transverse myelitis (101), Neuromyelitis optica (102), Acute disseminated encephalomyelitis (ADE) (103, 104), and multiple sclerosis (MS) (105).

1.2.3.1.1. Acute Disseminated Encephalomyelitis (ADE)

ADE is an acute demyelinating disease of the brain which is usually caused by a viral, bacterial, or parasitic infection, but spontaneous ADE can also occur (106-108). It affects a very small number of people (~8 in every 100,000), and is most common in younger children, especially those who have just experienced an upper tract infection or vaccination (106-108). It results in axonal demyelination, leading to neuronal degeneration and lesions in the white matter of the brain, but as the disease is associated with an acute pathology, and is most common in young people, the damage is often reversible and thus only fatal in ~5% of cases (106-108). The aetiology of the disease is not fully understood but it is thought to involve a defective immune response to myelin basic protein (MBP) (108). Symptoms can include, fever, malaise, nausea, and sometimes coma and/or death (106-108).

1.2.3.1.2. Multiple Sclerosis (MS)

MS is a far more serious condition to ADE, although the demyelinating pathology is the same (108, 109). Unlike the acute nature of ADE, MS is a progressive chronic condition which is ultimately fatal. MS is most common among Caucasian women living in Europe, North America, New Zealand, and parts of South East Australia, is much less common amongst Hispanics, Africans, and Asians, and is very rare amongst indigenous people such as Maori, Aboriginals, and the Inuit (110). Figure 1.16 outlines the geographical incidence of MS. The gender link to MS is yet to be

established, but the geographical link has been linked to Vitamin D, or a lack of it (111-115). Canada and Scotland have the highest incidences of MS in the world, countries which have relatively low annual rates of sunshine compared to the rest of the world. People of New Zealand and Australia are extremely vigilant when it comes to protecting against skin cancer due to a large hole in the ozone layer over New Zealand and South East Australia. This has led to an increase in the use of sun block and also to the rise of Vitamin D related conditions such as rickets (116). Consumption of dietary vitamin D is also low in western society, with people opting for a more meat rich diet over vitamin D rich vegetables such as spinach and broccoli (117), and in some countries like Scotland, changes in fishing regimes have seen a switch from the consumption of large amounts of vitamin D rich oily fish to white fish such as cod which has comparatively low amounts of vitamin D. This link between MS and vitamin D has also been associated with polymorphisms in genes involved in the vitamin D pathway (118), so there is definitely an established association between the two. This is far from the solution however. There are many potential causes of MS, and treatment is a multi-factorial process depending on the progression of the disease (119-125), but this is one very active field of research in what is a far from well understood condition.

Figure 1.16: Map of the world highlighting the most prevalent areas of MS worldwide. Taken from multiplesclerosis.net (506).

MS is characterised by a malfunction of lymphocyte populations in the brain and spinal cord, neurons, and oligodendrocytes which leads to axonal demyelination, gliosis, and neuronal cell death affecting both gray and white matter (119-125). Attacks are transient, and endogenous repair can occur to an extent, but due to the chronic nature of the disease, the affected sites are progressively degraded over time until irreparable lesions are formed, leading to a loss of cognitive function, and ultimately death (119-125). There are four stages of MS pathology outlined by Lublin *et al*. (126). They are:

- Relapse remitting – the initial stage where symptoms are present, but can partially recede or even go completely
- Secondary progressive – can take 15 years to get to this stage, where symptoms cease to remit and start to persist
- Primary progressive – when symptoms start to progress to more serious cognitive complaints such as walking and speech impairment
- Progressive relapsing – the final stage of the disease where cognitive function gets progressively worse to a fatal conclusion. Patients at this stage will be wheelchair bound.

Initial symptoms of MS are malaise, nausea, headaches etc, quite general symptoms which often lead to the patients being undiagnosed for long periods.

There are a number of cells, factors, and signalling molecules involved in the pathogenesis of MS, making it incredibly difficult to understand the exact mechanisms involved. Studies have highlighted certain factors and interactions involved; Steinman (124) demonstrated a mechanism involving VLA4 secretion by T cells which triggers osteopontin (OPN) production by neuronal cell bodies, ultimately leading to damaged oligodendrocytes. This alongside the production of antibodies to proteins such as Myelin Oligodendrocyte Glycoprotein (MOG), MBP, and Proteolipid Protein (PLP) which lead to the destruction of myelin, and also the secretion by

astrocytes of αB crystallin, which has been shown to cause remission of MS. Hemmer *et al.* (125) showed a link between CD8+ T cells stimulating apoptosis of neuronal and glial cells via FAS ligation, a binding by glutamate of neurotoxins which are secreted by glial cells, antibody mediated compliment activation leading to a complex which attacks the myelin membrane, and the release of inflammatory cytokines from macrophages, microglia, and astrocytes. The full story of how and why MS occurs though is still not fully understood.

Much research is focused on reversing the effects of the disease such as looking at ways to stimulate re-myelination (127), and stimulating local glial populations to aid damage repair (128). Stimulation of myelin production is of great significance throughout this thesis. The potential of mesenchymal stem cells found in the olfactory mucosa to stimulate axonal myelination has been established by Lindsay *et al.* (1). The exact mechanisms involved have yet to be established however, and this project will set out to try and further understand these mechanisms and how they might be of any future therapeutic potential.

1.2.3.2. Spinal Cord Injury (SCI)

According to the World Health Organisation, up to half a million people each year are victims of a spinal cord injury, which can often result in a lifetime of complete paralysis (507). Statistics show that the vast majority of SCI's are the result of road traffic accidents, falls, sporting injuries, or violence (Figure 1.17) (508). Likely due to an increased exposure to risk factors such as fast driving, violence and reckless behaviour, SCI's are most common amongst young males between 20 and 29 years old (506). SCI's lead to irreversible paralysis when the spinal cord is severed, breaking any connection between the brain and motor neurons of the peripheral nervous system (129).

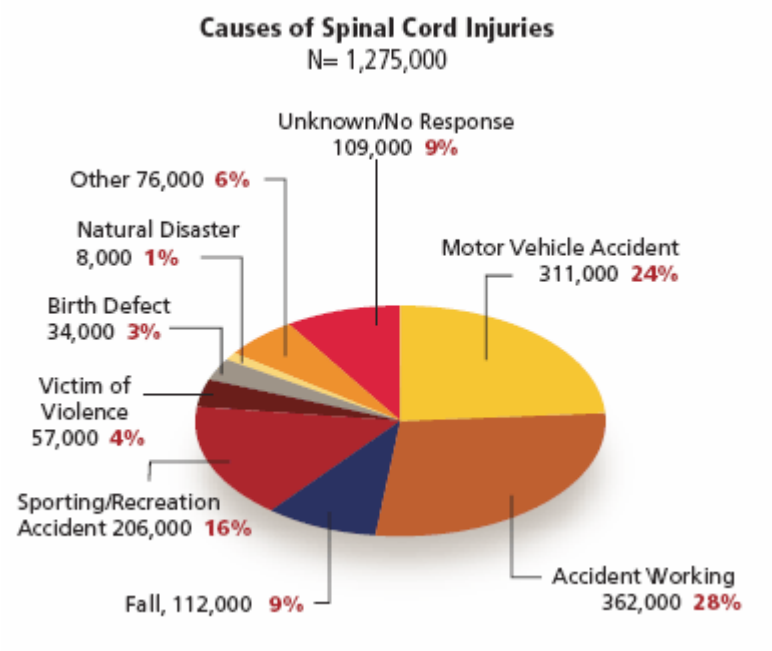

Figure 1.17: Pie chart representing the different causes of SCI and their relative percentages of prevalence. Taken from the Christopher and Dana Reeve Foundation (508)

SCI can be immediately fatal depending on the severity of the imposed trauma, but those who survive can be classified as to the severity of the injury, the location of the injury, and the secondary effects of the injury (130). Survival can lead to secondary complications which can cause fatalities years after the initial occurrence of the SCI. This most commonly occurs within two years of the initial injury, but even though SCI survivors can regain full fitness, life expectancy is generally lower compared to able bodied individuals (507).

To date there are no viable treatments regarding SCI repair other than physiotherapy. The spinal cord is a complex structure consisting of multiple different cell types, and damage to it results in a cascade of reparative mechanisms which ultimately result in the site of injury being unable to regenerate back to its normal functional state (69, 131-133). Possibly the most important local response to SCI is the formation of the glial scar. As the spinal cord is compromised, the danger of infiltration by

potentially harmful cells and immunomodulators is very high, so to prevent further damage, astrocytes flood the site of injury and form a protective barrier called a glial scar (Figure 1.18) (69, 131-133). Paradoxically however, this scar is impenetrable to neurons, preventing axonal regeneration, and inhibiting all signalling between neurons above and below the injury site (69, 131-133). This presents a major challenge to researchers, as any attempt to prevent the glial scar would undermine its protective nature and compromise the injury site further. Even if the glial scar could be prevented from forming, there is still a large empty lesion where all the damaged axons have retracted or degraded completely. Neurons are very large cells with long axons and multiple neurites extending from the terminal ends, it would be very difficult to bridge the lesion and encourage the neurons to extend far enough to make the required connections at the other side.

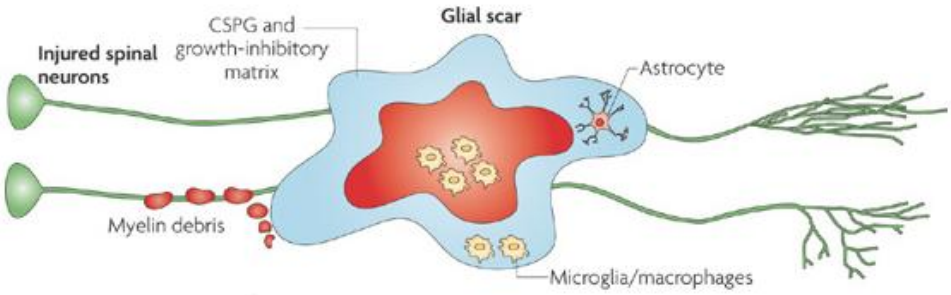

Figure 1.18: Schematic diagram of the glial scar formed post-spinal cord injury. Microglia and macrophages infiltrate the site of injury to clean up debris, and astrocytes fill the extremities of the injury site to prevent further damage. Adapted from Rolls *et al*. (131).

SCI repair is far from a unilateral approach, and all of these factors will have to be incorporated in order for a successful outcome. Studies are currently looking at factors to inhibit the glial scar (132) whilst modulating the environment to compensate for the loss of protection that the scar allows (69), and also looking into potential scaffolds to bridge the gap formed at the injury site (134) whilst encouraging neurite outgrowth to

extend neuroregeneration and re-establish connections across the lesion (135, 136).

1.2.4. The Olfactory System

Like the nervous system, the olfactory system (OS) has both a central and a peripheral component, although the whole system is an extension of the CNS (35, 137). The central component of the OS consists of the olfactory bulbs which extend from the base of the forebrain and rest on the cribriform plate, a piece of bone at the apical part of the nose which separates the brain and the nasal cavity (35, 137). The peripheral component of the OS consists of the olfactory mucosa (OM), which is located across the cribriform plate between it and the nasal cavity. Transcending the cribriform plate from the OM are olfactory receptor neurons (ORNs). These bipolar neurons have their cell bodies within the OM, and project axons down towards the basal edge of the OM, and upwards through the cribriform plate and into the olfactory bulb where they connect to mitral cells via glomeruli at the base of the bulbs (Figure 1.19) (509).

This whole system allows the CNS to capture and interpret smells, but is also a target of constant insult and damage due to the inhalation of chemically noxious and physically damaging airborne particles. Consequentially, the olfactory system, particularly the OM, is a locus of constant neuroregeneration, and thus of great interest to those concerned with conditions such as MS and spinal cord injury where neuroregeneration does not occur (138-140). To harness this endogenous reparative capability and replicate it ectopically would be extremely beneficial for a number of neurodegenerative conditions throughout the body.

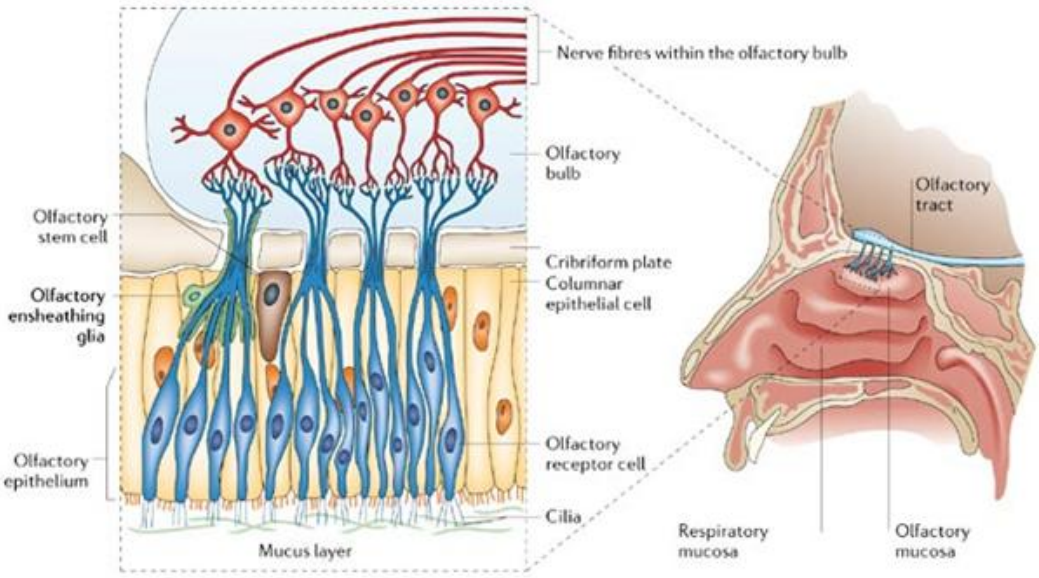

Figure 1.19: Schematic diagram of the olfactory system, taken from Thuret *et al*. (509).

1.2.4.1. The Olfactory Mucosa

For decades it was thought that you were born with your lifetime's supply of neurons and that the body was incapable of neurogenesis throughout adulthood. It has since been demonstrated however that there are certain areas throughout the CNS that are capable of neurogenesis throughout the life of humans. Sohur et al (141) identified 2 constituent neurogenic areas of the adult CNS in the olfactory bulb and the hippocampal dentate gyrus, and a number of other areas throughout the CNS which contain multipotent neural progenitor cells. More recently it was discovered that the OM contained not just neural progenitors but also multipotent adult stem cells which reside in the Lamina Propria of the OM (35, 36, 142-145).

The olfactory mucosa (OM) is a multicellular structure located at the apex of the nasal cavity, and consists of two distinct regions; the olfactory epithelium (OE) and the lamina propria (LP) (Figure 1.20) (35). Amongst the many cells which make up the OM are two distinct stem-like cell types located in the OE; The horizontal basal cells (HBC's) and globose basal cells (GBC's), referred to as putative stem cells or adult neural progenitors

of the olfactory system, that are considered to give rise to new neurons in the OM as well as help regenerate all the other constituent cells of the OM (146, 147). As the name suggests, the GBC's are more spherical in morphology than the HBC's, and they are dorsally situated relative to the HBC's (Figure 1.20).

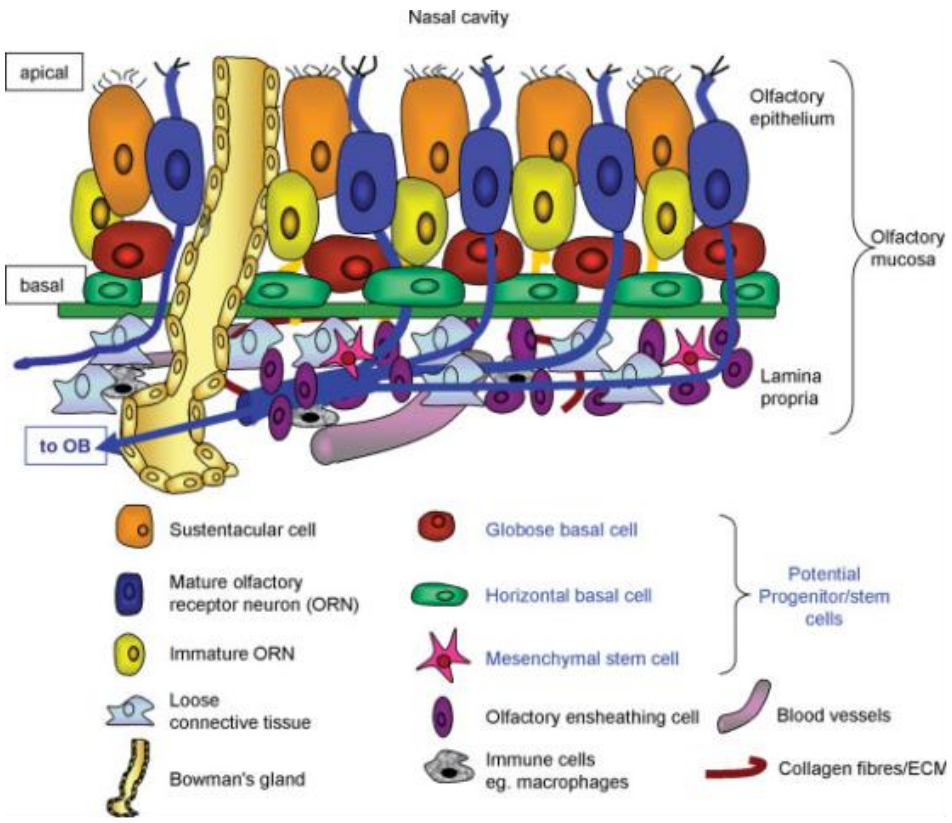

Figure 1.20: Schematic diagram depicting the cellular make up and physical structure of the olfactory mucosa (35).

As one of the first contacts of noxious or toxic inhalations, GBC turnover is relatively high, and consequentially they proliferate at a higher rate than the HBC's which are often in a state of quiescence (36). GBC's are thought to give rise to olfactory receptor neurons (ORN's) and sustentacular cells (support cells for ORN's) (148), and HBC's are thought to regenerate the GBC's themselves (146). HBC's have also been shown to differentiate *in vitro* towards both neuronal and non-neuronal lineages (146). Both cell types are capable of self-renewal, and their specific activation is

dependent on the extent of the damage to the OM, i.e. minor damage to the ORN's would only necessitate the activation of the GBC's to regenerate them, whereas more serious damage resulting in the degradation of multiple cell types including the GBC's would require the activation of HBC's (36, 146). This data has prompted the suggestion that it is the HBC that is the adult neural stem cell of the OM, although studies are still ongoing.

Also residing in the LP are a small population (~1% of total cells) of mesenchymal stem cells, which are thought to assist in the regeneration and the functional repair of damaged neurons post-injury (35). Only discovered quite recently, little is known about their function in the OM. Studies have confirmed them to express MSC markers such as CD90, CD105, CD166, and Nestin, and have demonstrated their ability to form bone and fat, so their identity as an MSC is no longer under dispute. MSCs are multi-functional cells so it's unlikely that they are limited to just one role in the OM, but their exact functions have yet to be fully determined. They may regenerate or replace local mesenchymal tissue such as the cribriform plate and cartilage in the nose, or they may have an immunomodulatory role to control the local immune system post-injury. Of most interest in terms of neuroregeneration however is their potential to aid in the repair of damaged neurons or to even regenerate new neurons altogether. MSCs are known to secrete large amounts of numerous hormones, growth factors, and chemokines, which could potentially be aiding HBCs and GBCs to replenish the olfactory system, or stimulating local glial populations to increase myelin production on damaged or demyelinated axons.

Lindsay *et al.* (1) have already demonstrated an ability for olfactory mucosa-derived MSCs (OM-MSCs) to stimulate axonal myelination in vitro. This pro-myelinating effect however was not observed with bone marrow-derived MSCs (BM-MSCs) so it is likely that OM-MSCs are secreting at least one factor which has a pro-myelinating effect.

1.2.5. Cell Transplantation into the CNS

Numerous regenerative therapies are being researched regarding the transplant of exogenous cells directly into the CNS (149-153). This covers such approaches as stimulating endogenous repair (154), replacing damaged tissue (155), grafting myelin producing cells (156), and transplanting stem cell populations to generate new cells such as damaged neurons (149). Such approaches are often coupled with biological scaffolds or devices to guide any cellular regeneration strategies (157, 158).

1.2.5.1. Stimulating Myelination via Exogenous Cell Transplant

CNS conditions such as MS and SCI result in the demyelination of axons and the deterioration of local populations of myelinating glial cells. If neurons aren't irreversibly damaged, repair could be initiated by the restoration of the local glial population. Studies have shown that transplantation of oligodendrocyte precursor cells (OPCs) can enhance myelination and even functional recovery in animal models of MS and SCI (159, 160). Even ectopic cell transplants have seen enhanced repair in the CNS. Schwann cells, the myelinating cells of the PNS which won't normally integrate in the CNS due to their inability to penetrate the astrocyte boundary, have been shown stimulate myelination when transplanted ectopically (156, 161, 162). Olfactory ensheathing cells (OECs), a type of glia which are responsible for supporting the repair of olfactory receptor neurons in the olfactory system, have been shown to stimulate myelin production *in vitro* (163), and also to increase axonal repair when transplanted into a compromised CNS (164-168).

1.2.5.2. Stem Cell Based Regeneration of Local Cell Populations

There are a number of candidate cells for the transplant-mediated regeneration of CNS tissue. Embryonic stem cells (ESCs), capable of differentiating into any cell from any of the three germ layers, could be transplanted directly to the injury site, and via endogenous cues, differentiate to re-form damaged cells (169). The behaviour of undifferentiated ESCs however, is very unpredictable, and cells may not

integrate at all with the surrounding niche, or they could proliferate uncontrollably and lead to tumour formation (170). The most sustainable approach regarding ESC transplantation is to part differentiate the cells towards neuronal and glial lineages post-transplant, an approach which has seen success is various disease models (171, 172).

Already part-programmed towards a neuronal fate, neuronal stem cells (NSCs) are also a candidate for transplant-mediated cell therapy (173). Not only are they capable of forming new neuronal and glial cells (174), they also elicit a neuroprotective "bystander effect", releasing trophic factors and signalling molecules which guide endogenous regeneration (149, 175).

1.3. MSCs in Health and Disease

MSCs have for some time now, been considered as potentially ideal candidates for the treatment of a number of conditions such as stroke (176), Alzheimer's (177), autoimmune diseases (178), amyotrophic lateral sclerosis (ALS) (179), and SCI (180). As well as these predominantly CNS and degenerative conditions, MSCs are also the subject of much research in the field of orthopaedics (181). The ability of MSCs to form bone in particular is of great importance when considering disorders of the musculoskeletal system and the body's need for repair post-injury or post-surgery.

1.3.1. MSCs and MS

MSCs have been considered as a candidate cell-based therapy to treat MS after studies in rodent Experimental Autoimmune Encephalomyelitis (EAE) models showed clinical and pathological improvements in animals treated intravenously with MSCs expanded *in vitro* (182). The suggested mechanisms of action of the MSCs on EAE were an induction of peripheral immune tolerance (183), the stimulation of endogenous neurotrophic factors (184), and the suppression of B cell activity (185). These findings led to numerous other studies which have demonstrated a therapeutic link

between MSCs and MS. It has been demonstrated that MSCs migrate to the EAE lesion site whether they are administered intravenously (186, 187), intrventricularly (188), or intraperitoneally (189), and although there is no definitive evidence of trans-differentiation occurring post-transplant (185-187, 189), MSCs have been shown to develop a neuronal morphology once in the CNS (188). Other proposed repair mechanisms in the EAE model were by inducing endogenous oligodendrogenesis and neurogenesis as previously mentioned via the "bystander effect" of secreting regulatory soluble factors (50, 57, 58, 190).

Current therapies involving patients at the relapse remitting phase of the MS are often insufficient to treat the disease, certainly insufficient to overcome it (191). Issues arise from patient intolerance (192) to a lack of control of the inflammatory effects of the disease (193), and there are often side effects (194-196). Even if the treatments were more robust, there are no current therapies which are able to reverse the neurodegenerative damage caused by the disease so a progression to the secondary progressive (SP) phase is inevitable (191). There are no currently available treatments for the primary progressive phase. For these reasons, MSC-based therapies are high on the agenda as potential treatments for MS. Further to their observed potential in EAE animal models, MSCs are also beneficial in terms of their autologous nature, their expansion capabilities, and their ease of administration into the patient.

Progress is slow however, and by 2012 only 4 human trials were taking place worldwide (197-200), and three of those focused only on patient safety, with the other focused on differences in visual capacity. Pre-clinical data is optimistic but purely anecdotal, with positive data regarding magnetic resonance imaging (MRI) and immunological studies. Low patient numbers and a general scope of study mean that these trials are very preliminary indeed. One post-2012 study however, has shown for the first time a neuroprotective effect elicited by MSC translplantation. Connick *et al*. demonstrated by analysis of visual endpoints that there

were physiological, structural, and functional improvements in patients treated with MSCs (201). There has been much excitement surrounding MSCs and MS, and their potential is undisputed. MS is a complex condition however, with multiple pathologies, and it is likely that MSC transplantation would be just one part of any successful therapy to treat MS.

1.3.2. MSCs and SCI

Although MS and SCI are pathologically distinct, they do share common symptomatic traits such as demyelination, apoptotic lesions, and local inflammation (180). Thus, for similar reasons as discussed with MSCs in MS, MSCs are also thought of as a potentially viable cell-based therapy for the treatment of SCI.

Trans-differentiation of MSCs is still a topic of much debate. Studies have demonstrated that MSCs possess numerous neuronal and glial genes, and have demonstrated an ability to form cells of a neurogenic morphology which express neurogenic markers, but whether these cells can perform as fully functioning neurons with the same electrophysiological capabilities has yet to be determined (202-206). Their potential for neuronal trans-differentiation *in situ* is still being investigated as a possible reparative mechanism.

The spinal cord is such a challenging environment for self-repair due to weak neuronal plasticity; i.e. an inherent remodelling incapacity due to numerous endogenous mechanisms designed to protect the injury site (180). MSCs have the potential to overcome these mechanisms whilst maintaining the integrity of the injured spinal cord via its substantial secretome (207). MSCs secrete neuroprotective and neuroregenerative growth factors such as neural growth factor (NGF), vascular endothelial growth factor (VEGF), glia-derived neurotrophic factor (GDNF), and brain-derived neurotrophic factor (BDNF) (56, 208-211), and also anti-inflammatory cytokines such as TGF-β1 which can overcome the

endogenous pro-inflammatory molecules such as IL-1β, and TNF-α which are upregulated post-injury (212-214). MSCs have also been shown to produce exosomes; microvesicles rich in lipids, proteins, growth factor receptors, and messenger (mRNA) and micro RNA (miRNA), all of which can help to stimulate an endogenous regeneration of the damaged spinal cord (215-218). Further to this, MSCs have an immunomodulatory effect which can regulate local natural killer (NK) cell, B cell, and cytoxic T cell populations, as well as inhibiting apoptosis, creating an environment which is much more permissive to neuro and gliogenesis (218-224). Figure 1.21 outlines the pathobiology of SCI and the potential MSC responses which counter these effects.

There have been a number of studies on SCI animal models which have demonstrated increased motor function after perfusion with MSCs (225-228). There are surprisingly few human clinical trials going ahead however, despite this success in animals. Early trials demonstrated the safety of the MSC transplants (229), highlighting the autologous nature of MSCs as one reason why they are such exciting prospects. Other more recent trials have shown therapeutic effects and increased neurological and motor function in patients of acute and sub-acute SCI (230, 231). For patients with chronic SCI, and indeed any patient looking to recover fully, strategies will likely have to be of a multi-lateral approach, incorporating MSC transplant and a dissolution of the glial scar to promote neurogenesis, and biomaterials technology to fill lesions and act as scaffolds for glia and neurite growth across the injury site (232).

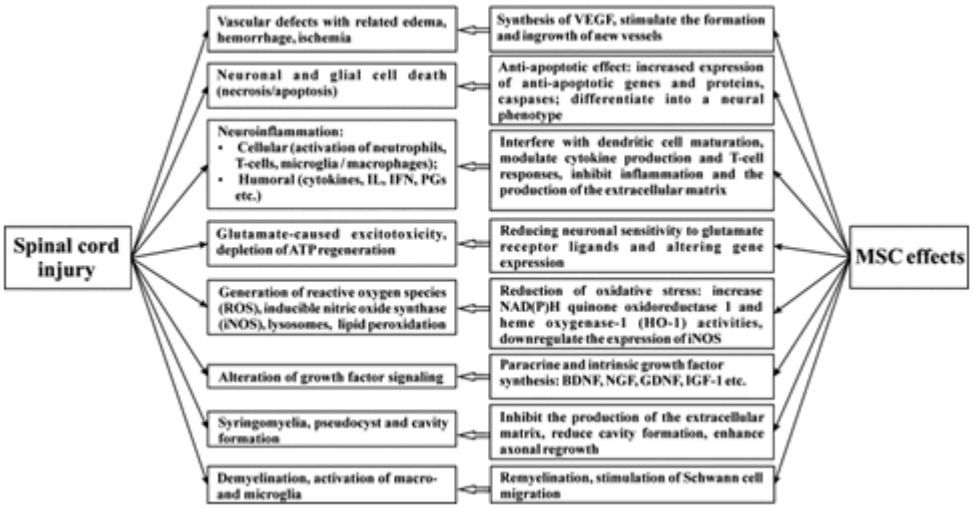

Figure 1.21: Diagram modified from Forostyak et al. outlining the potential therapeutic effects of MSCs on the different pathologies of SCI (180).

1.3.3. MSCs and Orthopaedics

Due to their ability to form bone, cartilage, fat, marrow stroma, tendons/ligaments, and muscle, MSCs have long been thought of as a potential therapeutic agent in the field of orthopaedics. Their natural function is to continually regenerate such tissues throughout the body, and throughout life, so when there is a malfunction of, or an interference to these processes, such as disease, injury, or surgery, the introduction of exogenous MSCs or the stimulation of endogenous MSCs become vitally important strategies. For example, genetic conditions such as osteo imperfecta (OI) affect the body's ability to properly form osteoblasts, leading to the formation of defective, brittle bones (181). These genetically defective MSCs could be replaced by MSC-derived osteoblasts which have been expanded *in vitro* and administered *in situ*, or exogenous MSCs could be simply transplanted into the patient to differentiate in vivo to form healthy osteoblasts (233-235).

For other more reparative methods such as regenerating damaged tissue, a more multi-lateral approach needs to be considered. Areas where damage from disease, injury, or surgery has resulted in empty lesions, simply

administering exogenous populations of cells would not be viable. Great advances in cell engineering technologies has led to the use of 3D scaffolds which not only hold the cells in place, but allow them to proliferate, and even encourage them to differentiate towards a specific lineage (181). For example, MSCs incorporated inside porous 3D scaffolds made from natural orthopaedic materials such as collagen, fibronectin, laminin etc., can be surgically implanted into the compromised area. The scaffolds must be porous to allow the movement of the MSCs and their produced matrices, as well as the movement of bioactive molecules, and they must also be natural to the niche so that they are not rejected by a local immune response, and so that they can naturally "dissolve" once the MSCs suitably regenerated the area of injury. This technique has been successfully implicated in repairing bone (236-238), cartilage (239-245), and tendons (246, 247).

1.3.3.1. Nanotopographies

MSCs don't just respond to biochemical cues *in vivo*. Different niches throughout the body are comprised of different structures of varying shapes, sizes, stiffness's, and roughness's. These parameters can alter a cell's behaviour on contact, and guide it down a particular path depending on cues relayed to the cell via cell/topography interactions (248-252). Changes in surface nanotopographies are felt by a cell's extracellular matrix (ECM), relaying signals into the cytoplasm to elicit changes in metabolic pathways which can alter the path towards which a cell can be guided (253-255). Engler *et al*. showed the importance of matrix stiffness in the fate of MSCs when he demonstrated changes in focal adhesion and differentiation patterns of MSCs cultured on substrates with different matrix elasticities (45), and Dalby *et al*. demonstrated the importance of nanotopography in the formation of bone, when he demonstrated the different osteogenic potentials of varying nanoscale patterns and pit heights to guide MSCs and osteoprogenitors towards an optimal osteogenic fate (256). These findings were ground-breaking in the field of orthopaedics, allowing surgeons, stem cell biologists, and engineers to

devise new implantable devices such as replacement hips which can stimulate endogenous populations of MSCs to form bone around the implanted device, and thus aid in a more successful and timely convalescence. Dalby *et al*. compared the osteogenic potential of cells cultured on 4 different nanotopographies; hexagonal, square, disordered square, and random, and showed that the disordered square pattern provided a significantly more osteogenic substrate compared to the other patterns, and to a non-patterned glass substrate (Figure 1.22) (256). Maclaine *et al*. also demonstrated the osteogenic potential of disordered square nanotopographies, and that different pit heights can also influence the cell's behaviour in terms of increasing proliferation or inducing terminal differentiation (257). These two studies were the basis of chapter 2 of my results, where I compared the behaviour of MSCs from the bone marrow and olfactory mucosa when cultured on nanotopography embossed polycaprolactone (PCL).

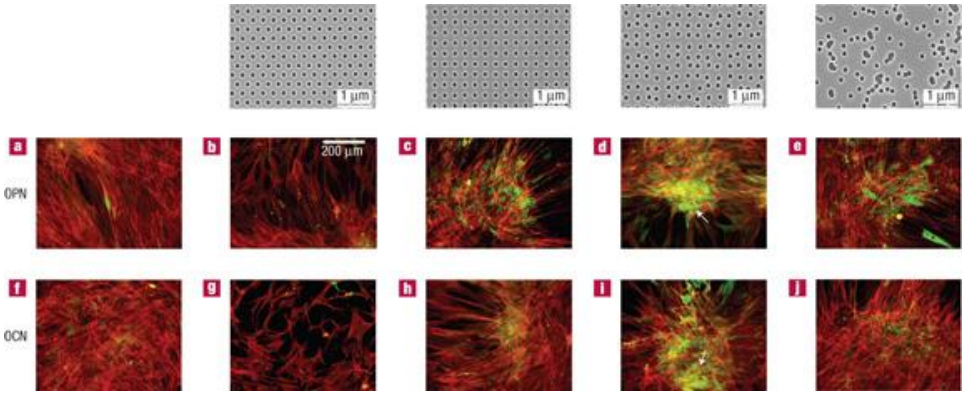

Figure 1.22: Figure taken from Dalby *et al*. depicting the four different nanotopographies; hexagonal, square, disordered square, and random, and their ability to stimulate the immunoreactivity of bone markers osteopontin (OPN) and osteocalcin (OCN) (green). Cells are highlighted by the immunoreactivity of actin (red) (256).

1.3.3.2. Polycaprolactone (PCL)

PCL is a biodegradable plastic polymer which I used as a cell culture substrate to gather data for chapter 2 of my results. Due to its low melting

point of 60°C, it was malleable and easy to emboss onto it different nanoscale topographies. For my experiments throughout this results section, squares of PCL were melted onto pre-manufactured metal shims which were patterned in a disordered square manner of differing pit heights. Full details of this process can be found in Materials and Methods section 2.12. Being a biodegradable polymer, and being so malleable, allows the use of PCL of unlimited nanotopographies with *in vivo* biological systems, such as nanopatterned implants and 3D scaffolds. Due to prior studies demonstrating the osteogenic induction capabilities of disordered square nanoembossed PCL, I will be using similarly nanoembossed PCL substrates to compare the osteogenic potential of BM-MSCs and OM-MSCs when cultured on these substrates.

1.4. The Myelinating Culture System

Measuring axonal myelination is at the forefront of this project. With only *in vitro* methods at my disposal, the myelinating culture system was an ideal experimental tool to manipulate and measure axonal myelination. First described by Sorensen *et al*. in 2008, the myelinating culture system allows the growth and myelination of embryonic spinal cord on glass cover slips (78). The full protocol is outlined in materials and methods section 2.17. As the support cells of the CNS, astrocytes are cultured from striatum-derived neurospheres onto 24-well plate glass cover slips. These act as a support matrix which feed and nurture the embryonic spinal cord mix which is layered on top. The embryonic spinal cord mix is a heterogenous suspension consisting of unmyelinated neurons, OPCs, astrocytes, and other glial cells. During the first 12 days of culture, the OPCs differentiate into mature myelinating oligodendrocytes, and for the remaining 14-16 days they myelinate the unmyelinated embryonic axons. After 28 days in culture, the amount of myelin in the cultures can be measured by immunocytochemistry, using fluorescent antibodies for myelin proteins such as PLP, MOG, MBP etc. The cultures have been shown to produce mature compact myelin with the correct location for nodal proteins (78, 258).

This is a very dynamic system, allowing the manipulation of myelin formation by the addition of soluble factors such as chemokines and hormones directly to the cultures. Factor-rich conditioned media taken from cells in culture can also be added, and even co-culture of these cover slips with other cover slips containing cells such as MSCs is possible and has been shown to have an influential effect on the way the axons are myelinated (1). This system is an excellent research tool in determining potential means of regulating myelination, and therefore has many implications in researching a number of demyelinating and degenerative conditions. Indeed a number of different studies have published data derived from the myelinating culture system (66, 70, 135, 136, 163, 197, 258-261). As an *in vitro* system, it is not an indication of what will definitely happen in vivo, but it is a solid testing base from which more exploratory *in vivo* work can be taken. Data from the lab have shown astrocytes are crucial in supporting myelination, but equally can become activated and inhibit myelination (66). Our lab has shown the importance of chemokines in regulating myelination and this has relevance for MSCs which secrete a huge number of chemokines.

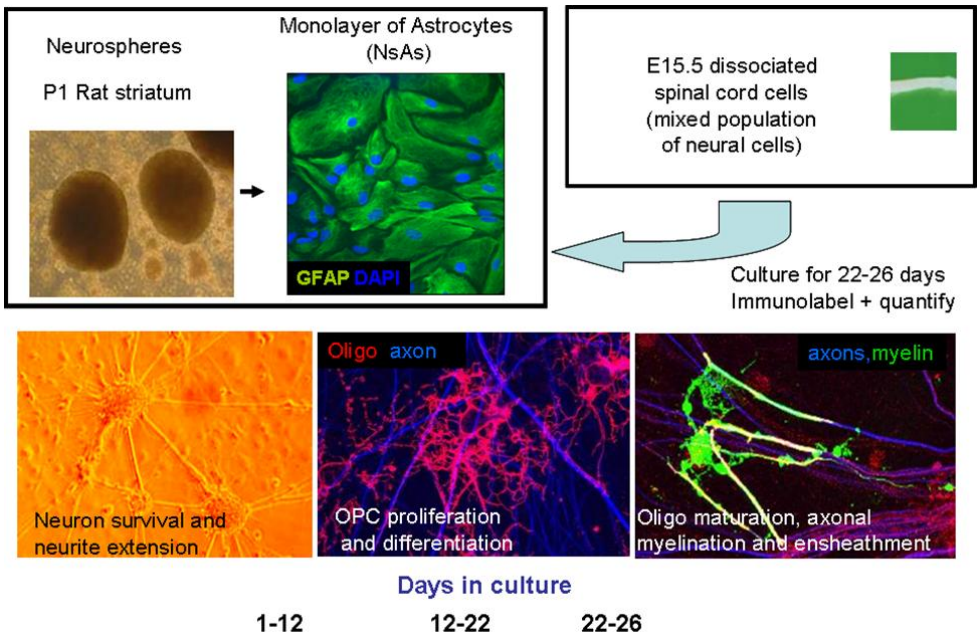

Figure 1.23: Schematic diagram outlining the different stages of the myelinating culture system. Antibodies used for immunocytochemistry analysis were SMI31 to label axons (blue), proteolipid protein (PLP) to label myelin (green), and O4 to label mature oligodendrocytes (red). Image compiled by Sue Barnett.

1.5. miRNA

MSCs have a vast secretome of numerous different cytokines which can be secreted at different concentrations under different conditions, depending on external cues (207). Secretion of particular cytokines at any particular time has to be regulated at a pre-translational level, and is done so by very short (~22 nucleotides) strands of RNA, called microRNA (miRNA). Their role is to bind to strands of mRNA to inhibit the translation of that mRNA, and thus inhibit the production of that particular cytokine (262, 263). miRNA have a promiscuous relationship with their respective cytokines which they regulate. Each individual miRNA is responsible for the regulation of numerous different cytokines, and each cytokine can be regulated by numerous different miRNA (262, 263). This allows for the specific regulation of one particular cytokine without there being a knock on inhibition of other cytokines which are regulated by that miRNA, but are required at that point also.

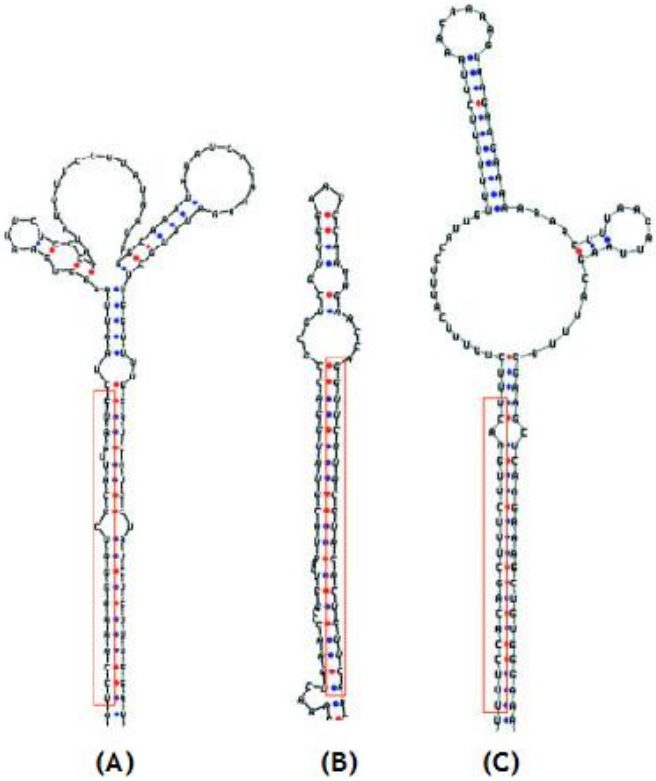

Figure 1.24: Diagram depicting three different pri-miRNA hairpin structures. Each pri-miRNA is from the Arabidopsis plant, and represent miR-393a (A), miR-416 (B), and miR-396b (C). The sequences inside the red boxes represent the mature miRNA strands. Image modified from Wang *et al*. (264).

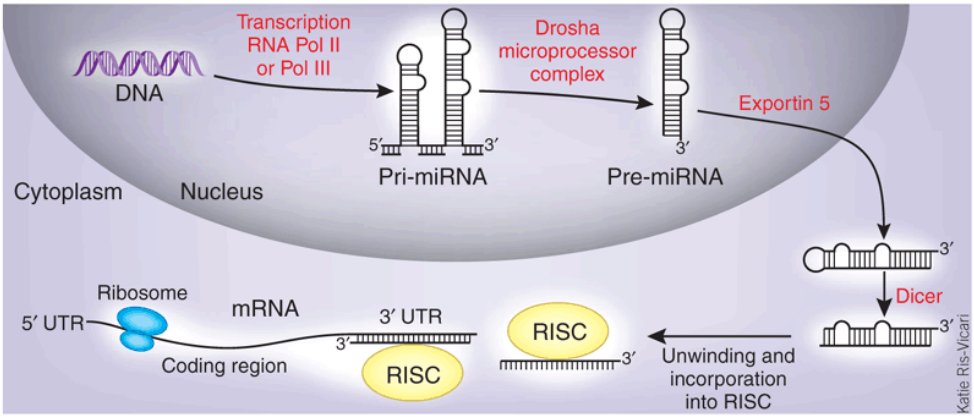

Figure 1.25: Schematic diagram of the genesis, transport from the nucleus, and inhibitory action of miRNA on mRNA translation. Image taken from Jeffrey *et al*. (265).

miRNA are produced in the nucleus either from introns or from their own genes. They are carried as needed into the cytoplasm by a protein called Exportin, in the form of a much larger hairpin structure called a pri-miRNA (Figure 1.24) (264). In the cytoplasm, the pri-miRNA are cleaved at the hairpin end by an enzyme called a Dicer, releasing a double stranded miRNA duplex. This duplex separates, and the single strand incorporates with a protein called an miRNA-induced silencing complex (RISC) and binds, not always in a fully complimentary way, to the target mRNA. The RISC/miRNA complex is then able to interfere with the translation of the mRNA by blocking it's entry through the ribosome (265) (Figure 1.25). Due to their regulation of numerous proteins, they are very significant in a number of biomedical conditions such as cancer (266), heart disease (267-269), obesity (270), and some neurological disorders such as schizophrenia (271, 272). For these same reasons, they are also a potential therapeutic target to treat such conditions, although any research into this is still in its infancy (273).

miRNA are a very important focus for this thesis. With Lindsay *et al*. having observed a very unique behavioural difference between BM-MSCs and OM-MSCs; an unknown pro-myelinating factor(s) secreted by OM-MSCs, it was essential for us to determine not only the secretory profiles of both cell types, but also the miRNA profiles of both, to see if there were any connections between the secretome and the miRNAome, and thus any potential therapeutic targets. If we could determine the secreted factor(s) which are/were responsible for this pro-myelinating effect, and then relate that/those to a particular miRNA, then we would be able to investigate whether or not regulation of that miRNA could be a potential therapeutic target for the manipulation of axonal myelination. For the determination of the miRNA profiles of BM-MSCs and OM-MSCs, we

collaborated with Sistemic, a developmental-stage biomedical company who specialise in miRNA technology, and miRNA fingerprinting techniques. More importantly they had the experience to compare two similar cell types and ask if they were related, and what, if anything, made them possess any differences in their biological behaviour like the poor myelinating potential of BM-MSCs.

1.6. Cytokine Array

Upon establishing a miRNA profile for each MSC, any pertinent miRNA which were differentially expressed between the two cell types, and the secreted factors associated with these miRNA, the next stage was to analyse the secretory profiles of both MSC types to investigate any differential secretion patterns which might relate to the differential miRNA expression. This was done using numerous cytokine arrays which allow the analysis of the media in which the MSCs have been cultured, and thus the secreted factors which have been released into the media. A number of commercially available arrays can be chosen, depending on which cytokines you wish to analyse your samples for, but each follow the same general mechanisms of action. Figure 1.26 outlines these mechanisms, and the full protocols can be found in Materials and Methods section 2.15.2. Briefly however, samples are combined with a number of beads which are each conjugated to an antibody to a specific cytokine. The antibody/bead conjugate binds to the cytokine, and is retained in the well whilst all unbound conjugate is washed away. Detectable secondary antibody then binds to the antibody/bead/cytokine complex, and the concentration of each cytokine is determined by a specific plate reader which measures the intensity of the fluorescence of each bound cytokine, and compares it to the fluorescence from the wells of a standard curve of pre-determined concentrations.

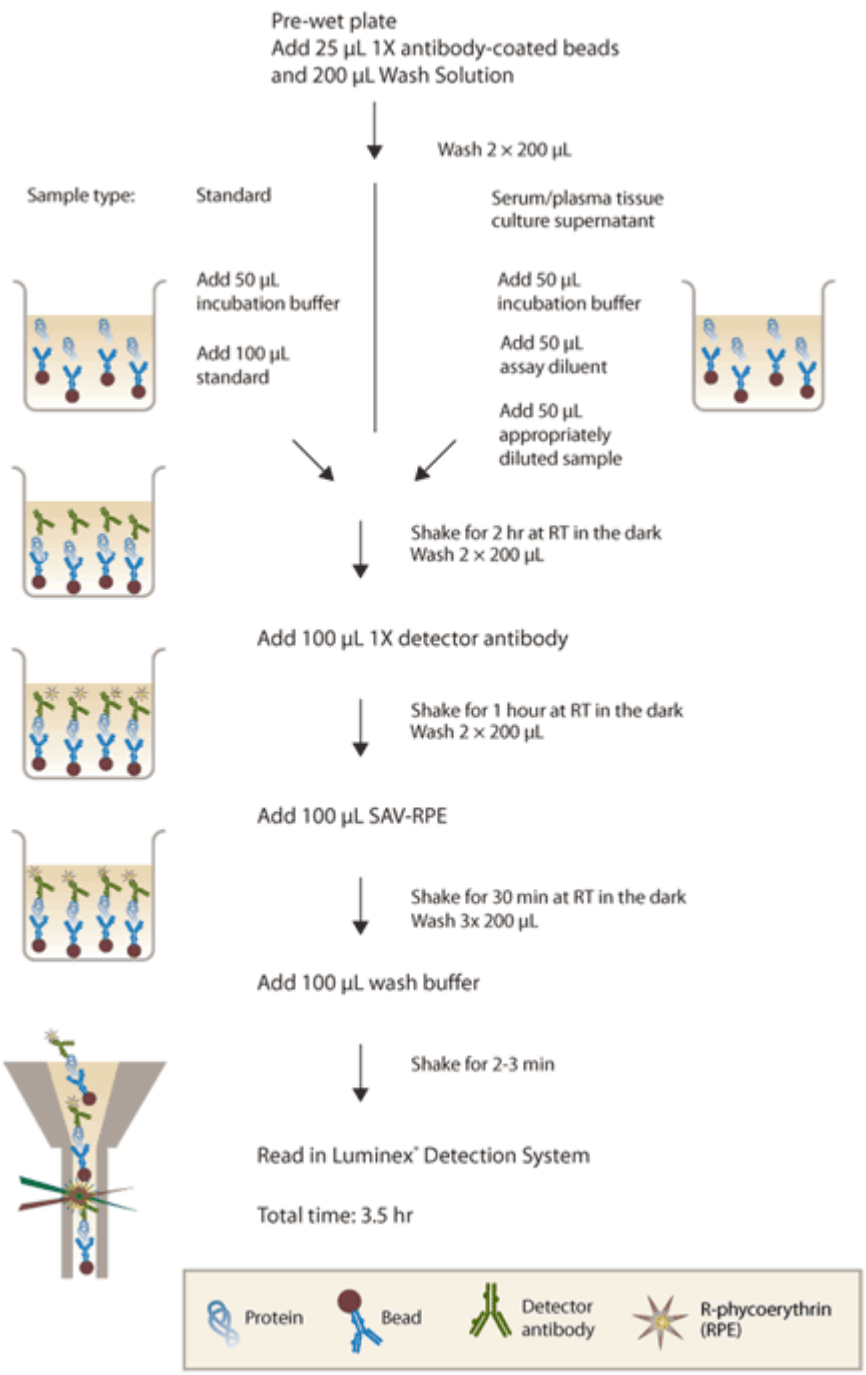

Figure 1.26: Schematic diagram representing the mechanisms of action occurring during a cytokine array. Image was taken from the LifeTechnologies website for Luminex® cytokine arrays (510).

The discovery by Lindsay *et al*. that OM-MSCs secrete a factor or factors which is/are responsible for stimulating axonal myelination and oligodendrocyte proliferation (1) is potentially ground breaking in the fields of MS and SCI research. MSCs have long been considered as potential therapeutic agents in a number of areas of biomedical research for their differentiation potential, immunomodulatory effects, and substantial secretome. OM-MSCs do not just offer up an alternative autologous source of MSCs, but may also be substantially more capable of contributing to the treatment of demyelinating conditions than those derived from bone marrow. Not only in MS and SCI research are OM-MSCs important. Breakthroughs in cell engineering and nanoscale cell/substrate interactions have revolutionised the field of orthopaedics. Research has focused predominantly on the behaviour of BM-MSCs on such substrates, but OM-MSCs could present a far more easily accessible autologous source for post-surgery or post-injury orthopaedic repair strategies.

Due to their relatively recent discovery, little has been researched with regard to OM-MSCs and their therapeutic potential, let alone their pro-myelinating potential. It is therefore my intention throughout this thesis to utilise well established analytical procedures such as RT-qPCR, immunocytochemistry, and cytokine arrays, as well as more neoteric technologies such as nanoscale cell engineering and miRNA fingerprinting, to compare and contrast the biochemical properties of BM-MSCs and OM-MSCs, their differentiation capabilities using factor rich induction media and nanotopographically embossed substrates, and also their behaviour and biological effects on neurobiological systems. I will not only be outlining any such differences between the two MSC phenotypes, but also fully investigating the possible mechanisms by which these changes are occurring.

The aim of my thesis is to identify the mechanism by which OM-MSc promote myelination and identify the optimal MSC for cell therapies. This will be carried out by:

1) Antigenic and morphologic characterisation using immunocytochemistry, RT-qPCR, and phase imaging techniques.

2) Comparing the differentiation capabilities of both MSC phenotypes, using factor-rich induction media and nanoscale topograhies

3) miRNA fingerprinting.

4) Bead-based multiplexing technology to identify and compare secreted factors

These studies will compare and contrast the two MSC types and determine their potential for use in regenerative medicine strategies.

Materials and Methods:

2. Materials and Methods

2.1. MSC and Astrocyte Culture Preparation

Lindsey *et al.* (1) showed previously that MSC culture was more efficient when the cells were seeded onto collagen coated surfaces compared to those of non-coated plastic or glass. Throughout this study, all glass and plastic surfaces onto which MSCs were cultured, were coated with collagen (Sigma, C4243) diluted 1:300 with sterile PBS, by simply incubating the surface with the collagen solution at RT for 30-60 min before washing with sterile ddH_2O and air drying.

Similarly, *Sørensen et al.* (78) showed that survival of astrocytes cultured onto plastic or glass surfaces relied on these surfaces being coated with Poly-L-Lysine (PLL) (Sigma, P4707), at a final concentration of 13 µg/mL in sterile ddH_2O. Plastic and glass surfaces are simply incubated at RT for 30-60 min before washing with sterile ddH2O and air drying.

2.2. Cell Culture

Three major cell types were compared throughout this study; bone marrow-derived-MSCs (BM-MSCs), CD271 positively selected bone marrow-derived-MSCs (BM271-MSCs), and CD271 positively selected olfactory mucosa-derived MSCs (OM-MSCs). Figure 2.1 details the methodology of these three cell types.

2.2.1. Human Bone Marrow-Derived MSC (BM-MSC) Culture

Human BM-MSCs were isolated from bone marrow aspirates obtained with ethics approval from 71 male and female patients (27 male, 44 female) undergoing routine hip replacement surgery from 2011 to 2013. Patients were predominantly elderly, but varied in age range from 32 to 86 years (average age 66.87 ± 12.55 (SD)), which was not significantly different from donor patients for OM-MSCs (all sample details are listed in Table 2.1). All surgeries were supervised by Mr David Allen, consultant orthopaedic surgeon at the Southern General Hospital in Glasgow. Bone marrow aspirates were isolated from the femoral heads and placed

immediately in 20 mL DMEM (low glucose) (Life Technologies, 10567-014) with 5% v/v foetal bovine serum (FBS) (Sigma, F7524), 0.5% v/v heparin (LEO Laboratories, PL0043/0041R), and 0.1% w/v Ethylinediaminetetraacetic acid (EDTA) (Sigma, E6758), and stored at 4°C for no longer than 24 hr before either collection from theatre, or delivery to the Glasgow Biomedical Research Centre (GBRC). Isolation of BM-MSCs from the bone marrow aspirate sample was carried out by carefully layering all aspirate onto 20 mL of Histopaque®-1077 (Sigma, 10771) cell separation media in a 50 mL centrifuge tube, ensuring to not break the surface of the Histopaque®-1077 with the aspirate, and ensuring not to layer any solid or particulate matter. The sample was then centrifuged at 604 x g (1500 rpm in a 24 cm radius centrifuge) for 35 min at RT, resulting in multi-layered content consisting (from top to bottom) of a waste media/adipose upper layer, an opaque interface layer termed the "buffy coat", a layer of Histopaque®-1077 (sometimes consisting of coagulated matter, depending on the sample), and a bottom layer of mononucleated cells such as erythrocytes (Figure 2.2). The layer containing the BM-MSCs is the buffy coat, and was collected by first aspirating and discarding the top layer to within 1 cm of the buffy coat. This 1 cm of media, plus the buffy coat and 1cm of Histopaque®-1077 below the buffy coat (avoiding any coagulated matter) was then collected, retained, and washed thrice with sterile phosphate buffered saline (PBS) with 5% v/v FBS and 0.1% w/v EDTA, centrifuging at 386 x g (1200 rpm in a 24 cm radius centrifuge) for 3 min between washes. The resultant pellet was then re-suspended in 7 ml DMEM (low glucose) plus 10% Hyclone™ FBS (Thermo Scientific™, SH3008803), and 0.05% L-Glutamine (Sigma, G7513) (henceforth referred to as DMEM:10% Hyclone), transferred to a collagen coated T75 cm^3 culture flask and incubated at 37°C for 72 hr. After 72 hr, the media containing all non-adherant cells was removed, the flask washed with sterile PBS, and a fresh 7 mL of DMEM:10% Hyclone added.

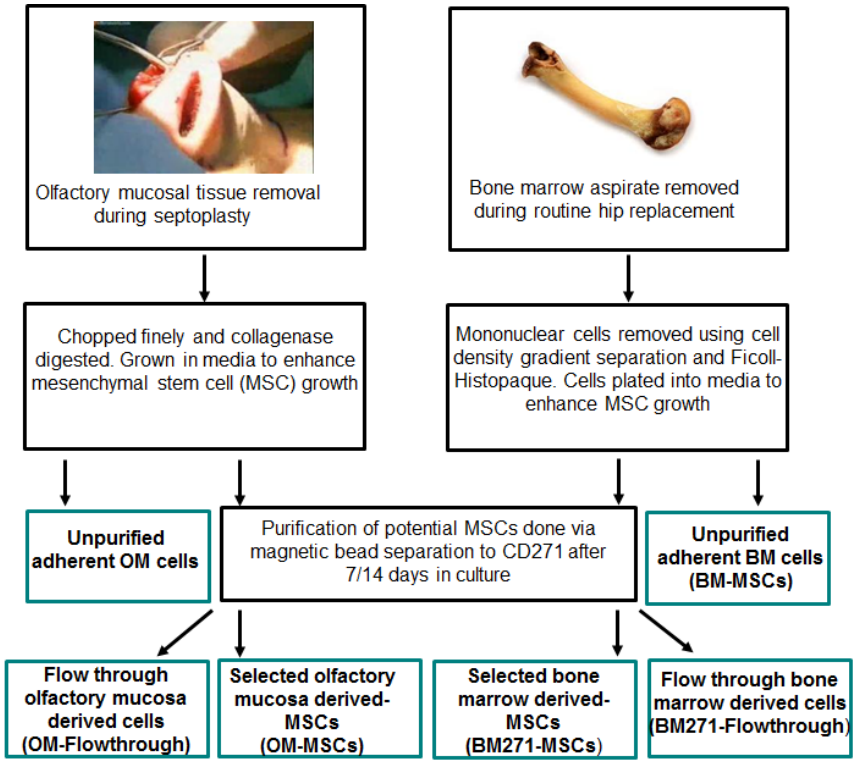

Figure 2.1: Schematic diagram detailing the methodology of the three major cell types used in this investigation; OM-MSCs, BM-MSCs, and BM271-MSCs.

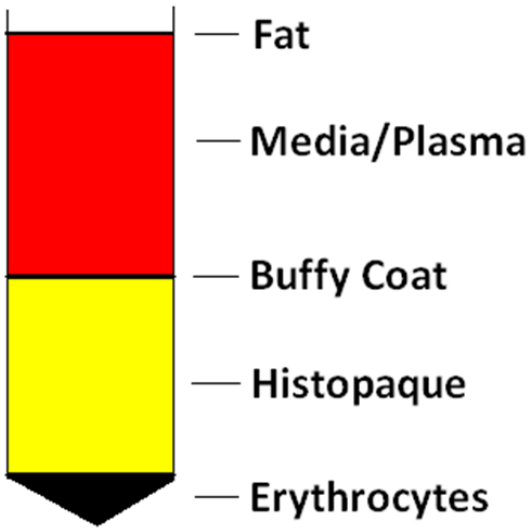

Figure 2.2: Diagram of the different layers resulting from the Histopaque® cell separation technique which isolates BM-MSCs from bone marrow aspirate samples. BM-MSCs are collected from the "buffy coat" layer, whilst all other layers are discarded to waste.

2.2.1.1. BM-MSC Purification to Isolate BM271-MSCs

Once the flask reached confluency (21-28 days), BM-MSCs were purified using the EasySep® Human MSC CD271 positive selection kit (StemCell Technologies, 18659). Figure 2.3 highlights the major steps involved in this process. During this process, adherent cells were enzymatically dislodged using 5 mL Trypsin-EDTA 0.5% (Sigma, S8636), which was neutralised after 5 min at 37°C using a further 5 mL of DMEM:10% Hyclone. The whole suspension was centrifuged at 386 x g for 3 min, and the pellet re-suspended in 500 µL DMEM:10% Hyclone + 12.5 µL of Fc receptor blocker and 25 µL of CD271 positive selection cocktail, and transferred to a FACS tube. This suspension was then incubated at RT for 15 min before the addition of 25 µL of magnetic bead particles and further incubation at RT for 15 min. 2.5 mL of DMEM:10% Hyclone was then added to the suspension, and the tube inserted into the EasySep® magnet for 5 min. Without removing the tube from the magnet, the liquid contents of the tube were removed to waste by inversion. The tube was then removed from the magnet, and a further 2.5 mL of DMEM:10% Hyclone was added before placing the tube back into the magnet for 5 min. This magnetic isolation of cells was repeated a further 2 times. After the final supernatant was discarded, the tube was centrifuged at 386 x g for 3 min, and the pellet of purified BM-MSCs (BM271-MSCs) re-suspended in 60 µL DMEM:10% Hyclone. This suspension was plated into T25 cm^3 culture flasks in 3 x 20 µL strips, and incubated at 37°C for 15 min for the cells to adhere to the flask. The flask was then flooded with 3 mL of DMEM:10% Hyclone and incubated at 37°C until use. These purified BM-MSCs were henceforth termed BM271-MSCs, and are to be treated distinctly to non-purified BM-MSCs. Cells were bulked up over time by enzymatically dislodging using trypsin-EDTA 0.5% (trypsinising), re-suspending them in fresh DMEM:10% Hyclone, and placing them back into a larger number of flasks. Any unused cells were trypsinised, re-suspended in 90% FBS + 10% dimethyl sulphoxide (DMSO), and stored in liquid nitrogen.

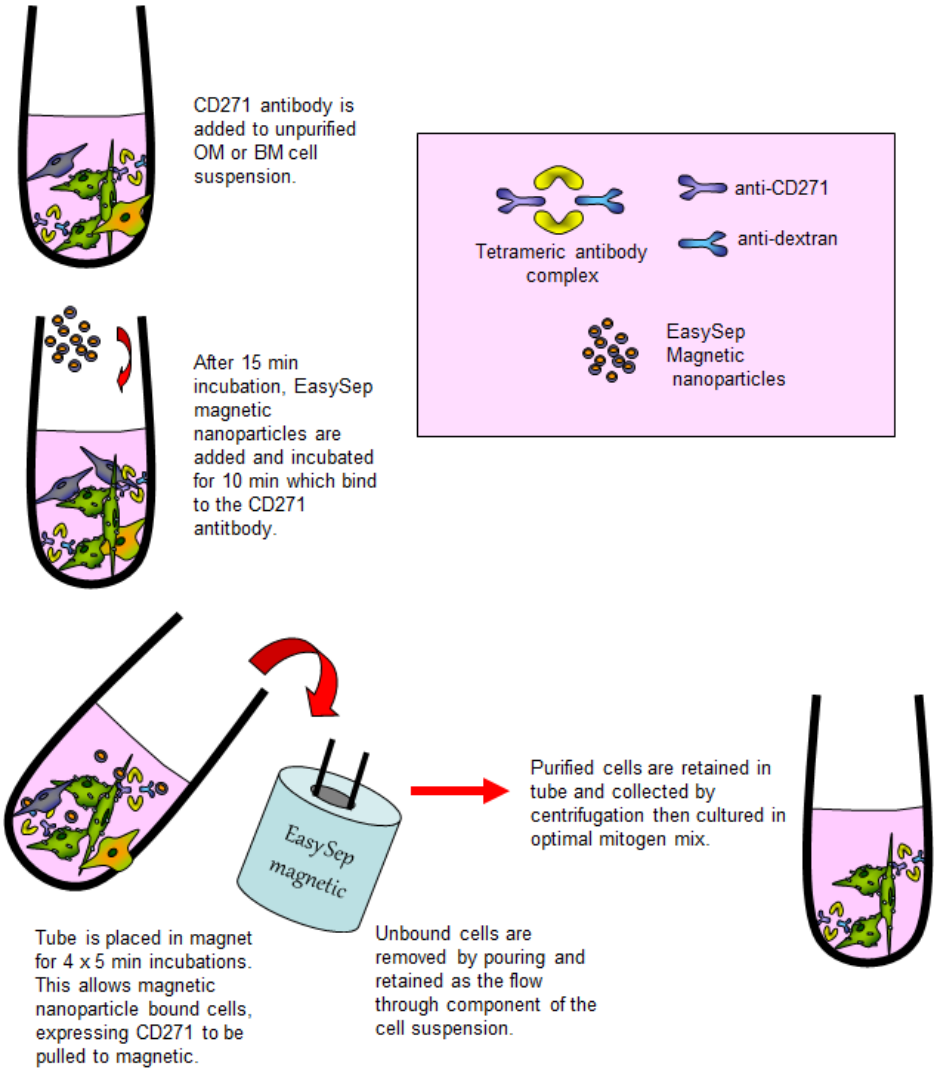

Figure 2.3: Schematic diagram of the EasySep® CD271 positive selection process carried out on BM-MSCs and on unpurified adherent OM cells. The resultant cells are termed BM271-MSCs and OM-MSCs.

Bone Marrow Aspirate Donors									
Sample ID	Date of Surgery	Year of Birth	Sex	Age	Sample ID	Date of Surgery	Year of Birth	Sex	Age
F43A	25/05/2011	1943	Female	68	M36R	05/07/2012	1936	Male	76
M39T	26/05/2011	1939	Male	72	M80C	09/07/2012	1980	Male	32
M70J	15/06/2011	1970	Male	41	M31J	11/07/2012	1931	Male	81
F34E	22/06/2011	1934	Female	77	F26H	12/07/2012	1926	Female	86
F33E	23/06/2011	1933	Female	78	M62J	09/07/2012	1962	Male	50
F35J	13/07/2011	1935	Female	76	F79G	26/07/2012	1979	Female	33
F48I	18/07/2011	1948	Female	63	F56MA	09/08/2012	1956	Female	56
F30A	20/07/2011	1930	Female	81	M51A	05/09/2012	1951	Male	61
F38I	27/07/2011	1938	Female	73	M33C	12/09/2012	1933	Male	79
F43E	03/08/2011	1943	Female	68	M42T	27/09/2012	1942	Male	70
M38R	04/08/2011	1938	Male	73	M55M	10/10/2012	1955	Male	57
F25I	11/08/2011	1925	Female	86	M43W	11/10/2012	1943	Male	69
F54H	18/08/2011	1954	Female	57	F28H	17/10/2012	1928	Female	84
F31M	24/08/2011	1931	Female	80	M63G	18/10/2012	1963	Male	49
F60M	25/08/2011	1960	Female	51	F34M	01/11/2012	1934	Female	78
M61K	06/09/2011	1961	Male	50	F50J	07/11/2012	1950	Female	62
F46I	19/09/2011	1946	Female	65	M44H	13/12/2012	1944	Male	68
F55I	20/09/2011	1955	Female	56	F45J	14/12/2012	1945	Female	67
F48J	28/09/2011	1948	Female	63	F56M	19/12/2012	1956	Female	56
M47R	26/10/2011	1947	Male	64	F52M	16/01/2013	1952	Female	61
F55S	27/10/2011	1955	Female	56	F35P	17/01/2013	1935	Female	78
F37F	04/11/2011	1937	Female	74	F32S	05/02/2013	1932	Female	81
M33J	11/11/2011	1933	Male	79	F30B	07/02/2013	1930	Female	83
F56M	16/11/2011	1956	Female	55	F37L	14/02/2013	1937	Female	76
F57K	01/12/2011	1957	Female	54	F45M	07/03/2013	1945	Female	68
M34K	04/01/2012	1934	Male	78	M49A	26/03/2013	1949	Male	64
M56J	01/02/2012	1956	Male	56	M49J	03/04/2013	1949	Male	64
F31I	02/03/2012	1931	Female	81	F47P	04/04/2013	1947	Female	66
M47RU	29/03/2012	1947	Male	65	F46P	30/05/2013	1946	Female	67
M33J2	17/04/2012	1933	Male	79	F32E	13/06/2013	1932	Female	81
M56P	18/04/2012	1956	Male	56	F40E	18/06/2013	1940	Female	73
F41C	24/05/2012	1941	Female	71	F59K	19/06/2013	1959	Female	54
F43C	26/05/2012	1943	Female	69	M39G	31/07/2013	1939	Male	74
F43M	14/06/2012	1943	Female	69	M32M	07/08/2013	1932	Male	81
M77A	24/06/2012	1977	Male	35	F37C	08/08/2013	1937	Female	76
F44E	05/07/2012	1944	Female	68					

Table 2.1: List of all bone marrow aspirate samples supplied between May 2011 and August 2013. All samples were donated with consent from patients of Mr David Allen, consultant orthopaedic surgeon at the Southern General Hospital, Glasgow, undergoing routine hip replacement surgery. All samples were taken from the iliac crests of male and female patients between the ages of 32 and 86.

2.2.2. Human Olfactory Mucosa-Derived MSC (OM-MSC) Culture

Human OM biopsies were obtained with ethics approval from 37 male and female patients (21 male, 16 female) undergoing routine nasal septoplasty/polypectomy surgery from 2011 to 2014. Patients were predominantly elderly, but varied in age range from 32 to 86 years (average age 55.32 ± 13.89 (SD)), which was not significantly different from donor patients for BM-MSCs (all sample details are listed in Table

2.2). Surgeries were supervised by Mr Saghir Sheihk and Mrs Louise Clark, consultant ENT surgeons at the Southern General Hospital and at the Victoria Hospital, both in Glasgow. Biopsies were taken from areas most commonly known to contain OM, the upper middle turbinates and uncinate process of the ethmoid bone. Biopsies were collected and placed immediately on ice in Hanks balanced salt solution (HBSS) (Life Technologies, 24020-117) containing 1% penicillin/streptomycin (Gibco, 15070), and 0.5% fungizone (Gibco, 15290-018) for no more than 24 hr before collection. After removing all solid and particulate matter from the tissue, it was homogenised with a scalpel blade, and digested in a 5 mL bijou using 1mL Leibovitz's L-15 media (Life Technologies, 11415064) + 100 µL of 1.33 % collagenase (Sigma-Aldrich, C0130) for 20 min at 37°C followed by incubation with DNAse to reduce cell clumping (0.04 mg/ml bovine pancreas DNAse (Sigma, DN25), 3.0 mg/ml bovine serum albumin-fraction A (Sigma, A9647) in L15 media). Cells were mechanically dissociated by pipetting, then triturating through a 23G needle, centrifuged at 386 x g for 5 min and the pellet re-suspended in DMEM:10% Hyclone and plated on collagen coated (10 mg/ml, Sigma-Aldrich, UK) 25 cm^2 tissue culture flasks. After 7 days, a heterogeneous monolayer of spindle shaped cells developed, and from this monolayer, human MSCs were purified using the EasySep® Human MSC CD271 positive selection kit previously described. After purification, cells were termed olfactory mucosa (OM)-MSCs. OM-MSCs were bulked up and stored long term using the same conditions as with BM-MSCs.

Olfactory Mucosa Donors									
Sample ID	Date of Surgery	Year of Birth	Sex	Age	Sample ID	Date of Surgery	Year of Birth	Sex	Age
M28.1.64	16/05/2011	1964	Male	47	M1952	05/10/2012	1952	Male	60
M6.12.61	22/06/2011	1961	Male	50	F26.2.1953	08/10/2012	1953	Female	59
F6.2.66	21/09/2011	1966	Female	45	F1960	15/10/2012	1960	Female	52
F24.7.52	17/10/2011	1952	Female	59	M1926	26/10/2012	1926	Male	86
M1956	31/10/2011	1956	Male	55	M7.10.80	26/11/2012	1980	Male	32
M26.6.47	28/11/2011	1947	Male	64	F16.11.79	19/11/2012	1979	Female	33
F1.12.1951	16/12/2011	1951	Female	60	F27.2.47	17/12/2012	1947	Female	65
M1971	06/01/2012	1971	Male	41	M11.2.30	07/01/2013	1930	Male	83
F01.01.59	16/01/2012	1959	Female	53	M23.9.51	18/01/2013	1951	Male	62
M08.12.56	30/01/2012	1956	Male	56	M1956	01/02/2013	1956	Male	57
M1943	10/02/2012	1943	Male	59	F28.1.53	15/01/2013	1953	Female	60
F24.7.68	23/03/2012	1968	Female	44	M4.6.71	01/03/2013	1971	Male	42
M23.1.51	02/04/2012	1951	Male	61	M1968	04/04/2013	1968	Male	45
F24.7.68	03/04/2012	1968	Female	44	M29.6.49	05/04/2013	1949	Male	64
F29.01.58	30/04/2012	1958	Female	54	F9.10.1972	28/08/2013	1972	Female	41
F1945	06/06/2012	1945	Female	67	M20.4.1987	28/08/2013	1987	Male	26
M1946	13/07/2012	1946	Male	66	F19.1.72	16/09/2013	1972	Female	41
M1960	20/07/2012	1960	Male	52	F1929	29/11/2013	1929	Female	84
M1976	30/07/2012	1976	Male	36	M23.12.1958	29/12/2013	1958	Male	55
F1948	06/08/2012	1948	Female	64	M2.3.1959	15/01/2014	1959	Male	55

Table 2.2: List of all olfactory mucosa samples supplied between May 2011 and January 2014. All samples were donated with consent from patients of either Mr Saghir Sheihk or Mrs Louise Clark, consultant ENT surgeons at the Southern General Hospital and at the Victoria Hospital, both in Glasgow, undergoing routine septoplasty/polypectomy surgery. All samples were taken from the upper middle turbinates and uncinate processes of the ethmoid bones of male and female patients between the ages of 32 and 86.

2.2.3. Human Dermal Fibroblast Culture

Human dermal fibroblasts were bought in, and were delivered frozen on dry ice (Life Technologies, C-013-5C). Cells were defrosted quickly in a water bath at 37°C, and immediately reconstituted in fibroblast culture media, Medium 106 (Life Technologies, M-106-500) which was fortified with Low Serum Growth Supplement (LSGS) (Life Technologies, S-003-10). Cells were centrifuged at 386 x g for 3 min to remove all transport media, the supernatant discarded, and the cells reconstituted in 7 mL of Medium 106 + LSGS, transferred to a collagen coated T75 cm^3 culture flask, and incubated at 37°C until confluent. Fibroblasts were bulked up and stored long term using the same conditions as with BM-MSCs and OM-MSCs.

2.2.4. "Flow through" Culture

Cell suspensions discarded during the EasySep® CD271 purification process, termed "flow through" cells, were collected in a 50 mL centrifuge tube, and centrifuged at 386 x g to remove any excess media and waste chemicals from the purification process. Cells were re-suspended in 7 mL of DMEM:10% Hyclone, transferred to a collagen coated T75 cm^3 culture flask, and incubated at 37°C until confluent. Flow through cells were bulked up and stored long term using the same conditions as with BM-MSCs, OM-MSCs, and fibroblasts.

2.2.5. Rat Bone Marrow-Derived MSC (rBM-MSC) Culture

Pregnant Adult Sprague-Dawley (SD) rats, euthanised for embryo removal, were harvested of their bone marrow by removing the whole back legs, stripping the bones of any tissue, and separating the femur from the rest of the leg. Both apical and dorsal ends of the femur were carefully removed, and DMEM passed through the central cavity of the bone by 1 mL syringe and 21 G needle, forcing the bone marrow from the bone by liquid pressure. Bone marrow was chopped thoroughly using a sterile scalpel blade, and transferred to a 5 mL bijou flask containing 2 mL DMEM:10% Hyclone. A cell suspension is created by triturating the marrow through a 1 mL pipette and a 21 G needle, before being transferred to a 15 mL centrifuge tube and centrifuged at 386 x G for 3 min. Cells are resuspended in 7 mL of DMEM:10% Hyclone and incubated in collagen coated T75 cm^3 culture flasks at 37°C for ~72 hr. All non-adherent cells were then removed by completely removing all media, washing with sterile PBS, and replacing with 7 mL DMEM:10% Hyclone. All adherent cells were henceforth termed rBM-MSCs, incubated at 37°C until confluent, and were bulked up and stored long term using the same conditions as with BM-MSCs, OM-MSCs, fibroblasts, and flow through cells.

2.2.6. Rat Olfactory Mucosa-Derived MSC (OM-MSC) Culture

Pregnant Adult SD rats, euthanised for embryo removal, were harvested of their olfactory mucosa by removing the whole head of the rat, stripping it

of all skin and tissue, and cutting it vertically down the centre of the skull from the tip of the nasal bone to the base of the occipital condyle (Figure 2.4). Situated at the posterior of the premaxilla bone, between the nasal passage and the olfactory bulbs (Figure 2.5), the olfactory mucosa is a green/brown tissue, quite obvious to the naked eye. The whole tissue was removed, separated from any solid particulate matter, placed in 1 mL of Liebovitz's L-15 media with 100 µL trypsin and 100 µL of 1.33 % collagenase, and cultured exactly as with human olfactory mucosa. As the rat olfactory mucosa contains large amounts of olfactory ensheathing cells (OECs) which are positive for the MSC selection marker CD271, the adherent rat OM tissue has to undergo an initial antigenic selection for the marker CD90, which is expressed on MSCs but not OECs. The remaining cells were cultured again until confluent before a 2nd antigenic selection for CD271. These final cells are termed rOM-MSCs, and were bulked up and stored long term using the same conditions as with BM-MSCs, OM-MSCs, fibroblasts, flow through cells, and rBM-MSCs.

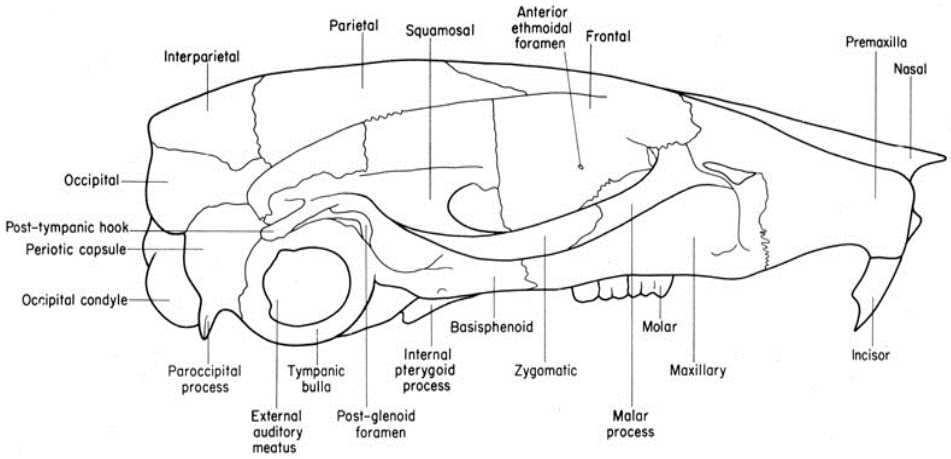

Figure 2.4: Diagram of the different bones of the rat skull

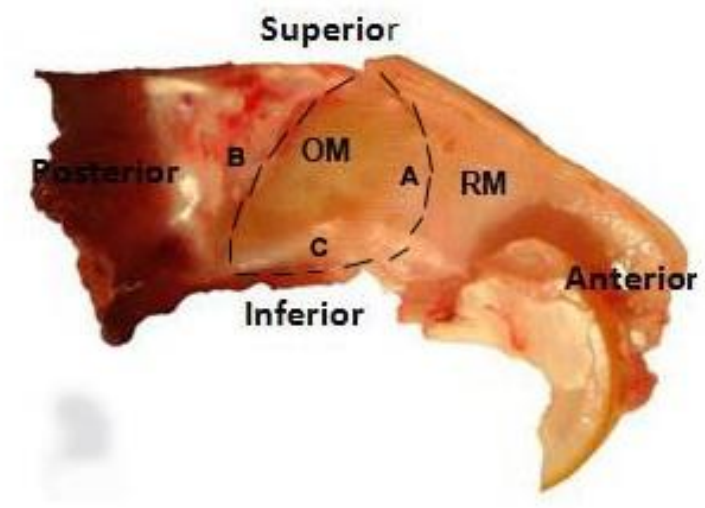

Figure 2.5: Diagram of a planar section of a rat skull showing the area from which the olfactory mucosa (OM) is removed (circled). The OM is surrounded by the arc of perpendicular plate (A), the cribriform plate (B), and the ceiling of oral cavity (C).

2.3. MSC Proliferation Study

BM-MSCs, BM271-MSCs, and OM-MSCs were seeded at 5 x10^3 cells/well in a 200 µL meniscus onto collagen coated 6-well plates. The 200 µL meniscus was deemed optimal, allowing for the cell-cell contact required for cell survival, and also for minimal cell clumping at the latter stages of the experiment. The menisci were incubated at 37°C for 15 min to allow cell adhesion, and each well flooded with 1 mL of DMEM:10% Hyclone. Cultures were simply trypsinised at 5, 10, 15, 20, and 25 days, and their cell numbers counted using a haemocytometer. Due to the vast diversity in proliferation between OM-derived MSCs and BM-derived MSCs, OM-MSCs became confluent in the 6-well plates after 7 days in culture, so were trypsinised and cultured in T75 cm^3 culture flasks henceforth. Trypsin/media suspensions were centrifuged at 386 x g, and re-suspended in 1 ml of DMEM:10% Hyclone. 10 µL of cell suspension was removed and added to the haemocytometer for visualisation under a phase microscope. The number of cells counted in one 4x4 grid x10^3 equates to the number of cells per 100 µL of cell suspension. All counts were multiplied a further 10

fold to give the total number of cells harvested in the 1 mL cell suspension.

2.4. Cell Profiling

2.4.1. By RT-qPCR

OM-MSCs, BM-MSCs, BM271-MSCs, unpurified OM tissue, OM flow through, BM flow through, and human dermal fibroblasts were compared by their expression profiles of a number of different genes by measuring the levels of messenger RNA (mRNA) related to these genes within each cell type. The full list of primers used in this section can be found in Tables 2.3 and 2.4, and the full list of samples used in sections 2.10.1 and 2.10.2 can be found in Tables 2.5 and 2.6. mRNA was extracted from each cell type using a Purelink® RNA mini kit (Life Technologies, 12183025) using their given protocol. Each cell type was cultured in DMEM:10% Hyclone on collagen coated cover slips, in triplicate at $5x10^4$ cells/cover slip in 24-well plates, for ~24 h at 37°C. After incubation, all media was removed and cover slips washed in sterile PBS. 350 µL of lysis buffer was then added to the first of the 3 triplicate cover slips, and all cells were detached and lysed by agitation with a 1mL pipette tip. The full lysate was then transferred to the second of the triplicate cover slips where lysis was carried out using the same agitation method, which was repeated for the third of the triplicate cover slips. The final lysate was triturated by passing through a 21G needle 5-10 times, and transferred to a 1.5 mL centrifuge tube on ice. All three of the triplicate wells were washed with one volume (350 µL) of 70% ethanol (EtOH), which was added to the lysate in the centrifuge tube (final volume 700 µL). The lysate was either stored at -80°C for use at a later date, or transferred straight to a spin column and centrifuged at 11337 x g (13,000 rpm in a 6cm radius centrifuge (Eppendorf mini spin)) for 15 sec. Columns were then washed by centrifuging at 11337 x g for 15 sec with 1 x 700 µL of wash buffer 1 followed by 2 x 500 µL of wash buffer 2, with all waste discarded between each spin. Columns were then dried by centrifugation at 11337 x g for 2 min. The waste collection tubes were replaced with 1.5 mL centrifuge tubes, and 50 µL of ddH_2O added to each

column, which were incubated at RT for ~60 sec before elution of mRNA by centrifugation at 11337 x g for 60 sec. mRNA samples were kept on ice whilst mRNA content was analysed using a Nanodrop 1000 spectrophotometer (Thermo Scientific) and Nanodrop 1000 3.7.1 software. 1 µL of sample was added to the nanodrop, and mRNA content recorded as a value of ng of RNA/µL of sample. mRNA purity was also measured by calculating the ratio of absorbance between 260 nm 280 nm wavelengths (a value of ~1.8 – 2.2 is accepted as pure for RNA). Samples were all equalised to 50 ng/µL total mRNA with ddH_2O before reverse transcription to cDNA. All mRNA samples were transcribed to cDNA using a Quantitect® Reverse Trancription Kit (Qiagen, 205311) using their supplied protocol. 12 µL of each sample was incubated with 2 µL of gDNA wipeout buffer (7x) in a thin walled PCR tube at 45°C for 2 min. 6 µL of reverse transcription master mix (1 µL reverse transcriptase, 4 µL RT buffer (5x), 1 µL RT primer mix) was added to each sample, which was then incubated at 42°C for 15 min followed by incubation at 95°C for 3 min. The resultant cDNA was stored at -20°C until analysis by RT-qPCR. All samples were analysed on the ABI7500 real-time PCR system, using the Livak ($\Delta\Delta C_T$) method with GAPDH as the reference control gene, each sample analysed in triplicate. Each sample was analysed as a 20 µL SybrGreen/cDNA mix in 96-well plates, with each sample well containing 10 µL of SybrGreen reagent containing low ROX (Primer Design, Precision-LR-SY), 0.4 µL of each target primer (forward and reverse), 2 µL of cDNA (from samples equalised at 50 ng/µL total mRNA), and 7.2 µL of ddH_2O. $2^{\Delta\Delta CT}$ values were calculated in Microsoft Excel® using the equations $\Delta\Delta C_T = (C_T \text{ (target, BM-MSC)} - C_T \text{ (ref, BM-MSC)}) - (C_T \text{ (target, BM271-MSC)} - C_T \text{ (ref, BM271-MSC)})$ and $\Delta\Delta C_T = (C_T \text{ (target, BM271-MSC)} - C_T \text{ (ref, BM271-MSC)}) - (C_T \text{ (target, OM-MSC)} - C_T \text{ (ref, OM-MSC)})$.

Oligo Name		Sequence (5'--> 3')	Yield (µg)	Reconstitution Vol. for 100 pmol/µL (µL)
CD90	Forward	CGTTAGGCTGGTCACCTTCT	422	695
	Reverse	CAGCGGAAGACCCCAGT	358	691
CD54	Forward	AGGGTAAGGTTCTTGCCCAC	407	664
	Reverse	TGCTATTCAAACTGCCCTGA	442	730
CD105	Forward	GATGCCTGGAGAGTCAGCTC	303	491
	Reverse	CACTAGCCAGGTCTCGAAGG	343	560
CD73	Forward	GAGTGGCTCGATCAGTCCTT	448	732
	Reverse	GGCACTATCTGGTTCACCGT	428	703
Nestin	Forward	GGGAGTTCTCAGCCTCCAG	407	701
	Reverse	GGAGAAACAGGGCCTACAGA	371	598
CD166	Forward	AGGTACGTCAAGTCGGCAAG	379	612
	Reverse	CGTCTGCTCTTCTGCCTCTT	383	641
CD271 ($p75_{NTR}$)	Forward	ACAAGGCTGGGCCACAC	263	506
	Reverse	CTGCTGCTGTTGCTGCTTCT	442	730

Table 2.3: List of all primers and their sequences used to identify MSC markers in BM-MSCs, BM271-MSCs, and OM-MSCs by RT-qPCR.

Oligo Name		Sequence (5'--> 3')	Yield (µg)	Reconstitution Vol. for 100 pmol/µL (µL)
GLUT4	Forward	CCCCAATGTTGTACCCAAAC	452	753
	Reverse	CTTCCAACAGATAGGCTCCG	390	643
Leptin	Forward	GGGCACAGCTTGGACATAGA	376	608
	Reverse	GTAGGAATCGCAGCGCC	345	661
Osteopontin	Forward	AGATGGGTCAGGGTTTAGCC	331	532
	Reverse	CATCACCTGTGCCATACCAG	398	661
Osteocalcin	Forward	CCTCCTGCTTGGACACAAAG	310	511
	Reverse	TGAGAGCCCTCACACTCCTC	474	791
Tuj-1	Forward	AGTCGCCCACGTAGTTGC	341	622
	Reverse	CGCCCAGTATGAGGGAGAT	304	517
MAP2	Forward	TGTGTCGTGTTCTCAAAGGG	345	558
	Reverse	TGCATATGCGCTGATTCTTC	336	554
MyoD	Forward	TAGTAGGCGCCTTCGTAGCA	402	655
	Reverse	AGCACTACAGCGGCGACTC	311	538
SMA	Forward	CAAAGCCGGCCTTACAGAG	377	649
	Reverse	AGCCCAGCCAAGCACTG	452	879
GFAP	Forward	ACAGACTTGGTGTCCAGGCT	288	469
	Reverse	GAGATCGCCACCTACAGGAA	386	631

Table 2.4: List of all primers and their sequences used to identify differentiation markers in BM-MSCs, BM271-MSCs, and OM-MSCs by RT-qPCR.

Tissue Type	n=	Sample	Sex	Age	Passage #
BM-MSC	1	F55I	F	56	1
	2	F37F	F	74	1
	3	F57K	F	54	2
BM271-MSC	1	F56M	F	55	3
	2	F55S	F	56	4
	3	M33J	M	79	2
BM271-Flowthrough	1	F63C	F	49	2
	2	M47RU	M	65	2
	3	F57K	F	54	3
Unpurified OM Tissue	1	M9.12.70	M	41	1
	2	M28.1.64	M	47	2
	3	M6.12.61	M	50	1
OM-MSC	1	F1966	F	45	4
	2	F1952	F	59	2
	3	F24.7.52	F	59	2
OM-Flowthrough	1	F26.7.68	F	43	2
	2	F1966	F	45	2
	3	F1952	F	59	2
Fibroblasts	1	N/A	N/A	N/A	1
	2				2
	3				3

Table 2.5: List of all samples and donors used for MSC classification experiments in sections 3.3 and 3.4

Tissue Type	n=	Sample	Sex	Age	Passage #
	1	F55I	F	56	1
	2	F37F	F	74	1
BM-MSC	3	F57K	F	54	2
	1	F56M	F	55	3
	2	F55S	F	56	4
BM271-MSC	3	M33J	M	79	2
	1	F1966	F	45	4
	2	F1952	F	59	2
OM-MSC	3	F24.7.52	F	59	2

Table 2.6: List of all samples and donors used for MSC classification experiments in section 3.5

Quantities of mRNA are reported as arbitrary -$\Delta\Delta C_T$ values, using the first sample analysed as a reference point against which all other samples are compared.

2.4.2. By Immunocytochemistry

OM-MSCs, BM-MSCs, BM271-MSCs, unpurified OM tissue, OM flow through, BM flow through, and human dermal fibroblasts were compared by their expression profiles of a number of different protein markers. The full list of primary (1°) antibody markers used can be found in Table 2.7. Each cell type was trypsinised and seeded at 1 x 10^3 in a 20 µL meniscus onto the centre of dry collagen coated glass cover slips, placed inside a 24-well plate (as cell-cell interactions are vital for MSC survival, the 20 µL meniscus allows for a close enough proximity to nurture survival, whilst also allowing for an optimal spacing to see good quality individual staining). Cells were seeded in triplicate for each antibody marker to be analysed for (2 normal stainings and 1 isotype control (secondary antibody only)), although due to a number of antibodies used having different isotypes, "double staining" was carried out where 2 antibodies were incubated onto the same sample. The menisci were incubated at 37°C for 15 min to allow the cells to adhere to the cover slip, before the wells were flooded with 500 µL of DMEM:10% Hyclone, and the plates incubated at

37°C for 24 hr. Each cover slip was then removed from the plate, washed in PBS, and placed cell side up on a mounted staining tray. Cells were then fixed at RT for 10 min using 50 µL of 4% paraformaldehyde (PFA) (Sigma, P6148) for extracellular staining, and at -20°C using 50 µL of 100% methanol (VWR, 20847.307) for intracellular staining. The coverslips were washed in PBS and dH_2O, and the cell's receptors "blocked" for any non-specific binding by adding 50 µL of 10% horse serum (HS) at RT for 30 min. Coverslips were washed again in PBS and ddH_2O before the addition of each 1° antibody in 50 µL of 10% HS. All dilutions can be found in Table 4. Cells were incubated with antibody either at RT for at least 60

Antibody	Isotype	Species Reactivity	Dilution	Intracellular or Extracellular	Marker For:	Company	Product code
CD90	IgG1	Human	1 in 100	Extracellular	MSC	AbD Serotec	MCA90
CD54	IgG2a	Human and rat	1 in 100	Extracellular	MSC	ABCAM	ab2213
CD105	IgG1	Human	1 in 50	Extracellular	MSC	ABCAM	ab107595
CD73	Rabbit Polyclonal	Human and rat	1 in 100	Extracellular	MSC	Santa Cruz	sc25603
Nestin	IgG1	Human	1 in 100	Intracellular	MSC	Millipore	MAB5326
CD166	Rabbit Polyclonal	Human and rat	1 in 100	Extracellular	MSC	Santa Cruz	sc25624
P75	Rabbit Polyclonal	Human and rat	1 in 500	Extracellular	MSC	ABCAM	ab8874
Stro-1	IgM	Human and rat	1 in 50	Extracellular	MSC	Santa Cruz	sc-47733
Glut-4	Rabbit Polyclonal	Human and rat	1 in 100	Intracellular	Fat	ABCAM	ab654
Leptin	Rabbit Polyclonal	Human and rat	1 in 100	Extracellular	Fat	ABCAM	ab3583
Osteopontin	IgG1	Human and rat	1 in 100	Extracellular	Bone	Santa Cruz	SC-21742
Osteocalcin	IgG1	Human and rat	1 in 100	Extracellular	Bone	Santa Cruz	SC-73464
Tuj-1	IgG2a	Human and rat	1 in 100	Intracellular	Neuron	Covance	MMS-435P
MAP2	Rabbit Polyclonal	Human and rat	1 in 100	Intracellular	Neuron	Cell Signalling Technologies	4542
Myo-D	IgG1	Human and rat	1 in 100	Intracellular	Smooth Muscle	Santa Cruz	sc-377186
SMA	IgG2b	Human and rat	1 in 100	Intracellular	Smooth Muscle	Sigma-Aldrich	A7607
GFAP	Rabbit Polyclonal	Human and rat	1 in 1000	Intracellular	Glia	DAKO	20334

Table 2.7: List of all primary antibodies used for MSC classification

min, or overnight at 4°C (isotype controls were incubated with 10% HS only), and were then washed once more in PBS and ddH_2O before incubation with the relevant secondary (2°) antibodies at RT for 60 min (prolonged incubation may lead to false staining and high background (auto) fluorescence). Finally, each coverslip was washed in PBS and ddH_2O and "mounted" cell side down onto 5 µL of Vectashield® mounting media containing the nuclear stain 4',6-diamidino-2-phenylindole, dihydrochloride (DAPI) (Vectorlabs, H-1200) which had been pipetted onto a glass microscope slide. DAPI immediately enters the nuclei and combines with A-T regions of DNA, resulting in the strong fluorescence of all live nuclei under UV light, allowing accurate cell counts to be made. Coverslips were then sealed with clear nail varnish and stored at 4°C to be imaged by Fluorescence microscopy. All imaging was carried out using an Olympus BX51 fluorescence microscope with a Lumen 200 Fluorescence Illumination System with Proscan 2 motorised stage system (Prior Scientific), and images taken using ImagePro 6.3 software. Images were analysed by taking the mean number of cells which positively express the protein of interest as a percentage of the total number of cells per image (field of view).

2.5. Differentiation of MSCs

A list of all samples and donors used in this section can be found in Tables 2.8 and 2.9.

2.5.1. Bone

Each MSC type was seeded in triplicate (1 untreated control, 2 treated) at 5×10^3 cells per well of collagen coated 6-well plates, as a 200 µL meniscus for 15 min. Untreated control wells were flooded with 1 mL of DMEM:10% Hyclone, and treated wells were flooded with 1 mL of osteogenic induction media (sodium L-ascorbate (Sigma, A4034), ß-glycerophosphate disodium salt hydrate (Sigma, G9891), and dexamethasone (Sigma, D4902) in DMEM:10% Hyclone). All induction media and their constituent compounds can be found in Table 2.10. Cells were incubated at 37°C for 28 days, replacing 50% of the media every 72 hr. After 28 days, all media was

removed from each well and the wells washed with PBS before fixing the cells in 500 µL of 4% PFA for 10 min. Wells were washed 5 x with ddH_2O prior to the addition of 1 mL of 40 mM Alizarin Red S Dye (Sigma, A5533). Plates were incubated at RT on a mechanical shaker at low speed for 60 min, after which any unincorporated dye was removed, and each well washed thoroughly with ddH_2O. All water was removed, air dried, and staining visualised by phase microscopy. All images were analysed using ImageJ version 1.47 software by calculating the number of pixels from the stained areas of the whole images.

Tissue Type	n=	Sample	Sex	Age	Passage #
	1	M39G	M	74	2
	2	M32M	M	81	3
BM271-MSC	3	F37C	F	76	2
	1	F9.10.1972	F	41	4
	2	M20.4.1987	M	26	2
OM-MSC	3	F19.1.72	F	41	2

Table 2.8: List of samples and donors used for experiments represented in Results sections 3.6.1, 3.6.3, and 3.7

Tissue Type	n=	Sample	Sex	Age	Passage #
	1	F43E	F	68	2
	2	F54H	F	57	3
BM-MSC	3	F60M	F	51	3
	1	F33N	F	78	3
	2	F35J	F	76	3
BM271-MSC	3	F48I	F	63	2
	1	F6.2.66	F	45	3
	2	F24.7.52	F	59	3
OM-MSC	3	M1956	M	55	4

Table 2.9: List of samples and donors used for experiments represented in Results sections 3.6.2 and 3.6.4

2.5.2. Fat

Each cell type was seeded and cultured as per the above bone method, except that the treated cells were cultured in adipogenic induction media (dexamethasone (Sigma, D4902), Indomethacin (Sigma, I7378), 3-isobutyl-1-methylxanthine (IBMX) (Sigma, I7018), and insulin (Sigma, I3536) in DMEM:10% Hyclone). Due to adipogenesis occurring more quickly than osteogenesis, cells were cultured for only 21 days, but were fixed as previously described in the bone protocol. Oil Red O dye (Sigma, O0625) was prepared by diluting the 5 mg/mL stock solution, 3 parts Oil Red O with 2 parts ddH_2O, and filtering through Whatman #1 filter paper. 1 mL of the Oil Red O working solution was added to each well and incubated at RT on a mechanical shaker at low speed for 60 min. Cells were washed, imaged, and analysed as previously described in the bone protocol.

Induction Media	Constituent Compound	Company	Catalogue Number	Conc. (mg/mL)	Volume in 50 mL DMEM:10% Hyclone (µL)	Final Conc. in 50 mL DMEM:10% Hyclone (mg/mL)
Fat	Dexamethasone	Sigma	D4902	0.020	500	1.00
	Indomethacin	Sigma	I7378	20.0	90	1000
	3-isobutyl-1-methylxanthine (IBMX)	Sigma	I7018	111	50	5550
	Insulin	Sigma	I3536	10.0	1000	500
Bone	Sodium L-Ascorbate	Sigma	A4034	10.0	500	500
	B-glycerophosphate disodium salt hydrate	Sigma	G9891	100	1080	5000
	Dexamethasone	Sigma	D4902	0.020	50	1.00
Neuron	Retinoic Acid	Sigma	R2625	0.035	50	1.75
	Fibroblast Growth Factor-Basic Human (FGF)	Peprotech	100-18b	0.001	500	0.05
Smooth Muscle	Dexamethasone	Sigma	D4902	0.020	50	1.00
	Hydrocortisone*	Sigma	H0888	3.62	25	181
Glia	Fibroblast Growth Factor-Basic Human (FGF)	Peprotech	100-18b	0.001	500	0.05
	Recombinant Human Glial Growth Factor 2 (rh-GGF2)	Reprokine	RKQ022979	1.29	5	64.5
	Forskolin	Sigma	F6886	4.10	70	205
	Platelet Derived Growth Factor-AA (PDGF-AA)	R&D Systems	221-AA	0.005	50	0.250

* Concentration as 10 mM

Table 2.10: Table of fat, bone, neuron, smooth muscle, and glia induction media and their constituent compounds, concentrations, and manufacturer's details. All media was made by diluting their constituent compounds in 50 mL of DMEM:10% Hyclone.

2.5.3. Neuron, Smooth Muscle, and Glia

Each cell type was trypsinised and seeded in a 20 µL meniscus at 1 x 10^3 cells/cover slip onto collagen coated glass cover slips in 24-well plates. Cells were seeded in triplicate (1 untreated control, 2 treated (one of which to be used as an isotype control (2° antibody only))), and incubated at 37°C for 15 min before wells were flooded with 500 µL DMEM:10% Hyclone for all untreated controls, and 500 µL of either neurogenic induction media (Retinoic acid (Sigma, R2625), and FGF (Sigma, F0291) in

DMEM:10% Hyclone), myogenic induction media (Dexamethasone (Sigma, D4902), and Hydrocortisone (Sigma, H0888) in DMEM:10% Hyclone), or glial induction media (FGF (Sigma, F0291), rhGGF2 (Reprokine, RKQ022979), Forskolin (Sigma, F6886), and PDGF-AA (R&D Systems, 221-AA) in DMEM:10% Hyclone). Cells were incubated at 37°C for 21 days, with 50% of the media being replaced every 72 hr. At day 21, coverslips were removed from their wells, washed in PBS, and fixed in methanol (MeOH) at -20°C for 10 min before any non-specific binding sites were blocked with 10% HS. Neurogenically induced cells and their associate untreated controls were then incubated either at RT for 60 min or at 4°C overnight with 1° antibodies Tuj-1 and MAP2 (all antibodies and dilutions can be found in Table 4), except for isotype controls which were incubated with PBS only. The same protocol was followed for myogenically and glial induced cells and their associate untreated controls, only using MyoD and SMA, and GFAP 1° antibodies respectively. All cover slips were incubated with their associate 2° antibodies at RT for 60 min before being mounted onto glass microscope slides, and analysed by immunofluorescence as previously described in section 4.2.

2.5.4. Analysis of Media Induced Differentiation by RT-qPCR

Media induced differentiation was carried out as previous described in section 2.11.3, except that each condition (treatments and untreated controls) was set up in triplicate to allow for a sufficient amount of mRNA collection. At day 21, mRNA was collected, reverse transcribed to cDNA, and analysed by RT-qPCR as previously described in section 2.10.1.

2.6. Nanotopographically Embossed PCL

2.6.1. Manufacture

Nickel shims from which the nanotopographically embossed PCL used in this chapter was formed, were pre-fabricated off-site using the following methods taken from Maclaine *et al.* (257)

2.6.2. Nanopatterning and Die Fabrication

PCL samples were fabricated using a three-step process utilizing a block co-polymer technique, nickel die fabrication, and thumb embossing. The embossing process produced samples "Smooth" (non-embossed, non-patterned), "Surface A" (embossed with a disordered near square (DNSQ) nanotopography with 25 nm high islands) and "Surface B" (embossed with a DNSQ nanotopography with 20 nm high islands) which are used throughout.

2.6.3. Block Co-Polymer Phase Separation

Poly(styrene-block-poly-2-vinylpyridine) (PS-b-P2VP) inverse micelles were prepared in o-xylene with a solution concentration of 0.5% weight percent. The two different molecular weight forms of PS-b-P2VP used to form the two different topographies ''A'' and ''B'' were 190 500b-190,000 g/mol and 91 500-b-105,000 g/mol, respectively. A thin film of PS-b-P2VP micelles was spin coated onto clean silicon wafers at 5,000 r.p.m. in a relative humidity of 20–35%. This completed the topography formation.

2.6.4. Nickel Shim Fabrication

Ni-V was sputter coated onto the masters, which were subsequently electroplated to a nickel shim thickness of 300 mm.

2.6.5. PCL Embossing

PCL beads (Sigma, 704105) were placed in a circular pile ~15-20 cm in diameter, in the centre of glass sheet which is ~30 cm^2 and ~1 cm thick. This was then placed in an oven at 80°C for 1.5 hr, along with another glass sheet of the same dimensions. Once the PCL beads have all melted, the 2nd glass sheet was placed on top of the melted PCL, and the two sheets held together with bulldog clips. This was returned to the oven at 80°C for a further 30 min until the liquid PCL had reached the edges of the glass sheets. This was left to cool down at RT (forcible cooling can damage and crack the PCL) until the PCL has returned to an opaque white colour. The PCL sheet was removed from between the glass sheets and cut into squares of ~ 15 mm. Each nickel shim used to form surfaces A and B were placed

topography upwards onto a hot plate pre-heated at 75°C, and a single 15 mm PCL square placed on top. Once the PCL has fully melted, a glass microscope slide was placed on top, the whole structure removed from the hot plate, and pressure applied to the PCL using the thumb, forcing the melted PCL onto the nanotopography of the nickel shim and creating a "mirror image" pattern in the PCL substrate. This was left again to cool at RT until fully opaque, before being trimmed to ~6-10 mm and placed nanotopography up in a well of a 24 well plate. Smooth surface controls were manufactured in the same way, only replacing the nickel shims for a glass microscope slide. All PCL substrates were sterilised under UV in a sealed tissue culture hood for 45 min. Figure 2.6 outlines the process of PCL nanoembossing in schematic form.

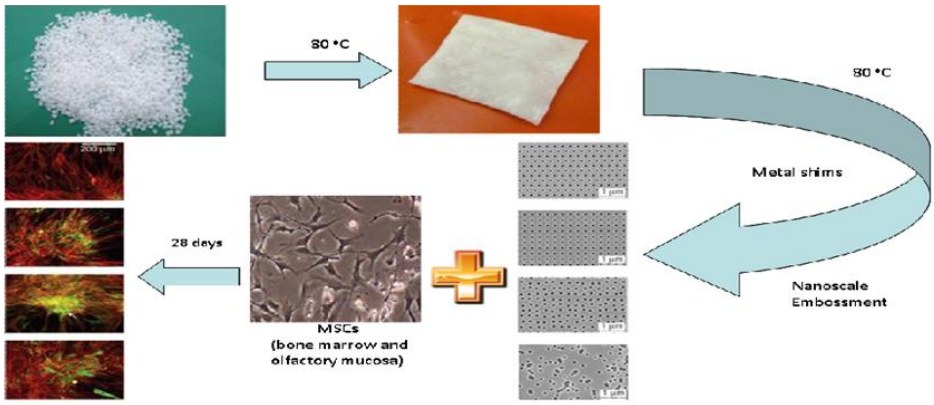

Figure 2.6: Schematic diagram of the process of nanoembossing PCL substrates onto which MSCs can be cultured and differentiated towards an osteogenic fate. Pellets of PCL were melted to form sheets which were cut into squares, melted, and pressed onto metal shims of varying nanotopographies. PCL squares then set hard, and cells can be seeded on top, and cultured under normal conditions.

2.7. Cell Culture and Differentiation Analysis

Cells were cultured onto PCL substrates exactly as they were when cultured onto glass cover slips. In all experiments, cells were cultured for 21 days before analysis. Differentiation was analysed by studying changes

in protein expression using the same immunocytochemistry protocol as previously described, and by studying changes in mRNA expression using the same RT-qPCR protocol as previously described. All samples used throughout this section can be found in Tables 2.11 and 2.12

Tissue Type	n=	Sample	Sex	Age	Passage #
	1	M56J	M	56	3
	2	M47RU	M	65	3
BM-MSC	3	M33J2	M	79	3
	1	F55S	F	56	3
	2	F56M	F	55	3
BM271-MSC	3	M55P	M	56	3
	1	M23.1.51	M	61	3
	2	F24.7.68	F	43	3
OM-MSC	3	F29.01.58	F	54	3

Table 2.11: List of samples donors used for experiments represented in section 4.2

Tissue Type	n=	Sample	Sex	Age	Passage #
	1*	F56M	F	56	3
	2*	M51A	M	61	2
BM-MSC	3*	M33C	M	79	3
	1*	F26H	F	86	2
	2*	M62J	M	50	3
	3*	F79G	F	33	3
	1**	F50J	F	62	2
	2**	M44H	M	68	2
BM271-MSC	3**	M63G	M	49	3
	1*	M1971	M	41	3
	2*	F01.01.59	F	53	3
	3*	M08.12.56	M	55	4
	1**	M29.3.51	M	61	4
	2**	M1956	M	56	3
OM-MSC	3**	F28.1.53	F	59	4

Table 2.12: List of samples donors used for experiments represented in section 4.3

* = Samples used for OPN and OCN immunocytochemistry

** = Samples used for Tuj-1, SMA, and GFAP immunocytochemistry

2.8. miRNA Analysis by Sistemic

4 x OM-MSC (all male, average age = 57.50 +/- 11) samples and 4 x BM271-MSC (3 Female, 1 male, average age = 56.25 +/- 22) samples were harvested each from a confluent T75 cm^3 culture flask by trypsinisation (a list of all samples used can be found in Tables 15 and 16). 5 mL of DMEM:10% Hyclone was added to each flask to neutralise the trypsin after 3 min, and samples were centrifuged at 386 x g for 3 min. All media/trypsin was removed and cells were reconstituted in 1 mL of DMEM:10% Hyclone before being transferred to 1.5 mL centrifuge tubes. Samples were centrifuged again at 11337 x g for 3 min before removing all media and snap freezing the cells in dry ice/H_2O. All samples were stored in dry ice and transported to Sistemic for miRNA analysis on that day. The following miRNA analysis protocol is taken from the final analytical report supplied to us by Sistemic:

2.8.1. Samples

Samples were from 8 individual donors; 4 from olfactory mucosa biopsies (OM-MSCs) and 4 from bone marrow aspirates (BM-MSCs) (Table 2.13 and 2.14). The 8 samples were received at Sistemic as total flash-frozen cell pellets on dry-ice, representing 2 types of sample designated as OM-MSC and BM-MSC. Upon receipt, samples were stored at -80^{0}C until processed through Sistemic's RNA isolation and QC checks and subsequently analysed on miRNA microarrays.

Sample number	Sample I.D.	Sistemic Sample I.D.	Sex	Location	Age	Passage cells used
LP1	M1941	SIS04397	Male	Turbinates	71	5
LP2	M1960	SIS04399	Male	Middle turbinates	52	3
LP3	M1952	SIS04401	Male	Middle turbinates (Uncinate process)	61	3
LP4	M1966	SIS04403	Male	Turbinates	46	3

Table 2.13: Details of all OM-MSC samples used throughout the Sistemic miRNA array. Note that at the time of the array, OM-MSCs were referred to as LP-MSCs (lamina propria-derived MSCs), and annotation was changed to OM-MSCs subsequent to the completion of the array.

Sample number	Sample I.D.	Sistemic Sample I.D.	Sex	Location	Age	Passage cells used
BM1	F56M	SIS04411	Female	Femoral head	56	3
BM2	F26H	SIS04405	Female	Femoral head	86	3
BM3	M62J	SIS04407	Male	Femoral head	50	3
BM4	F79G	SIS04409	Female	Femoral head	33	3

Table 2.14: Details of all BM-MSC samples used throughout the Sistemic miRNA array.

2.8.2. Sample Processing and Quality Control

All total RNA samples were checked for concentration, yield and quality of RNA. RNA concentration was measured following Sistemic's SOP (SSOP03). Absorbance ratios (Abs) at 260/280nm and 230/260nm were determined as indicators of sample yield and purity. For all samples, further RNA QC was performed using the Agilent 2100 Bioanalyser and the RNA 6000 Nano Kit following Sistemic's SOP (SSOP04.3) to determine the RNA Integrity Number (RIN). All samples passed Sistemic's RNA QC. A summary of the array QC metrics are in Appendix 1 and 2.

2.8.3. Microarray Profiling

Samples were analysed on the Agilent miRNA platform (using Agilent's SurePrint G3 Human v16 microRNA 8x60K microarray slides; miRBase version 16.0) following Sistemic SOP (SSOP07.3). One hundred nanograms of total RNA, from a working solution at 50ng/µl in nuclease-free water, was used as input for each microarray experiment. Each slide contains 8 individual arrays, each array represents 1,349 microRNAs (1,205 Human; 144 viral). The four key steps of the microarray process were:

1. Labelling of RNA with single-colour, Cy3-based reagent.
2. Hybridisation of the labelled RNA samples to the microarray.
3. Wash steps.
4. Slide scanning, data capture and feature extraction (matching array spots to miRNA IDs) and quality control checks on the resultant image and data files.

2.8.4. Data Pre-Processing and QC

The microarray data was normalised using Sistemic's in-house pre-processing and data quality control (QC) methods. Array quality control was performed using outlier testing based on the following metrics:

- average signal per array
- average background per array
- % present (% of miRNAs where expression is detected on each array)
- principal components 1-3 from PCA (Jackson JE, 1991) (511) of the full normalised sample set.

In addition, a sample-to-sample correlation analysis was performed on the normalised data set using Pearson's correlation metric. Outliers were identified using Grubbs' outlier test (Grubbs, 1969) (512) with significance called at $p < 0.05$.

2.8.5. Data Analysis

2.8.5.1. Overview of Detection Calls

Detection calls (present or absent) for individual miRNAs were compared across the samples. The detection calls were calculated using the Agilent Feature Extraction (AFE) software version 10.7.3.1. A detailed description of how these calls are made is available in the Feature Extraction Reference Guide on the Agilent website (http://www.genomics.agilent.com).

2.8.5.2. Variability Estimation

The overall variability of the 8 data sets was assessed in relation to other data sets of similar characteristics. The estimation of variability was performed by calculating the pooled standard deviation of all miRNAs for the current data set as well as Sistemic's in-house data sets.

2.8.5.3. Summary Overview Visualisation of miRNA Expression Data

A summary representation of the expression data was produced using Principal Component Analysis (PCA; Jackson JE, 1991) (511). PCA extracts the main effects from high-dimensional data such as microarray datasets, which for each sample have expression measurements from hundreds of miRNA. These main effects (principal components) can be displayed in a simplified graphical representation which retains the main properties of the data. The key point is that samples which have similar miRNA profiles cluster in the same space on the PCA plot.

2.8.5.4. Hypothesis Testing – Identification of Equivalently-Expressed miRNAs and Differentially-Expressed and Between the Different Sample Groups

Hypothesis testing was first utilised to identify a set of equivalently-expressed miRNAs. MiRNAs with equivalent expression levels (stably-expressed markers) were identified using the Two One-Sided Tests (TOST) approach; see e.g. (Barker *et al.*, 2002) (274). This approach is recommended for bioequivalence studies by the FDA (FDA guidance

document, 2001). The miRNAs with max (p_{FDR}) < 0.05 from the lower and upper limits, respectively, were considered equivalently expressed. The expression level range (Δ) allowed for the equivalence corresponds to a fold-change of ≤1.5 in log_2-space.

To identify differentially-expressed miRNAs, the differences in miRNA expression between each sample group were evaluated by performing unpaired t-tests. The p-values generated from the t-tests were adjusted for multiple test inflation using the Benjamini-Hochberg method (Benjamini and Hochberg, 1995) (513) and are referred to as p_{FDR} (FDR – False Discovery Rate). The miRNAs with significant differences were detected by hypothesis testing at p_{FDR} < 0.05 and an absolute fold-change (FC) ≥ 1.5.

2.8.5.5. Identification of Biological Processes and Pathways Enriched in the DE kmiR™ Lists

GeneGO MetaCore™ version 6.11 was used to map miRNAs to their validated mRNA targets and then to biological processes and pathways by generating networks for downstream interactions, including summary tables where the mRNA targets for each DE miRNA are listed along with the predicted or observed nature of the miRNA/mRNA interaction.

2.8.5.6. Validation of miRNA

BM-MSC and OM-MSC samples analysed by Sistemic were returned on dry ice, their mRNA concentrations determined using the Nanodrop 1000 spectrophotometer (Thermo Scientific) and Nanodrop 1000 3.7.1 software, and reverse transcription carried out using the miScript II Reverse Transcription Kit (Qiagen, 218161), following the supplied protocol: 50 ng/µL of mRNA was added to the reverse transcription master mix (5x miScript HiSpec Buffer (4 µL), 10x miScript Nucleics Mix (2 µL), Nuclease-Free ddH_2O (variable), and miScript Reverse Transcriptase Mix (2 µL)) and incubated at 37°C for 60 min, followed by incubation at 95°C for 5 min. cDNA samples were stored at -20°C until use. 100 ng of mRNA, from a

working stock of 50 ng/µL, was analysed in each well with SybrGreen Mastermix (Primer Design, Precision-LR-SY), nuclease-free ddH_2O, PerfeCta® universal primer (Quanta Biosciences, 95109-500), and either miR-140-5p primer (IDT, CAGUGGUUUUACCCUAUGGUAG), miR-146a-5p primer (IDT, UGAGAACUGAAUUCCAUGGGUU), or miR-335-5p primer (IDT, UCAAGAGCAAUAACGAAAAAUGU). Standard curves were created in seven increments from 0.625 ng, doubling up through to 40 ng of miRNA, from which the amounts of miRNA per sample were extrapolated. RT-qPCR was carried out using the standard curve method, to determine relative levels of miR-140-5p, miR-146a-5p, and miR-335-5p in each of the samples using the ABI7500 real-time PCR system, and data exported to excel where r^2 values were calculated to indicate the viability of the standard curve, each being above the required 0.96 threshold.

2.9. Luminex Array Analysis of Secreted Cytokines

2.9.1. Collection of Conditioned Media

4 x human Luminex arrays were carried out to analyse the presence of particular cytokines which had been secreted into the media in which each cell type was cultured, which we called "conditioned media" (CM). Each cell type; BM-MSC, BM271-MSC, OM-MSC, BM271-MSC Flowthrough (BM-FT), OM-MSC Flowthrough (OM-FT), and human dermal fibroblasts, was cultured as per standard protocol in T75 cm^2 flasks until confluent. All media was removed, washed thrice with sterile PBS, and replaced with 12 mL of differentiation media without insulin (DM-) (DMEM High Glucose (Invitrogen, 10566-016), Hydrocortisone (Sigma, H0888), N1 mix (Sigma, N6530), Biotin (Sigma, B4501)) for 72 h. To allow for a difference in cell proliferation, cell counts were taken after CM was collected at 72 h, and CM samples were diluted with DM- at a ratio determined by equalising each cell type's number to that of the lowest cell number in each case (BM-MSC) (data not shown). CM samples were then diluted 1:3 in DM-, and filtered to remove any cellular debris, then aliquoted and stored at -20 ^{o}C until use.

1 x rat Luminex array was also carried out using conditioned media collected from rat BM-MSCs, rat OM-MSCs, rat Olfactory Ensheathing Cells (OECs), and rat Schwann Cells by the same method as just described.

2.9.2. Analysis of Conditioned Media

2.9.2.1. Human

All media conditioned by human cells was analysed using 3 separate arrays:

- **MILLIPLEX $_{MAP}$ Human Cytokine/Chemokine Magnetic Bead Panel II – Premixed 23 Plex – Immunology Multiplex Assay (Millipore, HCP2MAG-62K-PX23).** Analyses the CM for 6Ckine, BCA-1, CTACK, ENA-78, Eotaxin-2, Eotaxin-3, I-309, IL-16, IL-20, IL-21, IL-23, IL-28A, IL-33, LIF, MCP-2, MCP-4, MIP-1d, SCF, SDF-1A+β, TARC, TPO, TRAIL, and TSLP.

- **MILLIPLEX $_{MAP}$ Human Cytokine/Chemokine Magnetic Bead Panel II – Premixed 41 Plex – Immunology Multiplex Assay (Millipore, HCYTMAG-60K-PX41).** Analyses the CM for EGF, Eotaxin, FGF-2, Flt-3 ligand, Fractalkine, G-CSF, GM-CSF, GRO, IFN-α2, IFN-γ, IL-10, IL-12 (p40), IL-12 (p70), IL-13, IL-15, IL-17, IL-1ra, IL-1α, IL-1β, IL-2, IL-3, IL-4, IL-5, IL-6, IL-7, IL-8, IL-9, IP-10, MCP-1, MCP-3, MDC (CCL22), MIP-1α, MIP-1β, PDGF-AA, PDGF-AB/BB, RANTES, TGFα, TNF-α, TNF-β, VEGF, and sCD40L.

- **Cytokine Human 30-Plex Panel (Invitrogen, LHC6003).** Analyses the CM for IL-1RA, IL-12 (p40/p70) IL-13, FGF-Basic, G-CSF, IL-7, IFN-α, IP-10, IL-17, IL-8, EGF, HGF, VEGF, MIG, RANTES, Eotaxin, MIP-1β, GM-CSF, TNF-α, IL-1β, IL-2, IL-4, IL-5, IL-6, IL-10, MIP-1α, IL-2R, IL-15, MCP-1, and IFN-γ.

2.9.2.2. Rat

All media conditioned by rat cells was analysed using the MILLIPLEX $_{MAP}$ Rat Cytokine/Chemokine Magnetic Bead Panel 27-plex Assay (Millipore, RECYMAG65K27PMX), which analyses the CM for EGF, Eotaxin, Fractalkine, G-CSF, GM-CSF, GRO/KC, IFN-γ, IL-10, IL-12 (p70), IL-13, IL-17A, IL-18, IL-

1α, IL-1ß, IL-2, IL-4, IL-5, IL-6, IP-10, LIX, Leptin, MCP-1, MIP-1α, MIP-2, RANTES, TNF-α, and VEGF.

2.9.3. MILLIPLEX assays

2.9.3.1. Preparing Reagents

All reagents were left on the bench for 1 hr to allow them to return to RT before starting the assay. The bottle of pre-mixed beads was sonicated for 30 sec then vortexed for 60 sec. Quality control (QC) samples 1 and 2 were each reconstituted with 250 µL of ddH_2O, mixed by inversion several times, and left to sit for 10 min. Wash buffer (60 mL) was diluted in 540 mL of ddH_2O and mixed by inversion. Cytokine/Chemokine standard was reconstituted in 250 µL ddH_2O, mixed by inversion, vortexed for 10 sec, and allowed to sit for 10 min. Seven working standards (standard curve) were produced from this standard by serial dilution. These serial dilutions can be found in Table 2.15.

Standard No.	Volume of Assay Buffer Added (µL)	Volume of Standard Added (µL)
7	0	0
6	120	40 µL of Standard 7
5	120	40 µL of Standard 6
4	120	40 µL of Standard 5
3	120	40 µL of Standard 4
2	120	40 µL of Standard 3
1	120	40 µL of Standard 2

Table 2.15: Preparation of working standards 1-7 used in each MILLIPLEX MAP Cytokine/Chemokine Magnetic Bead Panel Assay.

2.9.3.2. Plate Preparation

The placement of each sample (including standards and controls) in the 96-well plate supplied was determined before any analysis occurred. All samples are analysed in triplicate, vertically from the top of the plate downwards. 200 µL of assay buffer was added to each well of the plate,

which was then sealed and mixed on a plate shaker for 10 min at RT. Assay buffer was decanted and all residual buffer removed by vigorous inversion and blotting on absorbent towels. 25 µL of each standard or control was added to the appropriate wells (assay buffer used for 0 ng/mL standard), along with 25 µL of assay buffer and 25 µL of control media (DM-). 25 µL of sample was added then added to each appropriate well, along with 25 µL of assay buffer and 25 µL of control media (DM-). 25 µL of pre-mixed beads was added to each well, the plate sealed and wrapped in foil, and incubated with agitation at RT on a plate shaker for 2 hr. The plate is placed into a hand held magnetic plate holder for 60 sec before gently removing the well contents by inversion and gentle blotting. The wells were washed with 200 µL of wash buffer by removing the plate from the magnet, adding the wash buffer, shaking for 30 sec, reattaching the plate to the magnet for 60 sec, and removing the entire wash buffer as previously described. This washed step was repeated twice more. 25 µL of detection antibodies were added to each well, the plate sealed and covered in foil, and incubated with agitation at RT on a plate shaker. 25 µL of streptavidin-phycoerythrin was added to each well, the plate sealed and covered in foil, and incubated with agitation at RT on a plate shaker. The plate was then washed with wash buffer as previously described. 125 µL of sheath fluid was added to each, and the beads re-suspended by agitation on a plate shaker for 5 min.

2.9.3.3. Plate analysis

The plate was finally analysed on a Bioplex 100 plate reader (BioRad) using Bioplex Manager software.

2.9.4. Invitrogen 30 plex assay

2.9.4.1. Preparing Reagents

All reagents were left on the bench for 1 hr to allow them to return to RT before starting the assay. Wash solution was prepared by diluting the entire contents of the supplied concentrate with 285 mL of ddH_2O. The standard solution was prepared by reconstituting the lyophilised standard

in 1 mL of ddH_2O, allowing to stand for 10 min, mixing by gentle inversion, and leaving to sit at RT for a further 5 min. The standard curve was prepared by serial dilutions of this standard in assay buffer. These serial dilutions can be found in Table 2.16. The 30-plex antibody beads were supplied ready to use for the assay without further dilution, but were sonicated for 30 sec, and vortexed for 30 sec immediately prior to use. Biotinylated antibody and Streptavidin-RPE working concentrations were prepared by diluting 1 mL of the supplied 10 x concentrate in 10 mL of assay buffer.

Standard No.	Volume of Assay Buffer Added (µL)	Volume of Standard Added (µL)
1	0	0
2	150	150 µL of Standard 1
3	150	150 µL of Standard 2
4	150	150 µL of Standard 3
5	150	150 µL of Standard 4
6	150	150 µL of Standard 5
7	150	150 µL of Standard 6

Table 2.16: Preparation of working standards 1-7 used in the Invitrogen Cytokine 30-Plex Panel Assay.

2.9.4.2. Plate Preparation

Each well of the supplied filter bottom plate is washed with wash buffer by filling each well, placing the plate in a vacuum manifold, and gently aspirating the liquid through (5 mm Hg max). Excess fluid was removed by lightly tapping or pressing the filter paper onto a clean paper towel, and wash repeated 2x more. 25 µL of antibody beads were added to each well, followed by 200 µL of wash solution, allowing the beads to soak for 30 sec. Fluid was aspirated using the vacuum manifold, and the wash step repeated. 50 µL of incubation buffer was added to each well. 100 µL of appropriate working standard solution was added to their appropriate wells, and 50 µL of sample + 50 µL of assay buffer was added to their

appropriately designated wells. Plate was sealed, covered in foil, and incubated with agitation on a plate shaker at RT for 2 hr. All liquid was aspirated by vacuum manifold, and wells washed twice with 200 µL of wash buffer, before the addition of 100 µL of biotinylated detector antibody to each well, and incubation with agitation at RT for 1 hr. All liquid was again aspirated by vacuum manifold, and washed twice with 200 µL of wash buffer, before the addition of 100 µL of Streptavidin-RPE to each well, and incubation with agitation at RT for 30 min. Each well was washed a further 3 times with wash buffer, 100 µL of working solution added to each well, and the plate incubated by agitation at RT for 3 min.

2.9.4.3. Plate analysis

The plate was finally analysed on a Bioplex 100 plate reader (BioRad) using Bioplex Manager software.

2.10. Transfection of BM-MSCs and OM-MSCs with miRNA inhibitors/mimics

3 x BM-MSC samples (2 x Female, 1 x Male, average age 53 +- 19), and 3 x OM-MSC samples (1 x Female, 2 x Male, average age 56 +- 4) were transfected with miR-140-5p inhibitor (Ambion, MH10205) and mimic (Ambion, MC10205), miR-146a-5p inhibitor (Ambion, MH10722) and mimic (Ambion, MC10722), miR-335-5p inhibitor (Ambion, MH10063) and mimic (Ambion, MC10063), miRNA negative (scrambled) control (Ambion, RNU58A), and no miRNA (H_2O), using the Attractene Fast-Forward Transfection Protocol. A full list of samples used can be found in Table 2.17. Lyophelised miRNA treatments (5 $nmol^{-1}$) were reconstituted in 100 µL of ddH_2O to make a 50 µM solution. Transfection reagent was prepared by incubating 1 µL/well of treatment miRNA (or ddH_2O for no miRNA controls) with 80 µL/well of StemPro® MSC serum-free media (Invitrogen, A10332-01), and 3 µL/well of Attractene Transfection Reagent at RT for 15 min. 10^5 cells were seeded in 1 mL of DMEM:10% Hyclone into each well of a 6-well plate, and 84 µL of the Attactene transfection complex immediately added and mixed by gently pipetting up and down. Due to the

method of analysis for cells transfected with miR-335-5p inhibitor/mimic, cells had to be seeded onto collagen coated cover slips, so the 1 mL transefctant/cell suspension was seeded as 2 x 500 µL suspensions onto collagen coated glass cover slips in 24-well plates.

Tissue Type	n=	Sample	Sex	Age	Passage #
BM271-MSC	1	F52M	F	60	3
	2	M80C	M	32	3
	3	F45P	F	67	1
OM-MSC	1	M11.2.60	M	53	3
	2	F29.1.58	F	55	3
	3	F28.1.53	F	60	3

Table 2.17: List of samples donors used for experiments represented in section 5.3.1.

2.10.1. miR140-5p

Experiment was set up in duplicate; one for collection of conditioned media, and one for collection of mRNA for RT-qPCR analysis.

2.10.1.1. Conditioned Media Collection

Each condition was seeded in triplicate. Cells were incubated for 24 hr at 37°C before removing all media, washing thrice with sterile PBS, and incubating further in 1 mL of DM- at 37°C for 48 hr. Each media was collected, the triplicates of each condition pooled together and diluted 1:3 with DM-, filtered through Minisart® hydrophobic syringe filters (Sartorius Stedim, 16534), and stored at -20°C until use.

2.10.1.2. mRNA/miRNA Collection

Each condition was seeded in duplicate; one for CXCL12 analysis (mRNA), and one for miR-140-5p analysis (miRNA). Cells were incubated for 24 hr at 37°C before removing all media, washing with PBS, and adding fresh media for a further 24 hour incubation. Cells were washed again in sterile PBS

before collecting either mRNA using a Purelink® RNA mini kit as described in section 2.10.1, or miRNA using a miRNEASY mini kit (Qiagen, 217004) following the supplied protocol: 700 µL of QIAzol Lysis Reagent was added to each well, and the cells disrupted with a 1 mL pipette tip. This suspension was transferred to a 1.5 mL centrifuge tube, and incubated at RT for 5 min before 140 µL of chloroform was added, and the tubes shaken vigorously for 15 sec. Samples were centrifuged at 12,000 x g at 4°C for 15 min, and the upper aqueous layer transferred to a fresh 1.5 mL centrifuge tube. 525 µL of ethanol (EtOH) was added to each tube, and mixed thoroughly by pipetting, before transferring 700 µL into an RNeasy® Mini Column. Columns were centrifuged at 11,337 x g for 30 sec, the waste discarded, and the remainder of the sample added to the column and centrifuged as before. Waste was discarded again, and each column washed with 700 µL of wash buffer 1 by centrifugation as before, which was then repeated with 2 x 500 µL of wash buffer 2. Columns were centrifuged at 11,337 x g for 2 min to fully dry the membrane, before miRNA was eluted with 50 µL of nuclease-free ddH_2O into a nuclease-free 1.5 mL centrifuge tube. Samples were stored on ice whilst total miRNA content was analysed using the nanodrop method as previously described, and samples reverse transcribed using the miSCRIPT II RT kit as previously described. Samples were then stored at -20°C until analysed.

2.10.1.3. RT-qPCR

miRNA samples were analysed for miR-140-5p content using the primers and RT-qPCR standard curve method previously described in section 2.14.5.6. mRNA samples were analysed using primers for CXCL12 (IDT, TGGGCTCCTACTGTAAGGGTT (forward), TTGACCCGAAGCTAAAGTGG (reverse)). Both primers were delivered in lyophilised form, and were resuspended in ddH_2O (331 µL (forward) and 281 µL (reverse)) to produce 100 µM solutions. All samples were analysed using the RT-qPCR standard curve method as preciously described.

2.10.2. miR-146a-5p

Cells were transfected and lysed for western blot analysis to determine any increase/decrease in levels of expression of the Fas receptor protein CD95. Experiments were set up in duplicate so that transfection can be validated by RT-qPCR.

2.10.2.1. Protein Collection

2.10.2.1.1. "Normal" Expression Profile of CD95 on BM271-MSCs and OM-MSCs

Four separate donor samples of both BM271-MSCs and OM-MSCs were cultured under normal conditions for 24 hours before being trypsinised and lysed for protein harvesting. All cells used for this experiment can be found in Table 2.18. Cells were washed in sterile PBS and lysed by the addition of 500 µL of CellLytic™ MT cell lysis buffer (Sigma, C3228) and agitation with a 1 mL pipette tip. Lysates were triturated through a 21G needle, and transferred to a 1.5 mL centrifuge tube before protein concentrations were determined using the nanodrop 1000. Samples were diluted to a working concentration of 1 µg/µL, 16 µL of which was added to 6 µL of 4x LDS sample buffer (Invitrogen, NP0007) and 2 µL of sample reducing agent (Invitrogen, NO0004), and the whole protein suspension was incubated at 80°C for 10 min. Samples were transferred directly to ice or stored at -20°C until needed. Stock samples were stored at -80°C long term.

Tissue Type	n=	Sample	Sex	Age	Passage #
	1	F30B	F	83	2
	2	F37L	F	76	2
	3	F45M	F	68	3
BM271-MSC	4	M49A	M	64	2
	1	F19.1.72	F	41	2
	2	F1929	F	84	3
	3	M23.12.1958	M	55	3
OM-MSC	4	M2.3.1959	M	54	2

Table 2.18: List of samples donors used for experiments represented in section 5.4

2.10.2.1.2. Expression of CD95 Post-Transfection with Inhibitor and Mimic of miR-146a-5p

Cells were incubated at 37°C for 24 hour post-transfection before all media was removed from each well, wells washed with PBS, and Fresh media was added for a further 24 hour incubation at 37°C. Cells were lysed and protein harvested by the same method as previously described in section 2.16.2.1.1.

2.10.2.2. Western Blot

The western blot dock was prepared by adding 800 mL of MES SDS running buffer (Novex, NP0002, 40 mL of 20x diluted to 800 µL with ddH_2O) to the dock, and placing in a NuPage 4-12% Bis-Tris 15-well gel (Novex, NP0323BOX). 5 µL of SeeBlue Plus 2 Prestained Standard (Invitrogen, LC5925) was added to the first well of the gel, and 20 µL of each sample was added to each subsequent well. Electrodes were attached, and the gel exposed to 200 V of electricity for 1 hr. The gel was then removed from its case, and blotted onto a membrane using an iBlot® Gel Transfer System (Invitrogen). Membranes were cut from the iBlot and any non-specific protein binding sites were blocked with a 5% milk solution, made up in PBS + 0.01% Tween from Marvel® milk powder at RT for 30 min. The milk was poured to waste, primary (1°) antibody to CD95 (Abcam, ab82419) was diluted 1:1000 in 5% milk:PBS Tween solution and added to the blot, which was incubated at RT for 1 hr. 1° antibody was poured to waste, the blot washed for 3 x 20 min at RT, or overnight at 4°C, before addition of secondary (2°) antibody ECL anti-rabbit IgG, Horseradish peroxidase linked whole antibody from donkey (GE Healthcare, NA934V), 1:1000 in 5% milk:PBS Tween for 60 min at RT. Blot was washed for 3 x 20 min at RT, or overnight at 4°C, and developed by addition of 1 mL of Pierce ECL Western Blotting Substrate (Solutions A and B mixed 1:1) (Thermo Scientific, 32106) straight onto the membrane for 5 min at RT. ECL solution was then poured

off the membrane, and the blot developed onto x-ray film under dark room conditions. The membrane was "stripped" of its CD95 antibody by immersion in Western Blot Stripping Buffer (Thermo Scientific, 21059), re-blocked in 5% milk:PBS Tween, and incubated in 1° antibody as before, but with anti-GAPDH antibody as a loading control. ECL peroxidase labelled anti-mouse antibody (GE Healthcare, NA931VS) was added as a 2° antibody, and the blot developed onto film as before.

2.10.2.3. RT-qPCR

miRNA was collected as previously described with miR-140-5p, samples were analysed for miR-146a-5p content using the primers and RT-qPCR standard curve method previously described in section 2.14.5.6.

2.10.3. miR-335-5p

Cells were analysed for any increase/decrease in proliferation prior to transfection with either an inhibitor or mimic of miR-335-5p. The experiment was set up for time-points at 48, 72, and 96 hr post transfection, and in duplicate so that transfection can be validated by RT-qPCR.

2.10.3.1. Cell Counting

At each of the three time-points, all media was removed, cells washed with PBS, and fixed for 5 min in 4% PFA. Cells were mounted onto glass cover slips using Vectashield® mounting media with DAPI, and imaged using the same fluorescence microscope and software as previously described. 30 images per condition per time-point were taken, and cell counts taken by counting the DAPI stained fluorescent nuclei using CellProfiler cell image analysis software.

2.10.3.2. RT-qPCR

miRNA was collected as previously described with miR-140-5p, samples were analysed for miR-335-5p content using the primers and RT-qPCR standard curve method previously described in section 2.14.5.6.

2.11. Myelination Model using Rat Spinal Cord Cultures

2.11.1. Astrocyte Culture

Whole brains were removed from postnatal day 1 (P1) Sprague-Dawley (SD) rat pups immediately after euthanisation, and the striatum (caudate, putamen, and thalamus) removed and placed on ice in Leibovitz's L-15 media. Striata were homogenised by pipetting up and down with a 1 mL pipette, and triturated through a 21 G needle, before transferring to a 15 mL centrifuge tube, and centrifuging at 386 x g for 3 min. Media was decanted to waste, and the cells reconstituted in 2 mL of neurosphere media (ddH_2O, 10x DMEM/F12 (Invitrogen, 52100-021), 10x hormone mix (10x DMEM/F-12, 30% w/v glucose (Sigma, G7021), 7.5% $NaHCO_3$ (Sigma, S5761), 1M HEPES (Sigma, H4034), ddH_2O, transferrin (Sigma, T2252), Insulin (Sigma, I9278), Putrecine (Sigma, P7505), Selenium (Sigma, S9133), Progesterone (Sigma, P6149)), 30% w/v glucose, 1M HEPES, L-Glutamine (Gibco, 25030-081), Pen/Strep (Gibco, 15070-022), and 4% BSA (Sigma, A-3059) in HBSS (Sigma, H4891)). This cell suspension was added to 18 mL of neurosphere media + 4 µL of endothelial growth factor (EGF) (Peprotech, 315-09) in a T75 cm^3 culture flask. A further 5 mL of neurosphere media and 4 µL of EGF was added every 72 hr until numerous neurospheres formed suspended in the media. Once the neurospheres reached a sufficient number and size, the whole suspension was transferred to a 50 mL centrifuge tube, and spun down at 386 x g for 3 min. The formed pellet was re-suspended in 5 mL of DMEM (low glucose) (Invitrogen, 21885-025) plus 10% FBS (Sigma, F7524), and 0.05% L-Glutamine (Sigma, G7513), henceforth known as DMEM:10% FBS. Neurospheres were triturated gently through a 21 G needle, diluted further to 48 mL with DMEM:10% FBS, and 500 µL transferred to each well of 4 x 24-well plates containing PLL coated glass cover slips (Section 1). Cells were incubated at 37°C, replacing 50% of the media every 72 hr until a confluent monolayer of astrocytes had formed.

2.11.2. Spinal Cord Dissection

Embryos at 15 days gestation (E15) were removed from a female SD rat immediately after euthanisation. Whole spinal cord was removed from the embryos, all attached tissue and meninges removed, and placed on ice in a 5 mL bijou flask containing 1 mL of Leibovitz's L-15 media. For optimal enzymatic digestion, no more than 4 spinal cords were added to each bijou. Cords were homogenised by gently passing up and down a glass Pasteur pipette, and enzymatically digested by adding 100 µL of 2.5 mg/mL trypsin (T8253)) and 100 µL of 1.33% collagenase, and incubating at 37°C for 15 min. 1 mL of SD was added to neutralise the trypsin and collagenase, and reduce clumping, and the whole suspension transferred to a 15 mL centrifuge tube and spun down for 3 min at 386 x g. Waste media was decanted, and cells re-suspended in 2 mL of Plating Media (DMEM (Low Glucose), Hank's Balanced Salt Solution (HBSS) (Invitrogen, 24020-091), Horse Serum (HS) (Sigma, H1270), L-Glutamine). 10 µL of suspension was added to a haemocytometer and a cell count determined per 100 µL of suspension, which was further diluted to give a total of 150,000 cells/100 µL.

2.11.3. Mixed Myelinating Culture Set-up

Astrocyte cover slips were removed from their 24-well plates, and placed 3 at a time in small petri dishes. 100 µL of spinal cord cell suspension was added as a meniscus on top of the astrocyte monolayer, and incubated at 37°C for at least 2 hr. Each small petri dish is then "flooded" with 1 mL of plating media:DM+ (DMEM (High Glucose) (Invitrogen, 41966-029), Insulin, Hydrocortisone, N1, and biotin) at a ratio of 6:4, before incubation at 37°C for 28 days. 500 µL of the media is replaced with 600 µL of DM+ every 48-72 hr until day 12. Henceforth, feeding with DM+ was replaced with treatments as desired or with DM- for control conditions.

2.11.4. Mixed Myelinating Culture Analysis

On day 28, cultures were stained using the immunocytochemistry protocol previously described, using AA3 antibody (hybridoma-derived) as an

indicator of the myelin protein phospholipoprotein (PLP), and SMI31 as an axonal marker. Fluorescent images were taken using the previously described method, and percentages of myelinated axons per condition were calculated using CellProfiler Cell Image Analysis software. Myelination of axons under experimental conditions was presented as fold increases of myelinated axons relative to untreated controls.

2.11.5. Treatment of Mixed Spinal Cord Cultures with CXCL12, anti-CXCL12, and CXCR4 blocker (AMD3100)

From day 12 of incubation, mixed rat spinal cord cultures were treated with a neutralising antibody to CXCL12 (anti-CXCL12 (R&D Systems, MAB310)), a blocker of the CXCL12 receptor CXCR4 (AMD3100 (Sima, A5602)), 100 ng of CXCL12 (Peprotech, 400-32B), OM-MSC-CM, 100 ng CXCL12 + AMD3100, OM-MSC-CM + AMD3100, and 100 ng CXCL12 + anti-CXCL12, using DM- treated cultures as an untreated control. AMD3100 (molecular weight 794.5 g) was diluted to 39.7 mg/mL in ddH_2O to give a 50 mM stock solution. This stock solution was added to each designated culture at 1:1000, 1-2 hr before feeding to allow for optimal receptor blocking, giving a final concentration in the dish of 50 μM. 5 μL of CXCL12 (1 μg/μL) was diluted in 2.5 mL of DM- to give a working solution of 200 ng/mL. When feeding, 400 μL of media was replaced with 500 μL of CXCL12 working solution to give a total of 100 ng per dish. 5 μL of anti-CXCL12 stock solution (50 μg/mL) was diluted in 500 μL of DM- to give a 500 ng/mL diluted stock solution. 5 μL of this was then added to either 5 mL of OM-MSC-CM or 5 mL of DM- 1-2 hr before feeding (final concentration 5 ng/mL), and incubated at 37°C. When feeding, 400 μL of media was replaced with 500 μL of anti-CXCL12/DM- or anti-CXCL12/OM-MSC-CM working solutions. Cultures were fed every 48-72 hr until day 28 when they were stained using the immunocytochemistry protocol as previously described in section 2.10.2.

2.11.6. Treatment of Mixed Spinal Cord Cultures with Conditioned Media from MSCs Transfected with Inhibitor and Mimic of miR-140-5p

From day 12, cultures were fed by removing 400 µL of media and replacing with 500 µL of conditioned media collected in section 2.16.1.1. Feeding occurred every 48-72 hr until day 28 when they were stained using the immunocytochemistry protocol as previously described in section 2.10.2.

2.12. Statistical Analysis

All statistical analysis was carried out using GraphPad Prism version 6.0. For comparing values taken from the analysis of each cell type over a single parameter, such as comparing the secretion of a single chemokine by each particular cell type, a 1-way ANOVA was carried out. When comparing values taken from the analysis of each cell type over multiple parameters, such as comparing the gene expression in each cell type on different topographies at different time points, a 2-way ANOVA was carried out. As each of the means of each column of data, which represent the biological replicates of a particular sample, were compared against each other, Tukey's multiple comparison test was employed for each 1-way and 2-way ANOVA. These analyses were consistant throughout the thesis, and no other statistical analysis was used, other than the Benjamini-Hochberg method of finding the false discovery rate which was utilised by Sistemic in Table 5.1.

Results:

3. Characterisation of MSCs

Previous data from our lab has shown that MSCs extracted from the lamina propria of the olfactory mucosa have very different effects on axonal myelination in vitro compared to those derived from bone marrow (1). In order to try to identify by which mechanisms this might occur, we first have to carry out a comparative characterisation of both MSC types. In this chapter I will compare the biology of both olfactory mucosa-derived MSCs (OM-MSCs) and bone marrow-derived MSCs (BM-MSCs) taken from human donors, by means of morphology and proliferation, by classic MSC identifiers such as genetic and protein markers, and by their ability to produce bone and fat. To further emphasise any distinct biological properties, human OM-MSCs and BM-MSCs will also be compared to BM271-MSCs (bone marrow-derived MSCs which have undergone the same CD271 positive selection process as OM-MSCs), as well as fibroblasts, non-purified adherent OM cells, and flow through (discarded) cells from both OM-MSC and BM-MSC purifications.

3.1. Morphological Comparison of MSCs by Phase Microscopy

The initial basic observation to characterise the three MSC types was simply to compare their morphology under normal culture conditions. Three separate samples of MSCs from 3 separate donors and 2 distinct niches (2 x bone marrow and 1 x olfactory mucosa) were imaged under phase microscopy at x20 magnification. Unpurified bone marrow-derived MSC samples were generated (selected from bone marrow aspirate by adhesion only) (BM-MSC) and purified by antigenic selection using a commercially available MSC stem cell purification kit using the CD271 antibody as a means for positive selection (BM271-MSC). OM-MSCs were also purified by antigenic selection using the same CD271 positive selection kit. Each cell type was cultured for the same number of passages before imaging, and by simply observing the images of each cell type by eye it was clear that each was indistinguishable from the next (Figure 3.1). Each cell type showed a very similar morphology which is characteristic of MSCs;

small cell bodies with few processes which grew together to form palisades in a typical “fingerprint”, fibroblast-like morphology.

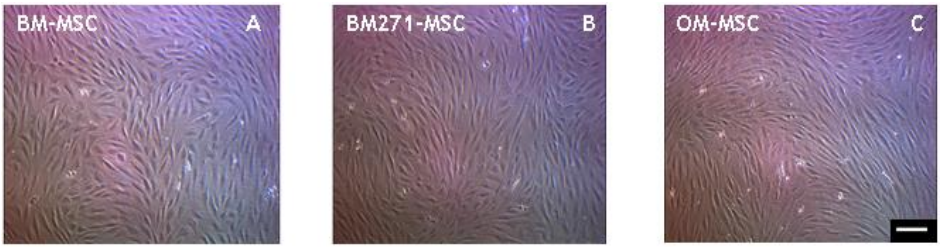

Figure 3.1: Phase images of BM-MSC (A, donor = Maggie, female, age 51, passage 3), BM271-MSC (B, donor = Hazel, female, age 57, passage 3), and OM-MSC (C, donor = M6.12.61, male, age 50, passage 3). Images were taken live at 20x magnification with the scale bar representing 50 µm.

3.2. Comparison of the Rates of Proliferation Between OM-MSCs and BM-MSCs

Coming from two completely distinct cellular niches, BM-MSCs and OM-MSCs are constantly influenced by environmental cues *in situ*. Although taking these cells from their niche and analysing them *in vitro* removes any niche dependant external cues, certain epigenetic changes may have occurred within the cells during their time within each niche. To begin to investigate any such effects, we first looked at the proliferation rates of each cell type by counting the number of cells in each culture at 5 day intervals over a 25 day period. Anecdotally, OM-MSCs displayed a much faster proliferative capacity than both BM and BM271-MSCs and were also able to survive longer numbers of passage, although their biological properties as MSCs were never analysed above passage 4 throughout this project. Table 3.1A lists each sample (n=3 experiments) and the actual cell counts at each 5 day period over the 25 day time course. Due to the impracticality of plotting such vastly differing figures in a line graph, log values were taken of each count (Table 3.1B) and plotted onto a line graph using GraphPad Prism 6 software (Figure 3.2). Statistical significance was determined via 1 way ANOVA using Tukey’s multiple comparison test, where *=$p<0.05$, **=$p<0.01$, ***=$p<0.005$, and ****=$p<0.001$, which showed

that OM-MSCs possess a vastly, and statistically significant ($p<0.001$) higher rate of proliferation compared to BM-MSCs and BM271-MSCs across every time point, with OM-MSCs showing an almost exponential growth pattern compared to the more linear pattern of growth displayed by BM-derived MSCs. Proliferation rates were significantly higher ($p<0.005$) in BM27-MSCs at day 5 decreasing to $p<0.05$ at day 10 compared to BM-MSCs, but by day 15 there was no significant difference between the two.

A

				Actual Cell Count					
			Age	Day 0	Day 5	Day 10	Day 15	Day 20	Day 25
BM271-MSC	n=1	F43M	69	5000	14000	22750	52000	98250	219900
	n=2	M33C	79	5000	10000	20000	47500	83250	198750
	n=3	M77A	35	5000	12500	20000	57500	94500	210000
	Mean		61	5000	12167	20917	52333	92000	209550
	S.D.		23.07	0	2021	1588	5008	7806	10582
	S.E.M.		13.32	0	1167	917	2892	4507	6110
BM-MSC	n=1	F79G	35	5000	20050	26000	57750	107200	218550
	n=2	M42T	70	5000	18750	25000	38750	90000	225000
	n=3	M49J	64	5000	17500	32000	47500	115700	258000
	Mean		56	5000	18767	27667	48000	104300	233850
	S.D.		18.72	0	1275	3786	9510	13093	21162
	S.E.M.		10.81	0	736	2186	5491	7559	12218
OM-MSC	n=1	M11.02.30	82	5000	99500	427500	1858750	5567480	20515500
	n=2	M1960	52	5000	82500	310000	1619089	4000050	16570890
	n=3	F26.2.53	59	5000	67500	245000	1492101	3599750	17955865
	Mean		64	5000	83167	327500	1656647	4389093	18347418
	S.D.		15.70	0	16010	92500	186188	1039955	2001243
	S.E.M.		9.06	0	9244	53405	107495	600418	1155418

B

				Log of Cell Count					
			Age	Day 0	Day 5	Day 10	Day 15	Day 20	Day 25
BM271-MSC	n=1	F43M	69	3.69897	4.14613	4.35698	4.71600	4.99233	5.34223
	n=2	M33C	79	3.69897	4.00000	4.30103	4.67669	4.92038	5.29831
	n=3	M77A	35	3.69897	4.09691	4.30103	4.75967	4.97543	5.32222
	Mean		61	3.69897	4.08101	4.31968	4.71745	4.96272	5.32092
	S.D.		23.07	0.00000	0.06071	0.02638	0.03389	0.03072	0.01795
	S.E.M.		13.32	0.00000	0.03505	0.01523	0.01957	0.01774	0.01037
BM-MSC	n=1	F79G	35	3.69897	4.30211	4.41497	4.76155	5.03019	5.33955
	n=2	M42T	70	3.69897	4.27300	4.39794	4.58827	4.95424	5.35218
	n=3	M49J	64	3.69897	4.24304	4.50515	4.67669	5.06333	5.41162
	Mean		56	3.69897	4.27272	4.43935	4.67551	5.01592	5.36778
	S.D.		18.72	0.00000	0.02954	0.05761	0.08665	0.05593	0.03848
	S.E.M.		10.81	0.00000	0.01705	0.03326	0.05003	0.03229	0.02222
OM-MSC	n=1	M11.02.30	82	3.69897	4.99782	5.63094	6.26922	6.74566	7.31208
	n=2	M1960	52	3.69897	4.91645	5.49136	6.20927	6.60207	7.21935
	n=3	F26.2.53	59	3.69897	4.82930	5.38917	6.17380	6.55627	7.25421
	Mean		64	3.69897	4.91453	5.50382	6.21743	6.63467	7.26188
	S.D.		15.70	0.00000	0.084276	0.121366	0.048232	0.098812	0.046842
	S.E.M.		9.06	0.00000	0.048657	0.07007	0.027847	0.057049	0.027044

Table 3.1: Cell counts (A), and the log values of these cell counts (B) comparing the proliferation of BM-MSCs, BM271-MSCs, and OM-MSCs over 25 days. Counts were taken every 5 days, and the log values were determined of these counts due to the exponential increase in proliferation of OM-MSCs compared to BM- and BM271-MSCs. There was no significant difference between the average ages of each set of sample donors.

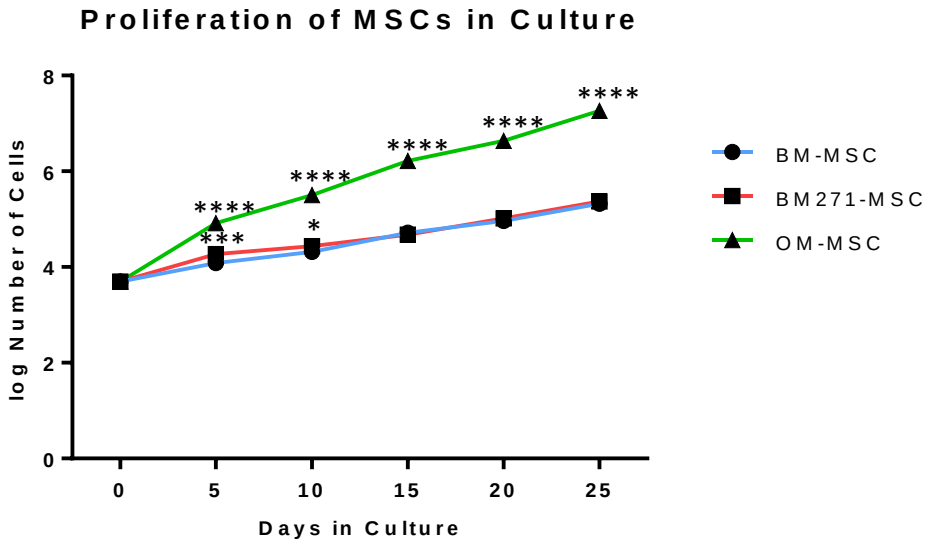

Figure 3.2: Line graph plotting the different rates of proliferation of BM-MSCs, BM271-MSCs, and OM-MSCs. Due to their advance proliferative capacity, OM-MSCs were passaged upon confluency from day 7 onwards to maintain cell survival. Statistical analysis was carried out by 1 way ANOVA using Tukey's multiple comparison test, where *=p<0.05, **=p<0.01, ***=p<0.005, and ****=p<0.001. n=3.

3.3. Comparative RT-qPCR of fibroblasts, BM- and OM- derived MSC, and their Resident Tissues

The niche in which a cell resides can influence cell behaviour via numerous environmental cues including the ECM and various gradients of growth factors (275-279). However, there will also be molecular changes that can be studied to compare any differences between each cell type, e.g. at a transcriptional level, to identify if any such differences may be cell type specific. This experiment is also to confirm the phenotype of OM-MSCs

which, as a relatively novel MSC type, have previously been suggested to be fibroblasts. Moreover, these experiments will also validate the CD271 positive selection process used to purify both BM- and OM-MSCs throughout this project. This was carried out by analysing cells normally discarded during the CD271 positive selection process (known as the flow through cells), as well as unpurified BM-MSCs and unpurified adherent OM cells (pre-enzymatic dissection) (see Materials and Methods Table 2.2 for full sample details). RT-qPCR was carried out, using the Livak (ΔΔCT) method, on cDNA from each cell type (BM-MSCs, BM271-MSCs, BM271-Flow through cells, unpurified adherent OM cells, OM-MSCs, OM-Flow through cells, and fibroblasts). This was done to identify a profile of mRNAs related to each cell, using a panel of MSC-related genetic markers (CD90, CD54, CD105, CD73, Nestin, CD166, and CD271 ($p75^{NTR}$)) (Figure 3.3). A full list of primers used can be found in Materials and Methods Table 3.3.

3.3.1. Comparison of the Transcription Profiles of OM-MSCs and Fibroblasts

Statistical significance was determined via 1 way ANOVA using Tukey's multiple comparison test, where *=$p<0.05$, **=$p<0.01$, ***=$p<0.005$, and ****=$p<0.001$, which showed first, that comparison of OM-MSCs and fibroblasts demonstrated little or no expression of CD54 (B), CD105 (C), Nestin (E), CD166 (F), and CD271 (G) in fibroblasts which were in contrast highly expressed in OM-MSCs (Figure 3.3). Due to a large sample variation in the expression of CD54 and CD105, the difference between fibroblasts and OM-MSCs wasn't statistically significant. However, the almost lack of CD54 and CD105 transcript in fibroblasts, coupled with significant differences in expression of Nestin, CD166, and CD271 ($p<0.01$) conclude that OM-MSCs are indeed distinct when compared to fibroblasts at a transcriptional level, when using this panel of MSC markers.

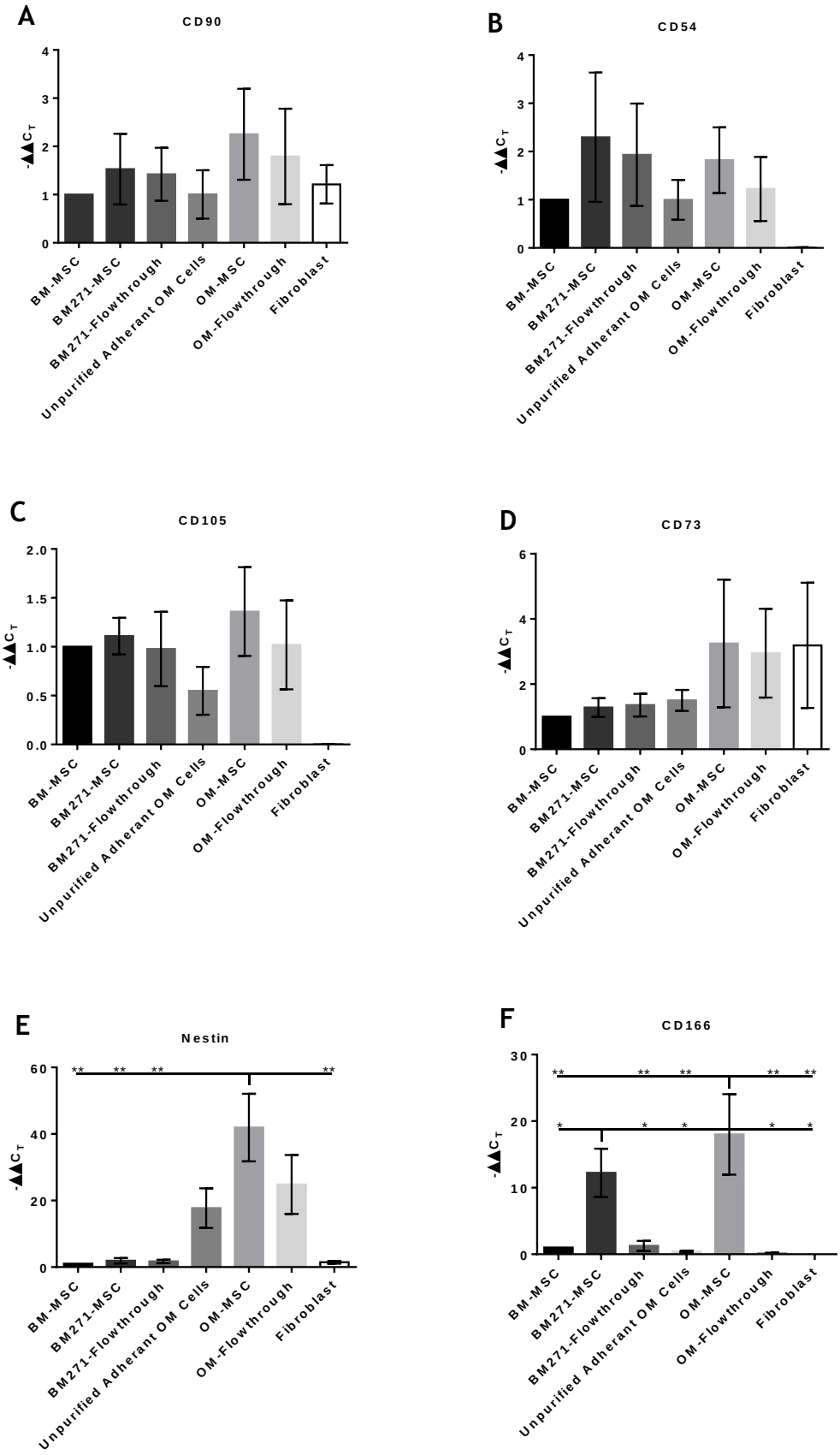
A
CD90
B
CD54
C
CD105
D
CD73
E
Nestin
F
CD166
-ΔΔC_T
BM-MSC
BM271-MSC
BM271-Flowthrough
Unpurified Adherant OM Cells
OM-MSC
OM-Flowthrough
Fibroblast

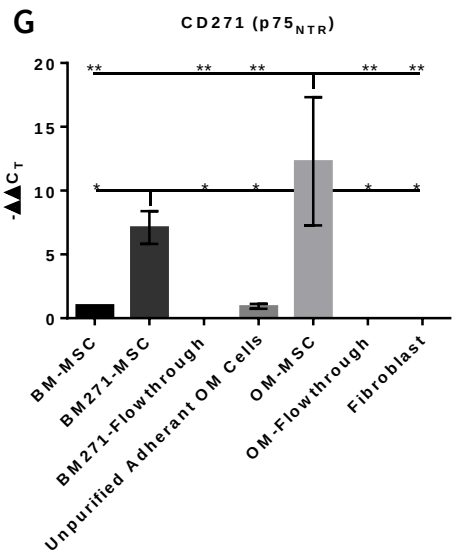

Figure 3.3: RT-qPCR analysis of MSC-associated transcripts CD90 (A), CD54 (B), CD105 (C), CD73 (D), Nestin, (E), CD166 (F), and CD271 ($p75^{NTR}$) (G) in n=3, BM-MSCs, BM271-MSCs, BM271-Flowthrough cells, unpurified OM tissue, OM-MSCs, OM-Flowthrough cells, and fibroblasts. Statistical analysis was carried out by 1 way ANOVA using Tukey's multiple comparison test, where *=p<0.05, **=p<0.01, ***=p<0.005, and ****=p<0.001. RT-qPCR was carried out using the Livak ($\Delta\Delta C_T$) method with GAPDH as the reference control gene.

3.3.2. Investigating the CD271 Positive Selection Method of MSC Isolation by RT-qPCR

Using the commercially available MSC purification kit it was observed for each cell type that the expression of CD271 (G) was expressed in BM-MSCs and OM-MSCs pre- and post-purification. However, post-purification BM271-MSCs and OM-MSCs express significantly higher levels of CD271 (BM-MSC vs BM271-MSC = p<0.05, and OM vs OM-MSC = p<0.01) than their parent tissue (Figure 3.3G), suggesting a much purer population of CD271 positive cells. Flow through cells collected from both BM271-MSC and OM-MSC purifications did not express CD271, suggesting that all CD271 positive cells were retained throughout the isolation procedure. In addition, as previously mentioned, fibroblasts also lacked expression of CD271. A similar expression profile for CD105 was detected in each cell type,

another typical MSC marker. CD166 was significantly more highly expressed in both BM271-MSCs and OM-MSCs ($p<0.05$ and $p<0.01$) compared to their unpurified counterparts, and expressed at very low levels, if at all, in flow through cells and fibroblasts. This further validates that BM271-MSCs and OM-MSCs are both pure populations of MSCs retained throughout the CD271 selection process, and distinct from fibroblasts.

3.3.3. Comparing Nestin mRNA Expression in OM-MSCs to that of Bone Marrow-Derived MSCs and Fibroblasts

The expression of Nestin mRNA was detected in all MSC types, although expression was highest in OM-MSCs (Figure 3.3E). Nestin mRNA levels were significantly differentially expressed in OM-MSCs ($p<0.01$) compared to BM-MSCs, BM271-MSCs, BM-Flowthrough cells, and fibroblasts. This greater expression was also observed in unpurified adherent OM cells and OM-flow through cells when compared to BM-MSCs, BM271-MSCs, BM-flow through cells, and fibroblasts, although this difference in expression was insignificant by 1-way ANOVA. These data suggest that the observed difference in expression of Nestin may be related to the tissue niche.

3.4. Validation of RT-qPCR Findings by Immunocytochemistry

To determine whether the differences in transcriptional expression were translated to differences in expression of their respective proteins, immunocytochemistry was carried out on each cell type using the antibodies to CD90, CD54, CD105, CD73, Nestin, CD166, CD271 ($p75^{NTR}$), and Stro-1 (Stro-1 gene has not been identified, so was unable to carry out RT-qPCR as primers could not be generated). A full list of antibodies used can be found in Materials and Methods Table 2.7. Protein expression profiles were determined by counting the number of immunoreactive cells for each of these MSC markers, and calculating a mean percentage of positive expressing cells per field of view (Figures 3.4 and 3.5).

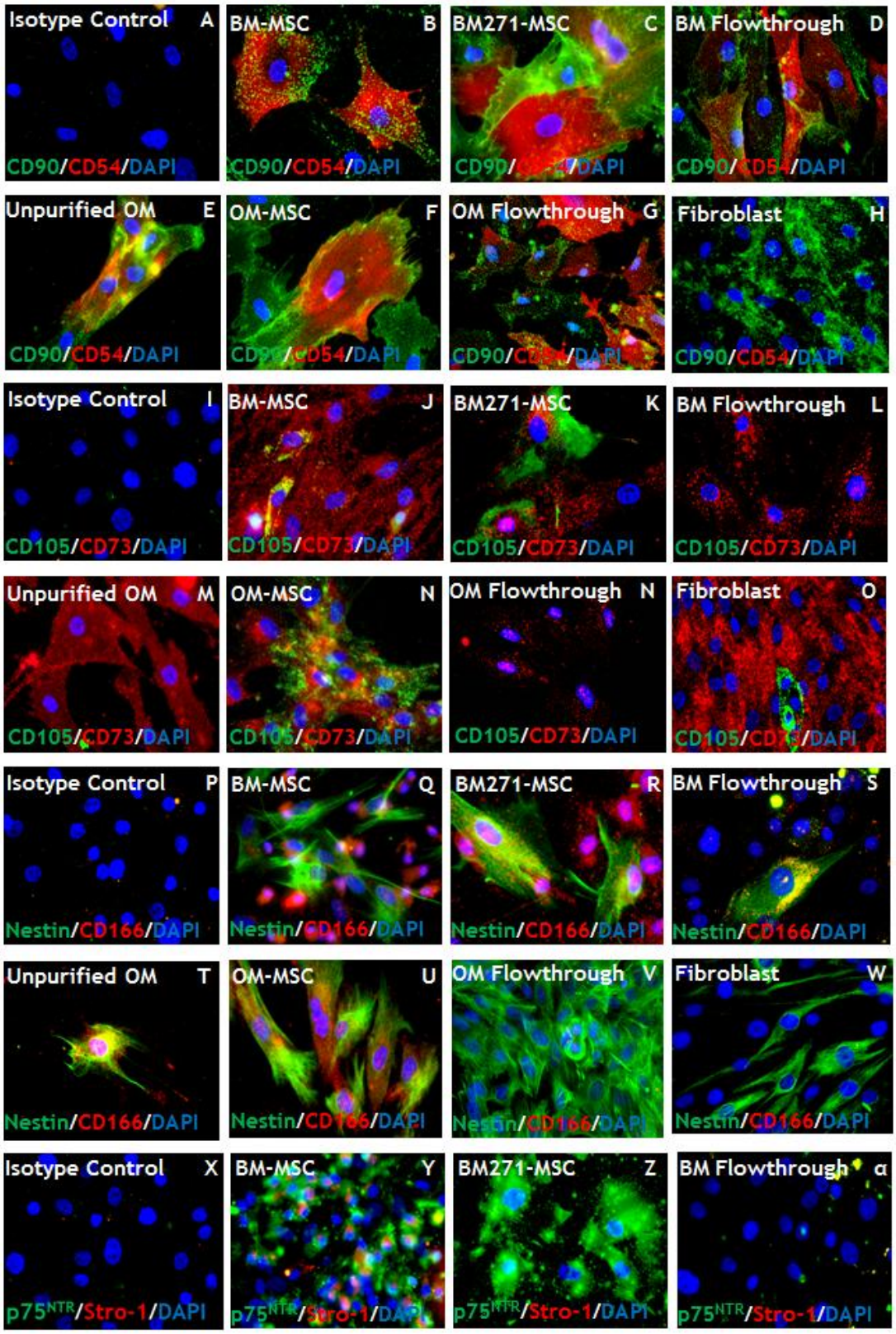
Isotype Control A
CD90/CD54/DAPI
BM-MSC B
CD90/CD54/DAPI
BM271-MSC C
BM Flowthrough D
Unpurified OM E
CD90/CD54/DAPI
OM-MSC F
OM Flowthrough G
Fibroblast H
Isotype Control I
CD105/CD73/DAPI
BM-MSC J
BM271-MSC K
BM Flowthrough L
Unpurified OM M
OM-MSC N
OM Flowthrough N
Fibroblast O
Isotype Control P
Nestin/CD166/DAPI
BM-MSC Q
BM271-MSC R
BM Flowthrough S
Unpurified OM T
OM-MSC U
OM Flowthrough V
Fibroblast W
Isotype Control X
p75NTR/Stro-1/DAPI
BM-MSC Y
BM271-MSC Z
BM Flowthrough α

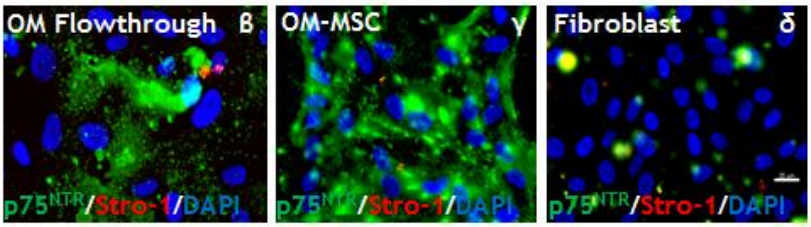

Figure 3.4: Representative images of Immunocytochemistry analysis of n=3 BM-MSCs, BM271-MSCs, BM271-flowthrough cells, OM-MSCs, OM-flowthrough cells, and fibroblasts. Staining was carried out for MSC markers CD90 (green) and CD54 (red) (A-H), CD105 (green) and CD73 (red) (I-P), Nestin (green) and CD166 (red) (Q-W), and CD271 ($p75^{NTR}$) (green) and Stro-1 (red) (X-δ). Isotype controls were stained with secondary antibody only. Images were taken at x40 magnification, scale bar represents 25 μm.

3.4.1. Comparing Protein Expression Profiles of OM-MSCs and Fibroblasts

CD90 immunoreactivity (IR) (Figure 3.5A), a well-known fibroblasts and MSC marker, was unsurprisingly highly expressed in fibroblasts, along with each of the other cell types. BM-MSCs however, displayed a significantly lower expression of CD90-IR compared to each of the other cell types ($p<0.05$) (Figure 3.5A). This may be due to the heterogenous nature of this population resulting in a "dilution" of CD90-IR positive cells. CD73-IR (Figure 3.5D) was also equivalently expressed in fibroblasts compared to each of the other cell types, it being a non-specific and relatively ubiquitous MSC marker. CD105-IR (Figure 3.5C) was expressed in a very small number of fibroblasts (<5%), compared to almost 40% of OM-MSCs, however, due to a very large sample variation in CD105-IR expression, this difference was not considered significant by 1-way ANOVA. Stro-1-IR (Figure 3.4H), regarded as a specific MSC marker (280-283), was expressed only in BM-MSCs and none of the other cell types ($p<0.01$). Stro-1-IR positive cells may not co-express CD271-IR, as all Stro-1-IR positive cells are lost during the CD271 positive selection process. It could be suggested that the loss of Stro-1-IR may be down to the fact that Stro-1 is an early MSC marker (514), and BM271-MSCs spend an extended time in culture

compared to BM-MSCs, however, CD271 is also an early MSC marker which is lost as MSCs differentiate (515), but CD271 positive BM-MSCs are still retained throughout this extended culture period. Stro-1-IR was also found to not be expressed in all OM-cell suspension samples or in fibroblasts. Each of the other markers (CD54-IR (Figure 3.5B), Nestin-IR (Figure 3.5E), CD166-IR (Figure 3.5F), and CD271-IR (Figure 3.5G)) were significantly differentially expressed in OM-MSCs compared to fibroblasts ($p<0.05$, $p<0.001$, and $p<0.001$ respectively). CD54-IR was expressed in ~50-60% of each cell type except fibroblasts, which lacked CD54 expression completely ($P<0.001$). Fibroblasts expressed Nestin-IR on ~45-55% of cells, in a similar manner to BM and BM271-MSCs. This was significantly different ($p<0.05$) to OM-MSCs which strongly express Nestin-IR in almost 100% of cells analysed. CD166-IR and CD271-IR were both weakly expressed in a very small number of fibroblasts (<5%) which was significantly lower ($p<0.001$) than OM-MSCs in both cases. These findings confirm that OM-MSCs and fibroblasts are two completely distinct cell populations. It also confirms the RT-qPCR data which shows an expression of all MSC markers on each of the three cell types; BM-MSCs, BM271-MSCs, and OM-MSCs, and that Nestin-IR is expressed at a significantly higher level in OM-MSCs compared to BM- and BM271-MSCs.

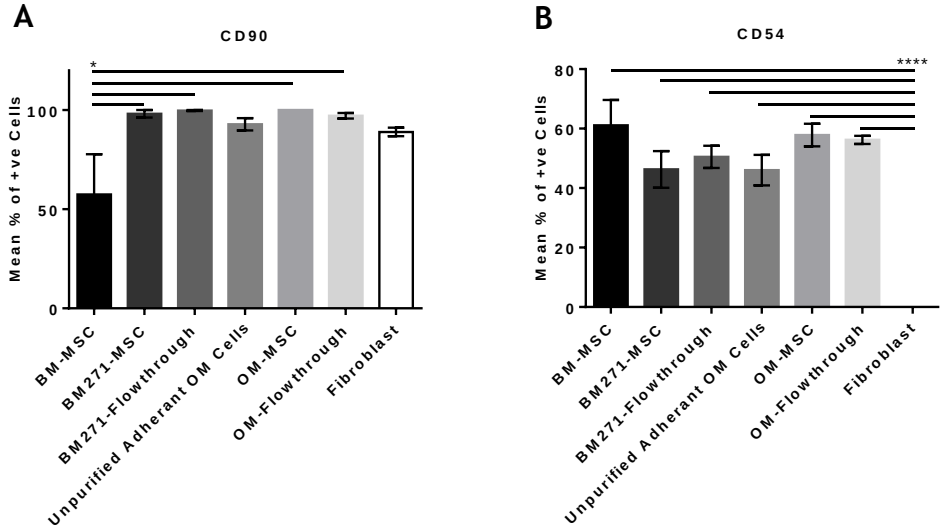

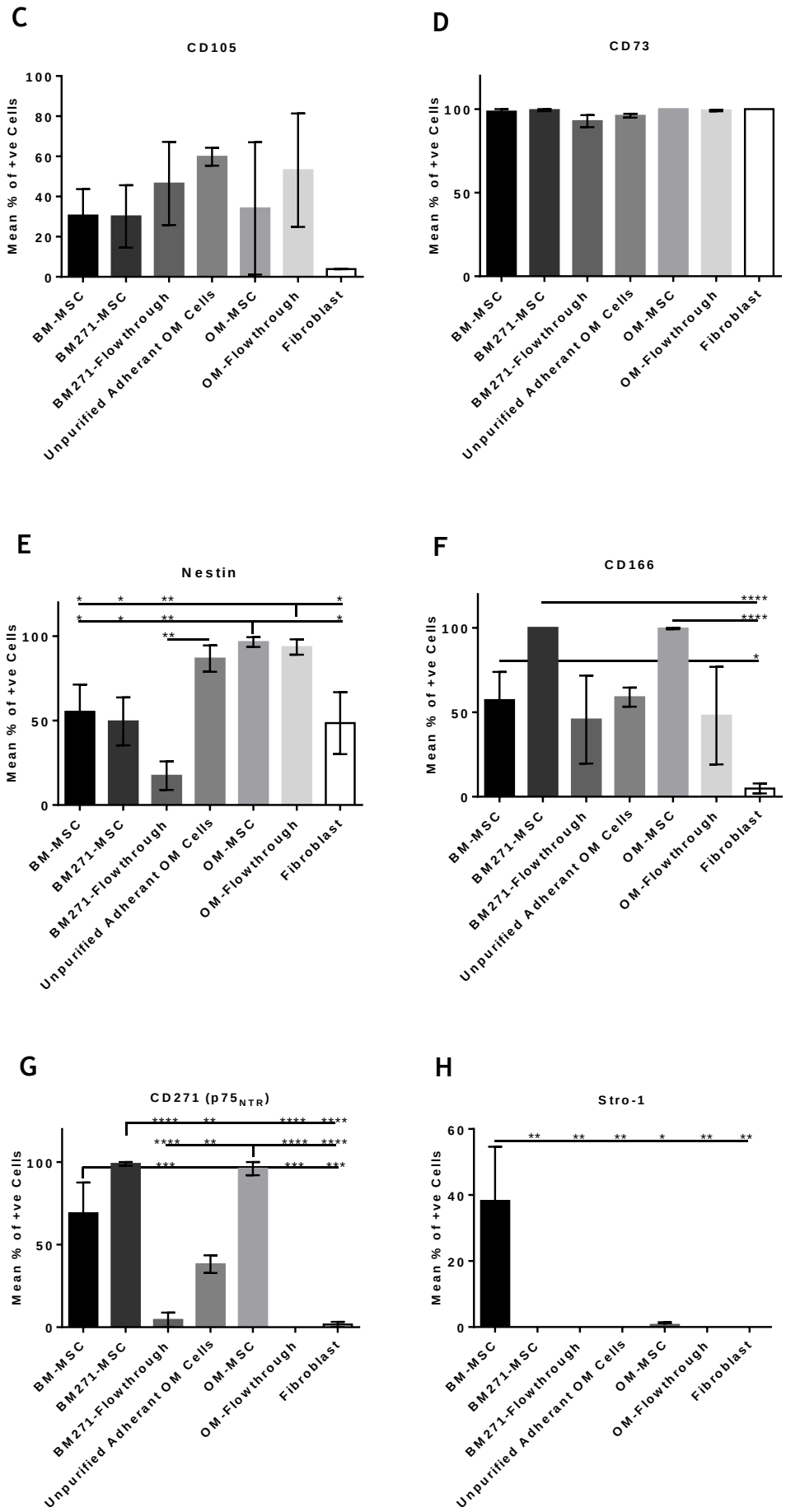
C
CD105
Mean % of +ve Cells
D
CD73
Mean % of +ve Cells
E
Nestin
Mean % of +ve Cells
F
CD166
Mean % of +ve Cells
G
CD271 (p75NTR)
Mean % of +ve Cells
H
Stro-1
Mean % of +ve Cells
BM-MSC
BM271-MSC
BM271-Flowthrough
Unpurified Adherant OM Cells
OM-MSC
OM-Flowthrough
Fibroblast

Figure 3.5: Graphical representations of Immunocytochemistry quantification of BM-MSCs, BM271-MSCs, BM271-flowthrough cells, Unpurified adherent OM cells, OM-MSCs, OM-flowthrough cells, and fibroblasts for the expression of MSC markers CD90 (A), CD54 (B), CD105 (C), CD73 (D), Nestin (E), CD166 (F), CD271 (G), and Stro-1 (H). Expression was calculated as the mean percentage of cells per field of view which expressed each marker, the mean being taken from 10 images per cell type per condition. Three separate sample donors were analysed throughout the experiment (n=3), and Statistical analysis was carried out by 1 way ANOVA using Tukey's multiple comparison test, where *=$p<0.05$, **=$p<0.01$, ***=$p<0.005$, and ****=$p<0.001$. n=3.

3.4.2. Investigating CD271 Positive Selection as a Valid Method of Isolation by Immunocytochemistry

These Immunocytochemistry data confirm findings from RT-qPCR that the CD271 positive selection protocol to generate MSCs used throughout this project is valid and reliable. Analysis of CD271 expression showed that ~40-80% of BM-MSCs and ~35-45% of unpurified adherent OM cells expressed CD271-IR. However, almost 100% of both BM271-MSCs and OM-MSCs were immunolabelled with CD271 antibody ($p<0.001$), which suggests that most of the MSCs collected at the end of the positive selection method were indeed immunolabelled with the CD271 antibody. This is validated by analysing the "flowthrough" cells which were discarded from both BM271-MSC and OM-MSC purifications, which showed that most of these cells analysed (>95%) did not label with the CD271 antibody.

3.4.3. Comparing Nestin Immunoreactivity on OM-MSCs to that on Bone Marrow-Derived MSCs and Fibroblasts

As shown using RT-qPCR, Nestin-IR was detected in almost 100% of OM-MSCs, as well as unpurified adherent OM cells and OM-Flowthrough cells. This is significantly different to Nestin-IR on BM-MSCs ($p<0.05$), BM271-MSCs ($p<0.05$), fibroblasts ($p<0.05$), and BM-Flowthrough cells ($p<0.01$). These significantly different levels of Nestin–IR appear niche dependant,

and possibly related to the high turnover of cells in the olfactory mucosa. Nestin is a marker for a number of cell types, but it is also an indicator of cell immaturity, as cells lose their expression of Nestin over time (284-288). The olfactory mucosa is an area of constant insult due to breathing in pollutants and xenoparticles. This requires a quick turnover of cellular regeneration compared to a far more protected environment in which the bone marrow tissue resides, where cells are able to turn over much more slowly (35, 36, 289-294).

3.5. Comparison of OM-MSCs and BM-MSCs by RT-qPCR and Immunocytochemistry, Using Markers of Fat, Bone, Neuron, Smooth Muscle, and Glia

MSCs are capable of differentiating into fat, bone, and cartilage, (295-299) and possibly to trans-differentiate to other cell types such as smooth muscle, neurons, and glia, although this theory is still under debate (300-304). Here we look at BM-MSCs, BM271-MSCs, and OM-MSCs, (Materials and Methods Table 2.5) and their inherent expression of mRNA associated with fat, bone, neuron, muscle, and glia differentiation. RT-qPCR was carried out using primers related to adipocytes (GLUT4 (Figure 3.6A) and Leptin (Figure 3.6B)), osteocytes (OPN (Figure 3.6C) and OCN (Figure 3.6D)), Neurons (Tuj-1 (Figure 3.6E) and MAP2 (Figure 3.6F)), myocytes (MyoD (Figure 3.6G), and SMA (Figure 3.6H)), and glia (GFAP (Figure 3.6I)) using the Livak ($\Delta\Delta C_T$) method. A full list of primers used can be found in Materials and Methods Table 2.4. With the exception of GFAP, SMA, and GLUT4, BM-MSCs had a trend towards higher mRNA expression of all other markers compared to BM271-MSCs and OM-MSCs, especially for OPN and OCN. None of these differences however, were statistically significant. Similar results were observed by immunocytochemistry when each cell type was immunolabelled with antibodies to each of the aforementioned markers. A full list of antibodies can be found in Materials and Methods Table 2.7. There was no significant difference in the expression of any of the protein markers across each cell type (Figure 3.8), with no expression

at all observed of OCN, MyoD, and MAP2 in any cell type. Representative images of these immunofluorescence can be found in Figure 3.7.

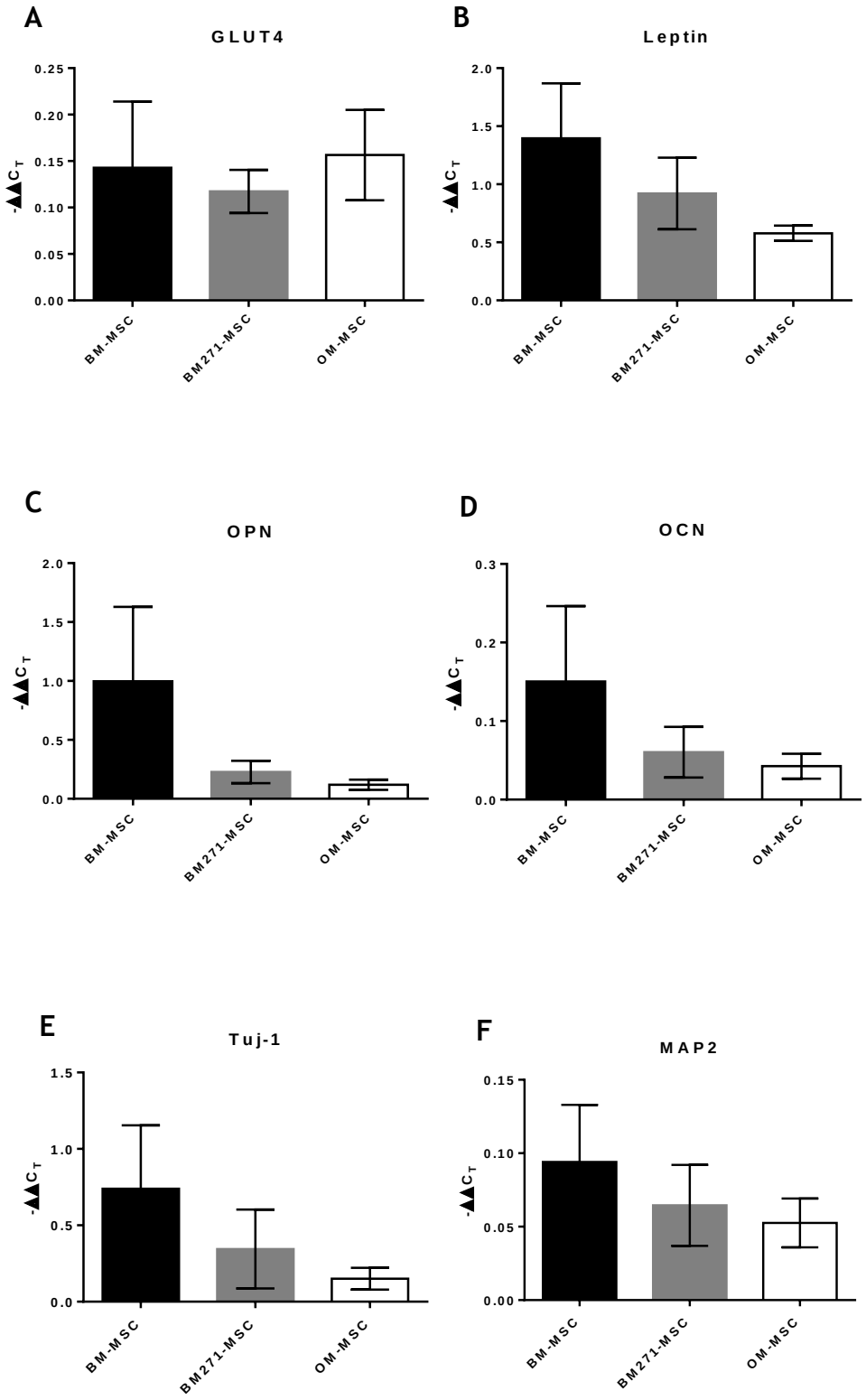

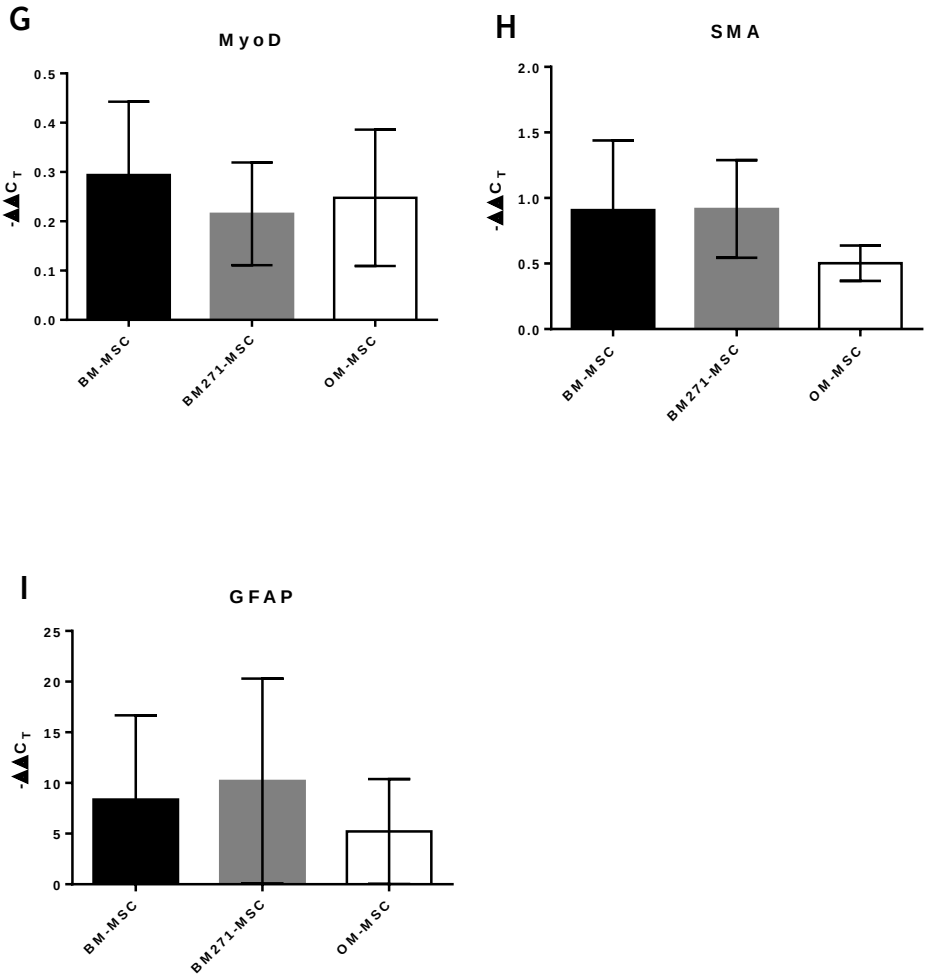

Figure 3.6: RT-qPCR analysis of transcripts associated to fat (GLUT4 (A) and Leptin (B)), bone (osteopontin (OPN) (C) and osteocalcin (D)), neuron (Tuj-1 (E) and MAP2 (F)), smooth muscle (SMA (G) and MyoD (H)), and glia (GFAP (I)) differentiation in n=3 BM-MSCs, BM271-MSCs, and OM-MSCs. Statistical analysis was carried out by 2 way ANOVA using Tukey's multiple comparison test, where *=p<0.05, **=p<0.01, ***=p<0.005, and ****=p<0.001. PCR was carried out using the Livak (ΔΔCT) method with GAPDH as the reference control gene.

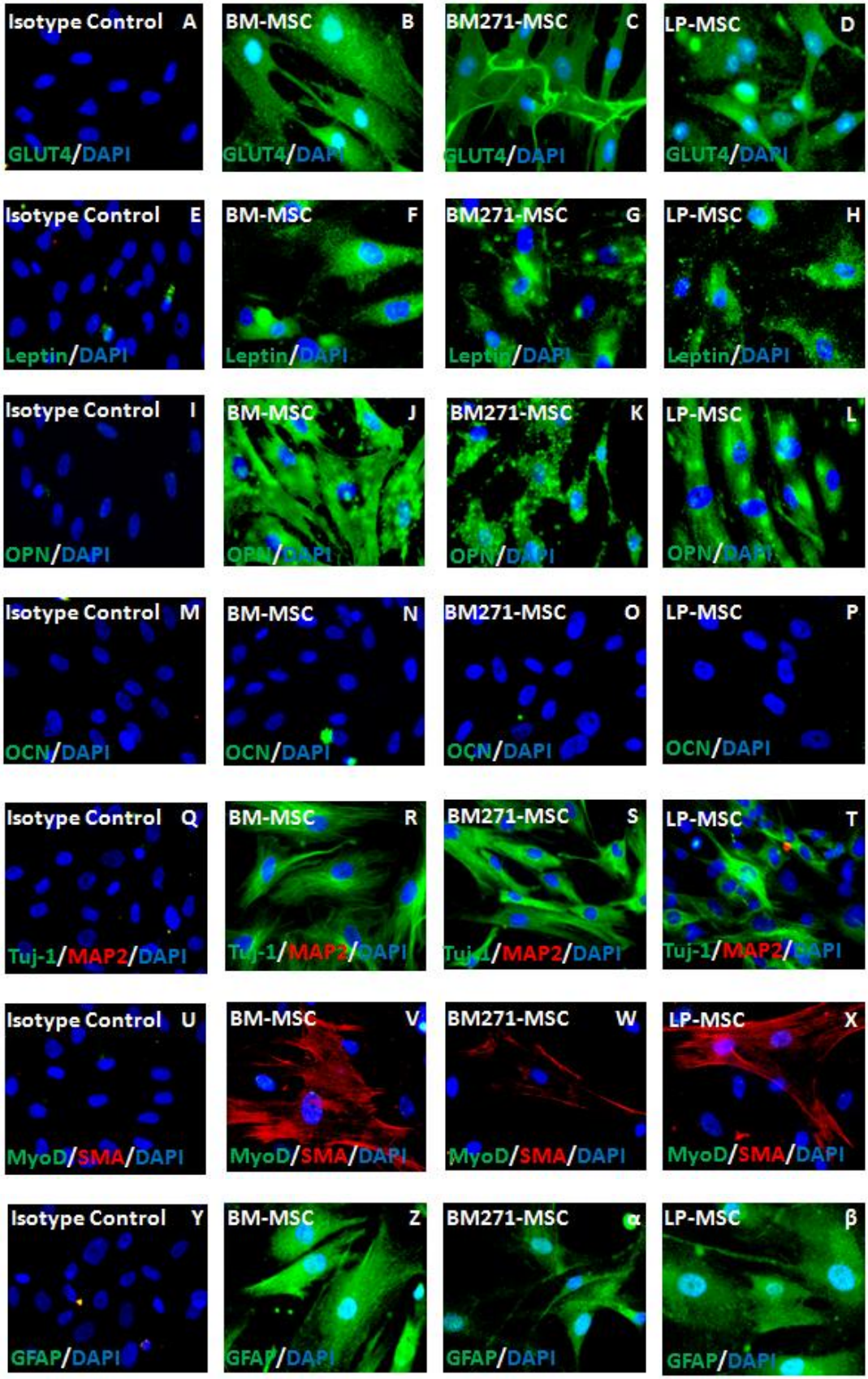
Isotype Control A
GLUT4/DAPI
BM-MSC B
GLUT4/DAPI
BM271-MSC C
GLUT4/DAPI
LP-MSC D
GLUT4/DAPI
Isotype Control E
Leptin/DAPI
BM-MSC F
Leptin/DAPI
BM271-MSC G
Leptin/DAPI
LP-MSC H
Leptin/DAPI
Isotype Control I
OPN/DAPI
BM-MSC J
OPN/DAPI
BM271-MSC K
OPN/DAPI
LP-MSC L
OPN/DAPI
Isotype Control M
OCN/DAPI
BM-MSC N
OCN/DAPI
BM271-MSC O
OCN/DAPI
LP-MSC P
OCN/DAPI
Isotype Control Q
Tuj-1/MAP2/DAPI
BM-MSC R
Tuj-1/MAP2/DAPI
BM271-MSC S
Tuj-1/MAP2/DAPI
LP-MSC T
Tuj-1/MAP2/DAPI
Isotype Control U
MyoD/SMA/DAPI
BM-MSC V
MyoD/SMA/DAPI
BM271-MSC W
MyoD/SMA/DAPI
LP-MSC X
MyoD/SMA/DAPI
Isotype Control Y
GFAP/DAPI
BM-MSC Z
GFAP/DAPI
BM271-MSC α
GFAP/DAPI
LP-MSC β
GFAP/DAPI

Figure 3.7: Representative images of Immunocytochemistry analysis of BM-MSCs, BM271-MSCs, and OM-MSCs. Staining was carried out for markers of fat (GLUT4 (green) (A-D) and Leptin (green) (E-H)), Bone (OPN (green) (I-L) and OCN (green) (M-P)), neuron (Tuj-1 (green) and MAP2 (red) (Q-T)), smooth muscle (MyoD (green) and SMA (red) (U-X)), and glia (GFAP (green)) (Y-ß) differentiation. Nuceli (blue) were stained with DAPI. Images were taken at x40 magnification, scale bar represents 25 µm. n=3.

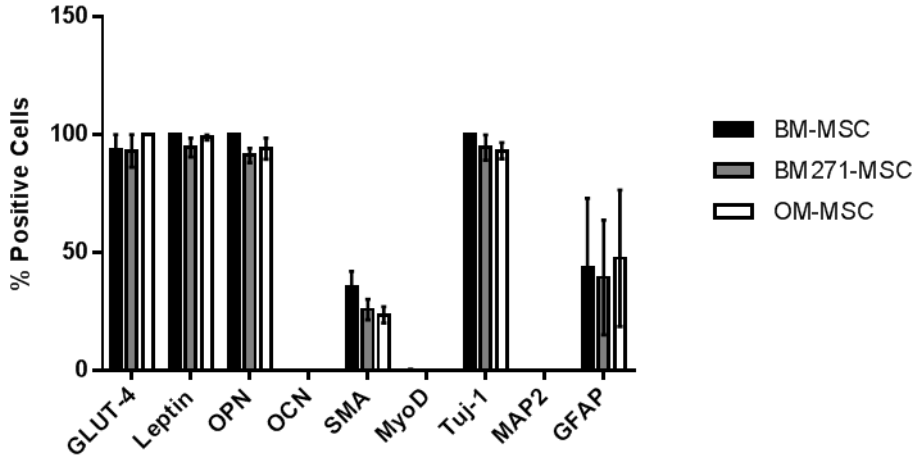

Figure 3.8: Graphical representations of Immunocytochemistry analysis of BM-MSCs, BM271-MSCs, and OM-MSCs for the expression of fat (GLUT4 and Leptin), bone (OPN and OCN), smooth muscle (SMA and MyoD), neuron (Tuj-1 and MAP2), and glia (GFAP) differentiation markers. Expression was calculated as the mean percentage of cells per field of view which expressed each marker, the mean being taken from 10 images per cell type per condition. Three separate sample donors were analysed throughout the experiment (n=3), and Statistical analysis was carried out by 1 way ANOVA using Tukey's multiple comparison test, where *=p<0.05, **=p<0.01, ***=p<0.005, and ****=p<0.001. n=3.

3.6. Comparison of the Ability of OM-MSCs and BM-MSCs to Differentiate Into Bone and Fat

Differentiation into both bone and fat is indicative of classical MSC behaviour (304-307). This property was investigated in BM-MSCs, BM271-

MSCs, and OM-MSCs (Materials and Methods Tables 2.8 and 2.9) by inducing bone and fat differentiation using osteogenic and adipogenic induction media (Materials and Methods Table 2.10). Visualisation of this differentiation can be detected by staining with Alizarin Red S and Oil Red O which bind to calcium deposits formed during osteogenesis, and to fat droplets formed during adipogenesis respectively. RT-qPCR analysis was also carried out on BM271-MSCs and OM-MSCs (Materials and Methods Tables 2.8 and 2.9) to assess any differences in the gene expression profile of these cells undergoing media induced differentiation. Samples were analysed using GLUT4 and Leptin primers as markers of fat differentiation, and using OPN and OCN primers for markers of bone differentiation.

3.6.1. Comparison of the Adipogenic Differentiation Potential of BM271-MSCs and OM-MSCs by RT-qPCR

RT-qPCR was carried out on BM271-MSCs and OM-MSCs to analyse levels of GLUT4 (Figure 3.9A) and Leptin (Figure 3.9B) transcripts after 21 days of media induced adipogenic differentiation. Treated samples were compared to untreated samples cultured for 1 day and 21 days in ordinary culture media. mRNA levels of GLUT4 and Leptin were significantly increased ($p<0.05$) in BM271-MSCs treated with adipogenic induction media compared to both untreated control conditions. Untreated day 21 samples show slightly elevated levels of mRNA for GLUT4 and Leptin compared to untreated day 1 samples, suggesting minor spontaneous differentiation, although these observations are not statistically significant. Levels of GLUT4 mRNA were significantly increased ($p<0.05$) in OM-MSCs treated with adipogenic induction media compared to both untreated control conditions. Levels of Leptin mRNA expression were also higher in treated OM-MSCs compared to untreated controls, although this differential expression was not statistically significant. As with BM271-MSCs, untreated day 21 samples show elevated but not statistically significant levels of GLUT4 mRNA and Leptin mRNA compared to untreated day 1 samples. Comparing expression levels of GLUT4 mRNA and Leptin mRNA in treated BM271-MSCs and OM-MSCs, it was seen that levels were much higher in

BM271-MSCs, although due to large sample variation, these differences are not statistically significant. We can conclude from this experiment that both BM271-MSCs and OM-MSCs are capable of significantly increasing levels of fat differentiation genes by adipogenic induction media, although this is observed with higher levels of efficacy in BM271-MSCs.

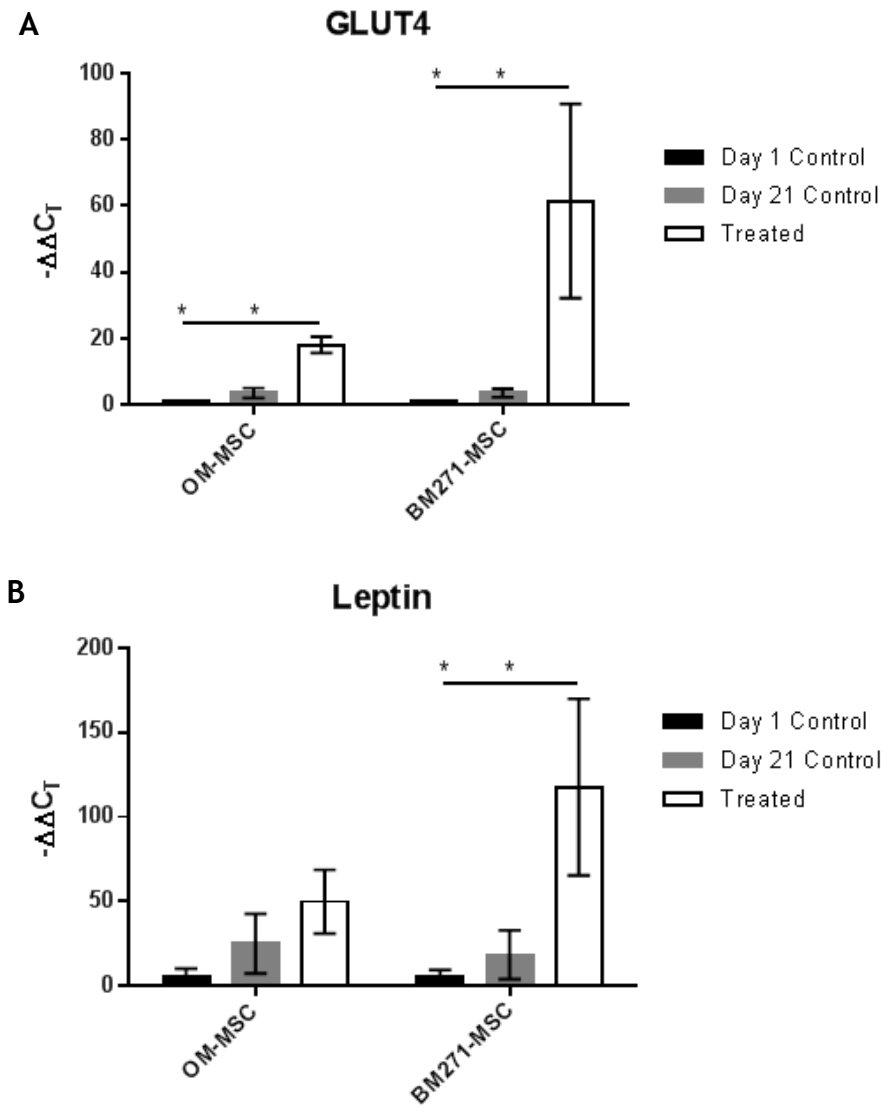

Figure 3.9: RT-qPCR analysis of transcripts associated with fat differentiation, GLUT4 (A) and Leptin (B) in BM-MSCs, BM271-MSCs, and OM-MSCs after 21 of culture with adipogenic induction media. Treated samples were compared to untreated samples collected after 24 hr and 21

days which were in culture with DMEM:10% Hyclone. Statistical analysis was carried out by 2 way ANOVA using Tukey's multiple comparison test, where *=p<0.05, **=p<0.01, ***=p<0.005, and ****=p<0.001. PCR was carried out using the Livak (ΔΔCT) method with GAPDH as the reference control gene. n=3.

3.6.2. Comparison of the Adipogenic Differentiation of BM-MSCs, BM271-MSCs, and OM-MSCs Using Oil Red O

BM-MSCs, BM271-MSCs, and OM-MSCs were stained with Oil Red O dye after 21 days of media induced adipogenic differentiation, to identify any fat droplets formed (Figure 3.10). Treated samples were compared to Oil Red O stained untreated samples which were cultured for 21 days in ordinary culture media. Staining demonstrates the ability of each cell type to form fat, with BM-MSCs seeming to be more effective at this compared to BM271-MSCs and OM-MSCs. This was confirmed by measuring the stained oil droplets from each condition using ImageJ software. BM-MSCs and BM271-MSCs produced significantly more oil droplets than untreated controls (p<0.001 and p<0.01 respectively) (Figure 3.11A). OM-MSCs produced noticeably more oil droplets than untreated controls, although due to a greater occurrence of spontaneous differentiation, the difference was not statistically significant (Figure 3.11A). This spontaneous differentiation likely occurred due to OM-MSCs becoming confluent quickly and the switching on of adipogenic mechanisms which occur under stressed conditions (516). Fold increases in fat droplet production in treated samples compared to untreated controls were calculated, confirming that BM-MSCs, produce fat droplets (~18-fold increase) with significantly more efficacy than both BM271-MSCs (p<0.01) (~8-fold increase) and OM-MSCs (~2-fold increase) (p<0.005) (Figure 3.11B). BM271-MSCs were also significantly more efficient at producing fat droplets compared to OM-MSCs (p<0.05) (Figure 3.11B). We can conclude from this experiment that BM-MSCs, BM271-MSCs, and OM-MSCs are capable of adipogenic differentiation, with BM-MSCs doing so with much better efficacy than BM271-MSCs and OM-MSCs. The CD271 positive selection may affect the cell's ability to

produce fat, but BM271-MSCs were still significantly more effective at this than OM-MSCs. These data correlate with the previous RT-qPCR data which showed significant increases in the expression of adipogenic markers GLUT4 and Leptin in cells treated with adipogenic induction media. Although the differences in expression of these mRNA was not significant in BM271-MSCs compared to OM-MSCs, there was a noticeable trend towards higher expression in BM271-MSCs.

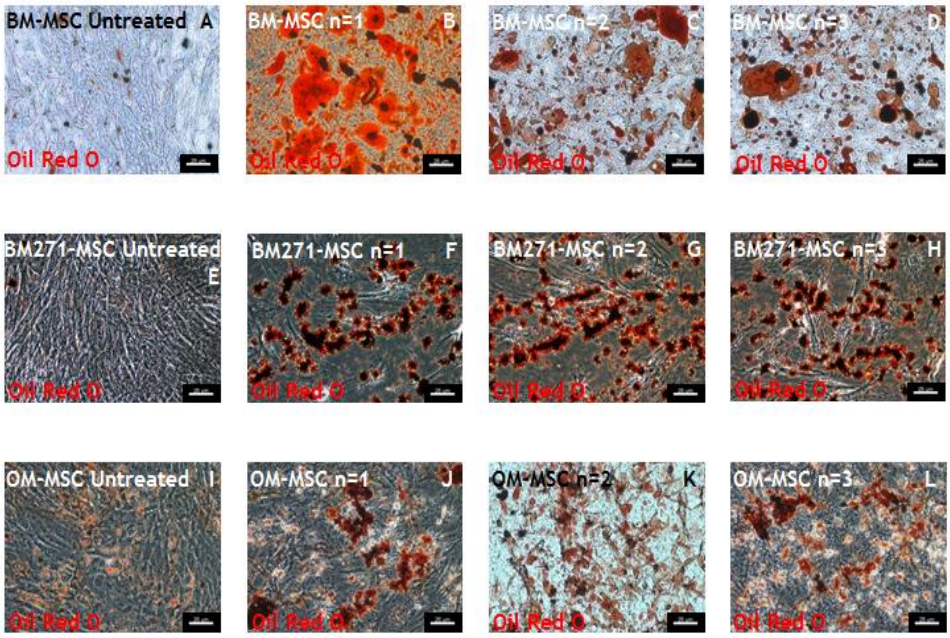

Figure 3.10: Representative images of adipogenic differentiation. BM-MSCs (B-D), BM271-MSCs (F-H), and OM-MSCs (J-L) after 21 days of culture with adipocyte induction media compared to those untreated after 21 days of culture in DMEM:10% Hyclone (A, E, and I). Adipocytes were stained red with Oil Red O dye, and images taken under phase microscope at x20 magnification, with the scale bar representing 50 µm, n=3.

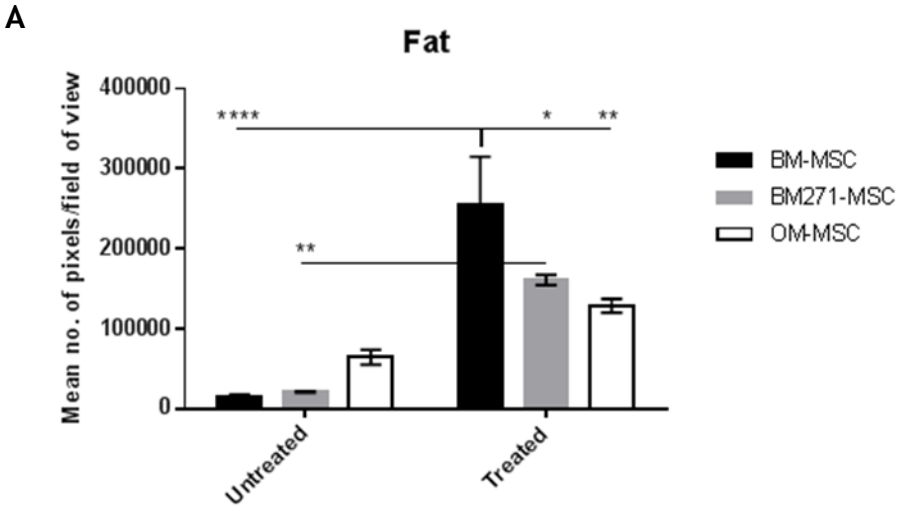

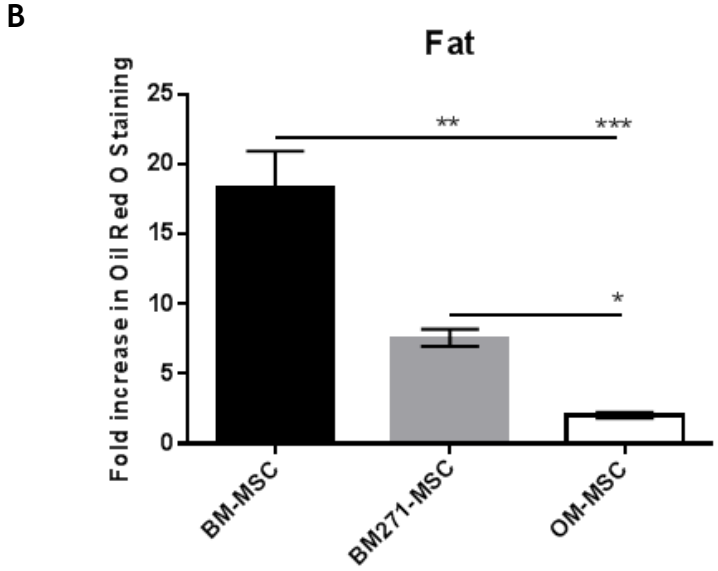

Figure 3.11: Graphical representations of adipogenic differentiation. BM-MSCs, BM271-MSCs, and OM-MSCs after 21 days of culture in adipocyte induction media, compared to untreated control samples cultured for 21 days in DMEM:10% Hyclone. Adipogenic differentiation was represented by analysing each of 10 images per condition using ImageJ software, and calculating the mean number of Oil Red O stained pixels per image (A). Fold increases in Oil Red O staining compared to untreated control samples are also represented (B). Statistical analysis was carried out by 2-way ANOVA using Tukey's multiple comparison test, where *=$p<0.05$, **=$p<0.01$, ***=$p<0.005$, and ****=$p<0.001$. n=3.

3.6.3. Comparison of the Osteogenic Differentiation Potential of BM271-MSCs and OM-MSCs by RT-qPCR

The same RT-qPCR analysis was carried out as in 3.6.1, only using primers for bone differentiation, OPN (Figure 3.12A) and OCN (Figure 3.12B). Levels of OPN and OCN transcript were similar at day 1 and day 21 in both untreated BM271- and OM-MSCs. Treated BM271-MSCs showed significantly higher expression of OPN mRNA ($p<0.01$) (Figure 3.12A) and OCN mRNA ($p<0.001$) (Figure 3.12B) compared to their untreated controls, and also a significantly higher expression of OCN compared to the OM-MSC treated samples ($p<0.05$) (Figure 3.12B). Levels of OPN and OCN transcript were markedly different in treated OM-MSC samples compared to their untreated controls (Figure 3.12), although this difference was not statistically significant by 1-way ANOVA. It can be concluded from this experiment that both BM271-MSCs and OM-MSCs are capable of increasing levels of bone differentiation genes by osteogenic induction media, although this observation is only statistically significant in BM271-MSCs.

3.6.4. Comparison of the Osteogenic Differentiation of BM-MSCs, BM271-MSCs, and OM-MSCs Using Alizarin Red S

Each cell type was stained with Alizarin Red S dye to identify calcified deposits formed after 21 days of culture in osteogenic induction media (Figure 3.13). Treated samples were compared to Alizarin Red S stained untreated samples which were cultured for 21 days in ordinary culture media. Staining demonstrates the ability of each cell type to form bone, with BM-MSCs seeming, like with fat differentiation, to be more effective at this compared to BM271-MSCs and OM-MSCs. This was again confirmed by measuring the stained calcified deposits from each condition using ImageJ software. BM-MSCs, BM271-MSCs, and OM-MSCs produced significantly more deposits than untreated controls ($p<0.001$) (Figure 3.14A), and both BM- and BM271-MSCs produced significantly more calcified deposits ($p<0.05$) compared to OM-MSCs (Figure 3.14A). Fold increases in calcified deposit production in treated samples compared to untreated controls was calculated, confirming that BM-MSCs produce

calcified deposits (~3.75-fold increase) with significantly more efficacy than both BM271-MSCs ($p<0.05$) (~3-fold increase) and OM-MSCs ($p<0.01$) (~2-fold increase) (Figure 3.14B). The difference in calcified deposit production between BM271-MSCs and OM-MSCs was not statistically significant. We can conclude from this experiment that each of BM-MSCs, BM271-MSCs, and OM-MSCs are capable of osteogenic differentiation, with BM-MSCs doing so with much better efficacy than BM271-MSCs and OM-MSCs. The CD271 positive selection clearly affects the cell's ability to produce bone, but BM271-MSCs were still more effective at this than OM-MSCs.

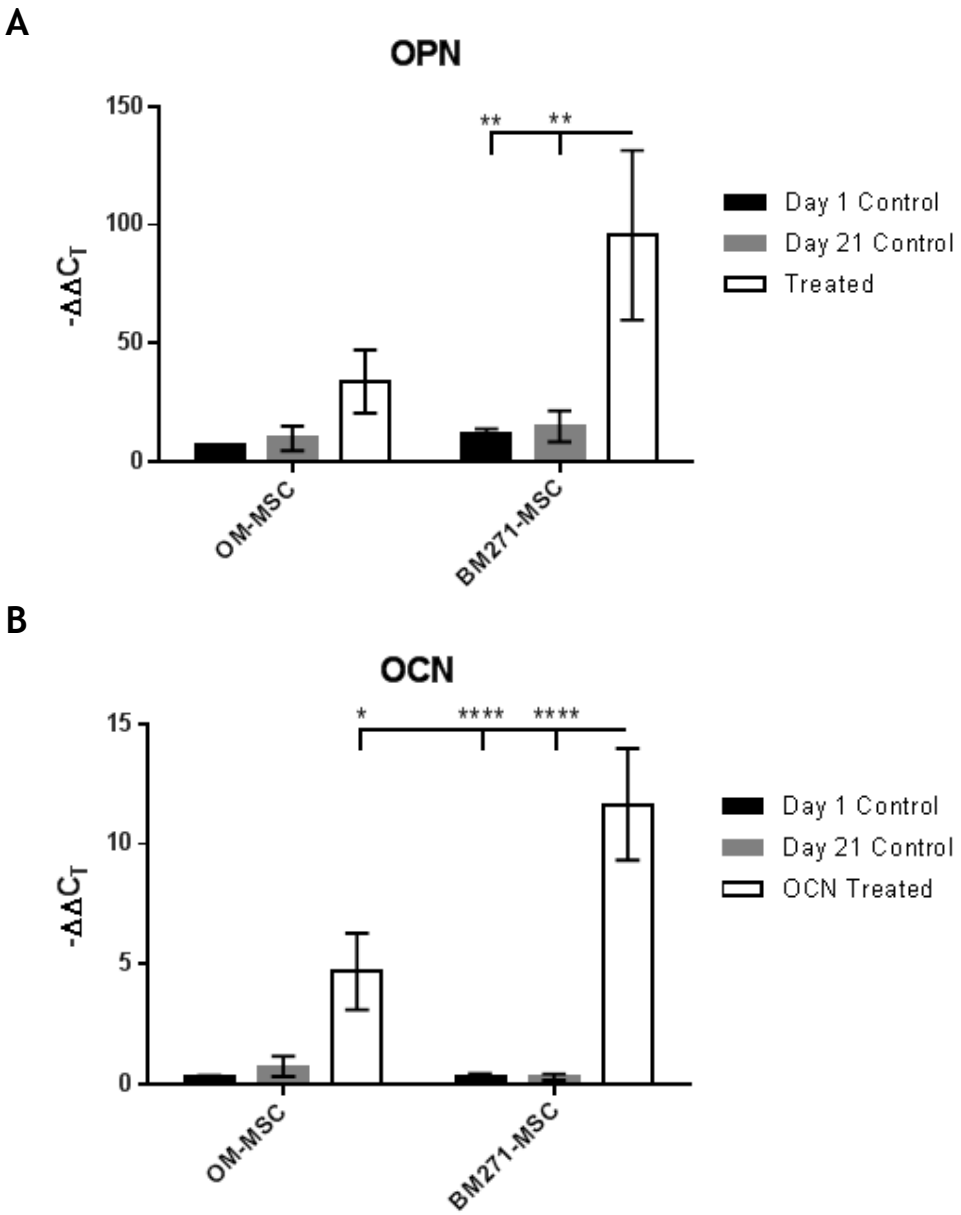

Figure 3.12: RT-qPCR analysis of transcripts associated with bone differentiation, OPN (A) and OCN (B) in BM-MSCs, BM271-MSCs, and OM-MSCs after 21 days of culture with osteogenic induction media. Treated samples were compared to untreated samples collected after 24 hr and 21 days in culture with DMEM:10% Hyclone. Statistical analysis was carried out by 2 way ANOVA using Tukey's multiple comparison test, where *=$p<0.05$, **=$p<0.01$, ***=$p<0.005$, and ****=$p<0.001$. PCR was carried out using the Livak ($\Delta\Delta C_T$) method with GAPDH as the reference control gene. n=3.

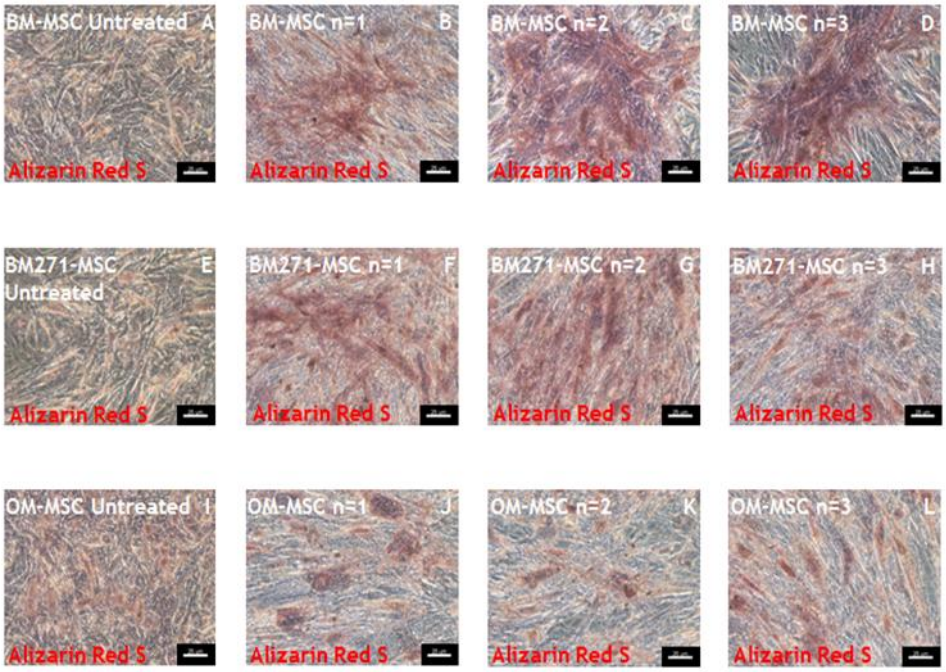

Figure 3.13: Representative images of osteogenic differentiation of BM-MSCs (B-D), BM271-MSCs (F-H), and OM-MSCs (J-L) after 21 days of culture with osteocyte induction media compared to those after 21 days of culture in DMEM:10% Hyclone (A, E, and I). Osteocytes were stained red with Alizarin Red S dye, and images taken under phase microscope at 20x magnification, with the scale bar representing 50 µm. n=3.

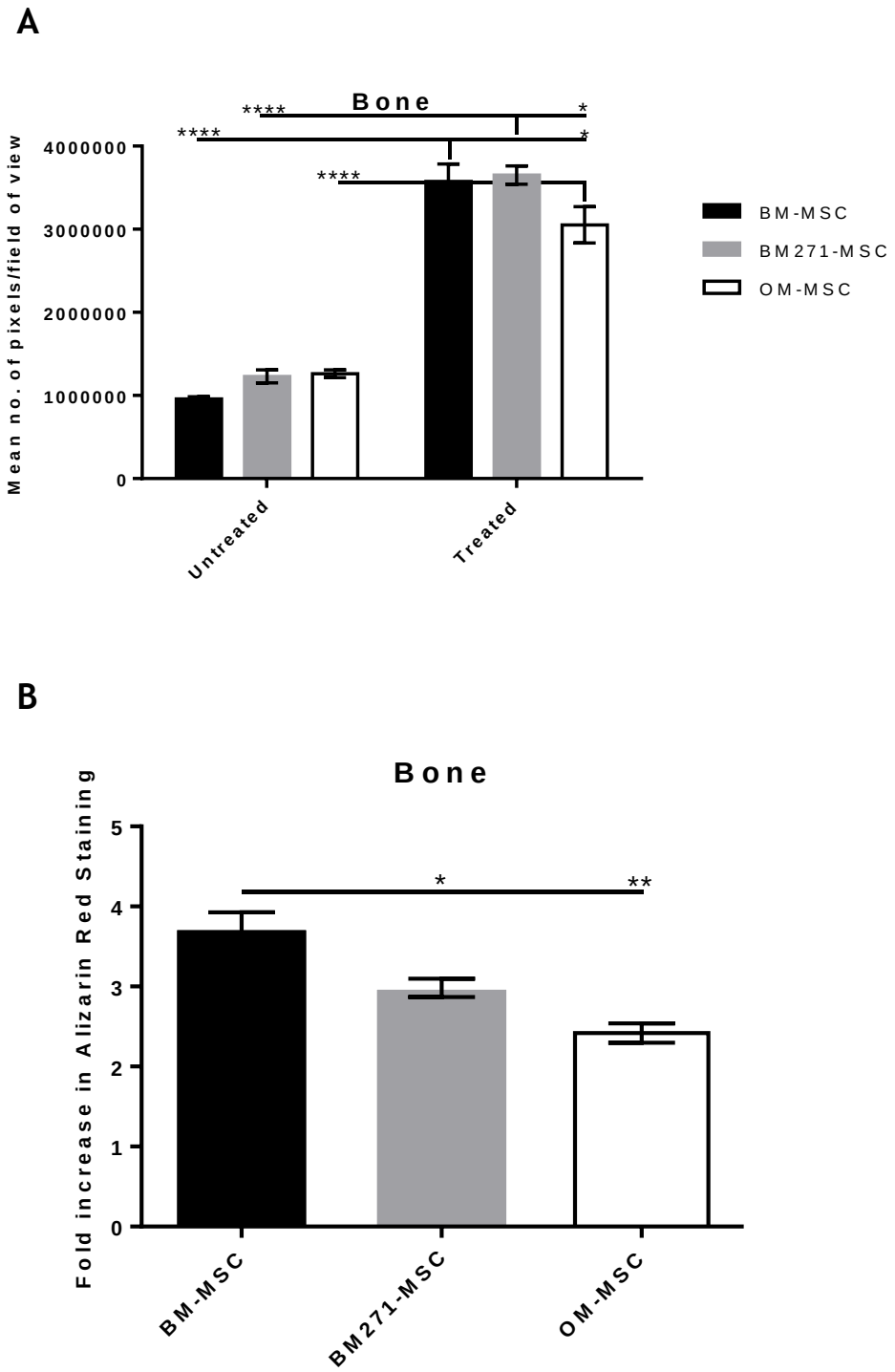

Figure 3.14: Graphical representations of osteogenic differentiation of BM-MSCs, BM271-MSCs, and OM-MSCs after 21 days of culture in osteocyte induction media, compared to untreated control samples cultured for 21 days in DMEM:10% Hyclone. Osteogenic differentiation was represented by analysing each of 10 images per condition using ImageJ software, and calculating the mean number of Alizarin Red S stained pixels per image (A).

Fold increases in Alizarin Red S staining compared to untreated control samples are also represented (B). Statistical analysis was carried out by 2 way ANOVA using Tukey's multiple comparison test, where *=p<0.05, **=p<0.01, ***=p<0.005, and ****=p<0.001. n=3.

3.7. Comparison of the Differentiation Potential of OM-MSCs and BM271-MSCs to Differentiate Towards Other Lineages

RT-qPCR analysis was carried out to determine levels of transcripts associated with differentiation towards neuronal, smooth muscle, and glial lineages in BM271 and OM-MSCs which were cultured for 21 days with induction media. RT-qPCR was carried out using primers for Tuj-1 (Figure 3.15A) and MAP2 (Figure 3.15B), MyoD (Figure 3.15C) and SMA (Figure 3.15D), and GFAP (Figure 3.15E). mRNA collected from untreated BM271 and OM-MSC samples at day 1 and day 21, and treated samples which were cultured for 21 days in the relevant induction media, was analysed to determine any increases in transcript expression within these treated samples, suggesting a potential to differentiate towards lineages other than bone and fat. Expression of mRNA for neuronal markers Tuj-1 and MAP2 was increased in treated BM271 and OM-MSCs, however these increases were only statistically significant with regards to Tuj-1 expression in BM271-MSCs (p<0.01). Levels of MAP2 mRNA expression were noticeably higher in treated samples of both BM271-MSCs and OM-MSCs, however, large sample variation meant that these differences were not statistically significant. Similarly, expression of myogenic markers MyoD and SMA were increased in treated BM271-MSCs and OM-MSCs compared to untreated controls, although these increases were only statistically significant in BM271-MSCs (p<0.001 and p<0.01 respectively). These observations were not only significant compared to their untreated control samples, but treated BM271-MSCs also expressed significantly higher levels of MyoD expression compared to treated OM-MSCs (p<0.05). Both BM271-MSCs and OM-MSCs showed significantly different expression of mRNA for GFAP compared to their untreated control (p<0.001 and p<0.05 respectively), with levels of mRNA GFAP expression being significantly

higher in treated BM271-MSC samples compared to OM-MSCs ($p<0.05$). These findings mimic those from the previous bone and fat differentiations, in that both types of MSC display the potential to differentiate towards neuronal, myogenic, and glial lineages, with MSCs from the bone marrow niche being more efficient at this than MSCs from the olfactory system.

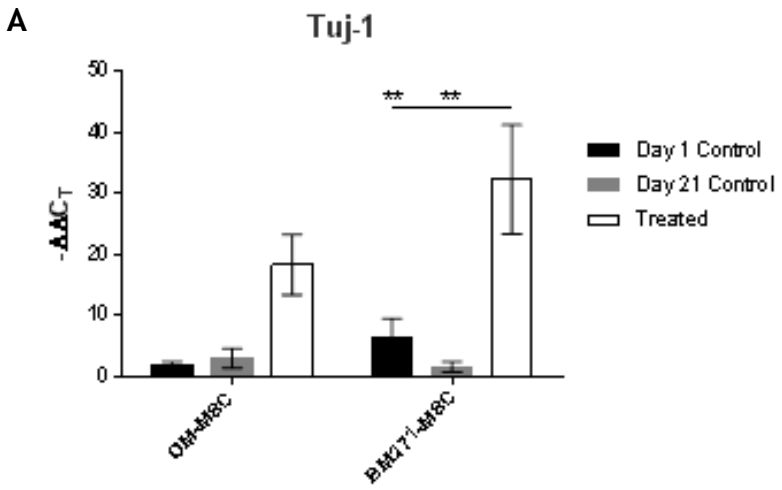

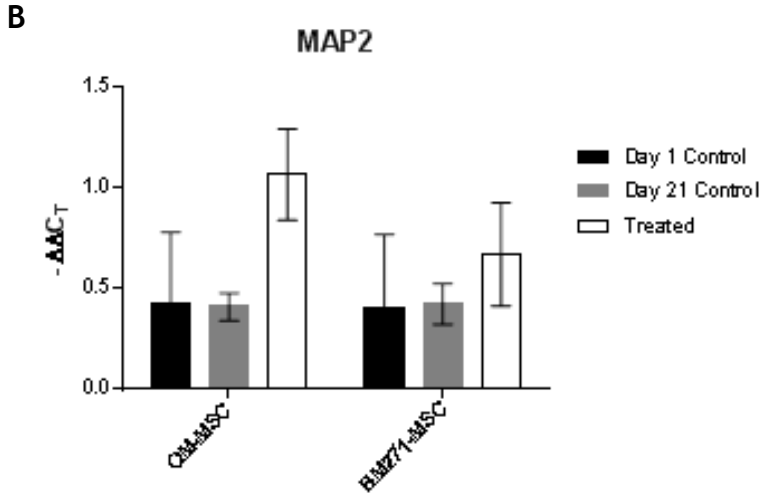

C

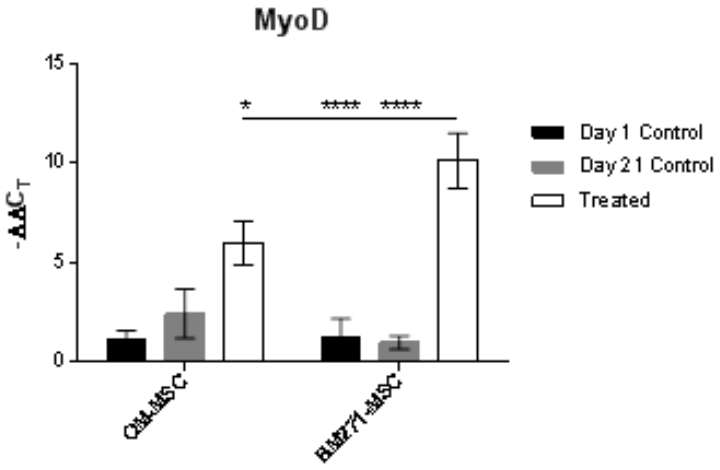
MyoD
15
10
5
0
-ΔΔC_T
*
****
****
Day 1 Control
Day 21 Control
Treated
QM-MSC
RM271-MSC

D

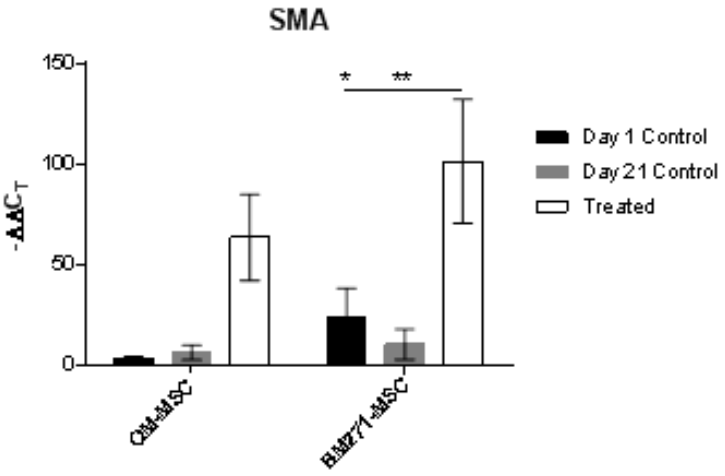
SMA
150
100
50
0
-ΔΔC_T
*
**
Day 1 Control
Day 21 Control
Treated
QM-MSC
RM271-MSC

E

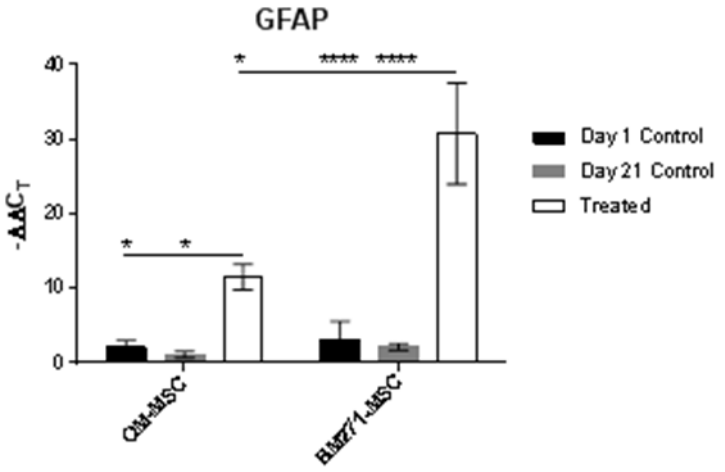
GFAP
40
30
20
10
0
-ΔΔC_T
*
****
****
*
*
Day 1 Control
Day 21 Control
Treated
QM-MSC
RM271-MSC

Figure 3.15: RT-qPCR analysis of transcripts associated with neuronal (Tuj-1 (A) and MAP2 (B)), smooth muscle (MyoD (C) and SMA (D)), and glial (GFAP (E)) differentiation in n=3 BM271-MSCs, and OM-MSCs after 21 of culture with neurogenic, myogenic, and glial induction medias respectively. Treated samples were compared to untreated samples collected after 24 hr and 21 days in culture with DMEM:10% Hyclone. Statistical analysis was carried out by 2 way ANOVA using Tukey's multiple comparison test, where *=$p<0.05$, **=$p<0.01$, ***=$p<0.005$, and ****=$p<0.001$. PCR was carried out using the Livak ($\Delta\Delta CT$) method with GAPDH as the reference control gene.

3.8. Discussion

MSCs are resident in a number of distinct cellular niches such as umbilical cord (308), adipose tissue (33, 309, 310), the developing tooth bud of the mandibular third molar (33), and amniotic fluid (34, 311), as well as the two niches identified throughout this study; bone marrow (312-314) and olfactory mucosa (1, 35, 36, 142). Although from completely distinct cellular niches, MSCs extracted from bone marrow were morphologically indistinguishable from those extracted from the lamina propria of the olfactory mucosa. This comparable morphology also extended to CD271 positive MSCs selected from cultures of adherent bone marrow cells. These findings mirror previous comparisons of BM-MSCs and OM-MSCs which showed not only a morphological similarity between the two MSC types, but also similar membrane marker expression, gene expression, ability of both to produce bone and fat, and a much higher rate of proliferation in OM-MSCs compared to BM-MSCs (1, 36). To confirm and extend previous studies, numerous experiments were carried out throughout this chapter to characterise and compare both MSC types.

Although the resident niche seems to have no effect on the cell's morphology, it may affect its molecular and biological properties. The bone marrow is an encapsulated, protected niche, mainly responsible for a steady production of blood, bone, fat, and cartilage progenitors (312-314),

whilst the olfactory system is a far less protected niche which is constantly exposed to external insult from noxious chemicals and xenoparticles during respiration, necessitating a high cellular turnover (1, 35, 36, 142). These environmental factors may have a profound effect on cellular turnover, as it was observed that OM-MSCs proliferate at a significantly faster rate than both BM and BM271-MSCs, with almost 100-fold more OM-MSCs compared to BM-MSCs after 25 days in culture.

As well as sharing morphology with each other, each MSC type shares a similar morphology to fibroblasts, hence being once known as colony forming unit fibroblasts (CFU-Fs) (11). It was important thus to distinguish these cells from fibroblasts as well as comparing each MSC to each other. Transcriptional analysis by RT-qRCR of each MSC type demonstrated that they share expression of a panel of typical MSC-associated genetic markers, which wasn't seen in human fibroblasts. This was mirrored by analysis of the protein expression by immunocytochemistry which showed that each MSC type expressed the equivalent panel of MSC-associated protein markers (except Stro-1, which was only expressed by BM-MSCs). The absence of Stro-1 in BM271-MSCs could suggest that Stro-1 positive cells do not express CD271, as all Stro-1 positive cells seem to be lost during the CD271 positive selection process. This protein expression pattern observed in each MSC type was not observed in fibroblasts, which confirms that the cells used throughout this project were indeed MSCs, and not fibroblasts.

This comparison also highlighted a significant difference in expression of Nestin at both a transcript and protein level. Nestin, although a relatively ubiquitous protein, is a generally transient one which is associated with naïve cells, as expression rarely persists into adulthood (284-287). This difference in Nestin expression could be related to the observed difference in proliferation between BM-derived and OM-derived MSCs, and the high cellular turnover of the olfactory niche. Williams *et al.* (291) identified a "rapid and reproducible" ability of the rat olfactory system to regenerate

and repair itself post-ablation by external insult, following on from previous studies outlining the unique regenerative capacity of sensory neurons within the olfactory epithelium (292-294). Arranz *et al.* (288) demonstrates a distinct correlation between nestin expression and proliferation of haematopoietic stem cells (HSCs), and numerous studies have described a high turnover of a number of cells within the olfactory niche (35, 36, 142), and that OM-MSCs have a much higher proliferative capacity *in vitro* compared to BM-MSCs (1, 36). These findings along with those from this chapter could suggest that the observed increased rate of proliferation in OM-MSCs could be related to their elevated expression of Nestin, and that these inherent biological properties may be a necessary consequence derived from residing in their native niche which is a source of constant insult and regeneration. Perhaps the MSCs in the OM have an inherent necessity to proliferate in order to keep up with the constant maintenance of the olfactory system?

Each MSC type was further compared using a panel of 9 differentiation-associated genetic and protein markers, showing no significant difference in expression of either of these markers. This expression pattern was similar to those of adipogenic MSCs, dental pulp MSCs, umbilical cord MSCs, and amniotic fluid MSCs which, although from completely distinct niches, are shown to share expression of MSC markers CD54, CD90, CD105, CD166, and Nestin, as well as stromal markers such as SMA, Tuj-1, OPN, and GFAP (315-317). It is difficult to assess any differential expression of markers between MSCs from other niches however, as no direct comparison has been done using one consistent panel of the same markers. Huang *et al.* (316) did show a differential expression of antigenic markers when comparing stem cells from different areas of the mouth and dentistry whilst still maintaining the equivalent expression of certain classic MSC markers such as CD90, CD73, CD105 and CD106. This could suggest that niche may necessitate an MSC to perform a specific niche-dependant function whilst still maintaining its capacity as an MSC.

Bone and fat differentiation studies showed that both BM-derived and OM-derived MSCs are capable of producing calcified bone deposits and fat droplets. BM-derived MSCs however, were much more efficient at this differentiation compared to OM-MSCs. This, again, could be niche dependant, as OM-MSCs are normally resident in a predominantly neurogenic environment where bone and fat production doesn't occur, so their primary function within the olfactory niche may not be to form bone and fat, but perhaps to form cartilage or connective tissue, or to play a supportive role in the neurogenesis of within the olfactory niche. However, these findings are slightly at odds with the findings of DeLorme *et al.* (36) who did find that both BM-MSCs and OM-MSCs could produce bone and fat, but that OM-MSCs produced more bone deposits identified by Von Kossa, Alizarin Red S, and Alkaline Phosphatase staining, and by expression of Runx2-IR. With regards to adipogenesis, DeLorme *et al.* (36) identified similar findings in that BM-MSCs were able to produce more adipocytes compared to OM-MSCs, although in his experiments both OM-MSCs and BM-MSCs were isolated using different methods, and neither were purified by CD271 (or any other antigenic) selection.

The lower efficacy to bone and fat differentiation in OM-MSCs observed throughout my experiments could also be related to the observed difference in Nestin expression between MSCs from the two niches. As Nestin is an indicator of naïve cells (284-287), they may not be mature enough to produce bone and fat at levels comparable to MSC from bone marrow where Nestin expression is significantly lower, although this is at odds with Delorme *et al.* who saw a 7 fold increase in Nestin expression in OM-MSCs but also an enhanced ability to form bone compared to BM-MSCs (36). As stated before though, the OM-MSCs and BM-MSCs were isolated using completely separate methods to the ones used throughout this study. OM-MSC cultures in Delorme's study did not go through CD271 positive selection and therefore could contain a more heterogenous population of cells. We also observed that BM271-MSCs were less efficient at producing bone and fat compared to non-purified BM-MSCs. CD271 is downregulated

throughout the culture of MSCs (318, 319), therefore whilst bulking up enough BM-MSCs to carry out the CD271 positive selection, a large number of BM-MSCs will lose their expression of CD271, and as a consequence the majority of these will be lost during the process. This downregulation of CD271 also meant that among these discarded cells are not only CD271 negative MSCs, but also populations of bone and fat progenitors, which by their part-differentiated nature would not express CD271. This might explain why we observed this increase in efficiency of bone and fat differentiation in BM-MSCs compared to BM271-MSCs. This also gives some credence to the hypothesis that Delorme's less purified OM-MSCs are capable of enhanced bone production compared to those in this study due to their differing isolation methods. It is entirely possible that the CD271 selection process results in the discarding of potentially osteogenic cells or osteogenic precursors.

These observations aren't limited to bone and fat differentiation. Using media induced differentiation we observed significant increases in transcript expression for genes related to neuronal, myogenic, and glial differentiation in each MSC type compared to their untreated controls. However as seen previously, BM-derived MSCs expressed the tested mRNA at a much higher level compared to those from the olfactory niche. This suggests that, although OM-MSCs possess an inherent ability to differentiate, this may not be their primary function within the olfactory system. It is perhaps more likely that they play a more supportive role in the neurogenesis of other cell types within the niche, whereas the primary function of BM-MSCs is to generate cells from the mesenchymal lineage.

3.9. Summary

- BM-MSCs, BM271-MSCs, and OM-MSCs are morphologically indistinguishable
- OM-MSCs proliferate at a significantly higher rate than BM and BM271-MSCs *in vitro*

- OM-MSCs are genetically and antigenically similar to BM and BM271-MSCs, and are completely distinct from fibroblasts
- OM-MSCs express significantly higher levels of Nestin at a transcript and protein level compared to BM-MSCs and BM271-MSCs
- BM-MSCs, BM271-MSCs, and OM-MSCs are each capable of differentiating to bone and fat, with BM- and BM271-MSCs being more efficient at this compared to OM-MSCs
- CD271 selection of BM-MSCs reduces the efficacy of these cells to differentiate towards bone and fat
- Media induced differentiation towards neuronal, myogenic, and glial lineages results in significant increases in transcripts related to these lineages in each of BM271-MSCs, and OM-MSCs, with bone marrow-derived MSCs expressing more of these mRNA compared to OM-MSCs
- CD271 selection of BM-MSCs results in a reduction of mRNA related to differentiation towards neuronal, myogenic, and glial lineages when compared to non-selected BM-MSCs

4. Cell/Substrate Interactions of MSCs

Cells throughout the body are exposed not only to external chemical cues (320-323), but also to physical ones (255, 324, 325). Receptors and matrices external to the cell surface can respond to stiffness (45, 326-330), and to symmetrical and non-symmetrical nanotpographies (46, 256, 325, 331-334) within the cellular niche in a manner which defines their fate. Previous studies have investigated niche effect on MSCs (335-337), and recreated environmental cues *in vitro* using artificial substrates such as hydrogels (338-343), matrigels (344, 345), and different plastic polymers (256, 257, 346-350). The previous chapter investigated the biological properties of each MSC type but in this chapter we look at cell/substrate interactions, and the ability of BM-derived and OM-derived MSCs to differentiate under normal culture conditions, using only nanotopographical cues via polycaprolactone surfaces which have been embossed with a controlled disordered pattern at heights of 20 – 25 nm.

4.1. Identification of the Nanotopographically embossed PCL Substrates by Atomic Force Microscopy (AFM)

Having demonstrated the ability of MSCs from both niches to differentiate under induction media conditions, here I investigated their ability to differentiate via their interactions with certain nanotopographies, without the use of exogenous chemical triggers. Also investigated were any differences between BM-MSCs and BM271-MSCs, and whether the CD271 selection process has any effect on their interactions with nanotopographically embossed substrates. Prior to this however, I had to determine the different nanotopographies onto which these MSCs were cultured. AFM analysis of each of the three surfaces; smooth, surface A, and surface B, confirmed the controlled disordered pattern on surfaces A and B (Figure 4.1), and also determined a relative roughness value (RQ) of each surface, a peak to valley roughness which measures the difference between the highest peak and the deepest valley, and a mean pit height value measuring the average height of each of the peaks over a 1 μm^2 area. All values can be found in Table 4.1, and confirm that the "smooth"

surface, although not actually smooth, is smooth in the sense that it has no nanotopography patterned onto its surface. The values also confirm that surfaces A and B are distinct, although having the same controlled disordered pattern, the relative roughness of surface A is much higher than surface B, and the mean pit height is also higher on surface A compared to surface B. Images taken from the AFM analysis also show that the width between each pit is greater in surface A compared to surface B (Figure 4.1).

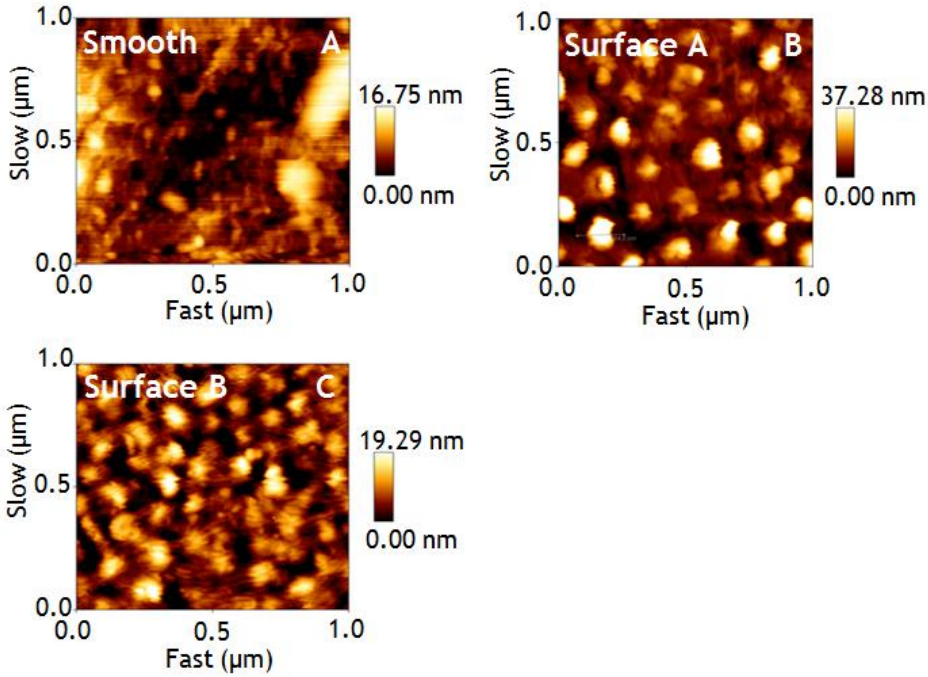

Figure 4.1: Atomic force microscopy (AFM) images of polycaprolactone (PCL) nanotopographically embossed with metal shims of controlled disordered patterns to give surface A (B) and surface B (C) substrates onto which cells can be cultured and differentiated. The control sample (A) is a non-embossed (smooth) PCL substrate formed between glass instead of a patterned metal shim.

	RMS Roughness (RQ) (nm)	Peak to valley Roughness (nm)	Mean Pit Height (nm)
Smooth	3.807	n/a	n/a
Surface A	8.473	81.87	24.64
Surface B	4.383	33.37	20.40

Table 4.1: Values of relative surface roughness (RQ), maximum peak to valley roughness, and mean pit height of each of the three PCL substrates (smooth, surface A, and surface B) used throughout this chapter. Values were calculated from 1 μm^2 images taken using atomic force microscopy and analysed using JPKSPM Data Processing software.

4.2. Comparison of the Expression of mRNA Markers of Differentiation in BM-MSCs and OM-MSCs when cultured on Nanotopographically Embossed PCL

The effects of these substrates on the biological properties of MSCs were looked at in two ways; how the nanotopgraphy of the substrate effects cell behaviour, and how this behaviour differs from cell to cell. Three different substrates were used throughout the comparison of cells; PCL nanotopographically embossed with surface A and surface B patterns, and a non-embossed "smooth" surface control. It is important to first identify how these different surfaces influence MSC differentiation. The cell-cell comparison was divided into BM-MSC vs. BM271-MSC to investigate whether or not the CD271 selection process influences the behaviour of BM-MSCs on these substrates, and into BM271-MSC vs OM-MSC to investigate any potential influence of niche on MSC behaviour on these substrates. RT-qPCR was carried out on each sample using the Livak ($\Delta\Delta C_T$) method at day 1, day 7, day 14, and day 21 time points, using BM-MSC day 1 samples as a point of reference for BM-MSC vs. BM271-MSC comparisons, and BM271-MSC day 1 samples as a point of reference for BM271-MSC vs. OM-MSC comparisons. A full list of samples used throughout this experiment can be found in Materials and Methods Table 2.11. All primers used are the same as in Materials and Methods Table 2.7.

4.2.1. Substrate vs. Substrate Comparison

Due to the complexity of the analysis of the RT-qPCR data, it was divided into two separate comparisons; substrate vs substrate and cell vs cell. Here each phenotype is separated to identify the differences in expression of each transcript by comparing the statistical analysis of each substrate to the other. Tables 4.2, 4.3, and 4.4 detail the statistical significance of the differences in gene expression laid out in figure 4.2 by comparing smooth surface vs surface A, smooth surface vs surface B, and surface A vs surface B effects on BM-MSCs (Table 4.2), BM271-MSCs (Table 4.3), and OM-MSCs (Table 4.4).

4.2.1.1. BM-MSCs

Expression of each transcript, except GFAP mRNA, was significantly increased via interactions with both surfaces A and B compared to controls by at least day 21 (Table 4.2). With the exception of Leptin mRNA, MyoD mRNA, and GFAP mRNA, these observations occurred with all other transcripts by day 14 on at least one of either surface A or surface B (Table 4.2). GLUT4 mRNA was significantly differentially expressed in BM-MSCs interacting with surfaces A and B compared to controls at day 7, however expression dropped to non-significant levels at day 14 (Table 4.2). No significant difference in expression of any of the transcripts was observed when comparing surfaces A and B, except that of OCN mRNA in BM-MSCs cultured on surface B at day 21 (Table 4.2).

4.2.1.2. BM271-MSCs

Expression of each transcript was significantly increased via interactions with both surfaces A and B compared to controls by day 21, and via interactions with at least one of either surface A or surface B by day 14 (Table 4.3). Expression of GLUT4 mRNA was significantly differentially expressed by BM271-MSCs on surfaces A and B compared to controls at day 7 (Table 4.3). No significant difference in expression of any of the transcripts was observed when comparing surfaces A and B, except that of OCN mRNA in BM271-MSCs cultured on surface B at day 21 (Table 4.3).

BM-MSCs				
Marker	Time point	Statistical Significance		
		Smooth vs A	Smooth vs B	A vs B
GLUT4	Day 7	*	*	NS
	Day 14	NS	NS	NS
	Day 21	****	****	NS
Leptin	Day 7	NS	NS	NS
	Day 14	NS	NS	NS
	Day 21	****	****	NS
OPN	Day 7	NS	NS	NS
	Day 14	****	****	NS
	Day 21	****	****	NS
OCN	Day 7	NS	NS	NS
	Day 14	**	NS	*
	Day 21	****	****	NS
Tuj-1	Day 7	NS	NS	NS
	Day 14	**	***	NS
	Day 21	****	****	NS
MAP2	Day 7	NS	NS	NS
	Day 14	****	***	NS
	Day 21	*	*	NS
MyoD	Day 7	NS	NS	NS
	Day 14	NS	NS	NS
	Day 21	***	***	NS
SMA	Day 7	NS	NS	NS
	Day 14	*	**	NS
	Day 21	****	****	NS
GFAP	Day 7	NS	NS	NS
	Day 14	NS	NS	NS
	Day 21	NS	NS	NS

Table 4.2: Statistical analysis of data from Figure 4.2 comparing levels of expression of transcripts related to adipogenic (GLUT4 (Figure 4.2A and B) and Leptin (Figure 4.2C and D)), osteogenic (OPN (Figure 4.2E and F) and OCN (Figure 4.2G and H)), neurogenic (Tuj-1 (Figure 4.2I and J) and MAP2 (Figure 4.2K and L)), myogenic (MyoD (Figure 4.2M and N) and SMA (Figure 4.2O and P)), and glial (GFAP (Figure 4.2Q and R)) differentiation. Statistical analysis was carried out by comparing substrate vs. substrate levels of transcript expression in BM-MSCs cultured on Smooth, Surface A, and Surface B topographies for 7, 14, and 21 days. Statistical analysis was carried out by 2 way ANOVA using Tukey's multiple comparison test, where

ns = not significant, *=p<0.05, **=p<0.01, ***=p<0.005, and ****=p<0.001. n=3.

BM271-MSCs				
Marker	Time point	Statistical Significance		
		Smooth vs A	Smooth vs B	A vs B
GLUT4	Day 7	*	**	NS
	Day 14	NS	NS	NS
	Day 21	****	****	NS
Leptin	Day 7	NS	NS	NS
	Day 14	**	***	NS
	Day 21	****	****	NS
OPN	Day 7	NS	NS	NS
	Day 14	NS	*	NS
	Day 21	**	*	NS
OCN	Day 7	NS	NS	NS
	Day 14	***	NS	**
	Day 21	****	****	NS
Tuj-1	Day 7	NS	NS	NS
	Day 14	****	****	NS
	Day 21	****	****	NS
MAP2	Day 7	NS	NS	NS
	Day 14	***	***	NS
	Day 21	****	**	NS
MyoD	Day 7	NS	NS	NS
	Day 14	*	*	NS
	Day 21	****	****	NS
SMA	Day 7	NS	NS	NS
	Day 14	**	***	NS
	Day 21	****	****	NS
GFAP	Day 7	NS	*	NS
	Day 14	*	*	NS
	Day 21	**	***	NS

Table 4.3: Statistical analysis of data from Figure 4.2 comparing levels of expression of transcripts related to adipogenic (GLUT4 (Figure 4.2A and B) and Leptin (Figure 4.2C and D)), osteogenic (OPN (Figure 4.2E and F) and OCN (Figure 4.2G and H)), neurogenic (Tuj-1 (Figure 4.2I and J) and MAP2 (Figure 4.2K and L)), myogenic (MyoD (Figure 4.2M and N) and SMA (Figure 4.2O and P)), and glial (GFAP (Figure 4.2Q and R)) differentiation. Statistical analysis was carried out by comparing substrate vs. substrate levels of transcript expression in BM271-MSCs cultured on Smooth, Surface

A, and Surface B topographies for 7, 14, and 21 days. Statistical analysis was carried out by 2 way ANOVA using Tukey's multiple comparison test, where ns = not significant, *=p<0.05, **=p<0.01, ***=p<0.005, and ****=p<0.001. n=3.

4.2.1.3. OM-MSCs

Expression of each transcript was significantly increased via interactions with both surfaces A and B compared to controls by day 21, with the exceptions of GFAP, MAP2, and Tuj-1 (surface A only) (Table 4.4). No significant difference in GFAP mRNA expression was observed under any condition, and differential expression of GLUT4 mRNA was observed at day in OM-MSCs on surface B (Table 4.4). There was no significant difference in expression of any gene at any time point in OM-MSCs on surface A compared to surface B (Table 4.4).

OM-MSCs				
Marker	Time point	Statistical Significance		
		Smooth vs A	Smooth vs B	A vs B
GLUT4	Day 7	NS	**	NS
	Day 14	NS	**	NS
	Day 21	**	***	NS
Leptin	Day 7	NS	NS	NS
	Day 14	*	***	NS
	Day 21	***	**	NS
OPN	Day 7	NS	NS	NS
	Day 14	NS	*	NS
	Day 21	**	*	NS
OCN	Day 7	NS	NS	NS
	Day 14	NS	NS	NS
	Day 21	***	***	NS
Tuj-1	Day 7	NS	NS	NS
	Day 14	****	****	NS
	Day 21	NS	*	NS
MAP2	Day 7	NS	NS	NS
	Day 14	**	***	NS
	Day 21	NS	NS	NS
MyoD	Day 7	NS	NS	NS
	Day 14	***	***	NS
	Day 21	NS	**	NS
SMA	Day 7	NS	NS	NS
	Day 14	NS	NS	NS
	Day 21	***	***	NS
GFAP	Day 7	NS	NS	NS
	Day 14	NS	NS	NS
	Day 21	NS	NS	NS

Table 4.4: Statistical analysis of data from Figure 4.2 comparing levels of expression of transcripts related to adipogenic (GLUT4 (Figure 4.2A and B) and Leptin (Figure 4.2C and D)), osteogenic (OPN (Figure 4.2E and F) and OCN (Figure 4.2G and H)), neurogenic (Tuj-1 (Figure 4.2I and J) and MAP2 (Figure 4.2K and L)), myogenic (MyoD (Figure 4.2M and N) and SMA (Figure 4.2O and P)), and glial (GFAP (Figure 4.2Q and R)) differentiation. Statistical analysis was carried out by comparing substrate vs. substrate levels of transcript expression in OM-MSCs cultured on Smooth, Surface A, and Surface B topographies for 7, 14, and 21 days. Statistical analysis was carried out by 2 way ANOVA using Tukey's multiple comparison test, where

ns = not significant, *=p<0.05, **=p<0.01, ***=p<0.005, and ****=p<0.001. n=3.

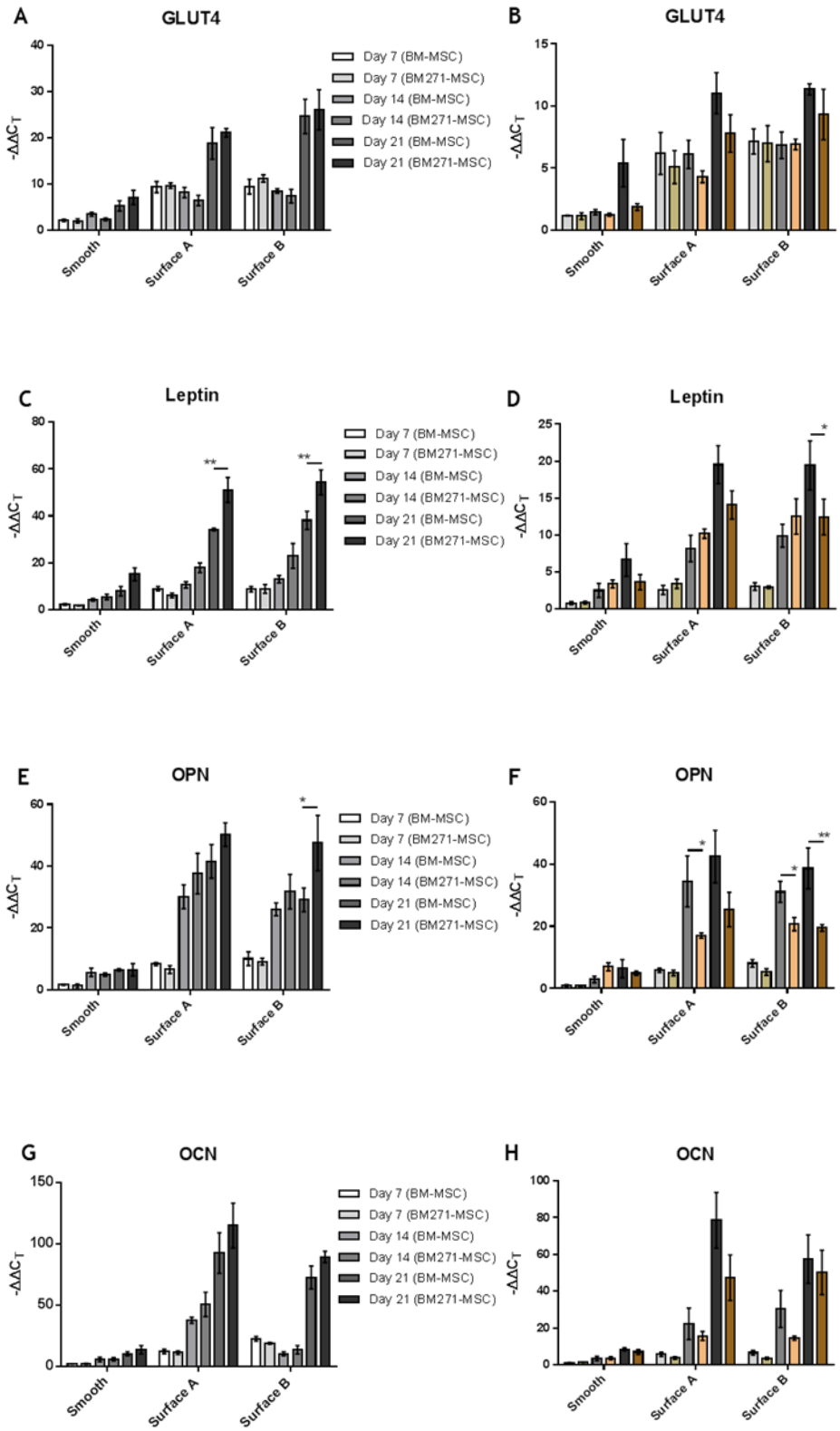

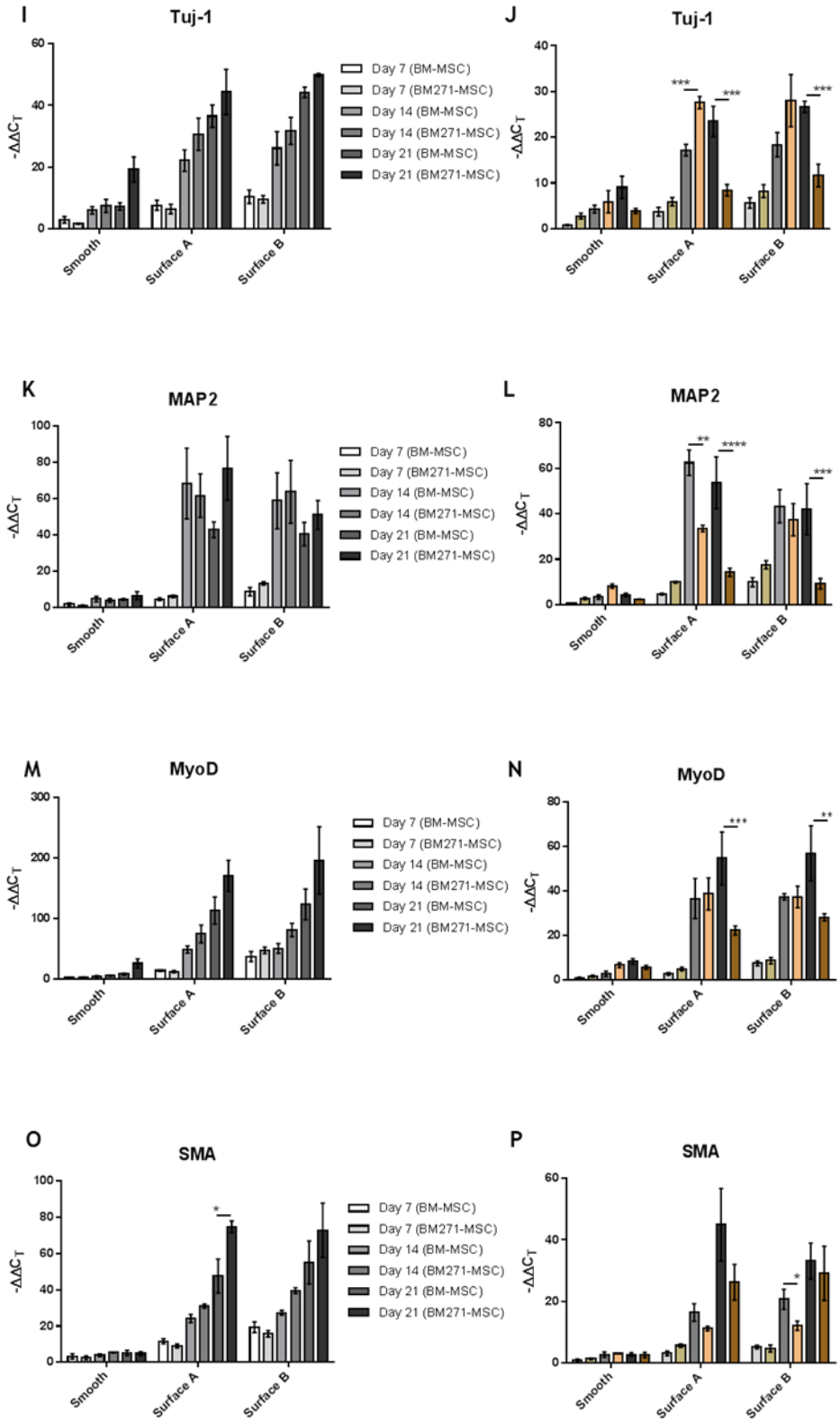
I
Tuj-1
J
Tuj-1
K
MAP2
L
MAP2
M
MyoD
N
MyoD
O
SMA
P
SMA
-ΔΔC_T
Smooth
Surface A
Surface B
Day 7 (BM-MSC)
Day 7 (BM271-MSC)
Day 14 (BM-MSC)
Day 14 (BM271-MSC)
Day 21 (BM-MSC)
Day 21 (BM271-MSC)

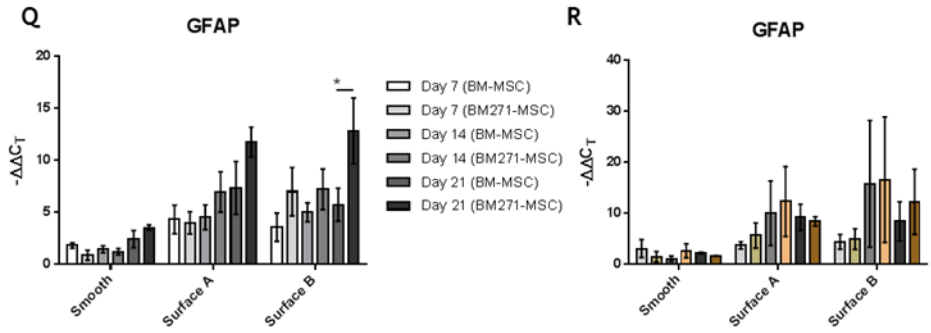

Figure 4.2: Key is for BM- and BM271-MSC only. No key for BM271- vs OM-MSC. Graphical representation of the transcript expression profiles of BM-MSCs vs BM271-MSCs, and BM271-MSCs vs OM-MSCs when cultured over 21 days on nanotopographically embossed PCL substrates of smooth, surface A, and surface B topographies. Gene expression was measured at days 7, 14, and 21, and values were all measured relative to the expression of each particular gene in BM-MSCs at day 1. Each condition was analysed for genetic markers of differentiation for fat (GLUT4 and Leptin) (A-D), bone (OPN and OCN) (E-H), neuron (Tuj-1 and MAP2) (I-L), smooth muscle (MyoD and SMA) (M-P), and Glia (GFAP) (Q-R). Statistical analysis was carried out by 2 way ANOVA using Tukey's multiple comparison test, where *=p<0.05, **=p<0.01, ***=p<0.005, and ****=p<0.001. PCR was carried out using the Livak (ΔΔCT) method with GAPDH as the reference control gene. Statistical analysis shows that both surfaces A and B have a significant influence on the expression of each gene compared to controls, so statistics bars on the graphs represent the cell vs cell comparison data found in section 4.2.2. Tables 4.2 – 4.7 contain all of the statistical analysis carried out in this experiment. n=3.

4.2.2. Cell vs. Cell Comparison

Here each surface was separated to identify the differences in expression of each transcript by comparing the statistical analysis of each phenotype to the other. Table 4.5, 4.6, and 4.7 detail the statistical significance of the differences in gene expression laid out in Figure 4.2 by comparing BM-MSCs vs BM271-MSC, and BM271-MSC vs OM-MSC on smooth surface controls (Table 4.5), surface A (Table 4.6), and surface B (Table 4.7).

4.2.2.1. Smooth surface

There was no significant difference in the expression of either transcript between BM-MSCs and BM271-MSCs, and between BM271-MSCs and OM-MSCs (Table 4.5).

4.2.2.2. Surface A

The only significant differences observed between BM-MSCs and BM271-MSCs on surface A were in the expression of Leptin at day 21 ($p<0.01$) and SMA at day 21 ($p<0.01$) (Table 4.6). More differential expression was observed when comparing BM271-MSCs and OM-MSCs, with OPN showing a significantly differential expression at day 14 ($p<0.05$), Tuj-1 at days 14 ($p<0.005$) and 21 ($p<0.005$), MAP2 at days 14 ($p<0.01$) and 21 ($p<0.001$), and MyoD at day 21 ($p<0.05$) (Table 4.6).

4.2.2.3. Surface B

The only significant differences observed between BM-MSCs and BM271-MSCs on surface B were in the expression of Leptin at day 21 ($p<0.01$), OPN at day 21 ($p<0.05$), and GFAP at day 21 ($p<0.05$) (Table 4.7). As with surface A, more significant differences were observed when comparing BM271-MSCs with OM-MSCs, with Leptin showing a significantly differential expression at day 21 ($p<0.05$), OPN at days 14 ($p<0.05$) and 21 ($p<0.01$), Tuj-1 at day 21 ($p<0.005$), MAP2 at day 21 ($p<0.005$), MyoD at day 21 ($p<0.01$), and SMA at day 21 ($p<0.05$) (Table 4.7).

From these observations it could be suggested that both surfaces A and B are capable of significant stimulation of a number of genetic markers within BM-MSCs, BM271-MSCs, and OM-MSCs, with surface A causing a higher level of bioreactivity compared to surface B. It was also observed that, with only a few exceptions, gene expression profiles of BM-MSCs and BM271-MSCs were very similar under these experimental conditions. OM-MSCs however, seemed less bioreactive compared to BM271-MSCs under these conditions, and their peak gene expression levels were generally at

an earlier time point compared to BM-derived MSCs, whose gene expression patterns showed a continuous rise to day 21.

Smooth Surface			
Marker	Time Point	Statistical Significance	
		BM-MSC vs BM271-MSC	BM271-MSC vs OM-MSC
GLUT4	Day 7	NS	NS
	Day 14	NS	NS
	Day 21	NS	NS
Leptin	Day 7	NS	NS
	Day 14	NS	NS
	Day 21	NS	NS
OPN	Day 7	NS	NS
	Day 14	NS	NS
	Day 21	NS	NS
OCN	Day 7	NS	NS
	Day 14	NS	NS
	Day 21	NS	NS
Tuj-1	Day 7	NS	NS
	Day 14	NS	NS
	Day 21	NS	NS
MAP2	Day 7	NS	NS
	Day 14	NS	NS
	Day 21	NS	NS
MyoD	Day 7	NS	NS
	Day 14	NS	NS
	Day 21	NS	NS
SMA	Day 7	NS	NS
	Day 14	NS	NS
	Day 21	NS	NS
GFAP	Day 7	NS	NS
	Day 14	NS	NS
	Day 21	NS	NS

Table 4.5: Statistical analysis of data from Figure 4.2 comparing levels of expression of transcripts related to adipogenic (GLUT4 (Figure 4.2A and B) and Leptin (Figure 4.2C and D)), osteogenic (OPN (Figure 4.2E and F) and OCN (Figure 4.2G and H)), neurogenic (Tuj-1 (Figure 4.2I and J) and MAP2 (Figure 4.2K and L)), myogenic (MyoD (Figure 4.2M and N) and SMA (Figure 4.2O and P)), and glial (GFAP (Figure 4.2Q and R)) differentiation. Statistical analysis was carried out by comparing levels of transcript expression in BM-MSCs vs BM271-MSCs, and in BM271-MSCs vs OM-MSCs cultured on smooth, non-patterned topographies for 7, 14, and 21 days.

Statistical analysis was carried out by 2 way ANOVA using Tukey's multiple comparison test, where ns = not significant, *=p<0.05, **=p<0.01, ***=p<0.005, and ****=p<0.001.

Surface A			
Marker	Time Point	Statistical Significance	
		BM-MSC vs BM271-MSC	BM271-MSC vs OM-MSC
GLUT4	Day 7	NS	NS
	Day 14	NS	NS
	Day 21	NS	NS
Leptin	Day 7	NS	NS
	Day 14	NS	NS
	Day 21	**	NS
OPN	Day 7	NS	NS
	Day 14	NS	*
	Day 21	NS	*
OCN	Day 7	NS	NS
	Day 14	NS	NS
	Day 21	NS	*
Tuj-1	Day 7	NS	NS
	Day 14	NS	*
	Day 21	NS	***
MAP2	Day 7	NS	NS
	Day 14	NS	**
	Day 21	NS	****
MyoD	Day 7	NS	NS
	Day 14	NS	NS
	Day 21	NS	***
SMA	Day 7	NS	NS
	Day 14	NS	NS
	Day 21	**	*
GFAP	Day 7	NS	NS
	Day 14	NS	NS
	Day 21	NS	NS

Table 4.6: Statistical analysis of data from Figure 4.2 comparing levels of expression of transcripts related to adipogenic (GLUT4 (Figure 4.2A and B) and Leptin (Figure 4.2C and D)), osteogenic (OPN (Figure 4.2E and F) and OCN (Figure 4.2G and H)), neurogenic (Tuj-1 (Figure 4.2I and J) and MAP2 (Figure 4.2K and L)), myogenic (MyoD (Figure 4.2M and N) and SMA (Figure 4.2O and P)), and glial (GFAP (Figure 4.2Q and R)) differentiation. Statistical analysis was carried out by comparing levels of transcript expression in BM-MSCs vs BM271-MSCs, and in BM271-MSCs vs OM-MSCs cultured on surface A topographies for 7, 14, and 21 days. Statistical

analysis was carried out by 2 way ANOVA using Tukey's multiple comparison test, where ns = not significant, *=p<0.05, **=p<0.01, ***=p<0.005, and ****=p<0.001.

Surface B			
Marker	Time Point	Statistical Significance	
		BM-MSC vs BM271-MSC	BM271-MSC vs OM-MSC
GLUT4	Day 7	NS	NS
	Day 14	NS	NS
	Day 21	NS	NS
Leptin	Day 7	NS	NS
	Day 14	NS	NS
	Day 21	**	*
OPN	Day 7	NS	NS
	Day 14	NS	NS
	Day 21	*	**
OCN	Day 7	NS	NS
	Day 14	NS	NS
	Day 21	NS	NS
Tuj-1	Day 7	NS	NS
	Day 14	NS	*
	Day 21	NS	***
MAP2	Day 7	NS	NS
	Day 14	NS	NS
	Day 21	NS	***
MyoD	Day 7	NS	NS
	Day 14	NS	NS
	Day 21	NS	**
SMA	Day 7	NS	NS
	Day 14	NS	NS
	Day 21	NS	NS
GFAP	Day 7	NS	NS
	Day 14	NS	NS
	Day 21	*	NS

Table 4.7: Statistical analysis of data from Figure 4.2 comparing levels of expression of transcripts related to adipogenic (GLUT4 (Figure 4.2A and B) and Leptin (Figure 4.2C and D)), osteogenic (OPN (Figure 4.2E and F) and OCN (Figure 4.2G and H)), neurogenic (Tuj-1 (Figure 4.2I and J) and MAP2 (Figure 4.2K and L)), myogenic (MyoD (Figure 4.2M and N) and SMA (Figure 4.2O and P)), and glial (GFAP (Figure 4.2Q and R)) differentiation. Statistical analysis was carried out by comparing levels of transcript expression in BM-MSCs vs BM271-MSCs, and in BM271-MSCs vs OM-MSCs cultured on surface B topographies for 7, 14, and 21 days. Statistical

analysis was carried out by 2 way ANOVA using Tukey's multiple comparison test, where ns = not significant, *=p<0.05, **=p<0.01, ***=p<0.005, and ****=p<0.001.

4.3. Confirmation of RT-qPCR Analysis of Cell/Substrate Reactions by Immunocytochemistry

To further investigate if these nanotopographically embossed PCL substrates were able to induce differentiation as seen for BM-MSC previously [16,36], the three MSC types described in this thesis, were cultured on the three substrates A, B, and smooth control. Immunocytochemistry was carried out on each cell type cultured on the three substrates (A, B, and Smooth), to see if the observed increases in transcript expression translated into protein expression. The same experimental conditions were carried out as in section 4.2, only cells were fixed in PFA at day 21 for immunocytochemistry. The day 21 time point was used for this study as it was the point when protein expression appeared comparatively optimal based on the PCR studies. A full list of samples used throughout this experiment can be found in Materials and Methods Table 2.12.

Figure 4.3 contains representative images of the immunocytochemistry. There was no observed immunoreactivity for either MAP2 or MyoD antibodies, so their representative images were omitted. For all other markers, more intense fluorescence immunoreactivity was observed on each MSC type when cultured on surfaces A and B compared to smooth surface controls. This suggests that more protein is being expressed within each cell or on each cell surface. To quantify this, ImageJ software was used to measure the intensity of fluorescence as the number of fluorescent pixels per cell per field of view. Figures 4.4 and 4.6 contain graphical representations of this data, displayed in 2 ways as described previously in section 2.2; comparing substrate vs. substrate (Figure 4.4), and comparing cell type vs. cell type (Figure 4.6). Immunoreactivity was also quantified by identifying the number of immunoreactive cells (Figures 4.5 and 4.7).

Cells showing any amount of immunoreactivity to any of the antibody markers were considered positive, and immunoreactivity quantified as a percentage of positive cells per field of view. The data was again displayed in 2 ways; comparing substrate vs. substrate (Figure 4.5), and comparing cell vs. cell (Figure 4.7). Due to numerous previous experiments determining no compelling difference between BM-MSC and BM271-MSC immunoreactivity, immunocytochemical analysis of Tuj-1, SMA, and GFAP immunoreactivity was restricted to BM271-MSCs vs OM-MSCs only. Immunocytochemistry for OPN and OCN was carried out before this conclusion, so BM-MSCs were analysed for these markers.

4.3.1. Substrate vs. Substrate Comparison

ImageJ analysis of immunocytochemistry images identified distinct immunoreactivity patterns. As with the RT-qPCR data in section 4.2, this is best described by separating each phenotype. A summary of all the statistical analysis carried out can be found in tables 4.8 – 4.10.

4.3.1.1. BM-MSCs

OPN and OCN immunoreactivity (IR) was significantly increased in BM-MSCs cultured on surfaces A and B compared to smooth surface controls (OPN = $p<0.001$ for A and B, OCN = $p<0.005$ for A and $p<0.001$ for B) (Figure 4.4A and B). Due to BM-MSCs expressing OPN-IR under normal conditions, there was no increase in the percentage of cells which were positive for OPN-IR (Figure 4.5A). However, there was a significant increase in the percentage of BM-MSCs expressing OCN-IR on surfaces A and B compared to smooth controls ($p<0.001$) (Figure 4.5B). Analysis for other IR markers was not carried out on BM-MSCs.

4.3.1.2. BM271-MSCs

OPN-IR and OCN-IR was significantly increased in BM271-MSCs cultured on surfaces A and B compared to smooth surface controls (OPN = $p<0.005$ for A and B, OCN = $p<0.01$ for A and B) (Figure 4.4A and B). This significant increase in IR was also seen when analysed for SMA ($p<0.001$ for A and B),

Tuj-1 ($p<0.005$ for A and $p<0.001$ for B), and GFAP ($p<0.01$). No immunoreactivity was observed for MyoD or MAP2. Due to BM271-MSCs expressing OPN-IR under normal conditions, there was no increase in the percentage of cells which were positive for OPN-IR (Figure 4.5A). However, there was a significant increase in the percentage of BM271-MSCs expressing OCN-IR on surfaces A and B compared to smooth controls ($p<0.001$) (Figure 4.5B). This significant increase was also observed for Tuj-1-IR ($p<0.01$), SMA ($p<0.05$), and GFAP ($p<0.05$) (Figure 4.5C, D, and E).

4.3.1.3. OM-MSCs

OPN-IR and OCN-IR was significantly increased in OM-MSCs cultured on surfaces A and B compared to smooth surface controls ($p<0.05$ for OPN and OCN on both A and B). This significant increase in IR was also seen when analysed for SMA and Tuj-1 ($p<0.05$ for both on both surfaces A and B). There was a slight increase in GFAP-IR in OM-MSCs cultured on surfaces A and B compared to smooth surface controls, but this difference was not significant. No immunoreactivity was observed for MyoD or MAP2. Due to OM-MSCs expressing OPN-IR under normal conditions, there was no increase in the percentage of cells which were positive for OPN-IR (Figure 4.5A). However, there was a significant increase in the percentage of OM-MSCs expressing OCN-IR on surfaces A and B compared to smooth controls ($p<0.001$) (Figure 4.5B). This significant increase was also observed for Tuj-1-IR (surface A = $p<0.01$, surface B = $p<0.005$), and SMA (surface A = $p<0.005$, surface B = $p<0.01$) (Figure 4.5C and D). There was no significant difference in the percentage of OM-MSCs showing positive GFAP-IR expression (Figure 4.5E).

These observations show that IR for OPN, OCN, SMA, Tuj-1, and GFAP was significantly increased in each phenotype when cultured on the controlled disordered surfaces A and B (except GFAP-IR in OM-MSCs) compared to non-patterned surfaces when looking at both intensity of IR and the percentage of positively expressing cells. The absence of MyoD and MAP2 IR suggests that no trans-differentiation has occurred via this mechanism.

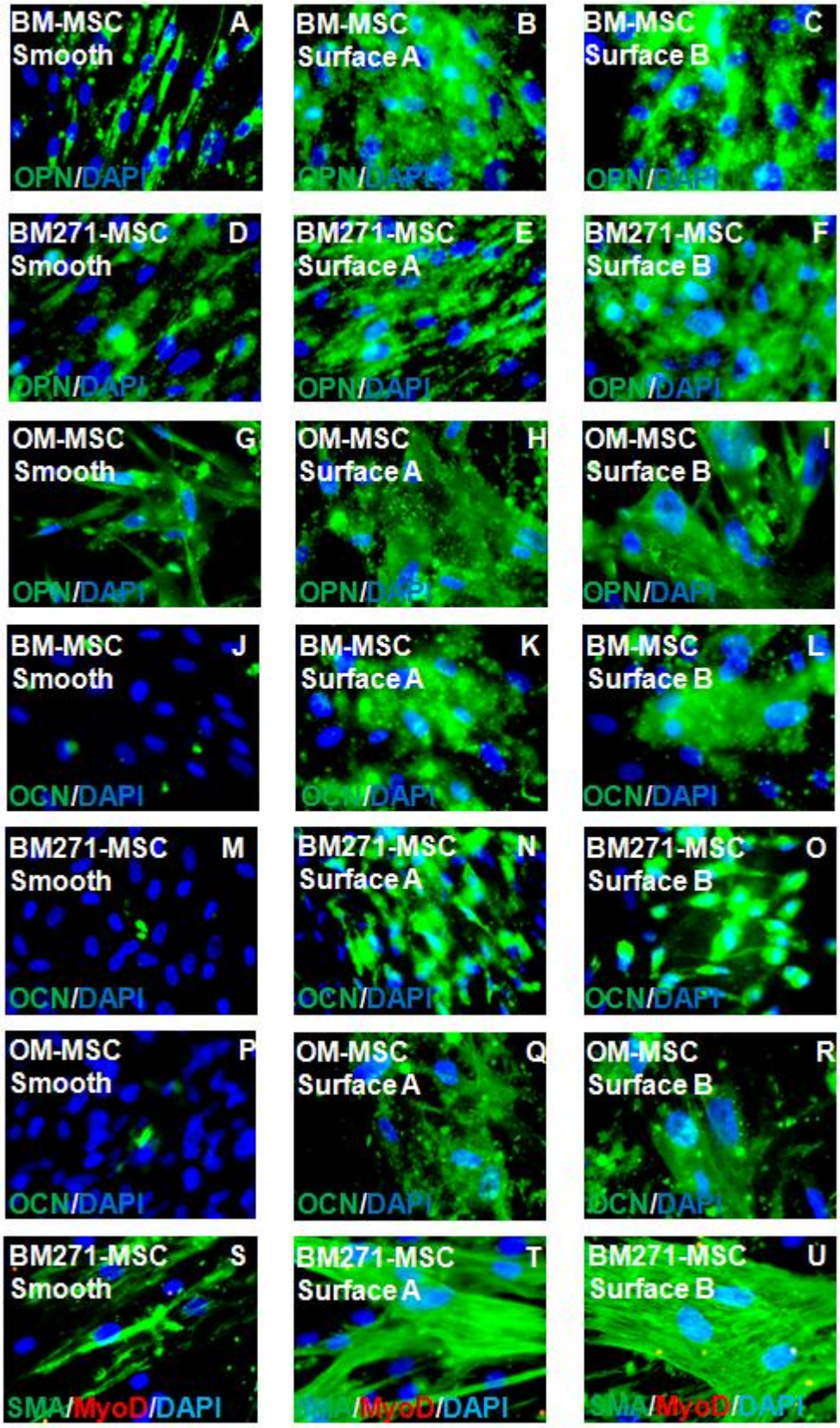
BM-MSC
Smooth
A
OPN/DAPI
BM-MSC
Surface A
B
OPN/DAPI
BM-MSC
Surface B
C
OPN/DAPI
BM271-MSC
Smooth
D
OPN/DAPI
BM271-MSC
Surface A
E
OPN/DAPI
BM271-MSC
Surface B
F
OPN/DAPI
OM-MSC
Smooth
G
OPN/DAPI
OM-MSC
Surface A
H
OPN/DAPI
OM-MSC
Surface B
I
OPN/DAPI
BM-MSC
Smooth
J
OCN/DAPI
BM-MSC
Surface A
K
OCN/DAPI
BM-MSC
Surface B
L
OCN/DAPI
BM271-MSC
Smooth
M
OCN/DAPI
BM271-MSC
Surface A
N
OCN/DAPI
BM271-MSC
Surface B
O
OCN/DAPI
OM-MSC
Smooth
P
OCN/DAPI
OM-MSC
Surface A
Q
OCN/DAPI
OM-MSC
Surface B
R
OCN/DAPI
BM271-MSC
Smooth
S
SMA/MyoD/DAPI
BM271-MSC
Surface A
T
/MyoD/DAPI
BM271-MSC
Surface B
U
SMA/MyoD/DAPI

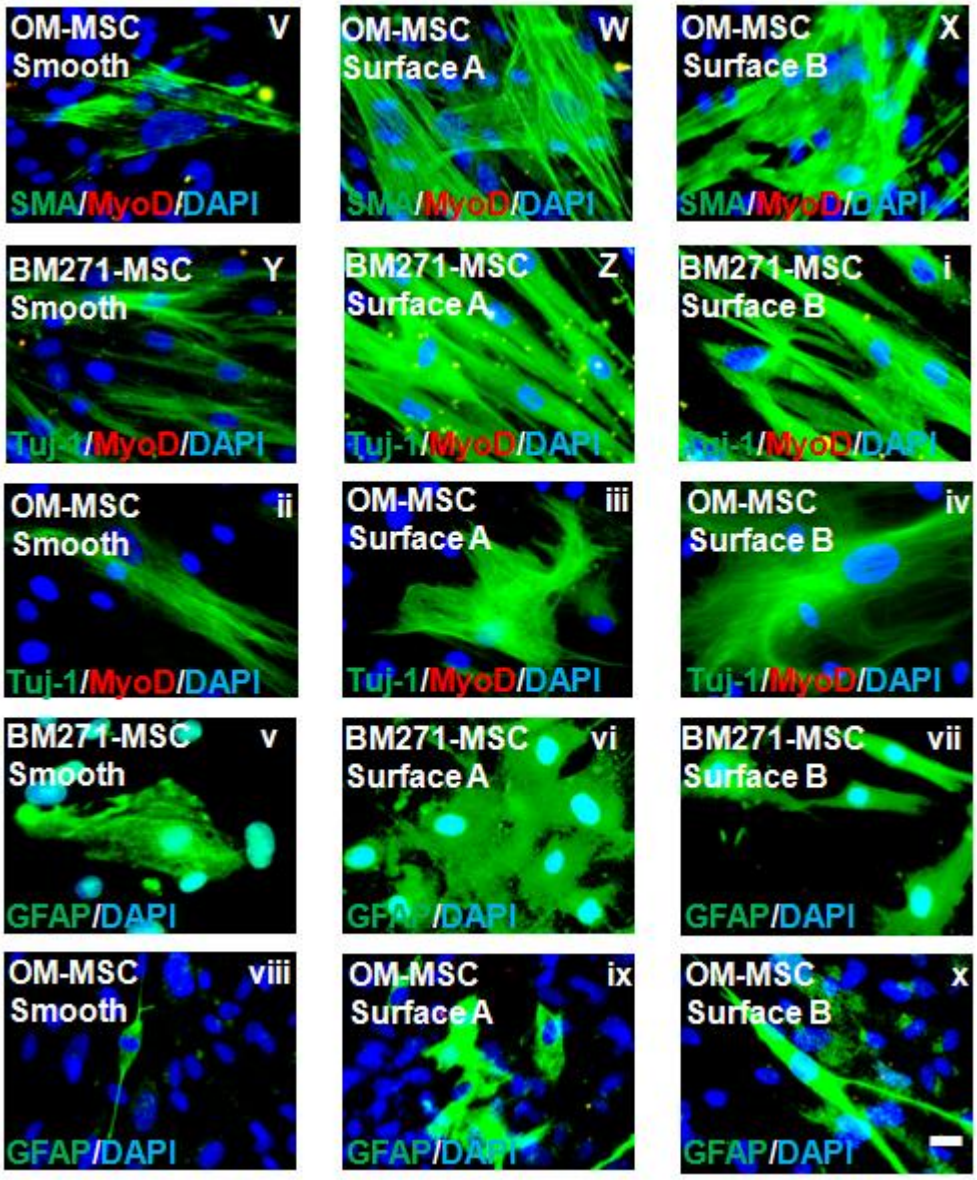

Figure 4.3: Representative images of immunocytochemistry for BM-MSCs (OPN and OCN only), BM271-MSCs, and OM-MSCs seeded onto nanotopographically embossed PCL substrates A and B, and smooth surface controls. Fluorescent markers of osteogenic differentiation, OPN (A-I) and OCN (J-R) myogenic differentiation, SMA (S-X) and MyoD (no MyoD-IR obeserved), neurogenic differentiation, Tuj-1 (Y-iv) and MAP2 (no MAP2-IR observed), and glial differentiation, GFAP (v-x) were used to identify immunoreactivity. Nuclei (blue) were visualised with DAPI. Images were taken at x40 magnification, scale bar represents 25 µm. n=3.

BM-MSCs				
Marker	Analysis	Statistical Significance		
		Smooth vs A	Smooth vs B	A vs B
OPN	IR Intensity	****	****	NS
	% Positive Cells	NS	NS	NS
OCN	IR Intensity	***	****	NS
	% Positive Cells	****	****	NS

Table 4.8: Statistical analysis of data from Figures 4.4 and 4.5 comparing intensity of IR expression and percentage of IR positive cells expressing markers related to osteogenic (OPN (Figure 4.4 and 4.5A)) and OCN (Figures 4.4 and 4.5B)) differentiation. Statistical analysis was carried out by comparing intensity of IR expression, and percentage of IR positive BM-MSCs cultured on smooth vs surface A, smooth vs surface B, and surface A vs surface B topographies for 21 days. Statistical analysis was carried out by 2 way ANOVA using Tukey's multiple comparison test, where ns = not significant, *=p<0.05, **=p<0.01, ***=p<0.005, and ****=p<0.001.

BM271-MSCs				
Marker	Analysis	Statistical Significance		
		Smooth vs A	Smooth vs B	A vs B
OPN	IR Intensity	***	***	NS
	% Positive Cells	NS	NS	NS
OCN	IR Intensity	**	**	NS
	% Positive Cells	****	****	NS
Tuj-1	IR Intensity	***	****	NS
	% Positive Cells	**	**	NS
MAP2	IR Intensity	No Immunoreactivity Observed		
	% Positive Cells			
MyoD	IR Intensity			
	% Positive Cells			
SMA	IR Intensity	****	****	NS
	% Positive Cells	*	*	NS
GFAP	IR Intensity	**	**	NS
	% Positive Cells	*	*	NS

Table 4.9: Statistical analysis of data from Figures 4.4 and 4.5 comparing intensity of IR expression and percentage of IR positive cells expressing markers related to osteogenic (OPN (Figure 4.4 and 4.5A)) and OCN (Figures 4.4 and 4.5B)), neurogenic (Tuj-1 (Figures 4.4 and 4.5C)), myogenic (SMA (Figures 4.4 and 4.5D)), and glial (GFAP (Figures 4.4 and 4.5E)) differentiation. Statistical analysis was carried out by comparing intensity of IR expression, and percentage of IR positive BM271-MSCs cultured on smooth vs surface A, smooth vs surface B, and surface A vs surface B topographies for 21 days. Statistical analysis was carried out by 2 way ANOVA using Tukey's multiple comparison test, where ns = not significant, *=p<0.05, **=p<0.01, ***=p<0.005, and ****=p<0.001.

OM-MSCs				
Marker	**Analysis**	**Statistical Significance**		
		Smooth vs A	**Smooth vs B**	**A vs B**
OPN	IR Intensity	*	*	NS
	% Positive Cells	NS	NS	NS
OCN	IR Intensity	*	*	NS
	% Positive Cells	****	****	NS
Tuj-1	IR Intensity	*	*	NS
	% Positive Cells	**	***	NS
MAP2	IR Intensity	No Immunoreactivity Observed		
	% Positive Cells			
MyoD	IR Intensity			
	% Positive Cells			
SMA	IR Intensity	*	*	NS
	% Positive Cells	**	*	NS
GFAP	IR Intensity	NS	NS	NS
	% Positive Cells	NS	NS	NS

Table 4.10: Statistical analysis of data from Figures 4.4 and 4.5 comparing intensity of IR expression and percentage of IR positive cells expressing markers related to osteogenic (OPN (Figure 4.4 and 4.5A)) and OCN (Figures 4.4 and 4.5B)), neurogenic (Tuj-1 (Figures 4.4 and 4.5C)), myogenic (SMA (Figures 4.4 and 4.5D)), and glial (GFAP (Figures 4.4 and 4.5E)) differentiation. Statistical analysis was carried out by comparing

intensity of IR expression, and percentage of IR positive OM-MSCs cultured on smooth vs surface A, smooth vs surface B, and surface A vs surface B topographies for 21 days. Statistical analysis was carried out by 2 way ANOVA using Tukey's multiple comparison test, where ns = not significant, *=p<0.05, **=p<0.01, ***=p<0.005, and ****=p<0.001.

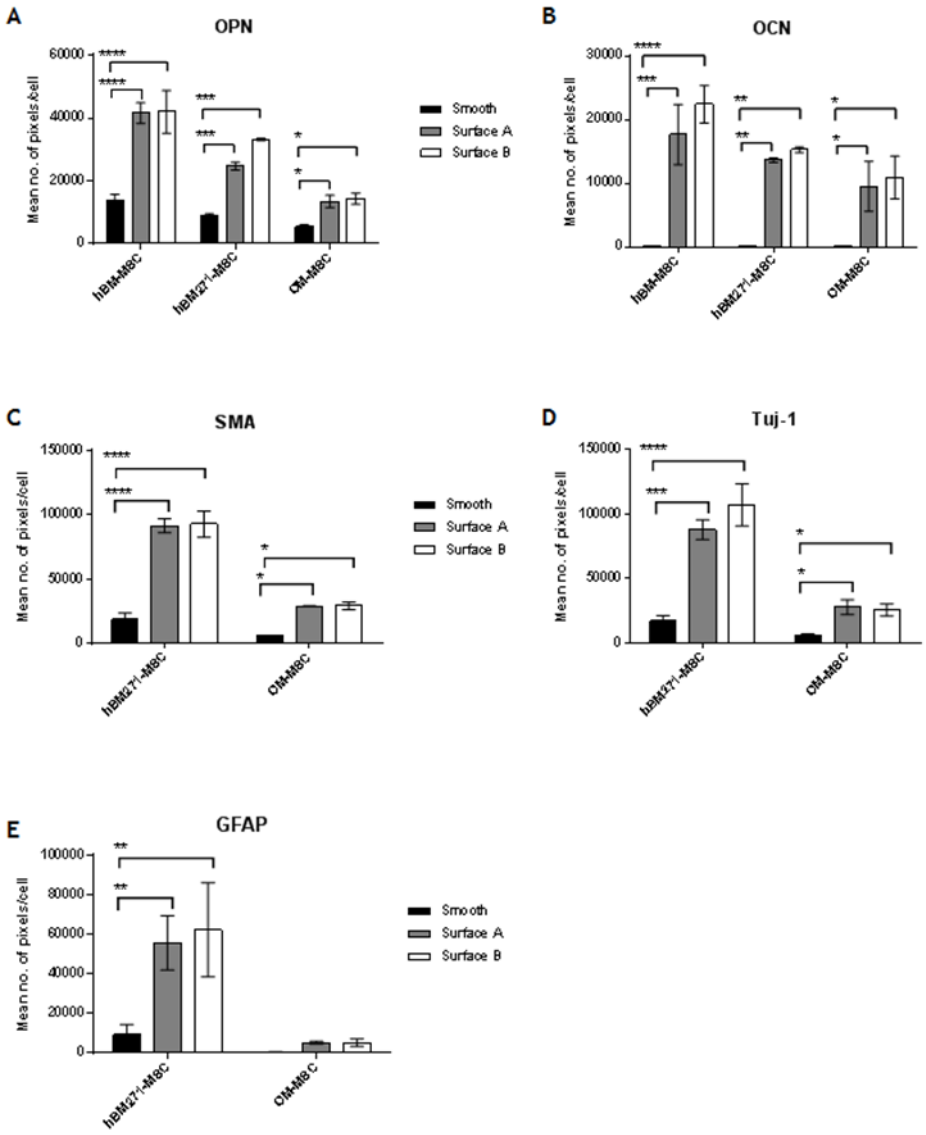

Figure 4.4: Graphical representations of immunocytochemistry for BM-MSCs (OPN and OCN only), BM271-MSCs, and OM-MSCs seeded onto nanotopographically embossed PCL substrates A and B, and smooth surface controls. Markers of osteogenic differentiation, OPN (A) and OCN (B), myogenic differentiation, SMA (C) and MyoD (no MyoD-IR obeserved),

neurogenic differentiation, Tuj-1 (D) and MAP2 (no MAP2-IR observed), and glial differentiation, GFAP (E) were used to identify protein expression. Analysis was carried out using ImageJ software by measuring intensity of fluorescence by counting the mean number of fluorescent pixels per cell per image. Statistical analysis was carried out by 2 way ANOVA using Tukey's multiple comparison test, where *=p<0.05, **=p<0.01, ***=p<0.005, and ****=p<0.001, n=3.

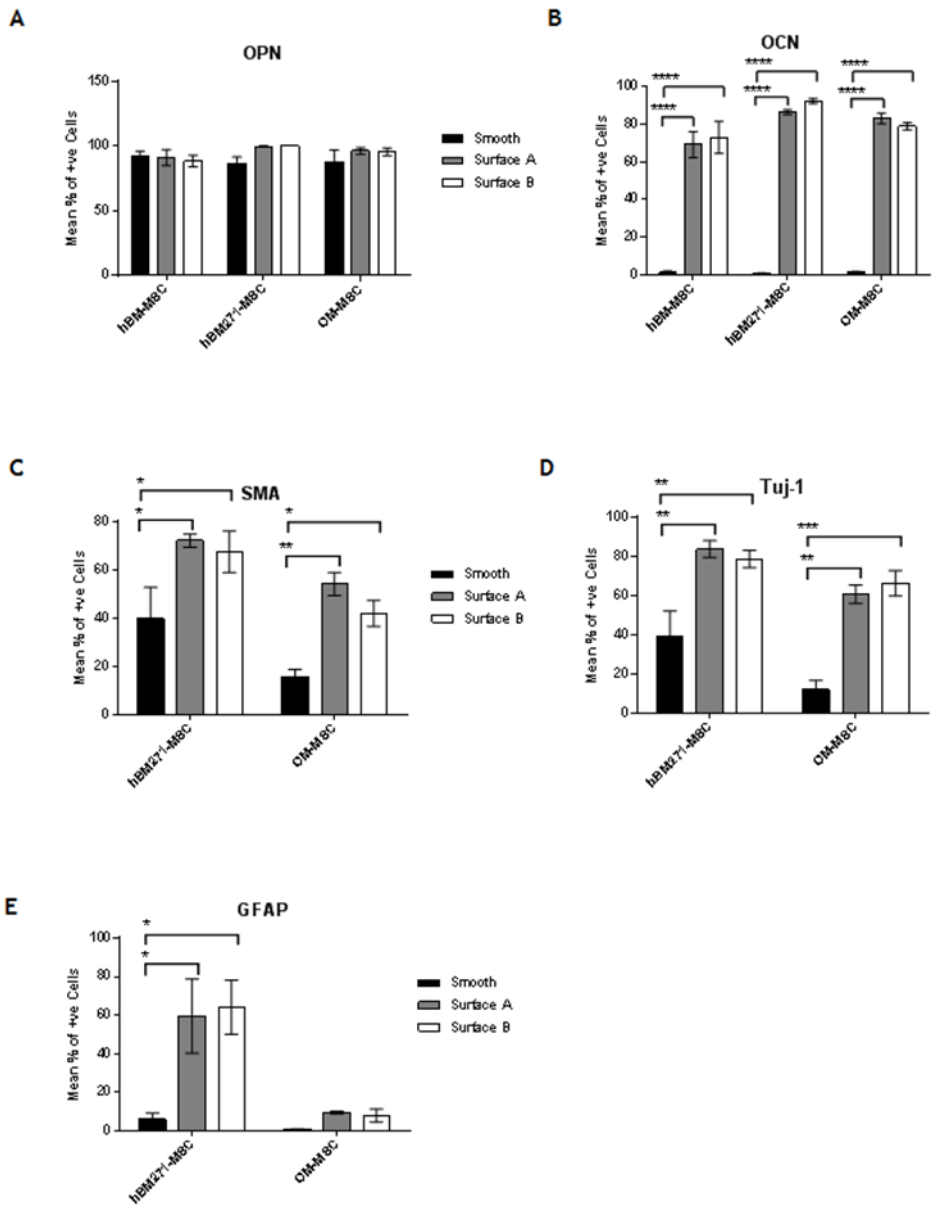

Figure 4.5: Graphical representations of immunocytochemistry for BM-MSCs (OPN and OCN only), BM271-MSCs, and OM-MSCs seeded onto

nanotopographically embossed PCL substrates A and B, and smooth surface controls. Markers of osteogenic differentiation, OPN (A) and OCN (B), myogenic differentiation, SMA (C) and MyoD (no MyoD-IR obeserved), neurogenic differentiation, Tuj-1 (D) and MAP2 (no MAP2-IR observed), and glial differentiation, GFAP (E) were used to identify protein expression. Analysis was carried out by calculating the mean number of positively expressing cells per image. Statistical analysis was carried out by 2 way ANOVA using Tukey's multiple comparison test, where *=p<0.05, **=p<0.01, ***=p<0.005, and ****=p<0.001, n=3.

4.3.2. Cell vs. Cell Comparison

When analysing the immunocytochemistry data from this perspective, similar patterns were observed as were seen when comparing substrate vs substrate. All statistical analysis is summarised in tables 4.11-4.13, and showed that when analysing intensity of IR expression, BM-derived MSCs showed significantly higher immunoreactivity of each marker where IR was observed (no MyoD or MAP2-IR was observed) compared to OM-MSCs (Figure 4.6). With regards to bone markers OPN and OCN, BM-MSCs demonstrated a significantly higher IR expression compared to both BM271-MSCs and OM-MSCs (Figure 4.6A and B), suggesting that the ability of BM-MSCs to express OPN-IR and OCN-IR may be affected by the CD271 positive selection process. Due to the expression under normal conditions of OPN-IR, SMA-IR, and Tuj-1-IR, no significant difference was observed between the percentage of IR positive BM-MSCs, BM271-MSCs, and OM-MSCs, although expression was noticeably higher in BM271-MSCs for SMA-IR and Tuj-1-IR (Figure 4.7A, C, and D). The only significant difference in OCN-IR expression between the phenotypes was observed in BM271-MSCs compared to BM-MSCs (figure 4.7B), which goes against what was earlier hypothesised. Finally, GFAP-IR was observed in a significantly higher percentage of BM2721-MSCs compared to OM-MSCs.

These findings back up the substrate vs substrate observations, and the RT-qPCR analysis, which suggests that BM-MSCs have more bioactive potential

compared to both BM271-MSCs and OM-MSCs when cultured on controlled disordered nanotopographies compared to smooth surfaces, although all three show significantly increased bioreactivity using both RT-qPCR and immunocytochemistry.

Smooth				
		Statistical Significance		
Marker	Analysis	BM-MSC vs BM271-MSC	BM-MSC vs OM-MSC	BM271-MSC vs OM-MSC
OPN	IR Intensity	NS	NS	NS
	% Positive Cells	NS	NS	NS
OCN	IR Intensity	NS	NS	NS
	% Positive Cells	NS	NS	NS
Tuj-1	IR Intensity	N/A	N/A	NS
	% Positive Cells	N/A	N/A	NS
MAP2	IR Intensity	No Immunoreactivity Observed		
	% Positive Cells			
MyoD	IR Intensity			
	% Positive Cells			
SMA	IR Intensity	N/A	N/A	NS
	% Positive Cells	N/A	N/A	NS
GFAP	IR Intensity	N/A	N/A	NS
	% Positive Cells	N/A	N/A	NS

Table 4.11: Statistical analysis of data from Figures 4.6 and 4.7 comparing intensity of IR expression and percentage of IR positive cells expressing markers related to osteogenic (OPN (Figure 4.6A and 4.7A)) and OCN (Figures 4.6B and 4.7B)), neurogenic (Tuj-1 (Figures 4.6C and 4.7C)), myogenic (SMA (Figures 4.6D and 4.7D)), and glial (GFAP (Figures 4.6E and 4.7E)) differentiation. Statistical analysis was carried out by comparing intensity of IR expression, and percentage of IR positive cells cultured on smooth surface topographies for 21 days, comparing BM-MSCs vs BM271-MSCs, BM-MSCs vs OM-MSCs, and BM271-MSCs vs OM-MSCs. Statistical analysis was carried out by 2 way ANOVA using Tukey's multiple comparison test, where ns = not significant, *=$p<0.05$, **=$p<0.01$, ***=$p<0.005$, and ****=$p<0.001$.

Surface A				
		Statistical Significance		
Marker	Analysis	BM-MSC vs BM271-MSC	BM-MSC vs OM-MSC	BM271-MSC vs OM-MSC
OPN	IR Intensity	**	****	*
	% Positive Cells	NS	NS	NS
OCN	IR Intensity	NS	NS	NS
	% Positive Cells	*	NS	NS
Tuj-1	IR Intensity	N/A	N/A	***
	% Positive Cells	N/A	N/A	NS
MAP2	IR Intensity	No Immunoreactivity Observed		
	% Positive Cells			
MyoD	IR Intensity			
	% Positive Cells			
SMA	IR Intensity	N/A	N/A	****
	% Positive Cells	N/A	N/A	NS
GFAP	IR Intensity	N/A	N/A	*
	% Positive Cells	N/A	N/A	*

Table 4.12: Statistical analysis of data from Figures 4.6 and 4.7 comparing intensity of IR expression and percentage of IR positive cells expressing markers related to osteogenic (OPN (Figure 4.6A and 4.7A)) and OCN (Figures 4.6B and 4.7B)), neurogenic (Tuj-1 (Figures 4.6C and 4.7C)), myogenic (SMA (Figures 4.6D and 4.7D)), and glial (GFAP (Figures 4.6E and 4.7E)) differentiation. Statistical analysis was carried out by comparing intensity of IR expression, and percentage of IR positive cells cultured on surface A topographies for 21 days, comparing BM-MSCs vs BM271-MSCs, BM-MSCs vs OM-MSCs, and BM271-MSCs vs OM-MSCs. Statistical analysis was carried out by 2 way ANOVA using Tukey's multiple comparison test, where ns = not significant, *=$p<0.05$, **=$p<0.01$, ***=$p<0.005$, and ****=$p<0.001$.

Surface B				
		Statistical Significance		
Marker	Analysis	BM-MSC vs BM271-MSC	BM-MSC vs OM-MSC	BM271-MSC vs OM-MSC
OPN	IR Intensity	NS	****	*
	% Positive Cells	NS	NS	NS
OCN	IR Intensity	NS	*	NS
	% Positive Cells	**	NS	NS
Tuj-1	IR Intensity	N/A	N/A	****
	% Positive Cells	N/A	N/A	NS
MAP2	IR Intensity	No Immunoreactivity Observed		
	% Positive Cells			
MyoD	IR Intensity			
	% Positive Cells			
SMA	IR Intensity	N/A	N/A	****
	% Positive Cells	N/A	N/A	NS
GFAP	IR Intensity	N/A	N/A	*
	% Positive Cells	N/A	N/A	*

Table 4.13: Statistical analysis of data from Figures 4.6 and 4.7 comparing intensity of IR expression and percentage of IR positive cells expressing markers related to osteogenic (OPN (Figure 4.6A and 4.7A)) and OCN (Figures 4.6B and 4.7B)), neurogenic (Tuj-1 (Figures 4.6C and 4.7C)), myogenic (SMA (Figures 4.6D and 4.7D)), and glial (GFAP (Figures 4.6E and 4.7E)) differentiation. Statistical analysis was carried out by comparing intensity of IR expression, and percentage of IR positive cells cultured on surface B topographies for 21 days, comparing BM-MSCs vs BM271-MSCs, BM-MSCs vs OM-MSCs, and BM271-MSCs vs OM-MSCs. Statistical analysis was carried out by 2 way ANOVA using Tukey's multiple comparison test, where ns = not significant, *=$p<0.05$, **=$p<0.01$, ***=$p<0.005$, and ****=$p<0.001$.

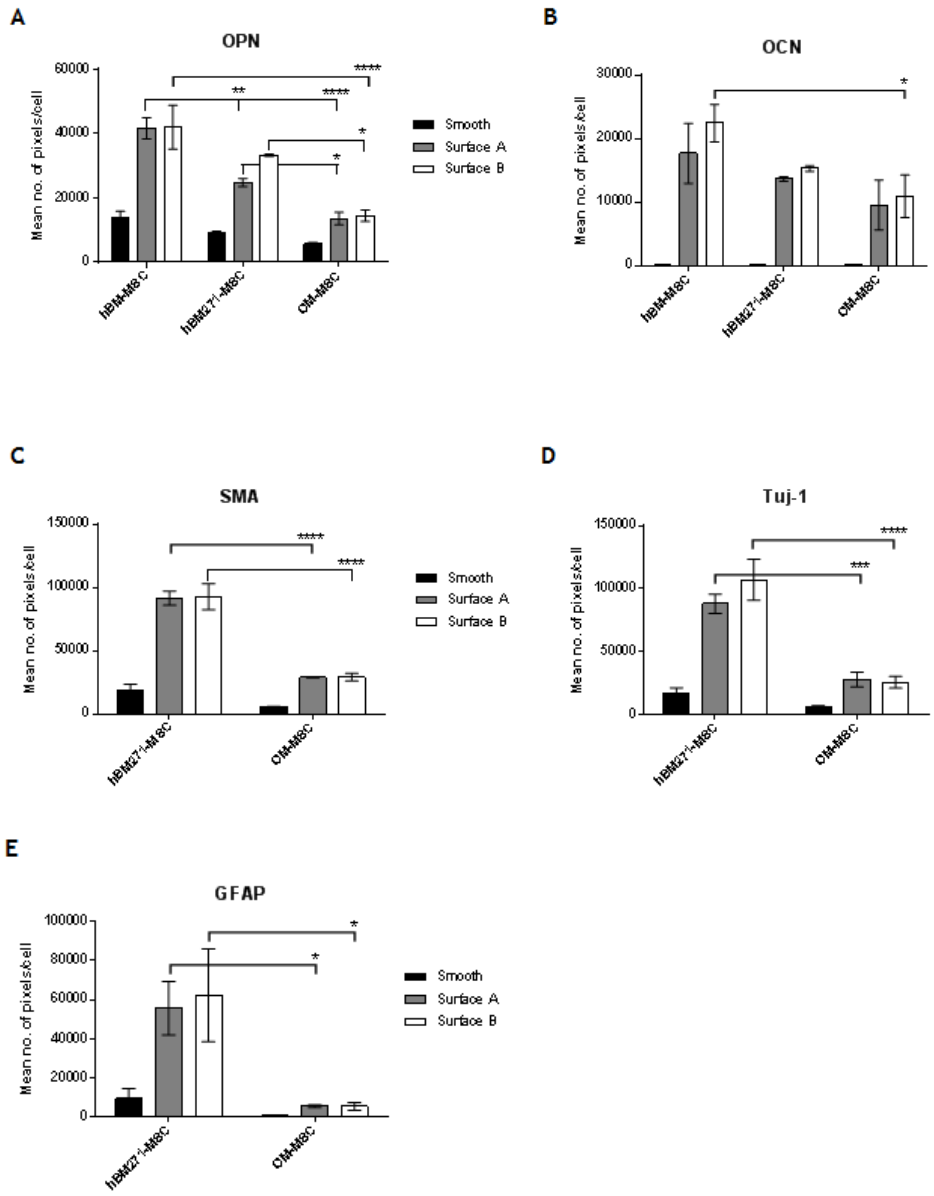

Figure 4.6: Figure 4.4 data with a statistical focus of a cell-cell comparison as opposed to a substrate-substrate comparison. Analysis was carried out using ImageJ software by measuring intensity of fluorescence by counting the mean number of fluorescent pixels per cell per image. Statistical analysis was carried out by 2 way ANOVA using Tukey's multiple comparison test, where *=p<0.05, **=p<0.01, ***=p<0.005, and ****=p<0.001. n=3.

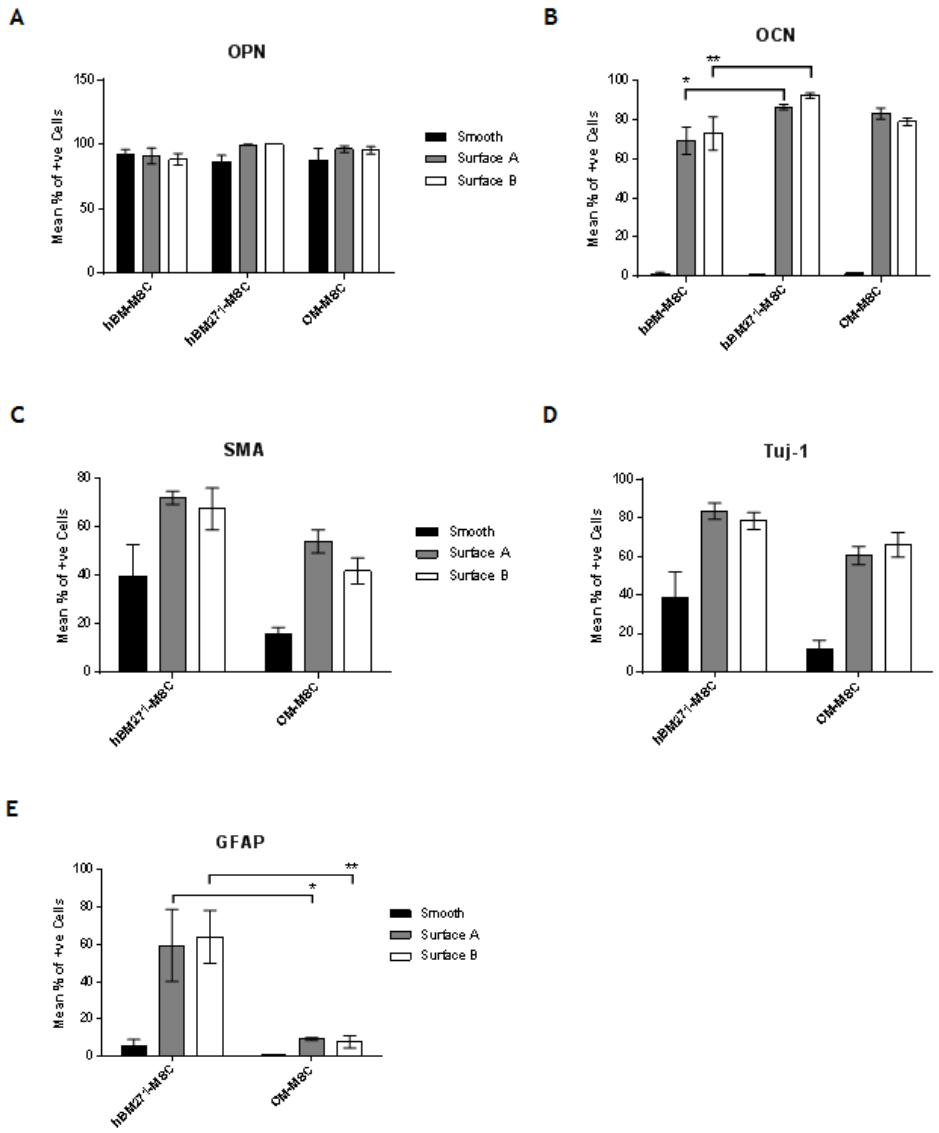

Figure 4.7: Figure 4.5 data with a statistical focus of a cell-cell comparison as opposed to a substrate-substrate comparison. Analysis was carried out using ImageJ software by measuring intensity of fluorescence by counting the mean number of fluorescent pixels per cell per image. Statistical analysis was carried out by 2 way ANOVA using Tukey's multiple comparison test, where *=p<0.05, **=p<0.01, ***=p<0.005, and ****=p<0.001. n=3.

4.4. Transcriptional Analysis of the Expression of Classic MSC Markers in BM-MSCs and OM-MSCs when Cultured on Nanotopographically Embossed PCL

To determine whether the observed increases in protein expression were in fact due to differentiation of the MSCs, we cultured BM-MSCs, BM271-MSCs, and OM-MSCs on the same nanotopographically embossed PCL substrates under the same conditions as in experiments 4.2 and 4.3. mRNA was collected and analysed as in experiment 4.2, excepting that transcripts analysed were typical MSC markers instead of differentiation markers. Levels of CD90, CD166, and Nestin were used as additional indicators of differentiation, as they are typical MSC markers whose expression is lost during differentiation (284-286, 351-353).

As observed in chapter three, expression of CD90, CD166, and Nestin at day 1 was expressed at higher levels in MSCs derived from the OM compared to those derived from BM, with little difference in expression of either marker in BM and BM271-MSCs (Figure 4.8). By day 7, expression of each marker had decreased significantly compared to day 1 levels across each of the three substrates, and expression continued to decrease with time until levels were negligible by day 21 ($p<0.01$ – $p<0.001$) (Figure 4.8). Expression levels of each marker were also much lower on patterned surfaces compared to smooth surface controls across each time point, although due to sample variation, these differences weren't always statistically significant (Figure 4.8). Levels of mRNA for CD90 expressed in BM-MSCs, BM271-MSCs, and OM-MSCs were significantly lower ($p<0.01$) in cells cultured on patterned surfaces compared to controls at each time point, except for in OM-MSCs at day 21, by which point levels of CD90 mRNA were very low (Figures 4.8A and B). Levels of nestin mRNA expression were significantly decreased in BM-MSCs cultured on patterned surfaces compared to controls at days 7 and 14 ($p<0.01$), and in BM271-MSCs cultured on patterned surfaces compared to controls at day 14 ($p<0.01$). All other differences in the expression of Nestin mRNA between patterned and smooth surfaces were not statistically significant (Figures 4.8E and F).

There were also marked decreases in the expression of CD166 mRNA in each MSC type cultured on patterned surfaces compared to smooth surface controls at each time point, although due to sample variation, these differences weren't statistically significant (Figures 4.8G and H).

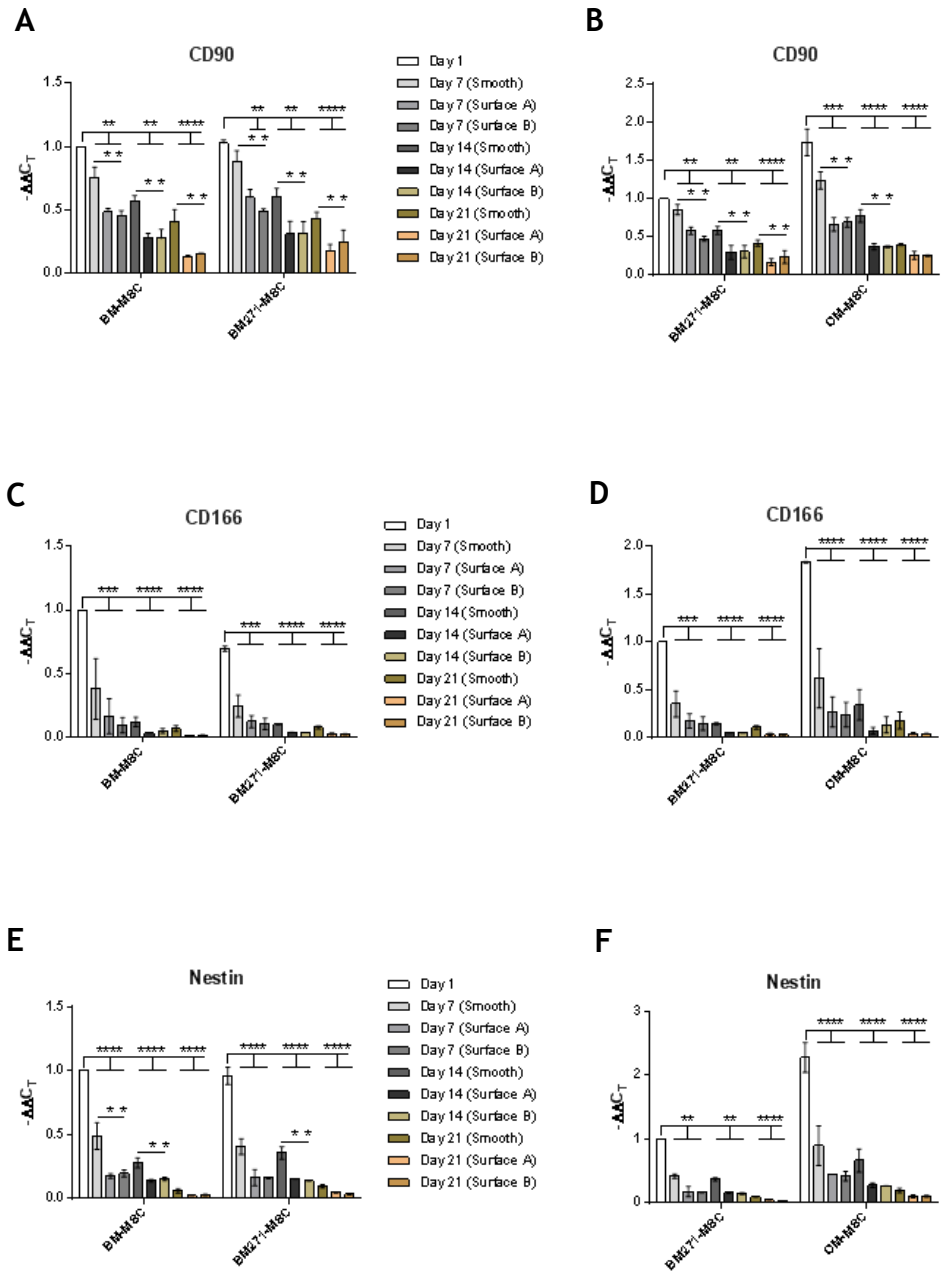

Figure 4.8: Graphical representations of RT-qPCR carried out on BM-MSCs, BM271-MSCs, and OM-MSCs cultured on smooth surface PCL, and PCL embossed with surface A and surface B nanotopographies for 21 days. Each

condition was analysed for MSC-related mRNA markers; CD90 (A-B), CD166 (C-D), and Nestin (E-F), and comparison was of BM-MSCs vs BM271-MSCs (A, C, and E) using the BM-MSC Day 1 condition as the point of comparison, and BM271-MSCs vs OM-MSCs (B, D, and F) using the BM271-MSC condition as the point of comparison. Statistical analysis was carried out by 2 way ANOVA using Tukey's multiple comparison test, where *=$p<0.05$, **=$p<0.01$, ***=$p<0.005$, and ****=$p<0.001$. PCR was carried out using the Livak ($\Delta\Delta CT$) method with GAPDH as the reference control gene, n=3.

4.6. Discussion

Previous studies have shown that nanotopographies of a controlled disordered pattern can stimulate osteoprogenitors to differentiate towards mature calcified bone cells (256, 354, 355), and have also suggested that this may be possible with bone marrow-derived MSCs (257, 346). The experiments in this chapter were designed to confirm whether this substrate induced osteogenic differentiation is possible in my BM-MSCs, BM271-MSCs, and OM-MSCs. From the data compiled throughout this chapter we can also see whether CD271 selected BM-MSCs behave in a similar manner to non-selected BM-MSCs, and whether or not there are any other differentiation mechanism taking place via these cell/substrate interactions.

Intially, the nanotopographies of the PCL substrates to be used throughout these experiments were confirmed. Using shims from previous studies which produced controlled disordered nanotopographies with pit heights of 16 nm (surface A) and 18 nm (surface B) (257), PCL was embossed and analysed using atomic force microscopy (AFM). This AFM analysis determined that surfaces A and B were both DNSQ and distinct in pit height, but pit heights were measured at 25 nm and 20 nm respectively. Non-embossed smooth surface controls were confirmed as being without any pattern.

BM-MSCs, BM271-MSCs, and OM-MSCs were cultured on these substrates and levels of mRNA analysed for changes in levels of differentiation markers for fat, bone, neuron, muscle, and glia. Levels of all transcripts were stimulated to some degree in cells cultured on the patterned surfaces compared to non-patterned controls, and in most cases to significant levels at later time points. This stimulation was much greater and in most cases significantly different in BM-derived MSCs compared to OM-derived MSCs, with there being little difference in expression of any transcript between BM-MSCs and BM271-MSCs. These findings were unexpected however. Upregulation of mRNA can suggest a measure of protein changes, and thus changes in function, but this clearly wasn't the case here. mRNA markers of adipogenesis, myogenesis, and neurogenesis were upregulated by the cell's interactions with the nanotopographies, but were not translated to their respective proteins. The MSCs seemed to be undergoing a certain differentiation but this was more likely to be towards a single lineage rather than multiple. The ability of controlled disordered nanotopographies to induce osteogenic differentiation is well documented (256, 257, 346, 354, 355). These studies, and others looking at genetic changes in MSCs during osteogenic differentiation (356-359) show a downregulation of indicators of other lineages of differentiation. This could suggest that the markers of differentiation used were perhaps not the most appropriate, i.e. GLUT4 and Leptin transcripts were stimulated by surfaces A and B but no fat droplets were observed to suggest any adipogenic differentiation had occurred.

Immunocytochemistry showed that as well as their respective transcripts, levels of OPN-IR, OCN-IR, Tuj-1-IR, SMA-IR, and GFAP-IR were also stimulated, suggesting that these transcripts were translated to increased protein expression. Expression of OPN-IR and OCN-IR, both bone differentiation markers, was significantly increased in each MSC type cultured on patterned PCL surfaces, with BM-derived MSCs showing much greater immunoreactive intensity and percentage of immunoreactive positive cells compared to OM-MSCs. Tuj-1 and SMA, although often

considered to be neuronal and myogenic differentiation markers respectively (360-364), are also quite ubiquitous structural proteins which are naturally present in undifferentiated MSCs (365-371). Their increase in expression doesn't necessarily suggest differentiation towards neuronal or myogenic lineages, but may be due to a cytoplasmic structural reorganisation that is occurring during osteogenic differentiation. This was seen by Chetakun *et al.* (372) who demonstrated an upregulation in ECM and skeletal proteins Tenascin and Fibronectin during osteogenesis, alongside bone-related proteins OPN, Bone Sialoprotein (BSP), and Bone Morphogenic Protein (BMP). Although GFAP is widely considered a classic glial marker (373, 374), previous studies have also identified that GFAP expression is stimulated during osteogenic differentiation (374), which would account for the observed increase in GFAP expression. Like with OPN and OCN, the observed increases in Tuj-1, SMA, and GFAP were significantly more pronounced in BM-derived MSCs compared to OM-MSCs. The observed increases in MAP2 and MyoD transcripts were not seen to be translated to their respective proteins. These proteins are specific markers of neuronal and myogenic differentiation, and their absence suggests that trans-differentiation may not have occurred in these MSCs via this particular mechanism, and that the up-regulation of Tuj-1 and GFAP may be related to the osteogenic differentiation that has more likely occured. This lack of translation seems inefficient but may be due to an absence of the required transcription factors.

To further confirm that differentiation has occurred, transcripts were analysed using classic MSC markers CD90, CD166, and Nestin which are lost during differentiation (284-286, 351-353). This analysis confirmed that expression of these transcripts was significantly decreased in each MSC type cultured on patterned surfaces compared to undifferentiated MSCs. This decrease in expression of these transcripts was very pronounced and continued over time until only negligible levels were observed by day 21.

These experiments collectively confirm that PCL substrates nanotopographically embossed in a controlled disorder of 20 nm and 25 nm pit heights are capable of inducing osteogenic differentiation in BM-MSCs, BM271-MSCs, and OM-MSCs, that BM-derived MSCs are more efficient at such differentiation compared to OM-derived MSCs, and that trans-differentiation did not occur via these specific cell/substrate mechanisms.

Although there have been numerous studies into the biological effects of nanotopography on stem cell adhesion, survival, and differentiation, these have mainly been focussed on bone marrow-derived MSCs and embryonic stem cells (ESCs) (334, 375-377). Here with OM-MSCs we have introduced another potential source of autologous MSCs which display the same osteogenic capabilities as bone marrow-derived MSCs when cultured on controlled disordered nanoscale topographies. This opens the door to many more studies to determine whether indeed OM-MSCs are a viable alternative to BM-MSCs in fields such as orthopaedics where the relationship between BM-MSCs and nanotopography has proved very successful. (248, 378).

4.8. Summary

- Three separate PCL substrates were confirmed as controlled disordered surface A; relative roughness = 8.473 nm, peak to valley roughness = 81.87 nm, and mean peak height = 24.64 nm, controlled disordered surface B; relative roughness = 4.383 nm, peak to valley roughness = 33.37 nm, and mean peak height = 20.40 nm, and smooth surface control; relative roughness = 3.807.
- BM-MSCs, BM271-MSCs, and OM-MSCs cultured on both surface A and surface B nanotopographies stimulated transcript expression of a number of differentiation markers compared to those MSCs cultured on non-patterned PCL substrates. This stimulation is more pronounced, often significantly, in bone marrow-derived MSCs compared to olfactory mucosa-derived MSCs, with very little difference at all between transcript profiles of BM-MSCs and BM271-MSCs.

- Observed increases in transcript expression were not always translated into increases in protein expression. Expression of OPN-IR, OCN-IR, Tuj-1-IR, SMA-IR, and GFAP-IR was stimulated significantly in BM and OM-derived MSCs, again with BM-derived MSCs expressing these proteins with more efficacy compared to OM-derived MSCs. Each of these proteins have been associated with bone differentiation, confirming previous studies which have demonstrated an ability of DNSQ nanotopographies to stimulate bone differentiation in MSCs and osteoprogenitors.
- Observed increases in expression of non-mesenchymal transcripts MyoD and MAP2 were not translated into increases in protein expression. These findings suggest that DNSQ surfaces A and B do not stimulate trans-differentiation in either bone marrow or olfactory mucosa-derived MSCs.

Expression of typical MSC markers using CD90, CD166, and Nestin mRNA decreased significantly in each MSC type when cultured on nanotopographically embossed PCL substrates over time, confirming that the MSCs are undergoing a differentiation process via these cell/substrate interactions.

5. Dissection of the Mechanisms of the Pro-Myelinating Effect of OM-MSCs

Previous studies have identified a pro-myelinating effect elicited by OM-MSCs but not by BM-MSCs (1). To investigate the possible mechanisms which drive this effect, a number of arrays were carried out comparing not only BM271-MSCs and OM-MSCs, but also other cells from within the bone marrow and olfactory niches, as well as fibroblasts. The first part of our investigation was a comparative analysis of BM271-MSC and OM-MSC miRNA. This analysis was performed by the biomedical company Sistemic using miRNA fingerprinting techniques. The data supplied by Sistemic is covered in detail in sections 5.1.1 and 5.1.2.

Experiments in the previous two chapters detected no significant or discernible difference in profile or behaviour patterns between CD271 selected BM271-MSCs and non-selected BM-MSCs. Therefore, subsequent experiments, detailed in this chapter, compare BM271-MSCs and OM-MSCs only, with the exception of the human cytokine arrays in which the secretory profiles of a number of different cell types were compared.

5.1. Comparison of Micro RNA (miRNA) Profiles of BM271-MSCs and OM-MSCs by SistemQC™ miRNA-Based Fingerprinting

Sistemic are a registered company who specialise in a range of technologies including miRNA fingerprinting. A collaboration was instigated aimed at comparing the miRNA profiles of MSCs from bone marrow and the olfactory system to determine how related they were, and to establish if they had characteristics of MSCs. We provided lysates of BM271-MSC (n=4) and OM-MSC samples (n=4) to Sistemic, and initial studies were made on the RNA of each sample with the view of establishing the viability of the RNA, and thus the comparative similarity of the samples submitted within each phenotype (Figure 5.1). Analysis was then carried out at miRNA level to create a full profile of all miRNA present in each cell type (Appendix 3), encompassing those which were equivalently expressed (EE) between each cell type (Appendix 4), and of those which were differentially expressed

(DE) between each cell type (Figure 5.3). Once these DE miRNAs were identified, Sistemic then identified key markers of cell phenotype (KmiRs™) which may be responsible for already identified differences in behaviour between BM-derived MSCs and OM-derived MSCs, namely cell survival, proliferation, and the ability to influence axonal myelination.

The SistemQC™ miRNA-based fingerprinting assay screened each sample for a total of 1205 human adult miRNAs, and identified from these 195 which were present in both BM271 and OM-MSCs. Details of all samples used throughout this experiment can be found in Material and Methods Tables 2.13 and 2.14.

5.1.1. Validation of Sample Groups by Principle Component Analysis (data provided by Sistemic)

A 3D PCA plot was configured to determine the relationship between each sample group, and between each sample within each group (Figure 5.1). This plot is derived from variations between each sample based on the 195 miRNAs identified (microRNA-ome), and is effectively an indicator of how similar each sample is compared to each other (points within elipse), and how different each sample set is compared to the other (distance between elipses). This PCA plot shows that the samples within each sample set are similar enough, and within Sistemic's QC parameters, to be considered part of the same data set. It also shows that each sample set is different enough to be considered as two distinct sample sets.

5.1.2. Identification of EE and DE miRNAs (data provided by Sistemic)

It was important to establish not only which miRNAs are expressed in MSCs, but also those which are expressed in both BM271-MSCs and OM-MSCs, as an observed homology between the two MSC types would further support OM-MSCs as a novel and distinct MSC. Most importantly however, is to establish any miRNAs which are highly expressed in one MSC type and not the other. These DE miRNAs could contribute to some of the observed behavioural

differences between the two MSC types which have been previously outlined in this study.

Of the 195 miRNAs identified during this array, 125 were considered to be equivalently expressed in both BM271-MSCs and OM-MSCs, giving a 64% homology between the 2 cell types at a miRNA level. Within these homologous miRNAs, 27 of the 195 have been previously identified as being associated with bone marrow-derived MSCs (Figure 5.2). Of the remaining 70 miRNAs, 26 were found to be differentially expressed between BM271 and OM-MSCs (Figure 5.3), leaving 44 which were in a statistical "grey area" in which the difference between expression of these miRNAs was too great to be considered equivalent, and too small to be considered differential. Of the 26 DE miRNAs, 16 were down-regulated in OM-MSCs compared to BM271-MSCs, and three were particularly identified in the Sistemic report as being associated with myelination (miR-140-5p), cell survival (miR-146a-5p), and proliferation (miR-335-5p) from previous studies (379-383). A full list of differentially expressed miRNAs and their relative fold changes can be found in Table 5.1.

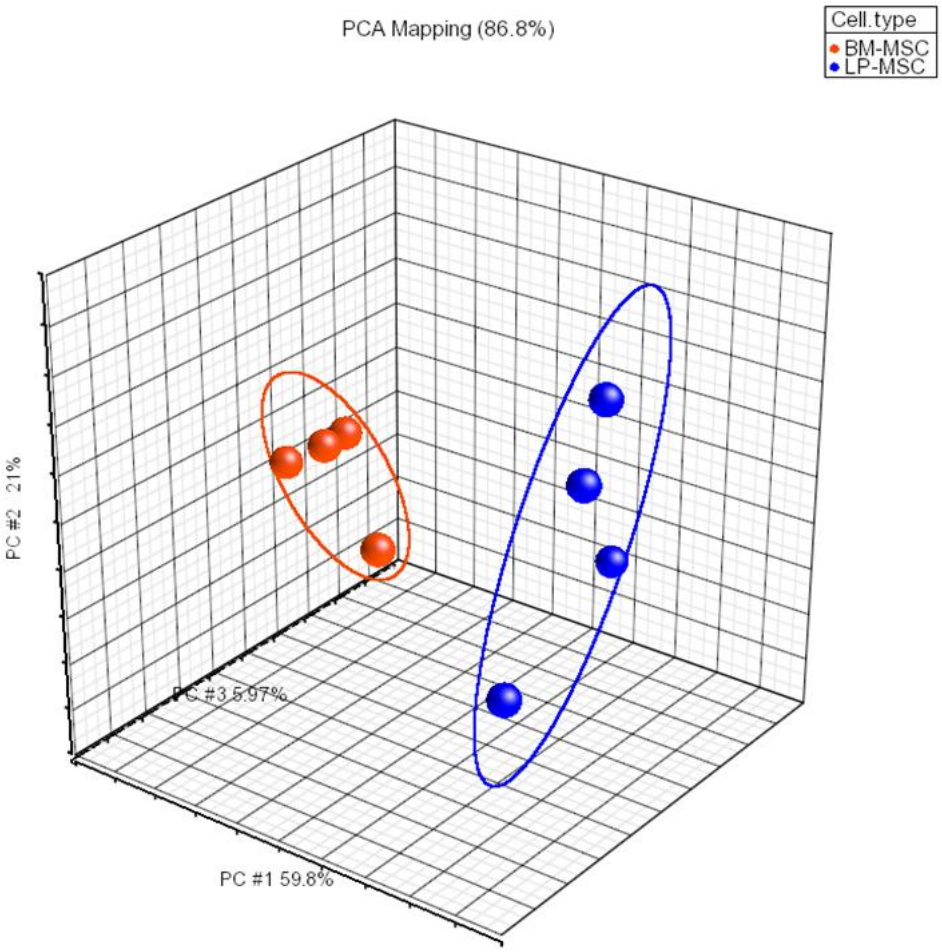

Figure 5.1: Principal Component Analysis (PCA) comparison of n=4 samples from both BM271-MSC and OM-MSC groups based on all 195 detected miRNAs in the Sistemic miRNA array. The ellipse around each sample set captures how much variation there is in each of the Principal Component Scores for each group. The centre of the ellipse is the mean PCA score for the first and second components for that cell group while the circumference represents points in the plane which are 2 standard deviations away from the centre. This Figure 3.1 was taken directly from Sistemic's final report.

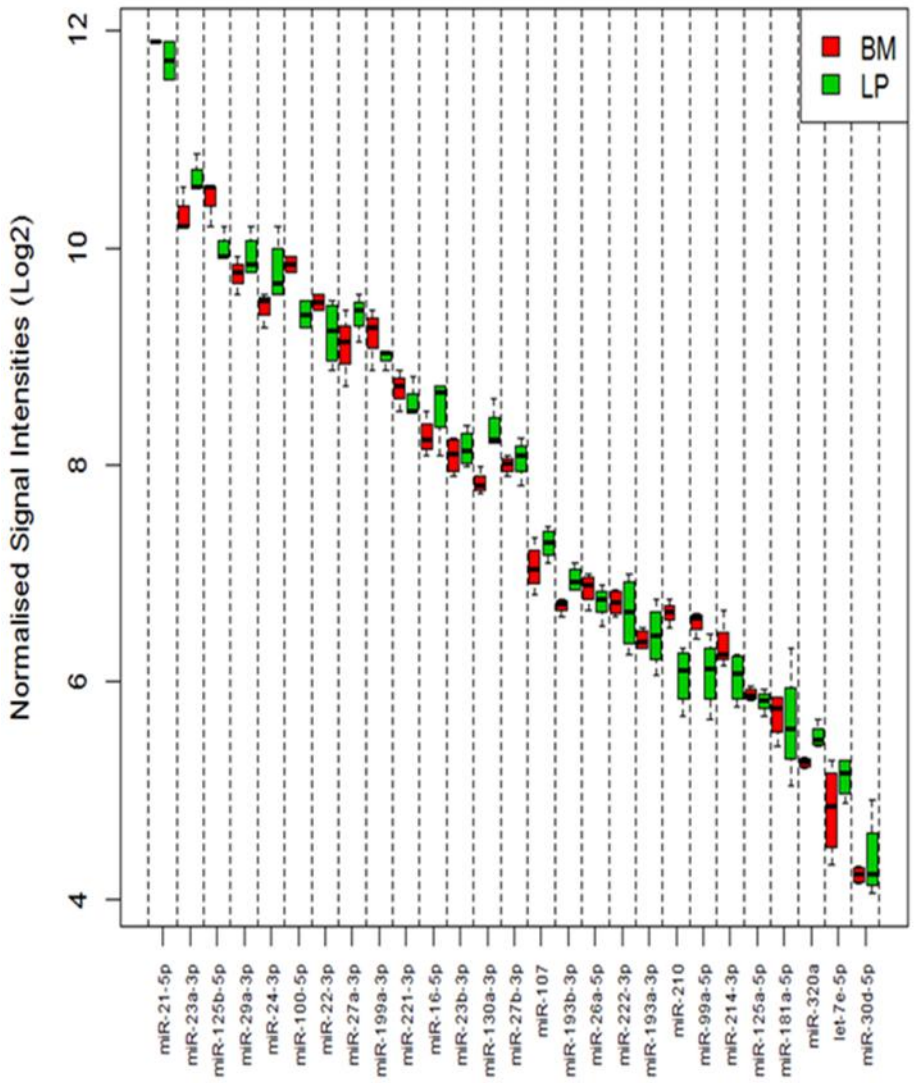

Figure 5.2: Box plot representation taken from Sistemic's final report, showing the 27 of the 125 miRNAs which were equivalently expressed (EE) between n=4 BM-MSCs and OM-MSCs (shown here as LP-MSCs) which have been shown in previous studies (Guo et al., 2011; Gao et al., 2011) to be consistently expressed in BM-MSCs. The full list of the 125 EE miRNAs can be found in Appendix 4. Significance was called at $p_{FDR} < 0.05$ and an absolute fold-change (FC) = 1.5 (i.e. the allowed 'equivalence range').

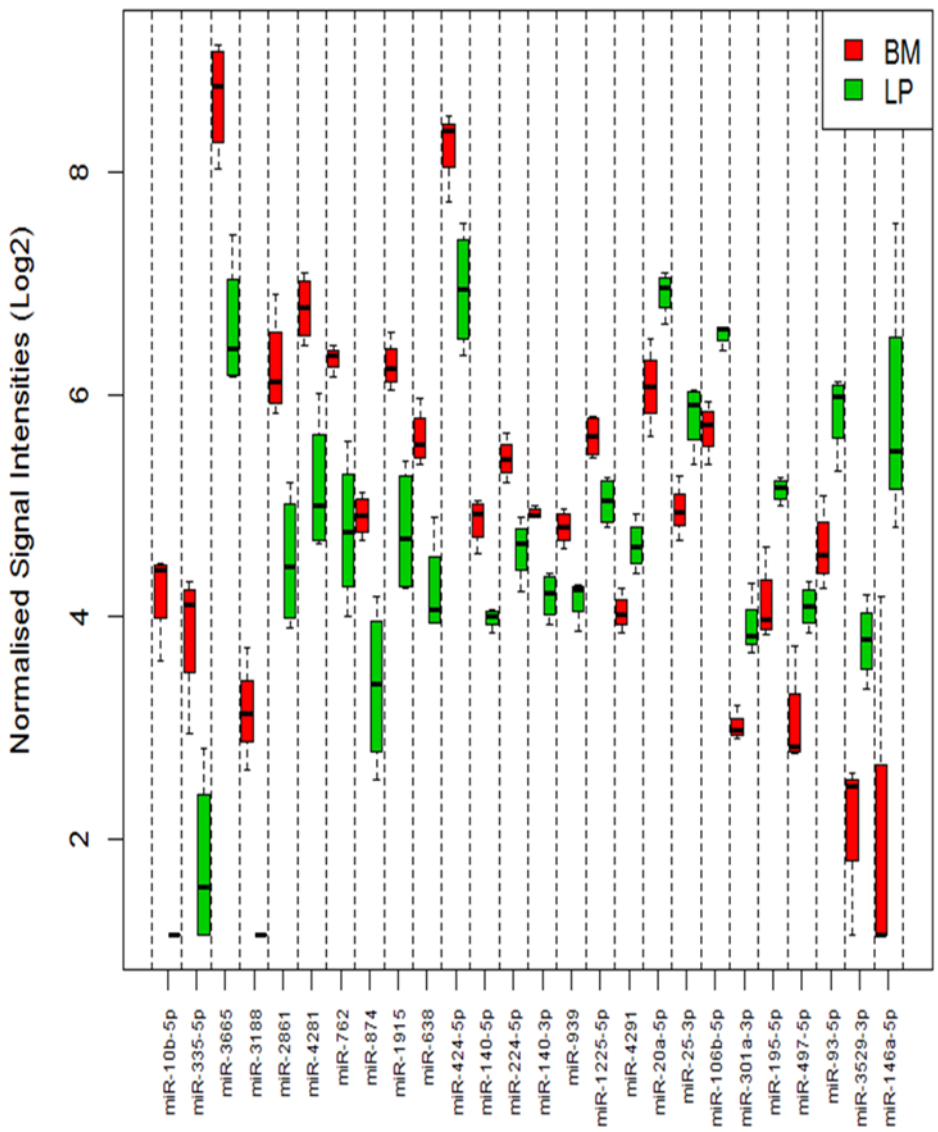

Figure 5.3: Box plot representation taken from Sistemic's final report, showing the 26 miRNAs which were differentially expressed (DE) between n=4 BM-MSCs and OM-MSCs (shown here as LP-MSCs). Significance was called at $p_{FDR} < 0.05$ and an absolute fold-change (FC) = 1.5 (i.e. the allowed 'equivalence range').

miRNA	pFDR*	Fold Change (FC)**	miRNA	pFDR*	Fold Change (FC)**
hsa-miR-10b-5p	0.0012	8.5189	hsa-miR-140-3p	0.0216	1.6697
hsa-miR-335-5p	0.0405	4.2807	hsa-miR-939	0.0304	1.5646
hsa-miR-3665	0.0304	4.2122	hsa-miR-1225-5p	0.0405	1.5027
hsa-miR-3188	0.011	4.0233	hsa-miR-4291	0.0405	-1.5192
hsa-miR-2861	0.0405	3.3465	hsa-miR-20a-5p	0.0405	-1.7979
hsa-miR-4281	0.0402	3.0499	hsa-miR-25-3p	0.0405	-1.798
hsa-miR-762	0.0405	2.9282	hsa-miR-106b-5p	0.0216	-1.8071
hsa-miR-874	0.0405	2.9067	hsa-miR-301a-3p	0.0304	-1.86
hsa-miR-1915	0.0365	2.828	hsa-miR-195-5p	0.0304	-2.057
hsa-miR-638	0.0304	2.5847	hsa-miR-497-5p	0.0405	-2.0666
hsa-miR-424-5p	0.0405	2.4546	hsa-miR-93-5p	0.0365	-2.3525
hsa-miR-140-5p	0.0151	1.8377	hsa-miR-3529-3p	0.0405	-3.0606
hsa-miR-224-5p	0.0365	1.7639	hsa-miR-146a-5p	0.0405	-15.2891

* False Discovery Rate (p value), calculated by Benjamini and Hochberg method

** Fold change in expression from BM-MSCs vs OM-MSCs

Table 5.1: List of each of the 26 miRNAs which were differentially expressed (DE) between n=4 BM-MSCs and OM-MSCs. Highlighted miRNAs miR-140-5p, miR-335-5p, and miR-146a-5p have been previously associated with the regulation of myelination, cell proliferation, and cell survival respectively, three mechanisms that have previously been noted as being different in BM-MSCs compared to OM-MSCs, and will therefore be the focus of the study forthwith.

5.1.3. Confirmation of DE miRNAs; miR-140-5p, miR-146a-5p, and miR-335-5p by RT-qPCR

From the list of 26 DE miRNAs, subsequent analysis will be focusing on the three DE miRNAs; miR-140-5p, miR-146a-5p, and miR-335-5p, which are

most pertinent to previously observed behavioural differences between BM271 and OM-MSCs; myelination, cell survival, and proliferation respectively. To confirm Sistemic's findings, RT-qPCR was carried out on each of the samples analysed by Sistemic using the standard curve method to determine the levels of miR-140-5p, miR-146a-5p, and miR-335-5p in each sample, and also the fold increases/decreases of expression in BM271-MSCs compared to OM-MSCs (Figure 5.4). Each RT-qPCR assay passed the minimum standard curve requirement of an r^2 value of >0.95 (each standard curve can be found in Figures 5.4 B, D, and F). A summary of the differential expression and fold increases can be found in Table 5.2, the results of the RT-qPCR were as follows:

The expression of miR-140-5p in OM-MSCs varied from ~1 to ~7 ng/sample, giving a mean value of 5.4 ng/sample (2.7 ng/µL). This was compared to expression in BM271-MSCs which varied from ~7 to ~28 ng/sample, with a mean value of 16.3 ng/sample (8.15 ng/µL). This difference was statistically significant ($p<0.05$) (Figure 5.4A), and gave a mean fold increase in expression of 3.66 in BM271-MSCs compared to OM-MSCs (Figure 5.4G).

The expression of miR-146a-5p in OM-MSCs varied from ~10 to ~50 ng/sample, giving a mean value of 26.5 ng/sample (13.25 ng/µL). This was compared to expression in BM271-MSCs which varied from ~1 to ~8 ng/sample, with a mean value of 3.3 ng/sample (1.65 ng/µL). This difference was statistically significant ($p<0.05$) (Figure 5.4C), and gave a mean fold decrease in expression of 15.45 in BM271-MSCs compared to OM-MSCs (Figure 5.4G).

The expression of miR-335-5p in OM-MSCs varied from ~2 to ~4 ng/sample, giving a mean value of 3.1 ng/sample (1.55 ng/µL). This was compared to expression in BM271-MSCs which varied from ~11 to ~34 ng/sample, with a mean value of 17.3 ng/sample (8.65 ng/µL). This difference was statistically significant ($p<0.05$) (Figure 5.4E), and gave a mean fold

increase in expression of 7.60 in BM271-MSCs compared to OM-MSCs (Figure 5.4G).

These data, although giving slightly different values to Sistemic's data, showed similar expression patterns to those found by Sistemic, and is therefore confirmation of their findings of differential expression of these miRNAs in BM271-MSCs compared to OM-MSCs.

miRNA	Phenotype	Minimum Quantity (ng)	Maximum Quantity (ng)	Mean Quantity (ng)	Fold Increase in BM271-MSCs
miR-140-5p	BM271-MSC	6.83	27.93	16.26	3.66
	OM-MSC	1.12	6.76	5.40	
miR-146a-5p	BM271-MSC	1.14	7.71	3.31	-15.45
	OM-MSC	9.83	49.64	26.45	
miR-335-5p	BM271-MSC	10.73	33.58	17.32	7.60
	OM-MSC	1.81	4.37	3.07	

Table 5.2: Summary of RT-qPCR analysis on BM271-MSCs and OM-MSCs outlined in section 3.1.3. showing minimum, maximum, mean, and fold change values regarding the expression of miR-140-5p, miR-146a-5p, and miR-335-5p in each phenotype.

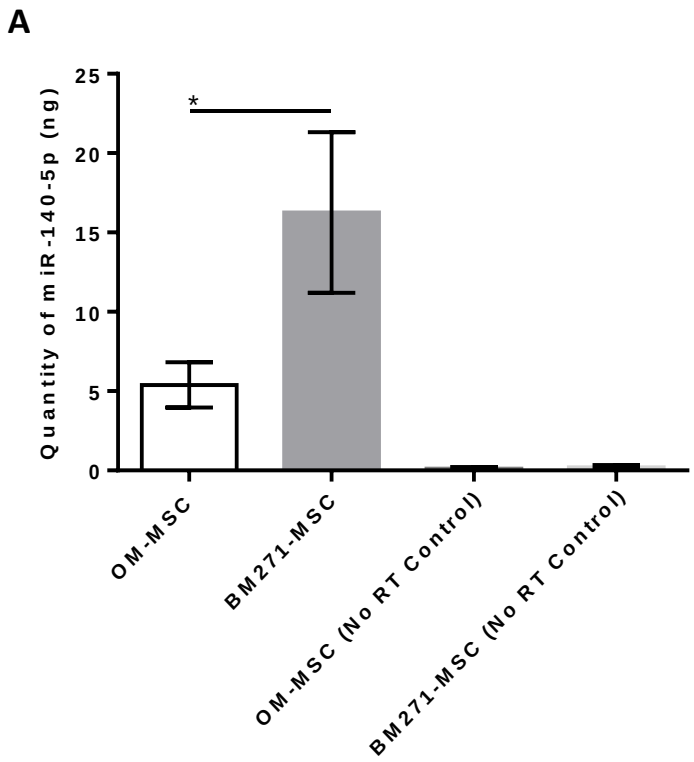

B

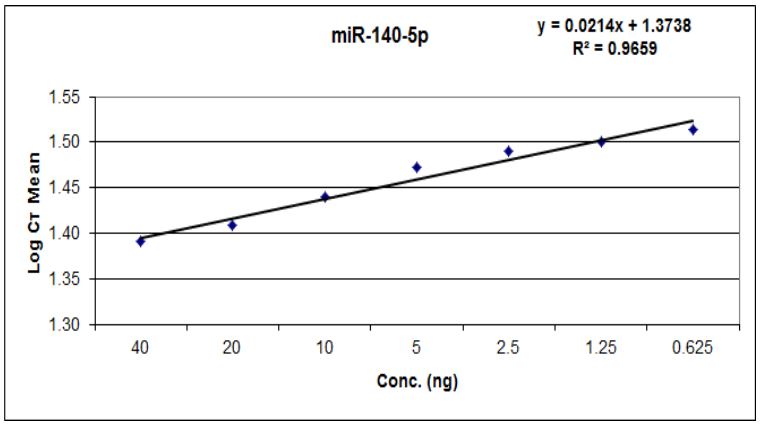
miR-140-5p
y = 0.0214x + 1.3738
R² = 0.9659
Log CT Mean
1.55
1.50
1.45
1.40
1.35
1.30
40
20
10
5
2.5
1.25
0.625
Conc. (ng)

C

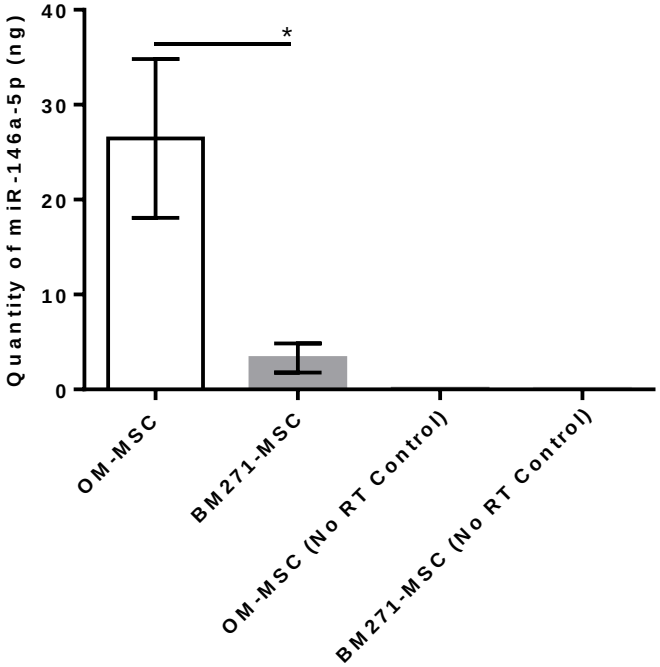
Quantity of miR-146a-5p (ng)
40
30
20
10
0
*
OM-MSC
BM271-MSC
OM-MSC (No RT Control)
BM271-MSC (No RT Control)

D

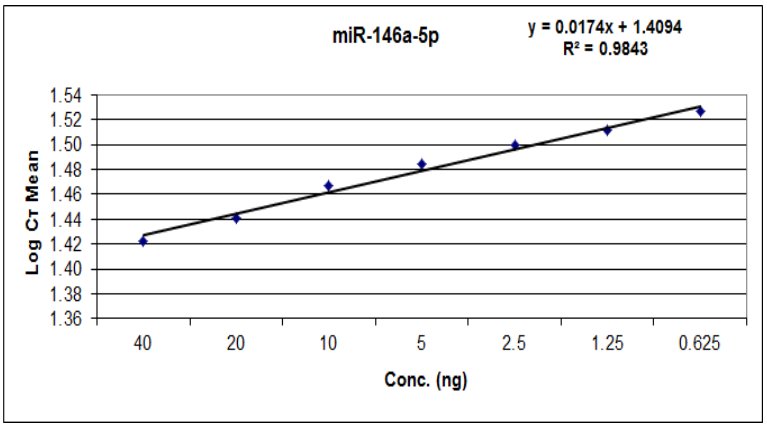
miR-146a-5p
y = 0.0174x + 1.4094
R² = 0.9843
Log CT Mean
1.54
1.52
1.50
1.48
1.46
1.44
1.42
1.40
1.38
1.36
40
20
10
5
2.5
1.25
0.625
Conc. (ng)

E

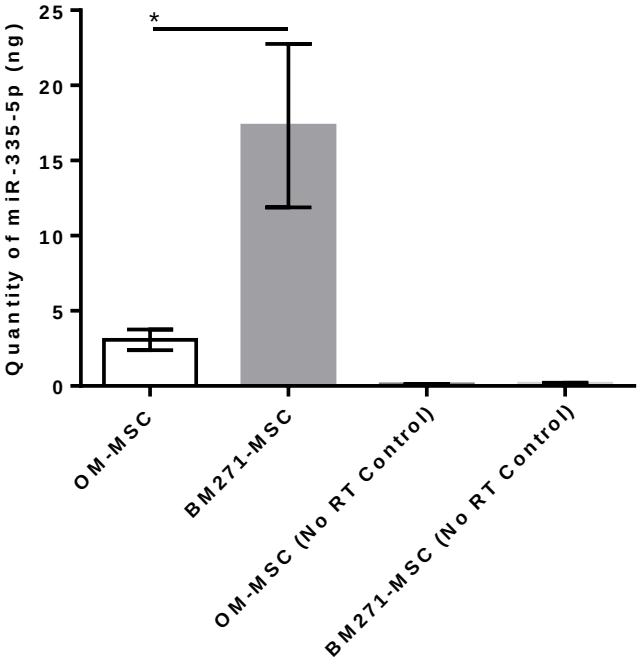
Quantity of miR-335-5p (ng)
25
20
15
10
5
0
*
OM-MSC
BM271-MSC
OM-MSC (No RT Control)
BM271-MSC (No RT Control)

F

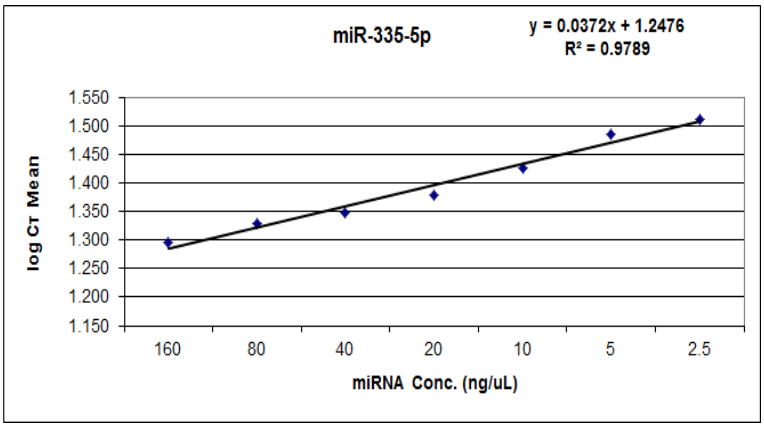

G

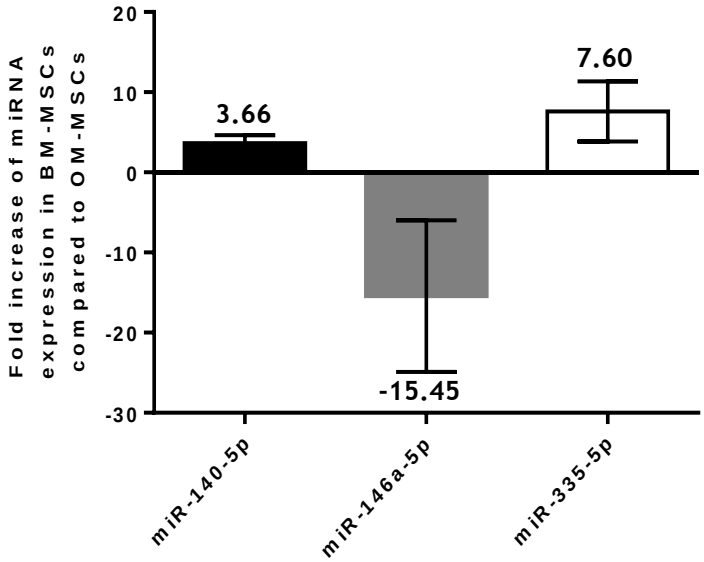

Figure 5.4: RT-qPCR analysis confirming Sistemics' findings of differential expression of miRNAs miR-140-5p (A), miR-335-5p (C), and miR-146a-5p (E) between BM271-MSCs and OM-MSCs. RT-qPCR was carried out using the standard curve method, and the standard curves from which the miRNA values were extrapolated are shown (B, D, and F), showing y-intercept, gradient, and R^2 values. Fold increases/decreases in expression of each of the miRNAs in BM271-MSCs relative to OM-MSCs are shown in graph G.

Statistical analysis was carried out using a two-tailed ratio paired t-test, where *=p<0.05. n=4 different biological samples.

5.2. Comparative analysis of chemokine/cytokine expression in media collected from BM-MSC and OM-MSCs

MSCs, as well as their function as precursors to cells from the mesenchymal lineage, can also play an immunoregulatory role throughout the body (214, 384-386). They are known to secrete a vast number of signalling molecules such as growth factors and chemokines which attract and modulate a range of different cells via chemotaxis to help repair and regenerate their niche (387-389). A number of studies have suggested that MSCs from different niches may secrete different signalling molecules according to the surrounding tissues and the unique regulation that each specific environment requires (390-394). In order to try and identify any cytokines which might be differentially secreted between BM-derived and OM-derived MSCs as well as other cells from their resident niches, conditioned media was collected and analysed from each cell type, with an aim to identify any potential factors which could instigate the different myelination capacity observed with the BM-MSCs and OM-MSCs.

Previously it has been shown that chemokines can affect myelination. Nash *et al.* demonstrated an inhibitory effect of CXCL10 on myelination (66), likely due to its IFN-γ induced pro-inflammatory effects via CXCR3 (395-403), whilst CXCL12, via its interactions with CXCR4 and CXCR7, has been shown to stimulate myelination, and promote neural cell function by increasing neuronal migration and proliferation of cells within the CNS (404-406). These conditioned media, in which each cell type had been cultured for 48 hours, is rich in all of the secreted factors unique to each cell type. Human Luminex cytokine arrays covering a wide range of cytokines were used to analyse each conditioned media sample for the presence of these molecules. Analysis of each sample was compared against the others to identify any which may be considered as being differentially secreted, and thus potentially important regarding

identifying possible mechanisms involved in the observed differences in behaviour between each MSC phenotype. Analysis was carried out using three commercially bought human Luminex® cytokine bead arrays comparing conditioned media collected from confluent flasks of BM-MSCs, BM271-MSCs, BM-flow through cells, OM-MSCs, OM-flow through cells, and fibroblasts, using non-conditioned DM- media as negative controls. Analysis of conditioned media from embryonic stem cell-derived MSCs was also carried out, however the data wasn't considered when comparing BM-MSCs and OM-MSCs as its secretory profile was so uniquely different to both.

Since data from the lab has shown that rat olfactory ensheathing cells (OECs) promote myelination in myelinating cultures while conditioned media from rat Schwann cells inhibits myelination (163), we had a good reason to compare this conditioned media with that of OM-MSCs and BM-MSCs which share similar pro-myelinating and non-myelinating properties. Thus, analysis of n=4 different biological samples of each rat CM was also carried out using a rat Luminex® cytokine array comparing conditioned media from rat BM-MSCs, rat OM-MSCs, rat olfactory ensheathing cells (OECs), and rat Schwann cells, using non-conditioned DM- media as a negative control.

5.2.1. Human Luminex® Cytokine Arrays

Lindsay *et al.* recently demonstrated that axonal myelination is stimulated by the use of OM-MSC conditioned media (OM-MSC-CM) *in vitro* (1), suggesting a secreted factor is playing a role. Numerous studies have demonstrated a link between the stimulation of axonal myelination and CXCL12 (396-399, 407) but here for the first time we show a common link between OM-MSCs, CXCL12, and the stimulation of myelination.

In total, conditioned media was analysed for 62 separate cytokines over three separate arrays (some cytokines overlapping in more than one array). Full details of all of the cytokines used throughout these arrays can be found in Materials and Methods section 2.15.2. Of these 62 cytokines, 18

were statistically differentially secreted between BM-derived MSCs and OM-derived MSCs. However, to determine whether or not this difference was completely specific to OM-MSCs, the secretory profiles of the other cells from their niche tissue has to also be considered. If a significant increase in the secretion of a particular cytokine is observed in OM-MSCs compared to BM-MSCs, but is also observed in the OM-flow through cells, then this differential secretion must be considered not specific to that cell type. For any significant difference in secretion of a particular cytokine to be considered unique to the MSC itself, it must be significantly different to OM-Flow through cells as well as those from the bone marrow niche, so factors were identified that were secreted by only one cell type. This was observed in just 4 of the 18 aforementioned cytokines; CCL11, IL-9, G-CSF, and CXCL12 (SDF-1). Table 5.3 summarises the cytokines which were differentially secreted by the various cell types identified using these arrays. In this table, secretion is assessed relative to OM-MSCs. Instead of a specific concentration value, cytokines are scored with either a + or – symbol depending on whether their secretion is higher or lower compared to the factors detected in OM-MSCs. Graphs of actual concentrations and statistics of the 4 cell-specific differentially secreted cytokines are represented in Figure 5.5.

CCL11 was found to be secreted at a significantly higher concentration in OM-MSCs compared to OM-flowthrough cells ($p<0.05$) and all other cells (except ESC-derived MSCs) ($p<0.001$) from the Invitrogen 41-plex array (Figure 5.5A), and significantly higher compared to all cell types ($p<0.001$) in the Millipore 30-plex array (Figure 5.5B).

BM-MSCs and BM271-MSCs were shown to secrete a significantly higher amount of IL-9 compared to each other cell type ($p<0.001$) (Figure 5.5C).

Human						
Relativity to OM-MSC (+/-)						
	Fibroblast	BM271	BM	OM-FT	BM-FT	Embryonic
Eotaxin-1	- -	- -	- -	-	- -	+
MCP-1	- -	-	-	=	-	-
MCP-2	- -	- -	N/A	=	N/A	N/A
MCP-3	-	-	-	+	-	-
MCP-4	-	-	N/A	=	N/A	N/A
IL-8	- -	- -	-	+	-	-
IL-9	-	+	++	=	=	-
IL-12	- -	-	-	=	-	-
MIP-1α	-	-	+	+	+	-
G-CSF	-	-	-	-	-	-
VEGF	-	=	+	+	+	+
IP-10	-	-	=	++	+	-
SCF	-	-	N/A	=	N/A	N/A
RANTES	-	-	-	++	-	-
CXCL12	-	-	N/A	-	N/A	N/A
HGF	+	=	+	+	-	-
Fractalkine	-	+	+	+	+	=
GRO	-	-	-	+	=	=

Table 5.3: Three luminex bead arrays using the kits outlined in materials and methods section 2.16 were carried out with conditioned medium collected from Fibroblasts, BM271-MSCs, BM-MSCs, OM-MSCs, OM-Flow through cells, BM-Flow through cells, and MSCs derived from ESCs. This table lists all differentially expressed chemokines taken from the combined results of the three separate human Luminex chemokine arrays. Highlighted cytokines are ones which are expressed at significantly different levels in BM-MSCs compared to both OM-MSCs and OM-flowthrough cells, i.e. the difference is specific to the OM-MSC and not just the other cell types that could be found isolated from this tissue. +/- refers to a <5-fold increase/decrease. ++/-- refers to a >5-fold increase/decrease.

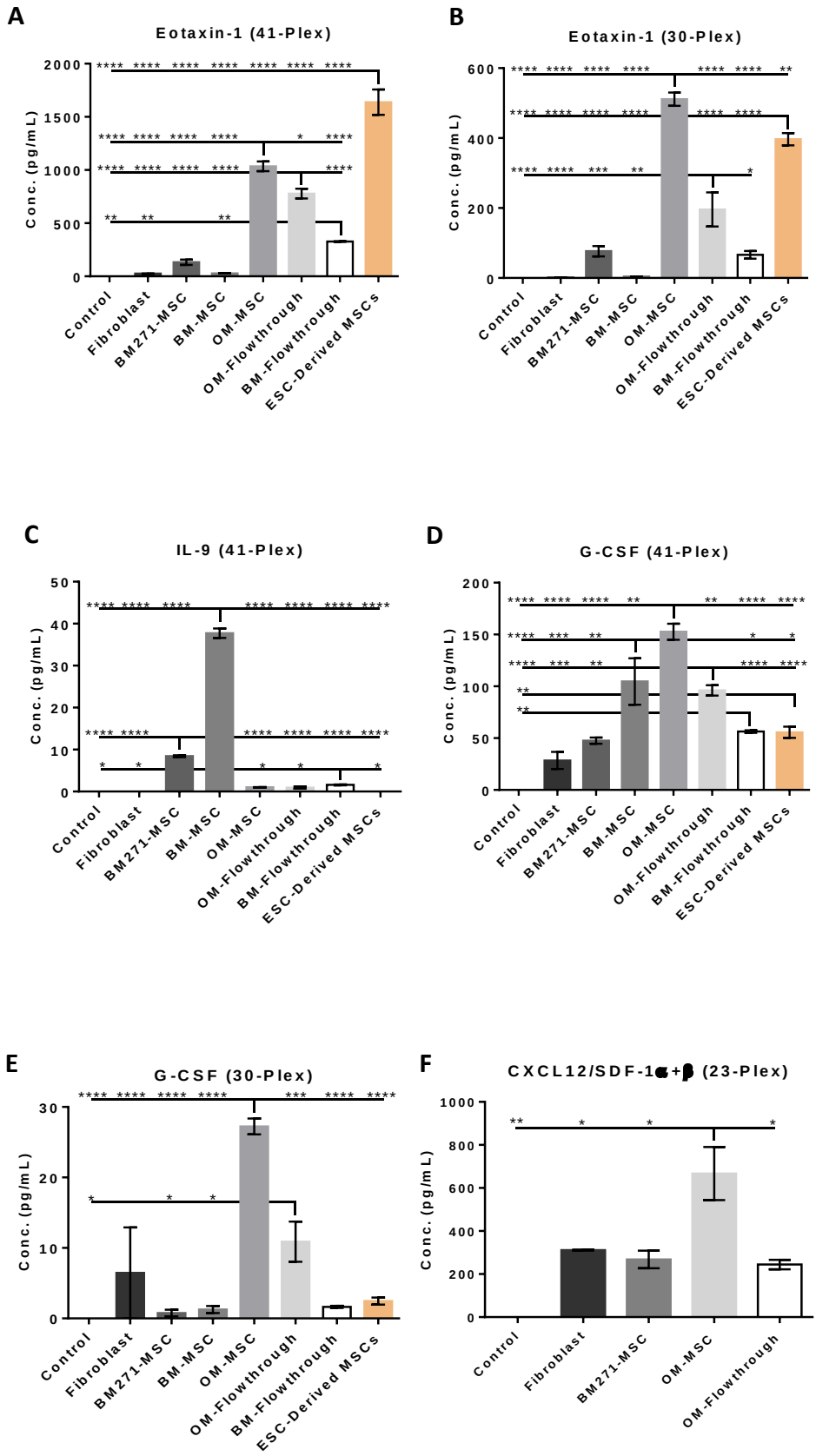
A
Eotaxin-1 (41-Plex)
Conc. (pg/mL)
2000
1500
1000
500
0
B
Eotaxin-1 (30-Plex)
Conc. (pg/mL)
600
400
200
0
C
IL-9 (41-Plex)
Conc. (pg/mL)
50
40
30
20
10
0
D
G-CSF (41-Plex)
Conc. (pg/mL)
200
150
100
50
0
E
G-CSF (30-Plex)
Conc. (pg/mL)
30
20
10
0
F
CXCL12/SDF-1α+β (23-Plex)
Conc. (pg/mL)
1000
800
600
400
200
0
Control
Fibroblast
BM271-MSC
BM-MSC
OM-MSC
OM-Flowthrough
BM-Flowthrough
ESC-Derived MSCs

Figure 5.5: Graphical representations of the concentration of factor in conditioned media taken from human BM-MSCs (n=3), BM271-MSCs (n=8), BM-flowthrough cells (n=3), OM-MSCs (n=8), OM-flowthrough cells (n=3), ESC-derived MSCs (n=3), and Fibroblasts (n=3). Figures show the chemokines taken from the three separate human Luminex arrays which were differentially expressed between OM-MSCs and all other cell types analysed for. CCL11 was shown in the 41-Plex array to be significantly differentially expressed in OM-MSCs compared to all other cell types except ESC-derived MSCs (A), and in the 30-Plex array to be significantly differentially expressed in OM-MSCs compared to all other cell types (B). IL-9, analysed only in the 41-Plex array, was significantly differentially expressed in OM-MSCs compared to all other cell types (C), G-CSF was shown to be significantly differentially expressed in OM-MSCs compared to all other cell types in both the 41-Plex and 30-Plex arrays (D-E), and CXCL12 was shown to be significantly differentially expressed in OM-MSCs compare to all other cell types in the 23-Plex array (F). Statistical analysis was carried out by 1 way ANOVA using Tukey's multiple comparison test, where *=$p<0.05$, **=$p<0.01$, ***=$p<0.005$, and ****=$p<0.001$.

The 41-plex array (Figure 5.5D) showed a high concentration of G-CSF was secreted by BM-MSCs, and to a significantly lower extent in BM271-MSCs ($p<0.01$) and BM-Flow through cells ($p<0.05$), suggesting that G-CSF producing cells may be lost during CD271 positive selection. This was not observed however in the 30-plex array, where G-CSF was secreted at very low concentrations from all bone marrow-derived cells (Figure 5.5E). In both arrays though, we see a very high concentration of G-CSF secreted from OM-MSCs which is significantly higher than that secreted by all other cells ($p<0.01$ – $p<0.001$).

Figure 5.5F shows that CXCL12 is secreted by BM-MSCs, OM-MSCs, and OM-Flow through cells. However, secretion of CXCL12 is at a significantly higher concentration in media collected from OM-MSCs compared to each of the other cell types. This would suggest that this difference in CXCL12

secretion is specific to OM-MSCs. This finding is of particular importance, as CXCL12 has been shown to be one of the signalling molecules regulated by miR-140-5p (Figure 5.7), which, as was shown in section 5.1, was upregulated 3.66 fold in BM-MSCs compared to OM-MSCs (Figure 5.4).

5.2.2. Rat Luminex Cytokine Array

Lamond *et al.* also showed a link between a pro-myelination effect and cells from the olfactory system. It was demonstrated that conditioned media from rat olfactory ensheathing cells (OEC-CM) stimulated myelination, as opposed to that from rat Schwann cells (SC-CM) which showed an inhibitory effect on myelination (163). As these opposing biological effects mirror those of OM-MSCs and BM-MSCs, analysis of each conditioned media was carried out by Luminex array to determine any cytokines which showed commonality in secretion patterns between OM-MSCs and OECs, and between BM-MSCs and Schwann cells. As it was technically demanding to isolate and culture human OECs, rat cells were used as an alternative. Conditioned media collected from rOM-MSCs, rBM-MSCs, rOECs, and rSCs was analysed for a panel of 27 different cytokines (n=4 different biological samples). Table 5.4 lists each cytokine which was significantly differentially secreted in at least one of the conditioned media. The highlighted cells show cytokines that showed a significant increase/decrease in concentration from OM-MSCs compared to BM-MSCs and OECs compared to SCs. These were MIP-1α (Figure 5.6A), MIP-2 (Figure 5.6B), IP-10 (Figure 5.6C), RANTES (Figure 5.6D), Fracktalkine (Figure 5.6E), and LIX (Figure 5.6F). Although these cytokines show a commonality between OM-MSCs and OECs, and between BM-MSCs and SCs, more work will have to be carried out to determine whether or not either of them have any effect of axonal myelination.

Rat		
	Relativity to LP-MSC (+/-)	Relativity to OEC (+/-)
	BM-MSC	SC
MCP-1	- -	+
MIP-1α	++	++
MIP-2	- -	- -
VEGF	-	++
IP-10	- -	-
RANTES	- -	-
Fractalkine	-	-
GRO/KC	- -	++
LIX	- -	- -

Table 5.4: List of all differentially expressed chemokines taken from the rat Luminex chemokine array comparing the conditioned media taken from rat-derived BM-MSCs and OM-MSCs, and rat OECs and Schwann cells. Highlighted cytokines are those which are secreted at significant different concentrations from both OM-MSCs compared to BM-MSCs and OECs compared to Schwann cells. +/- refers to a <5-fold increase/decrease, and ++/-- refers to a >5-fold increase/decrease.

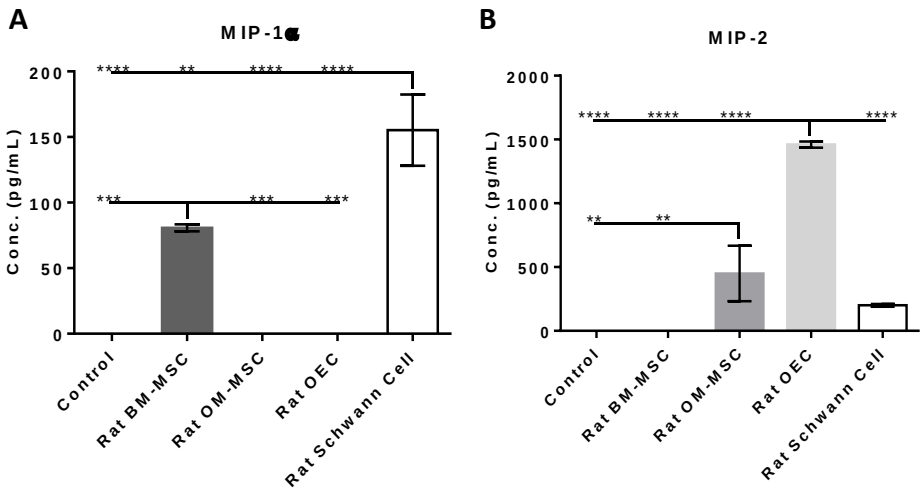

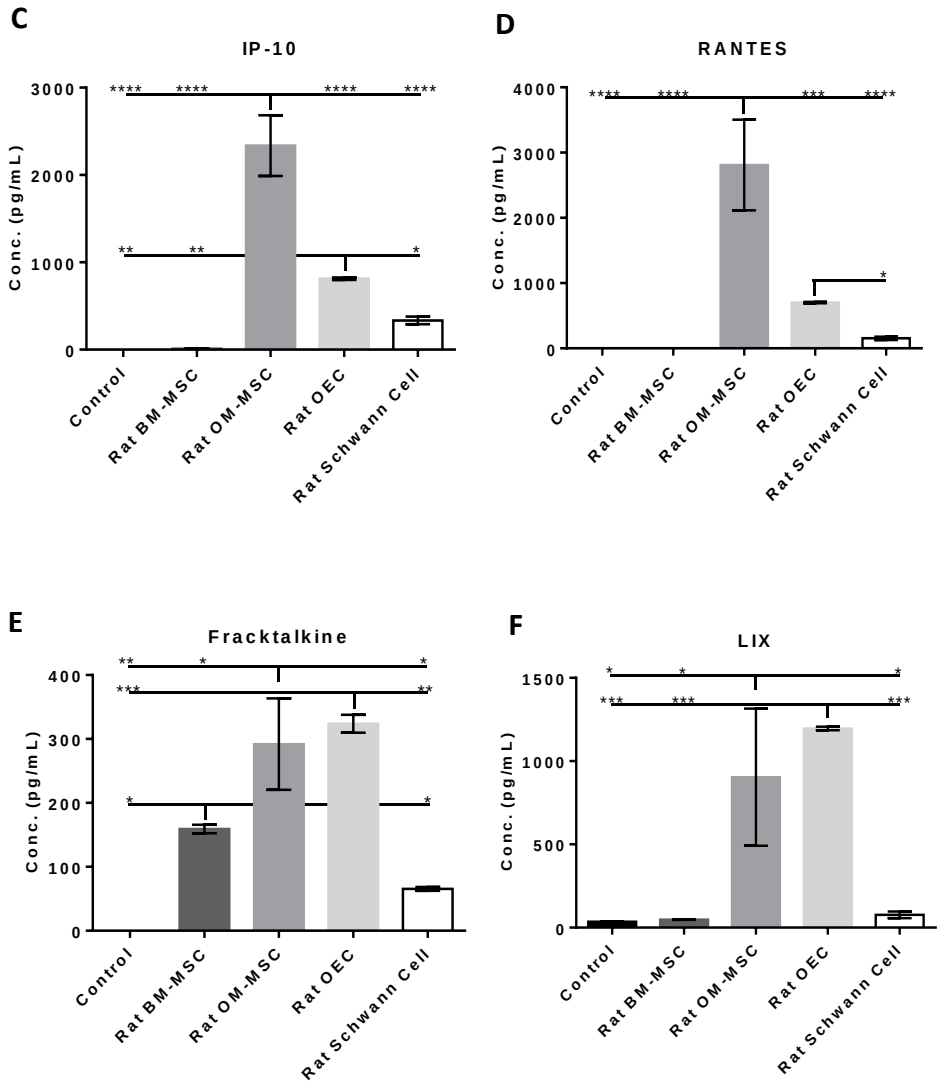

Figure 5.6: Graphical representations of the concentration of factors from conditioned media taken from rat BM-MSCs, OM-MSCs, OECs, and Schwann cells. Figures show the chemokines identified in the rat Luminex array which were differentially expressed between OM-MSCs and BM-MSCs, and between OECs and Schwann cells. Statistical analysis was carried out by 1 way ANOVA using Tukey's multiple comparison test, where *=p<0.05, **=p<0.01, ***=p<0.005, and ****=p<0.001. n=4.

5.3. Determining the Relationship Between miR-140-5p, OM-MSCs, CXCL12, and Myelination

Previous data has shown a significant increase in the expression of miR-140-5p in BM271-MSCs compared to OM-MSCs, and a significant decrease in

the secretion of CXCL12 in BM271-MSCs compared to OM-MSCs. Lindsay *et al.* (1) demonstrated that OM-MSC-CM promoted myelination significantly in mixed spinal cord cultures (myelinating cultures) when compared to BM-MSCs-CM, and as discussed previously, numerous studies have associated CXCL12 with enhanced myelination (396-399, 407). We also showed that miR-140-5p has an inverse correlation with CXCL12 expression (Figure 5.8) (379). All of these findings put together suggest that axonal myelination may be enhanced by CXCL12 secreted by OM-MSCs, and regulated by miR-140-5p. In this section we set out to confirm this link via a series of experiments including i) applying inhibitors and mimicks of miR-140-5p, ii) biological analysis of the subsequent conditioned media collected from these transfected cells on myelinating cultures, and iii) the use of CXCL12 receptor blocker, CXCL12 protein, and CXCL12 neutralising antibody on myelinating cultures.

5.3.1. RT-qPCR Demonstrates the Inverse Relationship of CXCL12 by miR-140-5p

Nicolas *et al.* (379) had previously identified miR-140-5p as a target for CXCL12 regulation (Figure 5.7), and separately, using SistemQC™ miRNA fingerprinting, we and Sistemic identified an upregulation of miR-140-5p in BM271-MSCs compared to OM-MSCs (section 5.1). As miR-140-5p is a negative regulator of CXCL12, it could be assumed that there would be an inverse relationship between miR-140-5p and CXCL12. Here we transfect BM271-MSCs and OM-MSCs with an inhibitor and mimic of miR-140-5p to simulate the regulation of miR-140-5p. RT-qPCR was used to identify any changes in the expression of CXCL12 mRNA with the view of confirming the relationship between miR-140-5p and CXCL12 (Figure 5.8). Figure 5.7 illustrates a miRNA map generated by Sistemic for their final report using high-confidence interactions from GeneGO MetaCore™ analyses. This miRNA map outlines signalling molecules which are known to be regulated by miR-140-5p. Figure 5.8 confirms the relationship between miR-140-5p and CXCL12, and demonstrates the role miR-140-5p plays in negatively regulating CXCL12. Confirmation that the transfections were successful is

shown in Figures 5.8A and 5.8C which demonstrate a downregulation of miR-140-5p in both BM271-MSCs and OM-MSCs when transfected with miR-140-5p inhibitor, and an upregulation of miR-140-5p in BM271-MSCs and OM-MSCs when transfected with mir-140-5p mimic. The negative control conditions are BM271-MSCs and OM-MSCs transfected with a "scrambled" piece of miRNA which has no affinity to miR-140-5p, and the "no miRNA" control is BM271-MSCs and OM-MSCs transfected with ddH_2O only. These controls both follow the expected mRNA expression pattern of miR-140-5p being normally expressed at a higher level in BM271-MSCs.

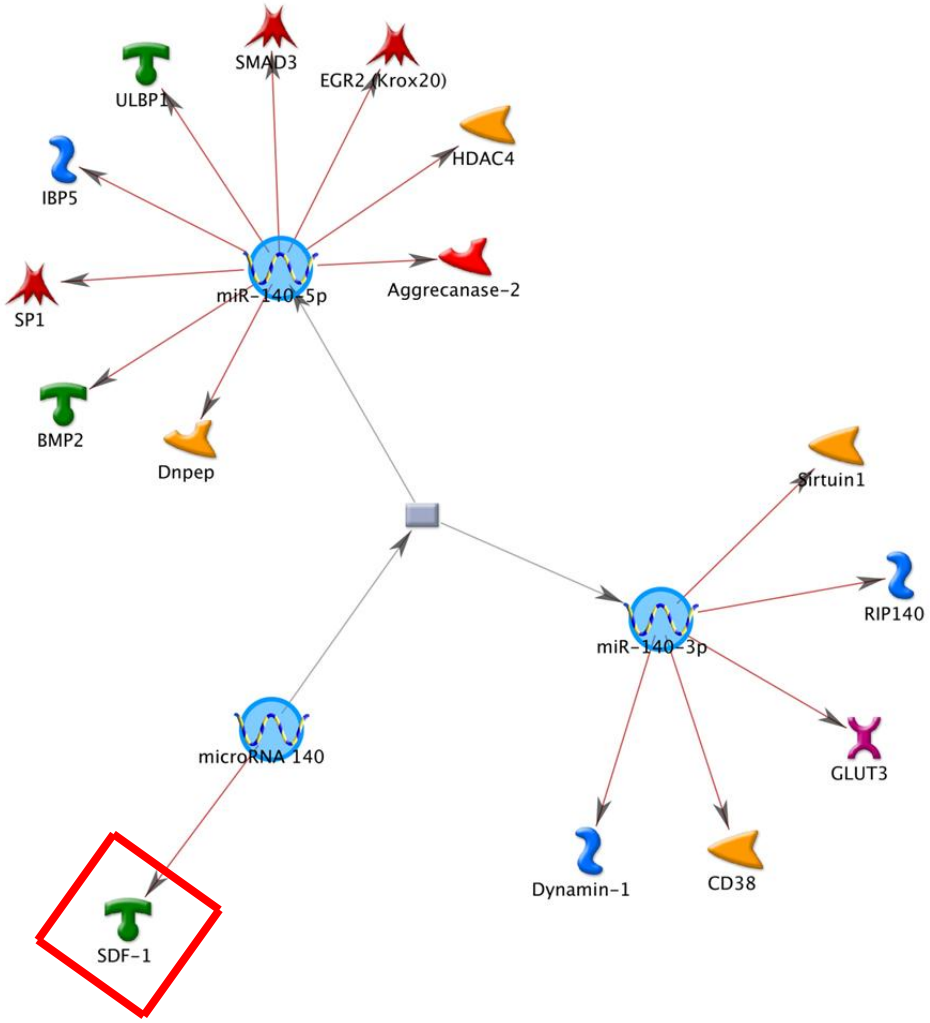

Figure 5.7: miRNA network plot built using high-confidence interactions form GeneGO MetaCoreTM analyses (taken from Sistemic's final report) showing a number of chemokines known to be regulated by miR-140, and

its constituent miRNAs miR-140-3p and miR-140-5p. The highlighted chemokine CXCL12 was shown in our previous Luminex analysis to be differentially expressed in OM-MSCs compared to BM-MSCs.

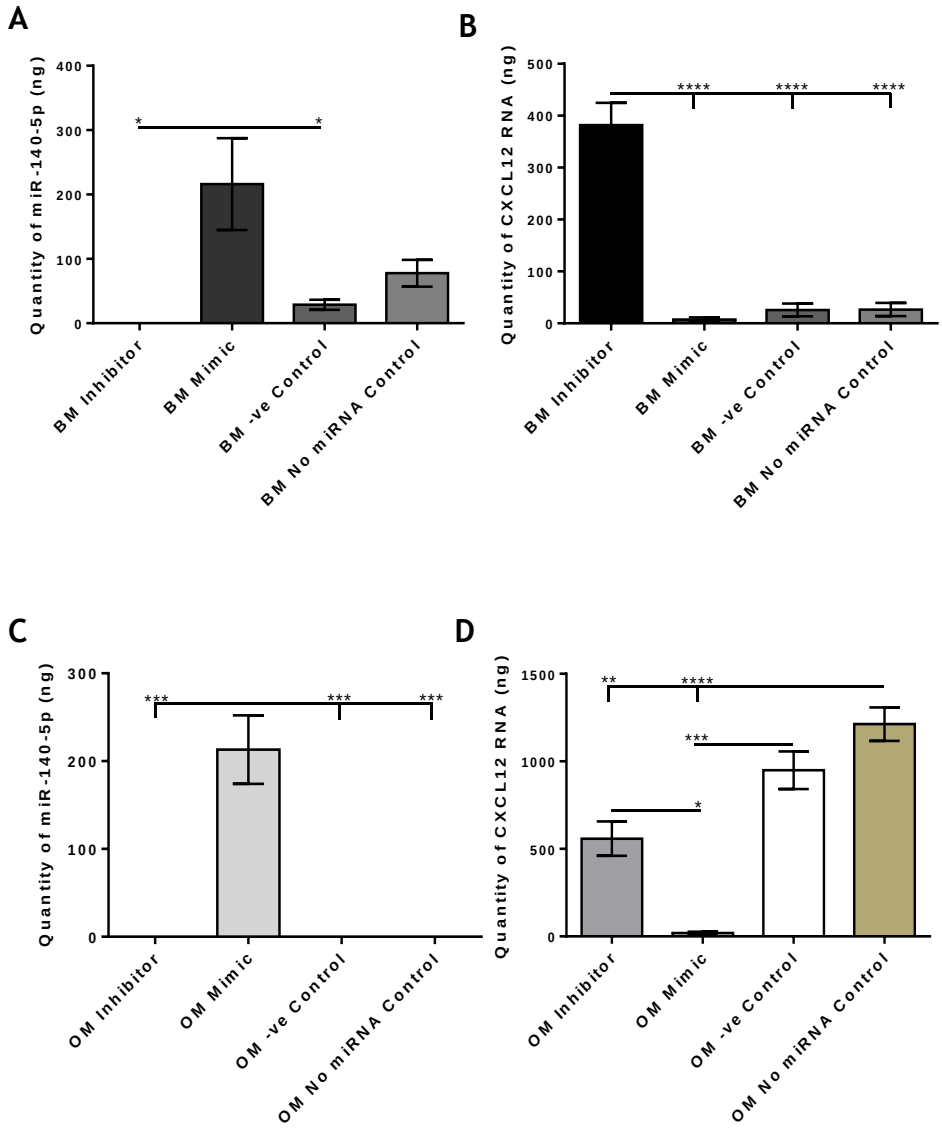

Figure 5.8: RT-qPCR analysis on BM271-MSCs (A-B) and OM-MSCs (C-D) which have been transfected with miR-140-5p inhibitor, miR-140-5p mimic, "scrambled" miRNA (-ve control), and ddH2O control in which no miRNA is transfected. Samples were analysed for miR-140-5p and its downstream effector CXCL12 to demonstrate a relationship between the miRNA and the chemokine. RT-qPCR was carried out using the standard curve method. All

standard curves can be found in supplementary data S3. Statistical analysis was carried out by 1 way ANOVA using Tukey's multiple comparison test, where *=p<0.05, **=p<0.01, ***=p<0.005, and ****=p<0.001, n=3.

Figures 5.8B and D confirm the negative regulatory effect of miR-140-5p on CXCL12, by demonstrating that an increase in the expression of miR-140-5p translates to a decrease in the expression of CXCL12 mRNA, and vice versa.

5.3.2. CXCL12 is Confirmed to Stimulate Axonal Myelination *in vitro*

As discussed previously in section 5.2, CXCL12 acts upon the receptors CXCR4 and CXCR7 (408-414). CXCL12 signalling can be abrogated by the blocking of CXCR4 using the chemical AMD-3100 (415-417) which also acts as an allosteric agonist to CXCR7 (418). CXCL12 in conditioned medium can also be neutralised using an antibody to CXCL12 which binds to the chemokine, thus rendering it unable to bind to its receptor. Here a number of conditions were set up whereby myelinating cultures were treated with CXCL12 to assess any stimulatory effects on myelination. Cultures were also treated with OM-MSC-CM to confirm the findings of Lindsay *et al*. that it stimulates myelination. Cultures were also pre-treated with AMD-3100 to block CXCL12 in the OM-MSC-CM from binding to CXCR4/CXCR7, and with a CXCL12 neutralising antibody to bind free CXCL12 in the OM-MSC-CM, preventing its interaction with CXCR4/CXCR7 (Figures 5.9 and 5.10). Controls were carried out using DM- only, DM- plus AMD-3100, and DM- plus anti-CXCL12.

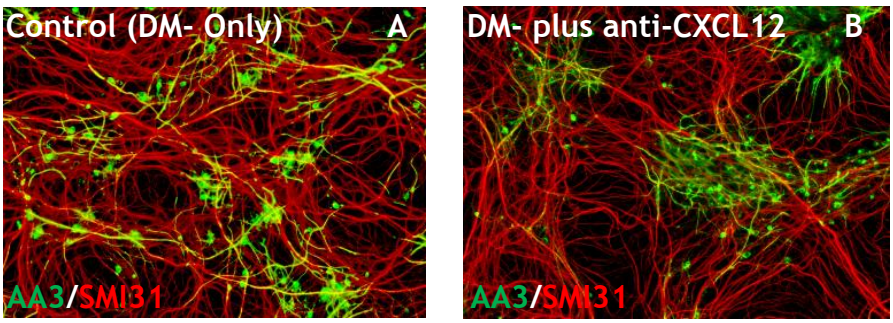

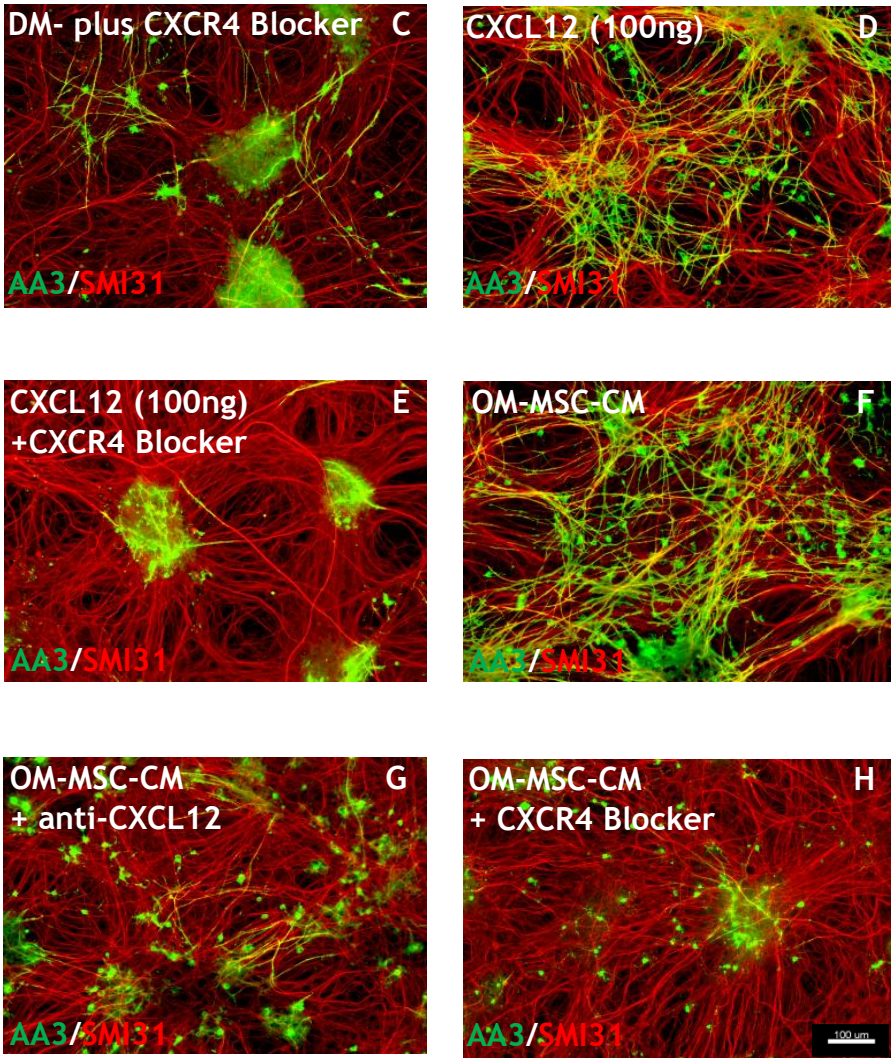

Figure 5.9: Representative immunocytochemistry images of the effects of CXCL12 on myelinating cultures (D), in the presence of the CXCR4 receptor blocker AMD3100 (E), the effects of OM-MSC conditioned media (CM) (taken from n=3 OM-MSC donors) on myelinating cultures (F); in the presence of neutralising antibody to CXCL12 (G), and in the presence of AMD3100 (H). These data suggest that the pro-myelinating effect may be CXCL12 dependant. Images (B) and (C) illustrate the effect of anti-CXCL12 antibody and AMD-3100 alone on myelination in culture. All conditions were compared to an untreated control (A). Immunocytochemistry was carried out using AA3, a myelin marker for Proteolipid protein 1 (PLP) (green), and

axons were visualised using SMI31 (red). All images were taken at x10 magnification, scale bar =100 µm. n=3.

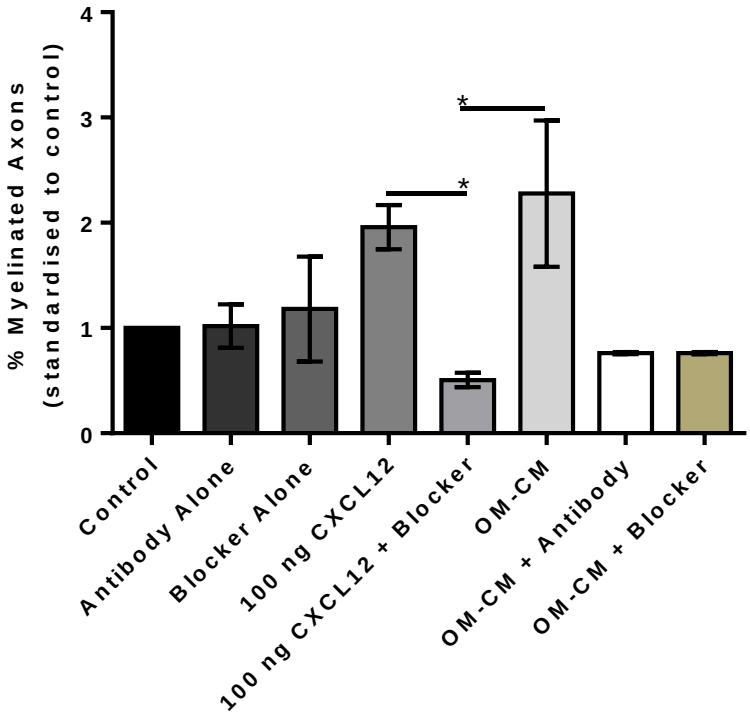

Figure 5.10: Graphical representation of the effects of CXCL12 and OM-MSC-CM (n=3 different OM-MSC donors) on myelination in vitro, in the presence of a neutralising antibody to CXCL12, and a blocker of the CXCL12 receptor (CXCR4), AMD3100. Myelination was quantified using CellProfiler Cell Image Analysis Software to calculate a percentage of myelinated axons per image. Mean values per condition were calculated, and a fold increase in myelination relative to the untreated control was represented in the graph. Statistical analysis was carried out by 1 way ANOVA using Tukey's multiple comparison test, where *=p<0.05, **=p<0.01, ***=p<0.005, and ****=p<0.001. n=3.

These data confirm the stimulatory effect of OM-MSC-CM on *in vitro* myelination, and correlate this with CXCL12 expression. Percentages of myelinated axons treated with CXCL12 and with OM-MSC-CM were >2-fold that observed in the untreated control samples. Untreated controls, AMD-3100 only, and anti-CXCL12 only controls showed very similar percentages of myelinated axons. Moreover, the percentage of myelinated axons decreased dramatically in cultures treated with CXCL12 that were pre-treated with AMD-3100, which confirms that AMD-3100 does indeed act in abrogating the signalling between CXCL12 and its receptors CXCR4 and CXCR7. The 2 fold increase in percentage of myelinated axons observed in cultures treated with OM-MSC-CM was diminished to around the levels of untreated controls by pre-treatment with AMD-3100 and with anti-CXCL12. This suggests that the pro-myelinating effect of the OM-MSC-CM may indeed be mediated by CXCL12 in OM-MSCs via CXCL12/CXCR4/CXCR7 interactions.

5.3.3. Inhibitors and Mimics of miR-140-5p Affect *in vitro* CNS Myelination.

It was demonstrated in section 5.5.1 that inhibition of miR-140-5p increases the ability of BM271-MSCs and OM-MSCs to produce CXCL12 mRNA, and contrastingly that mimicking of miR-140-5p decreases this ability. Conditioned media was collected from both BM271-MSCs and OM-MSCs which have been transfected with an inhibitor and mimic of miR-140-5p, to assess any effect on the myelinating cultures previously used in section 5.3.2 (Figures 5.11 and 5.12). This would validate biological activity of CXCL12 after transfection with modifiers of miR-140-5p. Controls included untreated control (DM- only), CM collected from cells transfected with negative “scrambled” miRNA, and CM collected from cells transfected with ddH_2O only.

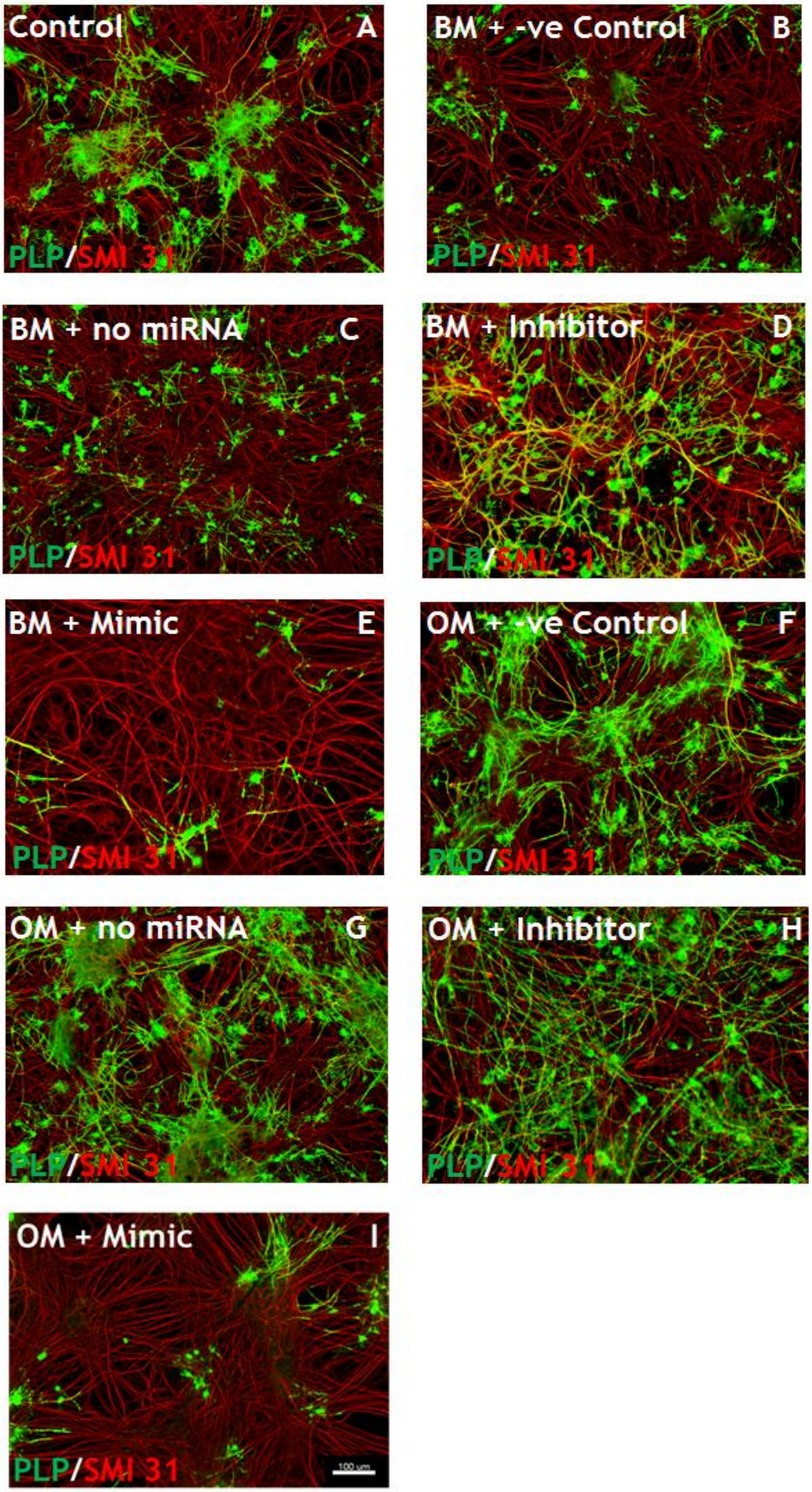
Control
A
PLP/SMI 31
BM + -ve Control
B
PLP/SMI 31
BM + no miRNA
C
PLP/SMI 31
BM + Inhibitor
D
PLP/SMI 31
BM + Mimic
E
PLP/SMI 31
OM + -ve Control
F
PLP/SMI 31
OM + no miRNA
G
PLP/SMI 31
OM + Inhibitor
H
PLP/SMI 31
OM + Mimic
I
PLP/SMI 31
100 µm

Figure 5.11: Representative images of the effect of conditioned media taken from BM271-MSCs and OM-MSCs transfected with inhibitor (D and H) and mimic (E and I) of miR-140-5p on *in vitro* myelination. Conditioned media was also used from BM-MSCs and OM-MSCs transfected with "scrambled" miRNA (-ve control) (B and F), and with H2O (No miRNA control) (C and G). All conditions were compared to an untreated control (A). Staining was carried out using AA31 as a myelin marker for polylipoprotein (green), and axons were visualised using SMI31 (red). All images were taken at x10 magnification, with the scale bar representing 100 µm. n=3.

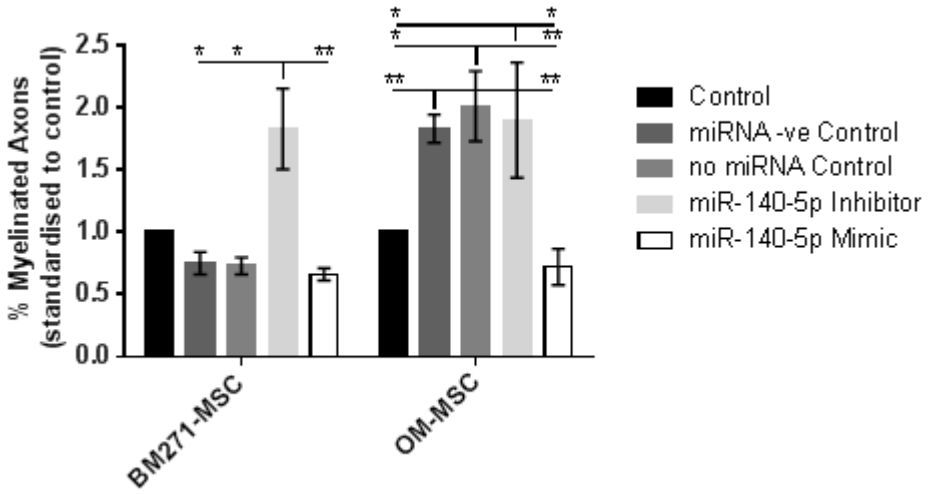

Figure 5.12: Graphical representation of the effect of conditioned media taken from BM271-MSCs and OM-MSCs transfected with inhibitor and mimic of miR-140-5p on in vitro myelination. Myelination under these conditions was compared to control conditions using BM-MSC-CM and OM-MSC-CM from cells transfected with "scrambled" miRNA (-ve control), and with H2O (No miRNA control). All conditions were compared to an untreated (non-transfected) control which was cultured as normal with DM-. Myelination was determined using CellProfiler Cell Image Analysis Software to calculate a percentage of myelinated axons per image. Mean values per condition were calculated, and a fold increase in myelination relative to the untreated control was represented in the graph. Statistical analysis was

carried out by 2 way ANOVA using Tukey's multiple comparison test, where *=p<0.05, **=p<0.01, ***=p<0.005, and ****=p<0.001. n=3.

These data confirm that manipulation of miR-140-5p in both BM271-MSCs and OM-MSCs can affect myelin production on *in vitro* myelination, and it is likely that this is due to subsequent changes in the secretion of CXCL12 from these cells. Figure 5.12 shows an almost 2 fold increase in the percent of myelinated axons when treated with CM from BM271-MSCs and OM-MSCs transfected with miR-140-5p inhibitor, suggesting inhibition resulted in an increase in secretion of CXCL12 into the CM. This percent of myelinated axons was significantly higher (p<0.01) than in cultures treated with CM from BM271-MSCs and OM-MSCs transfected with miR-140-5p mimic.

Cultures treated with OM-MSC-CM controls ("scrambled" miRNA and ddH_2O) showed increased percentages of myelinated axons compared to untreated controls and to cultures treated with OM-MSC-CM from cells transfected with miR-140-5p mimic. These increases were significant (scrambled → untreated and mimic = p<0.01), ddH_2O → untreated = p<0.05, ddH_2O → mimic = p<0.01) but were not different when compared to conditions treated with OM-MSC-CM transfected with miR-140-5p inhibitor. The observations in the control treatments were expected, but the lack of difference between the controls and the "inhibitor" treatment suggests a possible saturation point, where the pro-myelinating effect of the secreted CXCL12 cannot be further enhanced by more CXCL12 being secreted. The significant difference in axonal myelination between scrambled, ddH2O, and inhibitor treatments compared to mimic treatments shows that miR-140-5p is inhibiting at least one pro-myelinating factor secreted by OM-MSCs, most likely CXCL12 based on previous observations.

Cultures treated with BM271-MSC-CM controls ("scrambled" and ddH_2O) showed percentages of axonal myelination similar to those of untreated controls. This would be expected, as previous observations have shown no

pro-myelinating effect of BM271-MSC-CM on *in vitro* myelination. Cultures treated with the mimic transfected BM271-MSC-CM had less myelinated axons compared to untreated controls and transfected controls, but these differences were not significant. Cultures treated with BM271-MSC-CM from cells transfected with miR-140-5p inhibitor showed a significantly higher percentage of axonal myelination compared to untreated controls, transfected controls; scrambled and ddH_2O ($p<0.05$), and compared to cultures treated with BM271-MSC-CM from cells transfected with miR-140-5p mimic ($p<0.01$). This data illustrates that miR-140-5p inhibition results in increased secretion of at least one pro-myelinating factor, most likely CXCL12 based on previous experiments.

5.3.4. miR-140-5p Regulates the Secretion of Cytokines Other Than CXCL12

Data presented in Sections 5.3.2 and 5.3.3 showed a potential for miR-140-5p to regulate CXCL12 secretion by BM271-MSCs and OM-MSCs, and Figure 5.7 showed that miR-140-5p is responsible for the regulation of a number of different cytokines other than CXCL12, such as BMP2, SP1, HDAC4, and SMAD3. Here we try to identify other cytokines which may be regulated by miR-140 5p by analysing CM taken from BM271-MSCs which have been transfected with an inhibitor and mimic of miR-140-5p. Analysis was carried out by the same 30-plex and 41-plex Luminex arrays used in section 5.2.1 (Figure 5.13).

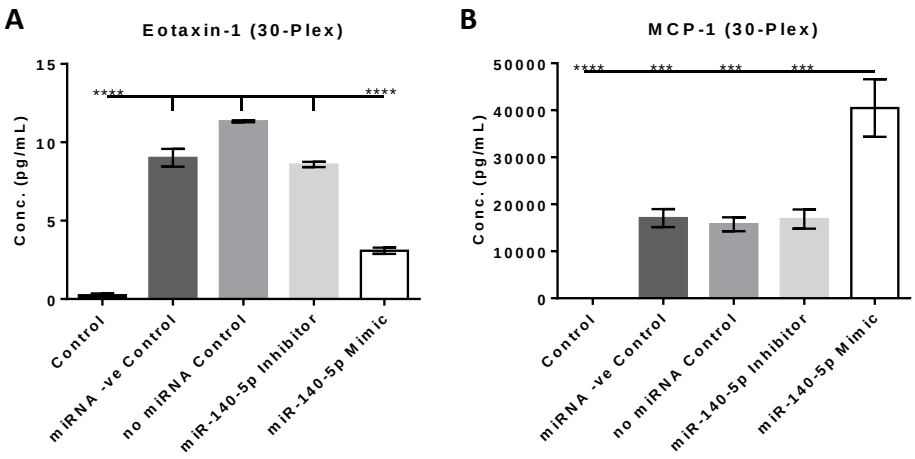

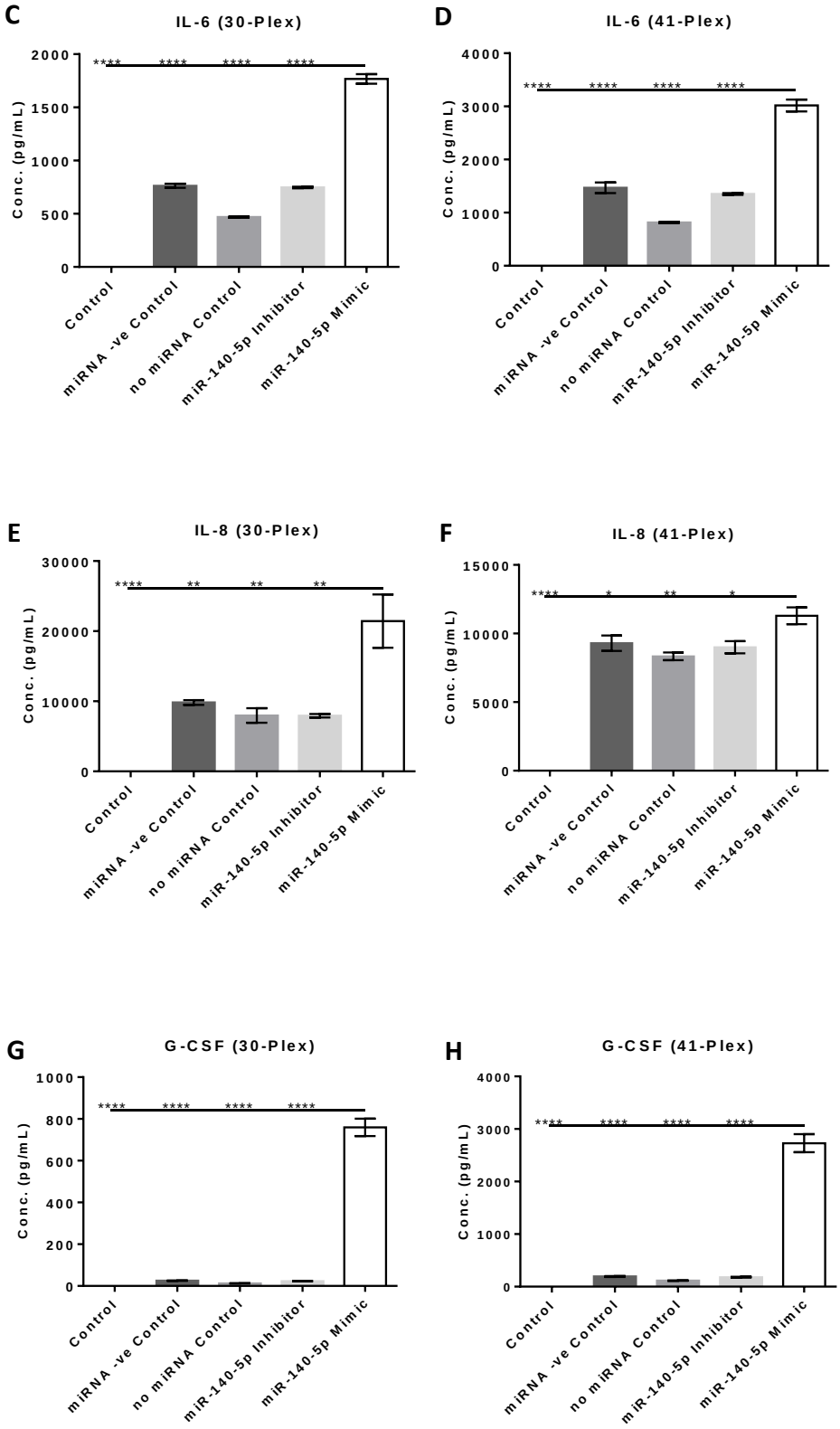
C
IL-6 (30-Plex)
Conc. (pg/mL)
2000
1500
1000
500
0
****
****
****
****
Control
miRNA -ve Control
no miRNA Control
miR-140-5p Inhibitor
miR-140-5p Mimic
D
IL-6 (41-Plex)
Conc. (pg/mL)
4000
3000
2000
1000
0
****
****
****
****
Control
miRNA -ve Control
no miRNA Control
miR-140-5p Inhibitor
miR-140-5p Mimic
E
IL-8 (30-Plex)
Conc. (pg/mL)
30000
20000
10000
0
****
**
**
**
Control
miRNA -ve Control
no miRNA Control
miR-140-5p Inhibitor
miR-140-5p Mimic
F
IL-8 (41-Plex)
Conc. (pg/mL)
15000
10000
5000
0
****
*
**
*
Control
miRNA -ve Control
no miRNA Control
miR-140-5p Inhibitor
miR-140-5p Mimic
G
G-CSF (30-Plex)
Conc. (pg/mL)
1000
800
600
400
200
0
****
****
****
****
Control
miRNA -ve Control
no miRNA Control
miR-140-5p Inhibitor
miR-140-5p Mimic
H
G-CSF (41-Plex)
Conc. (pg/mL)
4000
3000
2000
1000
0
****
****
****
****
Control
miRNA -ve Control
no miRNA Control
miR-140-5p Inhibitor
miR-140-5p Mimic

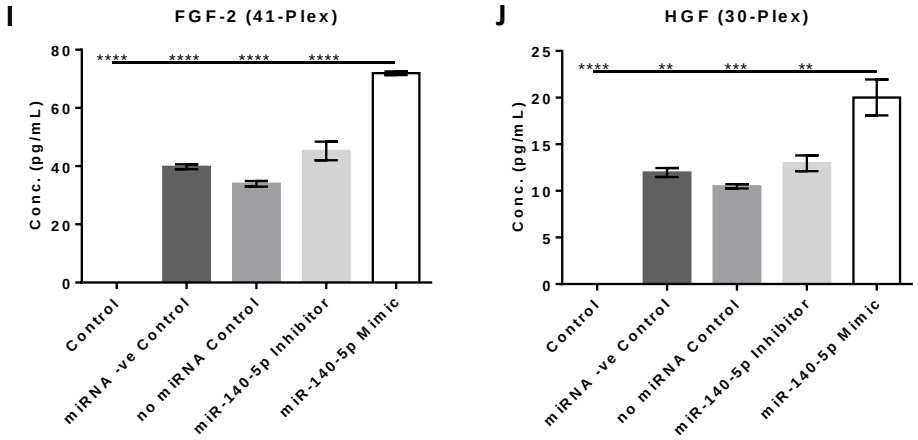

Figure 5.13: Graphical representation of human Luminex array analysis of CM taken from BM271-MSCs transfected with inhibitor and mimic of miR-140-5p. Also analysed was CM taken from BM-MSCs transfected with "scrambled" miRNA (-ve control), and H2O (no miRNA control), and a non-CM control of DM- alone. N=3 sets of CM were analysed on 30-Plex (A-C, E, G, J) and 41-Plex (D, F, H-I) arrays, and graphs presented represent chemokines which were differentially expressed in either mimic or inhibitor samples compared to each other, suggesting a possible regulatory effect on these chemokines by miR-140-5p. Statistical analysis was carried out by 1 way ANOVA using Tukey's multiple comparison test, where *=p<0.05, **=p<0.01, ***=p<0.005, and ****=p<0.001. n=3.

CCL11 (Eotaxin-1) was shown to be secreted at a significantly higher concentration from OM-MSCs compared to BM271-MSCs (Figure 5.5A). Figure 5.13A shows that when the amount of miR-140-5p produced by BM271-MSCs is increased (mimic), the cells secrete a significantly lower concentration of CCL11 compared to controls, and to those where miR-140-5p is inhibited. This mirrors previous data when looking at CXCL12, suggesting that CCL11 may also be negatively regulated by miR-140-5p.

Figure 5.13B shows a significant increase in the secretion of MCP-1 ($p<0.005$) from cells transfected with miR-140-5p mimic compared to controls, and to those transfected with inhibitor.

In both the 30-plex and 41-plex arrays we show a significant increase in the secretion of IL-6 from BM271-MSCs which have been transfected with miR-140-5p compared to controls and those transfected with inhibitor ($p<0.001$). This suggests that miR-140-5p may be inhibiting an upstream effector which regulates the secretion of IL-6.

In both the 30-plex and 41-plex arrays it was shown that BM271-MSCs transfected with miR-140-5p secreted a significantly higher concentration of IL-8 compared to controls and to those transfected with inhibitor ($p<0.05$ – $p<0.01$). This also could suggest that miR-140-5p may be inhibiting an upstream effector which regulates the secretion of IL-8.

G-CSF, described in section 5.2.1, was seen to be secreted at high concentrations in BM-MSCs but not so in BM271-MSCs (Figure 5.5D), suggesting a possible loss of G-CSF secreting cells during the CD271 positive selection process. However OM-MSCs, which also undergo this CD271 positive selection, were seen to secrete a significantly higher amount of G-CSF compared to all other cell types (Figures 5.5D and 5.5E), suggesting that this increased secretion is specific to OM-MSCs. This experiment shows us that BM271-MSCs which have been transfected with miR-140-5p mimic secrete a significantly higher amount of G-CSF compared to controls and to those transfected with miR-140-5p inhibitor ($p<0.001$) (Figures 5.13G and 5.13H).

FGF-2 (basic fibroblast growth factor) and HGF (hepatocyte growth factor) show a similar relationship between their secretion and miR-140-5p expression in BM271-MSCs in that mimicking of miR-140-5p increases the secretion of both of these factors compared to controls and to cells transfected by miR-140-5p inhibitor (Figures 5.13I and 5.13J). This

suggests, as before, that the secretion of these factors is regulated by an upstream effector that is directly regulated by miR-140-5p.

5.4. miR-146a-5p Regulates Fas Receptor (CD95) Expression. A Possible Mechanism for Increased Cell Survival?

Although neither BM-MSCs, BM271-MSCs, nor OM-MSCs were used throughout this study beyond passage 5, it was observed during numerous cell cultures that OM-MSCs had a much better survival rate compared to both BM-MSCs and BM271-MSCs (anecdotal evidence only). BM-derived MSCs would start to look very unhealthy by passage 7, and would die soon after, whereas OM-MSCs would look very healthy for numerous passages beyond that. No studies were carried out to assess the viability of OM-MSCs at such late passages, but these observations became quite pertinent with regards to miR-146a-5p expression. Suzuki et al. and Guo et al. (47-48) demonstrated a direct relationship between miR-146a-5p and CD95 (FasR) which is the receptor for the Fas ligand (CD95L) (Figure 5.14).CD95 is part of what's known as "the death receptor family" of ligands, as its interaction with CD95 induces apoptosis (49-53). In section 3.1 we demonstrated a 15.5 fold increase in miR-146a-5p expression in OM-MSCs compared to BM271-MSCs. This would suggest that downstream molecules which are suppressed by miR-146a-5p would be downregulated in OM-MSCs compared to BM271-MSCs. As CD95 (FasR) is one of these downstream molecules (Figure 5.14), its suppression could account for the increased survival of OM-MSCs compared to BM-MSCs that has been anecdotally observed during cell culture. The major flaw in this theory is that once you remove these cells from their respective niches and place them into culture, you are removing any exposure to the Fas ligand which would propagate the cell death effect. Unless of course the cells themselves secrete Fas ligand as a self-regulatory mechanism, but this is unlikely and was not investigated. The relationship between miR-146a-5p and CD95 will be further investigated in the preceding sub-chapters however, as any effects that this relationship might have *in situ* could cause epigenetic changes within the cells which are carried with them to *in vitro* cell

culture conditions. Any such relationship would have to be investigated with far more scrutiny however, before any connection could be made between miR-146a-5p, CD95, and cell survival.

5.4.1. Western Blot Analysis Shows Higher Expression of CD95 in BM271-MSCs Compared to OM-MSCs

Importantly we had to first identify and compare normal levels of CD95 expressed in both BM271-MSCs and OM-MSCs. Here we analysed 4 separate donor samples of each cell type by western blot, and demonstrated that there was a significantly higher expression of CD95 on BM271-MSCs compared to OM-MSCs ($p<0.01$) (Figure 5.15). A full list of sample donors can be found in Materials and Methods Table 2.18.

5.4.2. RT-qPCR Demonstrates the Viability of the miR-146a-5p Transfection

To further investigate the effect that miR-146a-5p has on CD95 expression, transfection experiments were carried out exactly as in section 3.3.1, only using miR-146a-5p transcripts as the transfected agent. Figures 5.16A and 5.16B demonstrate the ability of the transfection to mimic and inhibit expression of miR146a-5p, showing a significant increase in miR-146a-5p expression in cells transfected with miR-146a-5p mimic compared to controls and to those transfected with miR-146a-5p inhibitor ($p<0.01$ – $p<0.001$), and also showing a significant decrease in expression of miR-146a-5p in cells transfected with miR-146a-5p inhibitor compared to negative controls (BM271-MSCs = $p<0.01$, OM-MSCs = $p<0.05$).

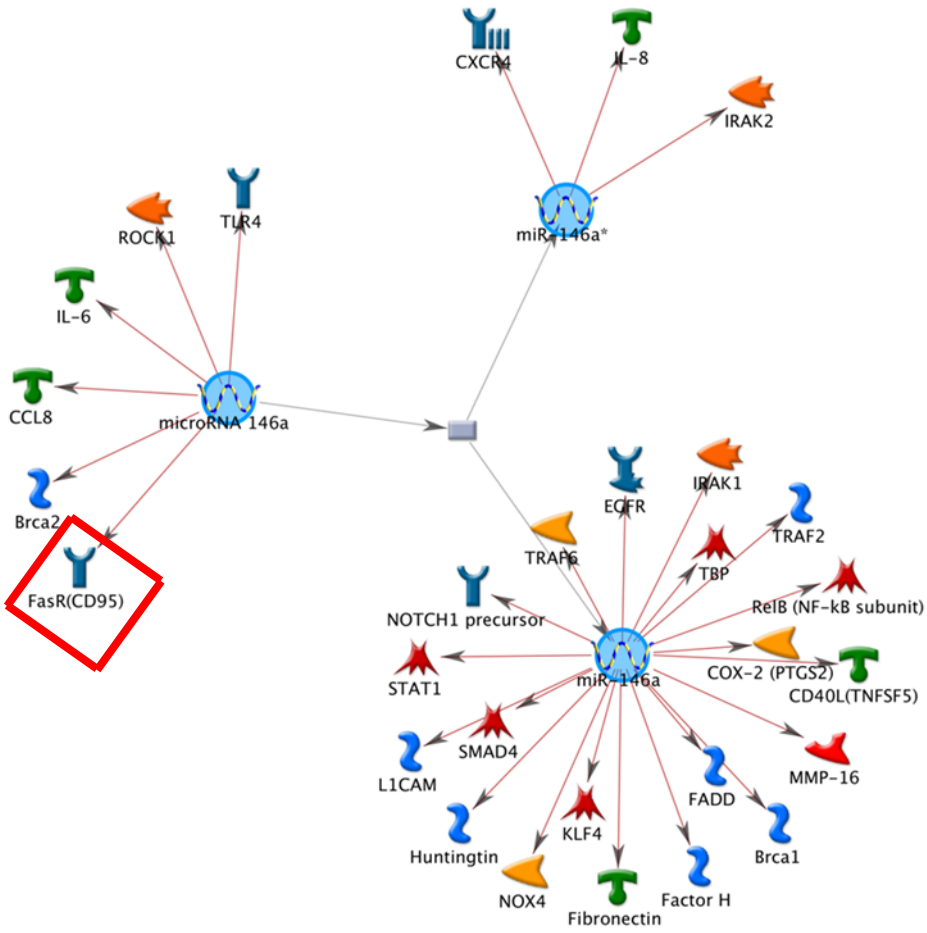

Figure 5.14: miRNA network plot built using high-confidence interactions form GeneGO MetaCoreTM analyses (taken from Sistemic's final report) showing a number of chemokines known to be regulated by miR-146a, the * denoting the minor products of miR-146a regulation. The highlighted molecule FasR (CD95) is one that is known to be related to cell survival.

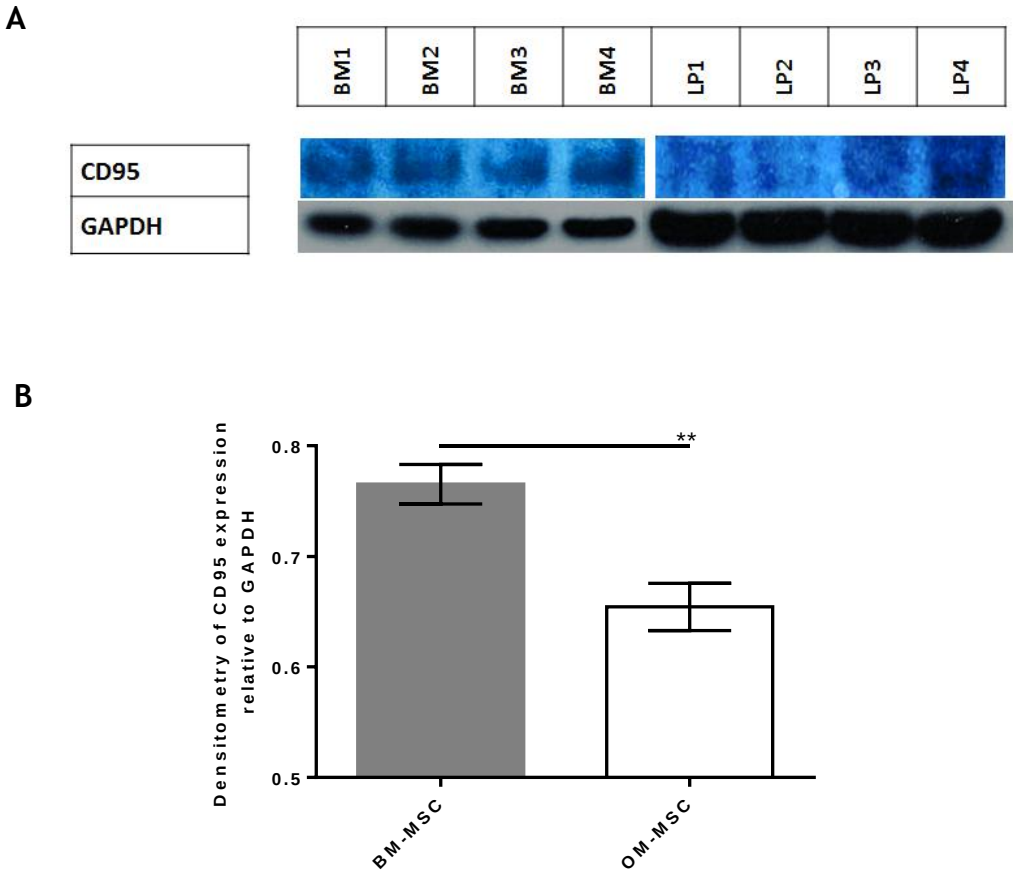

Figure 5.15: Scan of western blot of Fas Receptor (CD95) on BM271-MSCs and OM-MSCs, using GAPDH as a loading control (A), and a graphical representation of this western blot analysis (B). Densitometry of each protein band was analysed using ImageJ software, and amounts of CD95 were calculated relative to the loading control protein GAPDH. Statistical analysis was carried out using a two-tailed unpaired t-test, where *=p<0.05, **=p<0.01, ***=p<0.005, and ****=p<0.001. n=4.

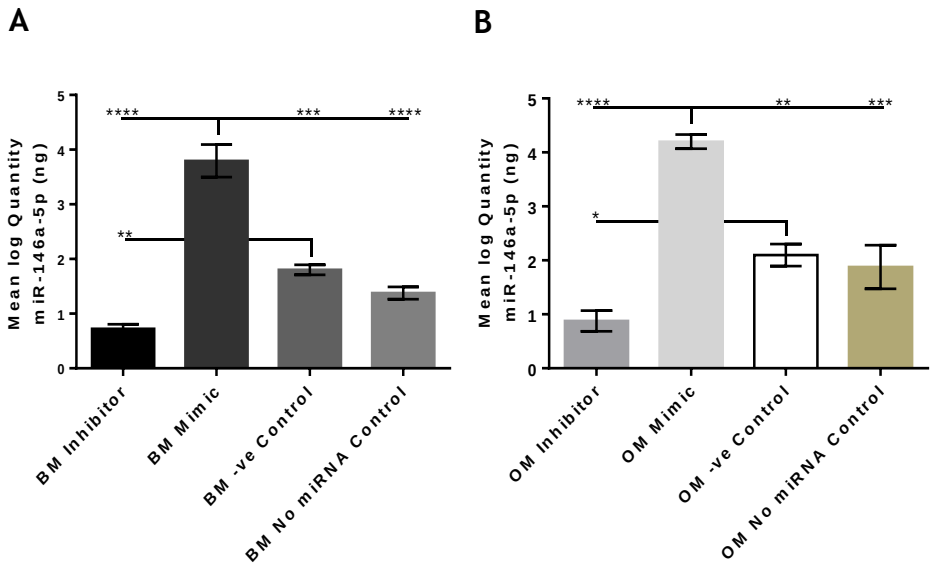

Figure 5.16: RT-qPCR analysis on BM271-MSCs (A) and OM-MSCs (B) which have been transfected with miR-146a-5p inhibitor, miR-146a-5p mimic, "scrambled" miRNA (-ve control), and ddH_2O as a control in which no miRNA is transfected. Samples were analysed for miR-146a-5p to demonstrate that the miRNA had been inhibited/stimulated. RT-qPCR was carried out using the standard curve method. Statistical analysis was carried out by 1 way ANOVA using Tukey's multiple comparison test, where *=p<0.05, **=p<0.01, ***=p<0.005, and ****=p<0.001. n=3.

5.4.3. Western Blot Analysis Confirms a Direct Relationship Between miR-146a-5p and CD95

CD95 as a molecule regulated by miR-146a-5p has been previously discussed. Here, the direct relationship between CD90 and miR-146a-5p is identified by manipulating levels of miR-146a-5p in each cell type, and analysing expression of CD95 by western blot (Figure 5.17).

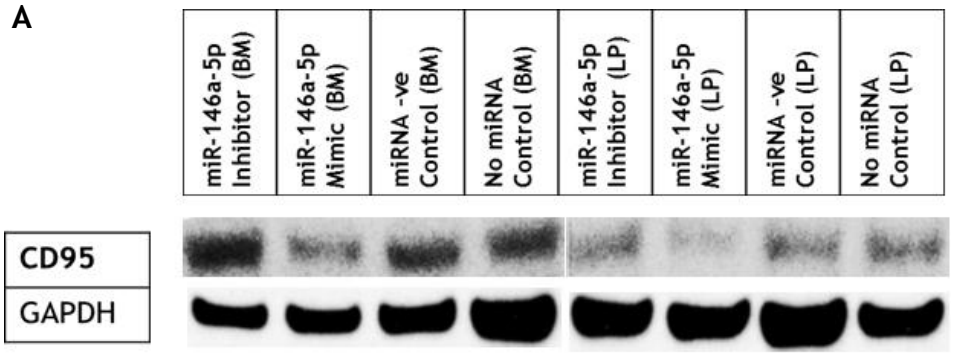

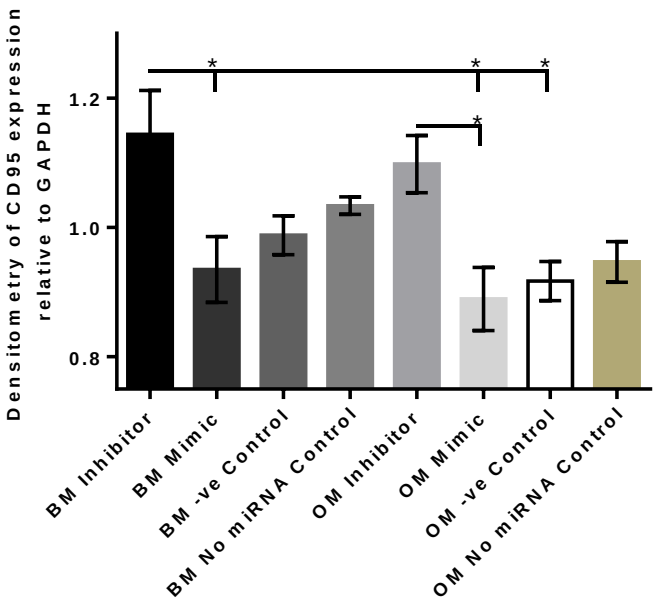

Figure 5.17: Representative scan of western blot analysis of protein from BM271-MSCs and OM-MSCs transfected with miR-146a-5p inhibitor and mimic (A). Cells were also transfected with a "scrambled" miRNA (-ve control) and H_2O (no miRNA control). Figure B is a Graphical representation of this western blot analysis. Densitometry of each protein band was analysed using ImageJ software, and values for CD95 were calculated relative to the loading control protein GAPDH. Statistical analysis was carried out by 1 way ANOVA using Tukey's multiple comparison test, where *=p<0.05, **=p<0.01, ***=p<0.005, and ****=p<0.001. n=3.

BM271-MSCs and OM-MSCs transfected with miR-146a-5p showed significantly higher levels of CD95 expression compared to their respected cells transfected with miR-146a-5p mimic ($p<0.05$). BM271-MSCs transfected with miR-146a-5p inhibitor also showed a significantly higher expression of CD95 compared to OM-MSCs transfected with mimic ($p<0.05$), and to OM-MSC negative controls ($p<0.05$). Although expression of CD95 was higher in BM271-MSC controls compared to OM-MSC controls, this difference was not statistically significant.

5.5. Determining the Relationship Between miR-335-5p and Proliferation

In section 3.2 it was demonstrated that OM-MSCs showed a significantly higher rate of proliferation compared to both BM-MSCs and BM271-MSCs ($p<0.001$). This observation may be quite pertinent with regards to miR-335-5p, which Figure 3.4 showed was upregulated 7.6 fold in BM271-MSCs compared to OM-MSCs. Tomé *et al*. (381) demonstrated a relationship between miR-335-5p and cell proliferation via the Wnt signalling pathway which regulates miR-335 expression. To try and confirm this relationship with proliferation, a transfection of BM271-MSCs and OM-MSCs with mimic and inhibitor of miR-335-5p was carried out using the same transfection methods as in sections 5.3 and 5.4.

5.5.1. RT-qPCR Confirms the Viability of the miR-335-5p Transfection

Before determining any effect of miR-335-5p manipulation on MSC proliferation, the transfection itself had to be validated. Transfection of each cell type was carried out in a similar manner as described in sections 5.3.1 and 5.4.2, only using miR-335-5p as the target transcript. Figure 5.18 shows the validation of the mimicking and inhibition of miR-335-5p in BM271-MSCs and OM-MSCs. Cells transfected with a “scrambled” miRNA transcript was used as a negative control. Due to the vast difference in expression of miR-335-5p between the inhibited and mimicked samples, log values of the actual quantities were plotted onto the graphs. In both

BM271-MSCs and OM-MSCs, cells transfected with miR-335-5p mimic expressed a significantly higher level of miR-335-5p compared to those transfected with miR-335-5p inhibitor ($p<0.001$) (Figure 5.18A and 5.18B). Mimic transfected cells also showed a significant increase in miR335-5p expression compared to negative controls (BM271-MSCs = $p<0.005$ (Figure 5.18A), OM-MSCs = $p<0.01$ (Figure 5.18B)), and BM271-MSCs transfected with miR335-5p inhibitor showed a significant decrease in miR-335-5p expression compared to negative controls ($p<0.01$) (Figure 5.18A).

5.5.2. Manipulation of miR-335-5p Led to Changes in Proliferation of BM271-MSCs and OM-MSCs

To assess any effect of mimicking and inhibition of miR-335-5p on MSC proliferation, transfected BM271-MSCs and OM-MSCs were fixed in 4% PFA and mounted onto glass cover slips using a mounting media containing the fluorescent nuclear dye DAPI. Samples of each MSC type under each condition were imaged under UV at 24, 48, and 72 hours post-transfection (Figure 5.20) and cell counts plotted against each other (Figure 5.19).

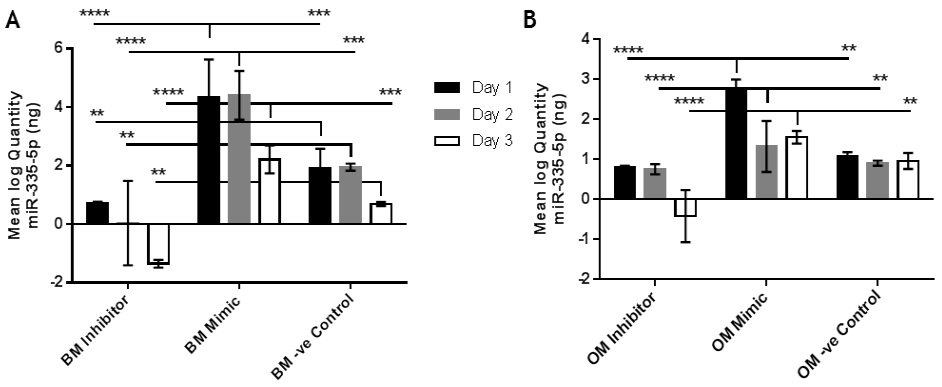

Figure 5.18: RT-qPCR analysis on BM271-MSCs and OM-MSCs transfected with miR-335-5p inhibitor and mimic, and with a "scrambled" miRNA (-ve control). Analysis was for the presence of miR-335-5p, 24, 48, and 72 hours post-transfection to demonstrate the effectiveness and transience of the transfection. Due to the substantial difference between cells transfected

with inhibitor and mimic, log values were calculated, and their means plotted. Statistical analysis was carried out by 2 way ANOVA using Tukey's multiple comparison test, where *=p<0.05, **=p<0.01, ***=p<0.005, and ****=p<0.001, n=3.

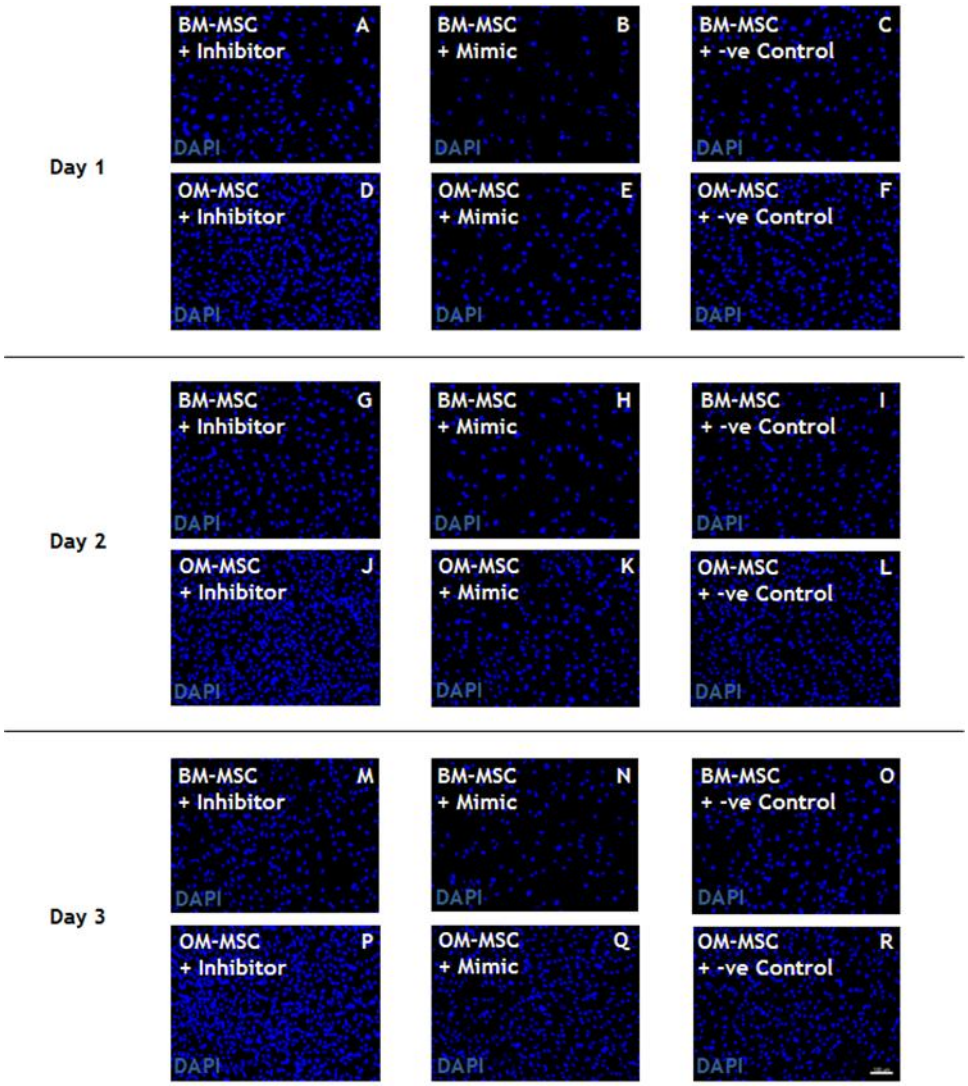

Figure 5.19: Representative images from n=3 BM271-MSCs and OM-MSCs transfected with miR-335-5p inhibitor and mimic, and with a "scrambled" miRNA (-ve control). Cell nuclei was stained with DAPI, and counted using CellProfiler Cell Image Analysis Software. Images were taken at x10 magnification, with the scale bar representing 100 µm. n=3.

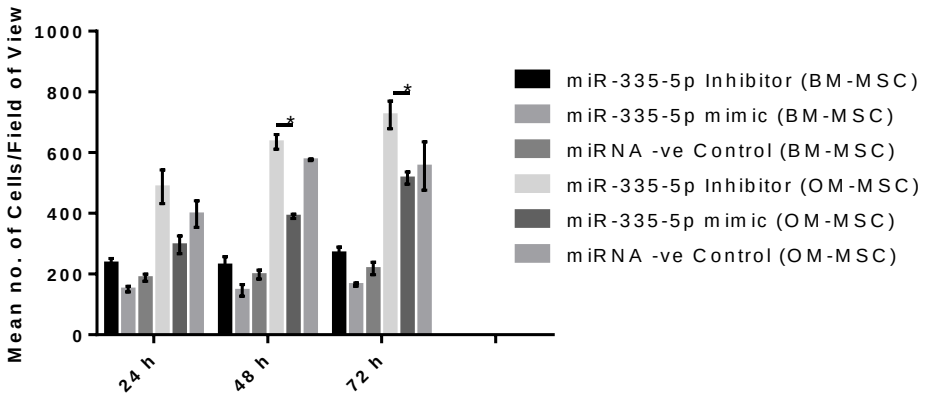

Figure 5.20: Graphical representation of the proliferation of BM271-MSCs and OM-MSCs transfected with miR-335-5p inhibitor and mimic, and "scrambled" miRNA (-ve control). DAPI stained nuclei was counted using CellProfiler Cell Image Analysis Software, and statistical analysis was carried out by 2 way ANOVA using Tukey's multiple comparison test, where *=p<0.05, **=p<0.01, ***=p<0.005, and ****=p<0.001. n=3.

Due to the relatively slow proliferation rates of BM271-MSCs under normal conditions, there was no significant difference in proliferation rates between either of the transfected conditions. There was a significant difference in proliferation between OM-MSCs transfected with miR-335-5p inhibitor and those transfected with mimic, however neither of these were significantly different to the control condition. These observations suggest that, while miR-335-5p may be involved in regulating certain molecules which are involved in cell proliferation, this may only be one of many mechanisms involved, and simply inhibiting or mimicking the production of miR-335-5p would not be sufficient to control the vast difference in the rates of proliferation between BM271-MSCs and OM-MSCs.

5.6. Discussion

Previously it was demonstrated that secreted factors from OM-MSCs but not BM-MSCs promoted myelinaton in vitro (Lindsay *et al*. (1)). Thus far, except for a significantly higher Nestin expression and proliferation rate, OM-MSCs have proved to be almost indistinguishable to their bone marrow-derived

counterparts. Throughout this chapter we analyse both MSC types at a molecular and miRNA level to better understand the underlying mechanisms which are responsible for OM-MSCs ability to stimulate myelin production in our myelinating culture system.

In collaboration with Sistemic we carried out a SistemQC™ miRNA fingerprint analysis on BM271-MSC and OM-MSC samples, and discovered a 64% homology in miRNA expression between BM271-MSCs and OM-MSCs, i.e. 125 of the 195 identified miRNAs were equivalently expressed (EE) between the two MSC types. Guo *et al*. (382) and Gao *et al*. (383) had previously identified 27 of these 125 miRNAs as being associated with BM-MSCs, but no such studies have been carried out using OM-MSCs. 13% (26 of 195 identified miRNAs) were considered to be differentially expressed (DE), leaving 23% of identified miRNAs as neither equivalently nor differentially expressed under Sistemic's experimental conditions. A focused contextual approach was adopted whereby miRNAs associated with MSC biology were identified. We chose miR-335-5p, miR-146a-5p and miR-140-5p from the DE kmiR™ list. Networks were built around these three miRNAs consisting of high-confidence mRNA targets for each miRNA. miR-140-5p, miR-146a-5p, and miR-335-5p have previously been associated with myelination (379, 419), cell survival (380), and proliferation (381) respectively; three behaviours which have been identified as significantly different between the two MSC types throughout. Focus therefore would be on these three miRNA for the remainder of the study. Each of these miRNAs were confirmed by RT-qPCR as significantly differentially expressed in BM271-MSCs compared to OM-MSCs.

Since previous studies have identified that chemokines could inhibit myelination (66), and that MSCs are known to secrete high levels of cytokines/chemokines (207, 214, 384-394) we were interested to see if there was a differential secretion of these by the two types of MSC. Luminex cytokine arrays, analysing molecules secreted by BM-MSCs, BM271-MSCs, OM-MSCs, Fibroblasts, and the flow through cells from BM- and OM-

MSC CD271 positive selection identified 4 cytokines which were secreted at significantly higher levels from OM-MSCs compared to all other cell types, or from BM-MSCs compared to all other cell types. Interleukin-9 (IL-9) and Granulocye colony stimulating factor (G-CSF) were secreted at significantly higher levels in BM-MSCs compared to all others. This could be expected considering the bone marrow niche, as IL-9 is a cytokine produced by T cells and Mast cells (420), and is important in the regulation of haematopoietic stem cells (421), and G-CSF, otherwise known as Colony Stimulating Factor 3, is a glycoprotein that is secreted by a number of immune cells which acts on precursor cells in the bone marrow, stimulating them to produce granulocytes and haematopoietic stem cells (422, 423). CCL11 (CCL11) and CXCL12 were both secreted at significantly higher levels from OM-MSCs compared to all other cell types, and have both been associated with myelination. CCL11, is a chemokine which is pertinent in the body's allergic response as it recruits eosinophils by chemotaxis (424-426). It has also been shown to decrease neurogenesis and hippocampal cognitive function in mice (427). It has been implicated in having a pro-myelinating effect by acting on its receptor CCR3 which is expressed on oligodendrocytes (428, 429), thus stimulating myelin production. CXCL12, is a ubiquitous chemokine which is secreted by a number of cells throughout the body (430-432), acting on its receptors CXCR4 (408-410, 414) and CXCR7 (411-414) to direct migration of cells such as haematopietic stem cells (432), astrocytes (407), neuronal cells (433), and immune cells (395). Like CCL11, it has been associated as having a pro-myelinating effect by acting on its receptors CXCR4 and CXCR7 which are also expressed on oligodendrocytes (395-399, 407, 410-414, 433).

Previous studies had shown a relationship between miR-140-5p and myelination, and also that miR-140-5p has an inverse relationship with CXCL12 (379, 419). This coupled with the decreased expression of miR-140-5p and increased secretion of CXCL12 in OM-MSCs observed in Figures 5.4 and 5.5, could suggest that the myelinating potential of OM-MSCs observed by Lindsay *et al*. (1) may be due, at least in part, to CXCL12.

The pro-myelinating effect of rat OECs observed by Lamond *et al*. (163) was also investigated in comparison to rat OM-MSCs to try and identify any commonly secreted cytokines between the two cell types, and also any commonly secreted cytokines between rat BM-MSCs and rat Schwann cells which have a de-myelinating effect on myelinating cultures (163). A number of cytokines common to both OECs and OM-MSCs were identified; MIP-2, IP-10, RANTES, Fraktalkine, and LIX were all secreted at significantly higher levels in OECs and OM-MSCs compared to BM-MSCs and Schwann cells, suggesting that there may be a possible stimulatory effect elicited by them on the *in vitro* myelination model. Interestingly though, despite the significant increase in secretion in OM-MSCs, ablation of MIP-2 (otherwise known as CXCL2) has been shown to have a neuroprotective role in the CNS by suppressing macrophage accumulation (434), so may not play any role in myelination. IP-10 (CXCL10), as previously discussed, has been shown to inhibit myelination (66) but it is possible that this could play a role in regulating myelin production so as to maintain equilibrium. RANTES (CCL5) however, could play a more direct role in myelination, as CCL5 defects have been identified in experimental autoimmune encephalomyelitis (EAE) mice, an *in vivo* model for de-myelinating disorders (435). Fractalkine (CX3CL1) has been shown to be highly up-regulated in EAE mice (436) which could suggest a potential role for this chemokine in neuroregeneration. The final chemokine which was up-regulated in OM-MSCs and OECs compared to BM-MSCs and Schwann cells was LIX (CXCL5). Stongly implicated in inflammatory conditions (437), CXCL5 has been identified as having a demyelinating effect, along with MIP-1α (438). This is contrary to what you might speculate from the significantly high secretion in OM-MSCs and OECs, but does support the significantly high secretion of MIP-1α seen in BM-MSCs and Schwann cells. These data indicate that more extensive work needs to be carried out on these chemokines to make any connection between them and an actual effect on myelination, or on any other biological functions which could potentially be modulated in this manner.

The connection between CXCL12 and OM-MSCs was confirmed earlier in this chapter. By blocking CXCR4 and CXCR7, and applying a CXCL12 neutralising antibody to OM-MSC-CM, we could firmly establish that CXCL12 was indeed secreted by OM-MSCs and was capable of increasing myelination *in vitro*. The relationship between CXCL12 and miR-140-5p was also confirmed by showing that CXCL12 secretion, and thus myelination, could be manipulated by inhibition and mimicking of miR-140-5p. Also identified was a potential relationship between CCL11 and miR-140-5p, when it was demonstrated that, as with CXCL12, mimicking of miR-140-5p significantly decreased the secretion of CCL11 from BM271-MSCs. This was discussed earlier as having a potential association with myelination, although further study will have to be carried out to determine any effect of CCL11 on our myelinating cultures.

Other chemokines outlined in this same array as being potentially regulated by miR-140-5p were MCP-1, IL-6, IL-8, and G-CSF. MCP-1, also known as CCL2 and small inducible cytokine A2, is a chemokine which recruits monocytes, memory T cells, and dendritic cells (439, 440) and has been associated with neuroinflammation (441), where its expression by glial cells is upregulated in a number of degenerative conditions in the CNS (442-447). As miRNAs generally have an inverse relationship with signalling molecules, it is unlikely that the significant increase in MCP-1 secretion in BM271-MSCs transfected with miR-140-5p mimic is due to a direct effect on MCP-1 by miR-140-5p, but it may be that enhanced inhibition of a separate downstream effector is resulting in an enhanced secretion of MCP-1. Interleukin 6 (IL-6) acts as a pro-inflammatory cytokine and anti-inflammatory myokine, and is important is a number of inflammatory conditions (448-451). It is also secreted by osteoblasts to induce bone resorption (452), which may explain why it is present in relatively high concentrations in BM271-MSC under control conditions. Its significantly higher secretion in cells transfected with miR-140-5p mimic might also suggest that this is perhaps not due to a direct relationship, but rather the

upstream effect of another molecule being inhibited directly by miR-140-5p. Interleukin 8 (IL-8), also known as neutrophil chemotactic factor, is another pro-inflammatory cytokine that induces chemotaxis in neutrophils and granulocytes so they migrate to the site of injury (453). As before, the observed effect is likely upstream of the direct inhibitory effect by miR-140-5p of a related chemokine. G-CSF was described previously as it was highlighted as being differentially secreted by OM-MSCs compared to BM271-MSCs (Figure 3.5). As miR-140-5p is upregulated in BM271-MSCs compared to OM-MSCs, mimicking miR-140-5p should result in a decrease in secretion of any molecule directly regulated by miR-140-5p, therefore the observed increased secretion of G-CSF in BM271-MSCs transfected with miR-140-5p mimic must mean that G-CSF is regulated by a separate downstream effector which is directly regulated by miR-140-5p.

A possible mechanism for the increased survival rates of OM-MSCs compared to BM-MSCs was explored via the miR-146a-5p relationship with the death receptor CD95. Figure 5.15 showed a significantly higher expression of CD95 in BM271-MSCs under normal conditions, which could be manipulated by inhibition and mimicking of miR-146a-5p (Figure 5.17).

A connection between miR-335-5p and proliferation was also explored using the same transfection techniques (Figures 5.19 and 5.20), although BM271-MSCs were not able to be manipulated in such a way as to increase their proliferation to that of OM-MSCs, suggesting that many more mechanisms are responsible for this difference than simply the effect of miR-335-5p.

As previously stated, there have been numerous studies associating CXCL12 and CCL11 with myelination via various mechanism and cell types such as astrocytes, neuronal cells, optic nerve cells, and oligodendrocytes, but none have made the connection with the pro-myelinating effect of CXCL12 via OM-MSCs or of CCL11 via OM-MSCs. Here the pro-myelinating effect of OM-MSCs can be attributed, at least in a contributory way, to the secretion

of CXCL12 which is regulated by miR-140-5p. The effect of CCL11 on our in vitro myelination model was not investigated here, but there is a case for the potential of CCL11 to influence myelination also, and that it too is regulated by miR-140-5p.

The secretome of the MSC is of vast important for vital biological functions, from immunomodulation (454-458) to regulation of haematopoiesis (459-462). Secretomes of MSCs from other niches such as umbilical cord have been shown to differ slightly from that of bone marrow-derived MSCs (388), but no studies have focused on the secretome of the OM-MSC. Not shown in this study were the full results of each cytokine array that was carried out, showing all of the cytokines that were expressed by both BM-MSCs and OM-MSCs. As a comparative study, my focus was on the differentially secreted cytokines, so equivalently secreted cytokines were not mentioned. Park *et al*. however, carried out an extensive study into the secretome of BM-MSCs (388), listing 120 cytokines found to be secreted by BM-MSCs. Interestingly, all of the cytokines found to be secreted by BM-MSCs and OM-MSCs during my analysis were found to be secreted by BM-MSCs in this study, which further validates both my data, and the identity of OM-MSCs as a unique MSC phenotype. This shows that although BM-MSCs and OM-MSCs share a similar secretome which is typical of the known MSC secretome, certain cytokines are secreted at significantly different levels from either BM-MSCs or OM-MSCs, suggesting that their niche may be regulating the secretion of certain cytokines, and thus the biology of the MSC, depending on its behavioural requirement in that particular environment.

As previously discussed with regard to the differentially secreted cytokines, they each have uniquely separate chemotactic or immunomodulatory functions. Although they may not be related to myelination, cell survival, or cell proliferation as focused on in this study, their differential expression suggests that they play a distinct role in regulating their niche via other mechanisms, which are very specific to

that particular niche. For example, a number of distinct signalling pathways such as wnt (463, 464), BMP (465), and notch (459, 466) regulate haematopoiesis via cytokines secreted by BM-MSCs. It would be very interesting to see if these same pathways are activated in a similar way by OM-MSCs whose primary role in the olfactory system may not be associated with haematopoiesis.

Throughout this chapter we demonstrated that the secretion of cytokines such as CXCL12 and CD95 could be manipulated by targeting their upstream regulatory miRNA. This has been demonstrated in other studies that have identified miRNA as targets for pathway regulation. For example, Selvamani *et al*. (467) demonstrated that the NF-κB pathway can be regulated by targeting miR-146a-5p. NF-κB was identified in Figure 3.14 by Sistemic's miRNA network map to be regulated by miR-146a-5p, and is a ubiquitous cytokine with numerous modulatory effects throughout the body such as Nitric Oxide production (468), cancer cell migration (469), apoptosis (470), and neuroinflammation (513). This ability to control cytokine secretion, and the promiscuity of these cytokine/miRNA relationships (numerous cytokines regulated by the same miRNA), mean that these targeting strategies have great therapeutic potential for the future.

5.7. Summary

- miR-140-5p and miR-335-5p are upregulated 3.7 and 7.6 fold respectively in BM271-MSCs compared to OM-MSCs, and miR-146a-5p is downregulated 15.5 fold in BM271-MSCs compared to OM-MSCs
- Cytokine arrays demonstrate a relationship between CXCL12 and CCL11 with the myelination associated miR-140-5p
- Pro-myelinating effect of CXCL12 is confirmed, and this effect is shown to be related to the secretion of CXCL12 by OM-MSCs
- Pro-myelinating effect of CXCL12 can be manipulated by controlling expression of miR-140-5p, as can levels of CCL11

- Rat cytokine arrays demonstrate comparable secretion patterns of cytokines MIP-2, IP-10, RANTES, Fraktalkine, and LIX in pro-myelinating cells OECs and OM-MSCs which isn't seen in de-myelinating cells BM-MSCs and Schwann cells
- Relationship between miR-146a-5p and "death receptor" CD95 was confirmed, suggesting a possible mechanism for the increased survival rates of OM-MSCs
- Manipulation of miR-335-5p showed significant differences in proliferation between OM-MSCs transfected with inhibitor and mimic of miR-335-5p but not compared to controls
- No significant difference in proliferation of BM271-MSCs was observed after transfection with inhibitor and mimic of miR-335-5p, suggesting additional mechanisms responsible for the observed difference in proliferation between the two MSC types

Discussion:

6. General Discussion

6.1. Overview

MSCs generated from any cellular niche within the body have a number of defining properties. As stem cells, they have the ability to self-replicate and to differentiate to a fully mature functioning cell, which is true for all stem cells. What makes MSCs unique is their combined ability to form any cell of mesenchymal lineage (bone, fat cartilage, connective tissue, and muscle), their ability to migrate to a specific site of injury, their plastic adhesion capabilities, their immunomodulatory effects, their "bystander effects" due to their substantial secretome, and their potential (disputed) to trans-differentiate towards cells of other lineages such as neurons (39, 40). It is the combination of these traits which separate MSCs from all other adult stem cells, and which give them such exciting potential in the field of regenerative medicine. These traits are true of all MSCs throughout the body, but are MSCs from different niches really the same? Do they express the same genes and possess the same cell surface markers? Do they differentiate in the same way or react to the same substrates in the same way? Do they have the same secretomes and pre-translation mechanisms? And most importantly of all, do they produce the same effect on various other biological systems that they will contact within the body, and thus have the same therapeutic potential? These are all questions which were addressed throughout this thesis when comparing MSCs from two completely distinct cellular niches; the bone marrow and the more neurogenic olfactory system.

It had been previously shown that MSCs from the olfactory system possess a pro-myelinating effect which is not observed with MSCs from the bone marrow. This thesis explored the differences and similarities of both MSC phenotypes to try and understand any underlying mechanisms pertaining to this effect, and more importantly, if these mechanisms can be potentially manipulated for therapeutic benefit with regards to certain neurodegenerative conditions such as Multiple Sclerosis and Spinal Cord Injury.

6.2. Summary of Results

Due to the different isolation methods of BM-MSCs and OM-MSCs, BM-MSCs were separated into two types; BM-MSCs which were isolated from bone marrow using normal plastic adhesion methods, and BM271-MSCs which were first isolated in this manner, and then underwent the same CD271 isolation as the OM-MSCs. This was to eliminate any question of effect of the different isolation methods on the cell's behaviour. Imaging under phase microscopy showed that each of the three MSC phenotypes were morphologically indistinguishable under normal culture conditions.

Behavioural analysis showed that OM-MSCs proliferated at a significantly higher rate than both BM phenotypes, which were very similar in their proliferation rates. This difference in proliferation was substantial, with OM-MSCs generating almost 100x more cells than both BM phenotypes after 25 days. This related to anecdotal observations of a fully confluent flask of OM-MSCs a week after isolation, compared to one month after isolation of BM-MSCs.

Profiling of each cell type comparing mRNA expression, and immunoreactivity of a number of MSCs markers, showed that each MSC type expressed all MSC classical markers at both a pre- and post-transcriptional level, except for the early MSC marker Stro-1, which was only expressed in around 40% of BM-MSCs. The lack of Stro-1 observed in OM-MSCs could be due to the fact that they simply don't express it, or that CD271 cells do not co-express Stro-1, and therefore all Stro-1 cells were lost during the isolation process. This reason could also be put forward for the lack of Stro-1 expression observed in BM271-MSCs, but this could also be down to the extended periods in which BM271-MSCs remain in culture due to the CD271 antibody mediated isolation process. Although each MSC type expressed all the same markers (except Stro-1), levels of expression of some of these markers were not the same. For example, levels of classic MSC markers CD90, CD166, and CD271 were significantly higher in OM-MSCs and BM271-MSCs at either mRNA or protein level, suggesting a "purer",

possibly more homogenous population of MSCs. Most interestingly however, was the significantly higher expression of Nestin mRNA and protein in OM-MSCs compared to both BM-MSC phenotypes confirming previous data of Delorme *et al*. (36). Nestin is not just an MSC marker but also a marker of a number of neuroectoderm-derived cells such as neurons and glia. Nestin expression was also significantly higher in non-purified OM tissue and OM-flowthrough cells compared to both BM-MSC types and fibroblasts, suggesting that this is likely associated with the olfactory niche. Nestin is also down regulated upon differentiation, and is associated with immature cells and cells which are generated post-pathological scenarios (471, 472). The vulnerable nature of the OM could be a possible explanation for this elevated nestin expression, and perhaps even the observed increase in proliferation. It is important to add that when compared against fibroblasts, it was demonstrated that neither MSC type exhibited a similar mRNA or profile of markers, and thus the OM-MSCs can be considered as legitimate MSC phenotypes. Figure 6.1 outlines the numerous different MSC phenotypes and their resident niches. I have added the olfactory mucosa to the figure as a new niche, as OM-MSCs have been shown to be a new addition to the MSC family, and a viable, easily accessible alternative to BM-MSCs for MSC transplant-based therapies.

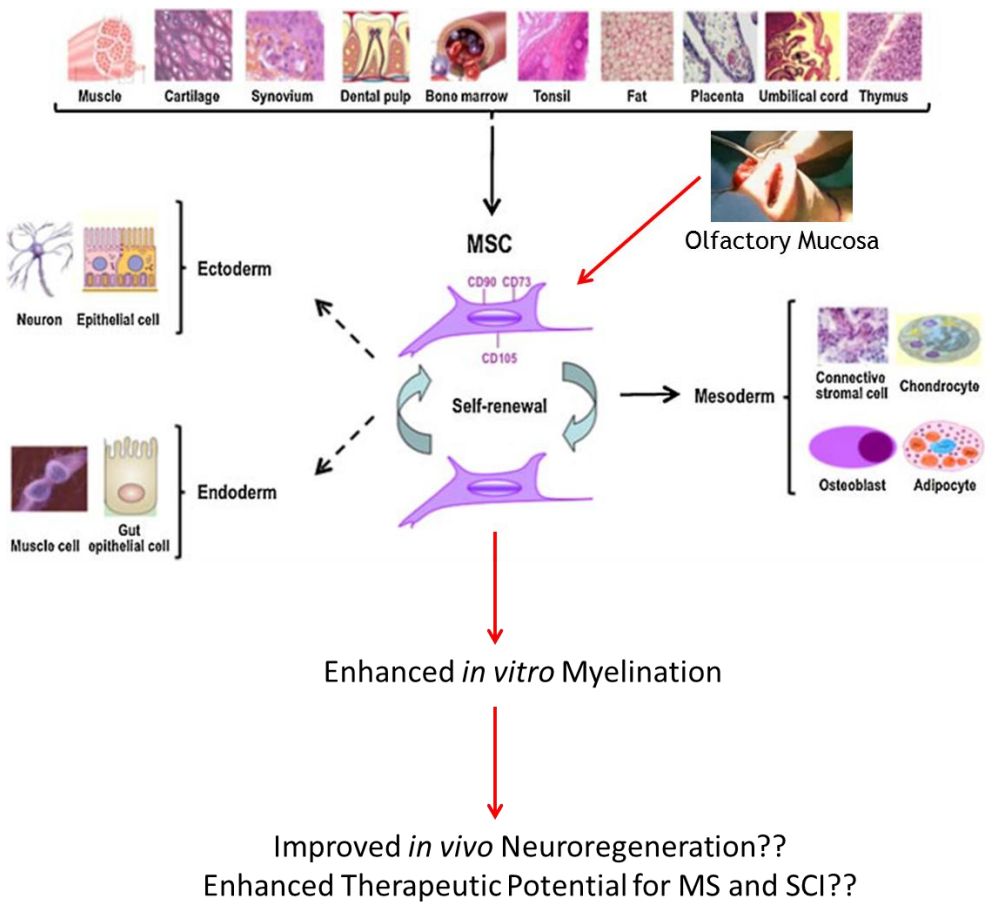

Figure 6.1: Schematic diagram representing the different MSC niches throughout the body. Adapted from Kuhn and Tuan (473).

Comparison of the differentiation capabilities of each MSC type demonstrated that each had the ability to form bone and fat, but that non-purified BM-MSCs produced significantly more bone and fat than OM-MSCs, and more fat compared to BM271-MSCs. These comparisons also show BM271-MSCs produced significantly more bone and fat than OM-MSCs. Non-purified BM-MSCs contain not just MSCs but also a range of mesenchymal progenitors (474). These data suggest that these progenitors are contributing to the increased bone and fat production, and that they may be lost during the CD271 selection process. The data also suggests that there may be an inherent niche-dependant effect on OM-MSCs which may be preventing them from differentiating into bone and fat as efficiently as those derived from BM, such as an increased expression of Nestin perhaps?

Due to the neuroregenerative nature of the OM, and the lack of mesenchymal tissue, the production of bone and fat may not be the primary role of MSCs within the OM.

Analysis of differentiation potential was not limited to bone and fat however, nor was it limited to media induced differentiation. BM271-MSCs and OM-MSCs were induced under different media conditions to differentiate towards neuronal, myogenic, and glial lineages. RT-qPCR showed a significant increase in expression of mRNA associated with each of these lineages in treated BM271-MSCs compared to untreated controls, except MAP2, a neuronal marker, which showed a trend of increased expression which was not significant. Any increased expression of these mRNA observed in OM-MSCs was either lower than that observed in BM271-MSCs or not significant. These data add credence to the hypothesis that the immature (Nestin positive) state of OM-MSCs, and the neuroregenerative, non-mesenchymal OM niche are not conducive to the production of mesenchymal tissue being the primary function of the OM-MSCs. i.e. OM-MSCs may help to generate new bone, fat and cartilage tissue in the nose and skull, but the soft tissue, neurogenic environment where they reside could require OM-MSCs to provide a more "bystander effect" role such as regulating neurogenesis via their secretome.

The ability to induce MSC differentiation along specific lineages was not limited to culture condition but could also be instigated by substrate topography (46, 256, 325, 331-334). Each cell type was cultured on nanotopography embossed PCL, a substrate that had been shown from previous studies to induce osteogenic differentiation (257). I observed an enhanced ability for BM-MSCs and BM271-MSCs to express not only mRNA associated with osteogenesis, but mRNA associated with other lineages too, compared to OM-MSCs. Immunocytochemistry showed that not all of these mRNA were translated into their respective proteins, but did demonstrate an increase in IR for OPN, OCN, SMA, Tuj-1, and GFAP, each of which can be associated with osteogenic differentiation. As before, each

of these proteins were expressed at significantly higher levels in BM- or BM271-MSCs compared to OM-MSCs, suggesting an enhanced ability for nanotopography induced osteogenic differentiation in MSCs derived from the bone marrow compared to those derived from the olfactory mucosa. No work has been done using these particular surfaces and MSCs from other niches, and indeed very little work has been carried out using MSCs isolated from other niches on any nanotopographies, however, Nemeth *et al*. (475) has shown an enhanced chondrocytic differentiation of dental pulp MSCs when cultured on nanopatterned hydrogels, and adipose-derived MSCs have been differentiated towards an endothelial lineage using nanograted quartz substrates (476). Little is known about the mechanisms of differentiation by cell/nanotopography interactions, but a number of studies have put forward hypotheses. Teo *et al*. and McNamara *et al*. (46, 477) both discuss how specific nanotopographies guide signals through the extracellular matrix via proteins such as Focal Adhesion Kinase (FAK). This triggers their phosphorylation, and in turn stimulates numerous signalling cascades which terminate in the nucleus and lead to specific translational events, such as increased production of bone proteins such as Runx2 and osteopontin. These hypotheses relate only to BM-MSCs however, as no such studies have been carried out using MSCs from any other niches. Importantly, with regards to my findings, although increases in expression of MAP2 mRNA and MyoD mRNA were observed, there was no evidence that any trans-differentiation occurred under these conditions. Additionally, by this stage in the thesis, there was nothing to suggest that any observed differences between BM- and OM-MSCs would be affected by the CD271 positive selection process, therefore only BM271-MSCs would be used as a comparison against OM-MSCs henceforth.

Analysis of pre-translational differences between BM271- and OM-MSCs enabled the investigation into possible mechanisms behind the pro-myelinating effects of OM-MSCs observed by Lindsay *et al*. SistemQC™ miRNA fingerprinting carried out by Sistemic uncovered a 64% homology in the miRNA expression of BM- and OM-MSCs, but more importantly, showed

26 miRNA which were significantly differentially expressed between the two MSC phenotypes. Through previous studies, three of these miRNA; miR-140-5p, miR-146a-5p, and miR-335-5p were linked to three important biological differences which have been observed between BM- and OM-MSCs; myelination, cell survival, and proliferation respectively. These differential expression were confirmed by RT-qPCR, and cytokines networks were provided by Sistemic, outlining a number of different cytokines known to regulated by each miRNA.

The secretomes of both cell types were compared to investigate any cytokines which were secreted at a significantly different concentration, and if so, to identify any links between them and the differentially expressed miRNA. A number of different cytokines were identified such as CCL11, and CXCL12, which have also been previously associated with myelination (424, 429). CXCL12 now became a very important molecule, as it had not only been shown to be secreted at a significantly higher concentration in OM-MSCs compared to BM271-MSCs and to OM-flowthrough cells, but had also been previously identified as being regulated by miR-140-5p, which was shown to be upregulated significantly in BM271-MSCs compared to OM-MSCs. This particular miRNA is important, as miR-140-5p has previously been associated with influencing CNS axonal myelination (379, 419). These data suggested that the decrease in miR-140-5p expression in OM-MSCs could lead to an increase in CXCL12 secretion, and thus a potential pro-myelinating effect. The pro-myelinating effect of CXCL12 was confirmed by its addition to the myelinating culture system at 100 ng/µL, and it's connection to OM-MSCs was confirmed using AMD3100, a blocker of CXCR4 and CXCR7 on which CXCL12 acts, and a neutralising antibody to CXCL12. When these were added to the myelinating culture system prior to the addition of pro-myelinating OM conditioned media, the result was a significant decrease in myelination. This confirmed that the promyelinating effects of OM-MSCs were at least in part due to the secretion of CXCL12. Further to this, it was demonstrated that the secretion of CXCL12 could be manipulated by targeting miR-140-5p.

Transfection of both MSC types with an inhibitor of miR-140-5p led to a significant increase in the secretion of CXCL12, which in turn led to an increase in myelination when the conditioned media from these transfections was added to the myelinating cultures.

This targeting was also carried out for miR-146a-5p, which has been associated with cell survival due to its regulation of FasR (CD95), a "death receptor" which triggers apoptosis. The ~15 fold increase in expression of miR-146a-5p in OM-MSCs compared to BM271-MSCs was proposed as a potential hypothesis as to why OM-MSCs are able to survive many more passages than BM271-MSCs. Western blotting confirmed that expression of CD95 was expressed at a significantly lower level in OM-MSCs compared to BM-MSCs, and also that CD95 expression could be manipulated by transfecting the cells with either an inhibitor or mimic of miR-146a-5p. Further experiments would have to be carried out however, to determine whether or not this manipulation of CD95 would actually have a significant effect of the cell survival rates of these MSCs.

Finally, under the same transfection procedure, miR-335-5p was targeted to determine any potential manipulation of cell proliferation rates. A considerable benefit of OM-MSCs over BM-MSCs is there advanced proliferative capacity, and miR-335-5p has been previously implicated in the regulation of cell proliferation. If BM-MSCs could be manipulated to achieve the same rates of cell production by way of a simple transfection, this would be of enormous benefit in MSC research. This experiment however, yielded little significant data. Although trends were observed which suggested an effect between OM-MSCs transfected with miR-335-5p inhibitor and miR335-5p mimic, these observations were not significant when compared to controls. BM271-MSCs which were transfected with miR-335-5p inhibitor certainly showed no suggestion of an ability to increase their proliferation via this mechanism. miR-335-5p may play a role in cell proliferation, but there are likely many other mechanisms involved, and

this one-step approach to manipulating MSC proliferation is unfortunately not a viable one.

6.3. Observed Differences

These data offer up a number of differences between MSCs derived from bone marrow and from the olfactory system. Their MSC phenotype has been firmly established, so why are OM-MSCs so different when they originate from the same mesenchymal lineage as BM-MSCs? I would first approach this question by asking, are OM-MSCs definitely from the mesenchymal lineage? As mentioned in the introduction, there are a population of ectodermally-derived mesenchymal cells which originate at the neural crest. These cells go on to form the bone and cartilage in the head, so it may be possible that OM-MSCs have their origins in the neural crest as opposed to the mesodermally derived BM-MSCs. Studies have looked at the potential of using neural crest mesenchymal cells in the treatment of SCI repair (478, 479), and Achilleos *et al*. has looked at neural crest stem cells in great detail regarding their properties and therapeutic potential (480), but there has been no direct comparison between mesodermally-derived BM-MSCs and ectodermally-derived mesenchymal cells (EDMCs), or indeed between OM-MSCs and EDMCs, so it may be that OM-MSCs and BM-MSCs do not share the same origins after all. Assuming that they do though, the observed differences must surely be a niche effect? The BM-MSC niche is an encapsulated, protected, and predominantly stromal environment. Matrices are stiff and topographies are rough, conducive of osteogenesis and chondrogenesis, but also with cues to encourage adipogenesis (248, 481). BM-MSCs are also the minority stem cell in the bone marrow which is essentially a haematopoietic niche with a slow and steady cell turnover (312-314). The olfactory mucosa is in complete contrast to bone marrow. Consisting predominantly of soft tissue, it is exposed with only the protection of a mucous membrane, and is therefore an area of high cellular turnover (1, 35, 36, 142). OM-MSCs are also the minority stem cell within the OM, which is essentially a neurogenic niche, so even if OM-MSCs and BM-MSCs are both mesodermally-derived

MSCs, they may perform very distinct functions driven by niche-dependant external cues. The chemokine arrays carried out in section 3.2.1 of the results showed an increased secretion from BM-MSCs of chemokines such as IL-9, a very important cytokine in the regulation of haematopoiesis (421), and IL-6 which is secreted by osteoblasts and is important in bone resorption (452). Whereas significant increases in the secretion of chemokines such as CCL11 and CXCL12 were observed in OM-MSCs, both of which are important in neurogenesis, glial proliferation, and myelination (395-399, 407, 410-414, 428, 429, 433). These observations add credence to the hypothesis that these two distinct MSC phenotypes have distinct inherent behaviours which are guided by the necessity of their particular niche for them to carry out particular functions which are unique to that niche. It would be very interesting to carry out *in vivo* experiments where each MSC is ectopically transplanted into the other's niche to investigate the niche effect further. Perhaps neurogenesis in the OM might be impaired by a replacement of OM-MSCs by BM-MSCs, or perhaps the BM-MSCs may inherit the features and behaviours of the OM-MSCs over time in the OM niche.

OM-MSC, although from a very different, neurogenic niche have very similar properties to BM-MSCs, and due to their promyelinating capacity could indeed be considered as viable alternatives to BM-MSCs. Moreover, their more accessible location within the olfactory mucosa adds extra credence to this proposal.

6.4. Therapeutic Potential of Phenotypic Differences

The observed differences between OM-MSCs and BM-MSCs have great research potential. The extensive proliferative capacity of OM-MSCs is a great asset in terms of tissue culture. One of the limitations of BM-MSCs in research is their slow proliferation. From a 20 mL bone marrow aspirate (a normal size from a patient donation), it is common to isolate a very small number of MSCs, often <20 cells. Under optimal conditions you may be able to bulk these 20 cells up to ~10^6 cells after one month in culture, by which

time you may already have passaged them twice. With only a maximum of six passages per sample, you really require a constant supply of bone marrow aspirates to allow for the amount of cells required for experimental purposes. Without a constant supply, often some techniques which require large volumes of cells, like FACS analysis for example, have to be discounted. With OM-MSCs however, their rate of proliferation is so high, and the cells are so much more robust, that 20 MSCs isolated from a tissue biopsy could be bulked up to ~$5x10^6$ within one week, with only one passage. This number can be doubled every 2-3 days forthwith, allowing for the collection of a vast number of low passage cells very quickly. OM-MSCs were able to survive passaging far beyond the recommended 6-8 passages which BM-MSCs cannot exceed, although throughout this study, cells were never used beyond passage 5. Anecdotally, OM-MSCs were still incredibly robust and viable beyond 10 passages, although their stemness was never investigated. BM-MSCs are known to lose their defining markers such as Nestin, CD271, and Stro-1 over time, and are also thought to spontaneously differentiate towards chondrocytes or osteocytes after multiple divisions on plastic surfaces, therefore losing their stemness (482, 483). It would be very interesting to find out if OM-MSCs are able to maintain their stem cell traits over multiple passages. Their enhanced expression of Nestin suggests that they may be more embryonic in terms of development, so may be able to survive much longer in culture.

MSCs currently have a number of potential therapeutic applications from stroke, Alzheimer's, autoimmune diseases, amyotrophic lateral sclerosis (ALS), and SCI, as well as orthopaedic conditions such as osteo imperfecta (176-181). These therapies are predominantly focused on the use of BM-MSCs, but OM-MSCs which display a number of similar behavioural and biomolecular properties compared to BM-MSCs can now be considered to be a viable alternative source for autologous MSC transplant-based therapies. They may also be considered a preferred alternative based on their location and relative ease of accessibility compared to BM-MSCs, retrieval of which requires very painful and invasive surgery. More research would

have to be carried out to determine exactly how viable an alternative they are, but the data presented in this thesis certainly highlights their potential as such. Connick *et al*. (197) studied 10 patients of secondary MS treated with *ex-vivo* expanded BM-MSCs, and observed a significant overall increase in many of the visual impairments which are symptomatic of the disease. It is not possible to determine the exact mechanisms involved in this improvement, but it is likely due to a regeneration of the optic nerve which gets progressively demyelinated throughout the course of the disease. It would be very interesting to see if OM-MSCs, which elicit an enhanced myelination response *in vitro* compared to BM-MSCs, could stimulated a more improved response and an increased regeneration of symptomatic MS damage.

The differences between BM-MSCs and OM-MSCs outlined in this thesis, and by Lindsay *et al*. also suggest potential therapeutic applications for OM-MSCs for which BM-MSCs may not be a viable candidate. The significantly increased secretion of CXCL12 observed in OM-MSCs is very important in terms of regenerative capabilities, especially neuroregeneration. CXCL12 is quite a ubiquitously expressed chemokine, acting on receptors CXCR4 and CXCR7, which are expressed on a number of different cells throughout the body (414). This receptor/ligand interaction results in the proliferation, and thus increased activity of the cells which express either (or both) receptor(s) (398, 414, 433). This is the proposed mechanism of action of the increased axonal myelination observed by Lindsay *et al*. (1) and throughout this thesis. It is hypothesised that CXCL12 stimulates the proliferation of CXCR4 expressing oligodendrocytes, and therefore increases the amount of myelin produced within that particular locus. It may also be possible that the CXCL12/CXCR4 interaction stimulates the oligodendrocytes themselves to produce more myelin. More work will have to be carried out to determine exactly how oligodendrocytes elicit this response, but recent data in our lab (not shown) has demonstrated this increase in *in vitro* myelination is by CXCL12/oligodendrocyte interactions. This has major therapeutic implications with regards to conditions such as

MS and SCI where stimulation of local oligodendrocyte populations to enhance myelination could have a profound effect on the pathologies and progression of these conditions. Studies have already shown a regeneration of optic nerve damage after treatment with CXCL12 (397), and CXCL12 has also been shown to decrease neuroinflammation and stimulate neuronal cell migration (395, 433), thus, the application of CXCL12 alongside other complimentary applications could provide the neuroregenerative capacity that is needed to reverse the effects of all demyelinating and neurodegenerative conditions.

6.5. Therapeutic Targets

CXCL12 is clearly a chemokine of therapeutic interest, but in what manner could its regulation be targeted? As mentioned in the introduction, the CNS is a very sensitive structure, vulnerable to secondary damage, so in situ administration would be difficult. As MSCs have been shown to migrate to a site of injury after intravenous, intracranial, or intraperitoneal administration (186-189), OM-MSCs could be administered in either of these ways to allow secretion of CXCL12 into the site of injury via exogenous and autologous OM-MSC populations. This could be coupled with an increase in the expression of CXCL12's receptors CXCR4 and CXCR7, to increase the amount of receptor/ligand interaction, and potentially stimulate an increase in myelin production. CXCR4 has been shown to be regulated by a number of transcription factors and signalling molecules. Nuclear Respiratory Factor-1 (NRF-1), YingYang-1 (YY-1), cyclic AMP (cAMP), Interleukin-2 (IL-2), IL-4, IL-7, IL-10, IL-15, TGF-1β, VEGF, and EGF have all been shown to stimulate the production of CXCR4, and Tumour Necrosis Factor-1 (TNF-1), Interferon-γ (IFN-γ), and IL-1β have all been shown to attenuate CXCR4 expression (473, 484-493). Therefore the effects of CXCL12/CXCR4 interactions in situ could be stimulated by gene knockouts directly effecting the production of these attenuating factors, or by knocking out genes of downstream effectors which would lead to the increased expression of the stimulatory factors. One other approach that was discussed in section 3 of the results chapter could be to target miR-

140-5p. It was shown in this chapter that inhibition of miR-140-5p lead to an increased expression of CXCL12 in both OM- and BM-MSCs, which led to an increase in axonal myelination. This approach could therefore be targeted to encourage endogenous populations of cells such as oligodendrocytes, whose myelinating effect is regulated by the action of CXCL12 on their cell surface receptors, CXCR4 and CXCR7 (398, 419), to increase their secretion of CXCL12, and thus potentially stimulate axonal remyelination at lesion sites. This however could pose the issue of an unwanted regulation of miR-140-5p in other local cell populations, which could result in a shift in equilibrium, and further potential issues. It would have to be established first, which potentially affected cells express miR-140-5p, and what knock on effects a regulation of this would have on other endogenous populations. Furthermore, with CNS injuries and disorders having so many different pathologies, any CXCL12-based therapies would have to be just one part of a multifaceted approach to be fully efficacious, encompassing many fields of biomedical science such as cell engineering, immunology, glial biology, stem cell biology, and neuroscience.

Conclusion:

7. Conclusion

Throughout this thesis, MSCs from bone marrow and from the olfactory system have proved to be very similar in many respects, but also profoundly different in a number of their behaviours. They certainly are a viable alternative autologous source for MSC-based therapies, which may even be better alternatives for some conditions, especially those dependant on remyelination and neuroregeneration strategies. Data compiled throughout suggests that the observed promyelinating effects of OM-MSCs is likely due to the secretion of CXCL12, which acts on CXCR4 and CXCR7, and which is regulated by the microRNA miR-140-5p. Each of these are credible target scenarios for CNS repair, and future research into complimentary therapies to accompany these scenarios could yield a very promising outlook in the field of cell-based regenerative medicine.

Appendices:

8. Appendices

GU020.001 sample ID	Yield (ng/µl)	rRNA ratio	RIN
OM-MSC 1	151.5	2	10
OM-MSC 2	90.56	2.1	10
OM-MSC 3	252.18	2	10
OM-MSC 4	103.47	2.2	10
BM-MSC1	150.91	2	10
BM-MSC2	121.81	2.1	10
BM-MSC3	145.91	2.1	10
BM-MSC4	105.94	1.9	10

Appendix 1: Summary of RNA QC checks, taken from Sistemic's draft report

GU020.001 sample ID	Array name	Agilent QC result
OM-MSC 1	253118112824_2_4	Good to excellent
OM-MSC 2	253118112824_1_2	Good to excellent
OM-MSC 3	253118112824_2_2	Good to excellent
OM-MSC 4	253118112824_1_4	Good to excellent
BM-MSC1	253118112824_2_1	Good to excellent
BM-MSC2	253118112824_1_3	Good to excellent
BM-MSC3	253118112824_2_3	Good to excellent
BM-MSC4	253118112824_1_1	Good to excellent

Appendix 2: Summary of miRNA array QC checks, taken from Sistemic's draft report

miRNA I.D.				
hsa-let-7a-5p	hsa-miR-140-3p	hsa-miR-214-3p	hsa-miR-320d	hsa-miR-4281
hsa-let-7b-5p	hsa-miR-140-5p	hsa-miR-218-5p	hsa-miR-320e	hsa-miR-4284
hsa-let-7c	hsa-miR-143-3p	hsa-miR-22-3p	hsa-miR-323a-3p	hsa-miR-4286
hsa-let-7d-5p	hsa-miR-145-3p	hsa-miR-22-5p	hsa-miR-324-3p	hsa-miR-4291
hsa-let-7e-5p	hsa-miR-145-5p	hsa-miR-221-3p	hsa-miR-324-5p	hsa-miR-4299
hsa-let-7f-5p	hsa-miR-146a-5p	hsa-miR-221-5p	hsa-miR-329	hsa-miR-4306
hsa-let-7g-5p	hsa-miR-148a-3p	hsa-miR-222-3p	hsa-miR-331-3p	hsa-miR-4313
hsa-let-7i-5p	hsa-miR-148b-3p	hsa-miR-224-5p	hsa-miR-335-5p	hsa-miR-4324
hsa-miR-100-5p	hsa-miR-150-3p	hsa-miR-23a-3p	hsa-miR-337-3p	hsa-miR-4327
hsa-miR-101-3p	hsa-miR-151a-3p	hsa-miR-23b-3p	hsa-miR-337-5p	hsa-miR-450a-5p
hsa-miR-103b	hsa-miR-151a-5p	hsa-miR-24-3p	hsa-miR-342-3p	hsa-miR-455-3p
hsa-miR-106a-5p	hsa-miR-152	hsa-miR-25-3p	hsa-miR-34a-5p	hsa-miR-487b
hsa-miR-106b-5p	hsa-miR-154-3p	hsa-miR-26a-5p	hsa-miR-34b-5p	hsa-miR-493-5p
hsa-miR-107	hsa-miR-155-5p	hsa-miR-26b-5p	hsa-miR-3529-3p	hsa-miR-494
hsa-miR-10b-5p	hsa-miR-15a-5p	hsa-miR-27a-3p	hsa-miR-361-5p	hsa-miR-495
hsa-miR-1202	hsa-miR-15b-5p	hsa-miR-27b-3p	hsa-miR-3651	hsa-miR-497-5p
hsa-miR-1207-5p	hsa-miR-16-5p	hsa-miR-28-5p	hsa-miR-3652	hsa-miR-503
hsa-miR-1225-3p	hsa-miR-181a-5p	hsa-miR-2861	hsa-miR-3653	hsa-miR-543
hsa-miR-1225-5p	hsa-miR-181b-5p	hsa-miR-299-5p	hsa-miR-3656	hsa-miR-551b-3p
hsa-miR-1228-3p	hsa-miR-1825	hsa-miR-29a-3p	hsa-miR-3659	hsa-miR-574-3p
hsa-miR-1234	hsa-miR-185-5p	hsa-miR-29b-3p	hsa-miR-365b-3p	hsa-miR-574-5p
hsa-miR-1238	hsa-miR-18a-5p	hsa-miR-29c-3p	hsa-miR-3663-3p	hsa-miR-575
hsa-miR-1246	hsa-miR-191-3p	hsa-miR-301a-3p	hsa-miR-3665	hsa-miR-638
hsa-miR-125a-5p	hsa-miR-1914-3p	hsa-miR-30a-3p	hsa-miR-3676-3p	hsa-miR-642b-3p
hsa-miR-125b-5p	hsa-miR-1915	hsa-miR-30a-5p	hsa-miR-3679-5p	hsa-miR-654-3p
hsa-miR-1260a	hsa-miR-193a-3p	hsa-miR-30b-5p	hsa-miR-374a-5p	hsa-miR-758
hsa-miR-1260b	hsa-miR-193a-5p	hsa-miR-30c-5p	hsa-miR-374c-3p	hsa-miR-762
hsa-miR-1268b	hsa-miR-193b-3p	hsa-miR-30d-5p	hsa-miR-376a-3p	hsa-miR-874
hsa-miR-127-3p	hsa-miR-195-5p	hsa-miR-30e-5p	hsa-miR-376b	hsa-miR-92a-3p
hsa-miR-1275	hsa-miR-1973	hsa-miR-31-3p	hsa-miR-376c	hsa-miR-93-5p
hsa-miR-128	hsa-miR-199a-3p	hsa-miR-31-5p	hsa-miR-377-3p	hsa-miR-939
hsa-miR-1280	hsa-miR-199a-5p	hsa-miR-3132	hsa-miR-379-5p	hsa-miR-940
hsa-miR-1281	hsa-miR-199b-5p	hsa-miR-3162-5p	hsa-miR-381	hsa-miR-98
hsa-miR-1305	hsa-miR-19a-3p	hsa-miR-3188	hsa-miR-409-3p	hsa-miR-99a-5p
hsa-miR-130a-3p	hsa-miR-19b-3p	hsa-miR-3195	hsa-miR-410	hsa-miR-99b-5p
hsa-miR-130b-3p	hsa-miR-20a-5p	hsa-miR-3196	hsa-miR-411-5p	
hsa-miR-136-3p	hsa-miR-20b-5p	hsa-miR-3198	hsa-miR-423-5p	
hsa-miR-136-5p	hsa-miR-21-3p	hsa-miR-320a	hsa-miR-424-5p	
hsa-miR-137	hsa-miR-21-5p	hsa-miR-320b	hsa-miR-425-3p	
hsa-miR-138-5p	hsa-miR-210	hsa-miR-320c	hsa-miR-425-5p	

Appendix 3: Table of the 195 miRNA detected in at least one sample

miRNA I.D.			
hsa-let-7b-5p	hsa-miR-1914-3p	hsa-miR-320c	hsa-miR-642b-3p
hsa-let-7c	hsa-miR-193a-3p	hsa-miR-320d	hsa-miR-92a-3p
hsa-let-7e-5p	hsa-miR-193a-5p	hsa-miR-320e	hsa-miR-940
hsa-let-7i-5p	hsa-miR-193b-3p	hsa-miR-324-3p	hsa-miR-99a-5p
hsa-miR-100-5p	hsa-miR-1973	hsa-miR-324-5p	hsa-miR-99b-5p
hsa-miR-103b	hsa-miR-199a-3p	hsa-miR-329	
hsa-miR-107	hsa-miR-199a-5p	hsa-miR-331-3p	
hsa-miR-1202	hsa-miR-19b-3p	hsa-miR-337-3p	
hsa-miR-1225-3p	hsa-miR-21-3p	hsa-miR-337-5p	
hsa-miR-1225-5p	hsa-miR-21-5p	hsa-miR-342-3p	
hsa-miR-1228-3p	hsa-miR-210	hsa-miR-361-5p	
hsa-miR-1234	hsa-miR-214-3p	hsa-miR-3651	
hsa-miR-1238	hsa-miR-22-3p	hsa-miR-365b-3p	
hsa-miR-1246	hsa-miR-22-5p	hsa-miR-3676-3p	
hsa-miR-125a-5p	hsa-miR-221-3p	hsa-miR-3679-5p	
hsa-miR-125b-5p	hsa-miR-221-5p	hsa-miR-374a-5p	
hsa-miR-1260a	hsa-miR-222-3p	hsa-miR-374c-3p	
hsa-miR-1260b	hsa-miR-23a-3p	hsa-miR-376a-3p	
hsa-miR-1268b	hsa-miR-23b-3p	hsa-miR-376c	
hsa-miR-127-3p	hsa-miR-24-3p	hsa-miR-377-3p	
hsa-miR-1275	hsa-miR-26a-5p	hsa-miR-381	
hsa-miR-128	hsa-miR-27a-3p	hsa-miR-410	
hsa-miR-1280	hsa-miR-27b-3p	hsa-miR-411-5p	
hsa-miR-1281	hsa-miR-28-5p	hsa-miR-423-5p	
hsa-miR-1305	hsa-miR-299-5p	hsa-miR-425-3p	
hsa-miR-130a-3p	hsa-miR-29a-3p	hsa-miR-4284	
hsa-miR-136-3p	hsa-miR-29c-3p	hsa-miR-4286	
hsa-miR-136-5p	hsa-miR-30a-3p	hsa-miR-4291	
hsa-miR-138-5p	hsa-miR-30a-5p	hsa-miR-4299	
hsa-miR-148b-3p	hsa-miR-30b-5p	hsa-miR-4306	
hsa-miR-151a-3p	hsa-miR-30c-5p	hsa-miR-4313	
hsa-miR-151a-5p	hsa-miR-30d-5p	hsa-miR-4324	
hsa-miR-152	hsa-miR-30e-5p	hsa-miR-487b	
hsa-miR-154-3p	hsa-miR-3132	hsa-miR-493-5p	
hsa-miR-15a-5p	hsa-miR-3162-5p	hsa-miR-494	
hsa-miR-16-5p	hsa-miR-3195	hsa-miR-495	
hsa-miR-181a-5p	hsa-miR-3196	hsa-miR-543	
hsa-miR-181b-5p	hsa-miR-3198	hsa-miR-574-3p	
hsa-miR-1825	hsa-miR-320a	hsa-miR-574-5p	
hsa-miR-191-3p	hsa-miR-320b	hsa-miR-575	

Appendix 4: Table of the 125 miRNA which were equivalently expressed in OM-MSCs and BM-MSCs

References:

References

1. Lindsay SL, Johnstone SA, Mountford JC, Sheikh S, Allan DB, Clark L, et al. Human mesenchymal stem cells isolated from olfactory biopsies but not bone enhance CNS myelination in vitro. Glia. 2013;61(3):368-82.

2. Little MT, Storb R. History of haematopoietic stem-cell transplantation. Nature reviews Cancer. 2002;2(3):231-8.

3. Mountford JC, Olivier E, Jordanides NE, de Sousa P, Turner ML. Red blood cells from pluripotent stem cells for use in transfusion. Regenerative medicine. 2010;5(3):411-23.

4. Maehle AH. Ambiguous cells: the emergence of the stem cell concept in the nineteenth and twentieth centuries. Notes and records of the Royal Society of London. 2011;65(4):359-78.

5. Carosella ED. From MAC to HLA: Professor Jean Dausset, the pioneer. Human immunology. 2009;70(9):661-2.

6. Till JE, Mc CE. A direct measurement of the radiation sensitivity of normal mouse bone marrow cells. Radiation research. 1961;14:213-22.

7. Bianco P, Robey PG, Simmons PJ. Mesenchymal stem cells: revisiting history, concepts, and assays. Cell stem cell. 2008;2(4):313-9.

8. Tavassoli M, Crosby WH. Transplantation of marrow to extramedullary sites. Science. 1968;161(3836):54-6.

9. Friedenstein AY. Induction of bone tissue by transitional epithelium. Clinical orthopaedics and related research. 1968;59:21-37.

10. Friedenstein AJ. Precursor cells of mechanocytes. International review of cytology. 1976;47:327-59.

11. Friedenstein AJ, Chailakhjan RK, Lalykina KS. The development of fibroblast colonies in monolayer cultures of guinea-pig bone marrow and spleen cells. Cell and tissue kinetics. 1970;3(4):393-403.

12. Caplan AI. Mesenchymal stem cells. Journal of orthopaedic research : official publication of the Orthopaedic Research Society. 1991;9(5):641-50.

13. Bishop MR, Logan BR, Gandham S, Bolwell BJ, Cahn JY, Lazarus HM, et al. Long-term outcomes of adults with acute lymphoblastic leukemia after autologous or unrelated donor bone marrow transplantation: a comparative analysis by the National Marrow Donor Program and Center for

International Blood and Marrow Transplant Research. Bone marrow transplantation. 2008;41(7):635-42.
14. Freedman AS, Takvorian T, Anderson KC, Mauch P, Rabinowe SN, Blake K, et al. Autologous bone marrow transplantation in B-cell non-Hodgkin's lymphoma: very low treatment-related mortality in 100 patients in sensitive relapse. Journal of clinical oncology : official journal of the American Society of Clinical Oncology. 1990;8(5):784-91.
15. Dezern AE, Brodsky RA. Clinical management of aplastic anemia. Expert review of hematology. 2011;4(2):221-30.
16. Grunebaum E, Mazzolari E, Porta F, Dallera D, Atkinson A, Reid B, et al. Bone marrow transplantation for severe combined immune deficiency. Jama. 2006;295(5):508-18.
17. Al-wahadneh AM, Haddadin I, Hamouri M, Omari K, Aejellat F. Bone marrow transplantation for leukocyte adhesion deficiency-I: case report. Saudi journal of kidney diseases and transplantation : an official publication of the Saudi Center for Organ Transplantation, Saudi Arabia. 2006;17(4):564-7.
18. Kwon HJ, Bhat N, Sweet EM, Cornell RA, Riley BB. Identification of early requirements for preplacodal ectoderm and sensory organ development. PLoS genetics. 2010;6(9):e1001133.
19. Pispa J, Thesleff I. Mechanisms of ectodermal organogenesis. Developmental biology. 2003;262(2):195-205.
20. O'Rahilly R, Muller F. Neurulation in the normal human embryo. Ciba Foundation symposium. 1994;181:70-82; discussion -9.
21. Jimenez-Rojo L, Granchi Z, Graf D, Mitsiadis TA. Stem Cell Fate Determination during Development and Regeneration of Ectodermal Organs. Frontiers in physiology. 2012;3:107.
22. Huang X, Saint-Jeannet JP. Induction of the neural crest and the opportunities of life on the edge. Developmental biology. 2004;275(1):1-11.
23. Zorn AM, Wells JM. Vertebrate endoderm development and organ formation. Annual review of cell and developmental biology. 2009;25:221-51.

24. Beyer Nardi N, da Silva Meirelles L. Mesenchymal stem cells: isolation, in vitro expansion and characterization. Handbook of experimental pharmacology. 2006(174):249-82.
25. Phinney DG, Prockop DJ. Concise review: mesenchymal stem/multipotent stromal cells: the state of transdifferentiation and modes of tissue repair--current views. Stem cells. 2007;25(11):2896-902.
26. Chamberlain G, Fox J, Ashton B, Middleton J. Concise review: mesenchymal stem cells: their phenotype, differentiation capacity, immunological features, and potential for homing. Stem cells. 2007;25(11):2739-49.
27. Friedenstein AJ. Marrow stromal fibroblasts. Calcified tissue international. 1995;56 Suppl 1:S17.
28. Friedenstein AJ, Latzinik NV, Gorskaya Yu F, Luria EA, Moskvina IL. Bone marrow stromal colony formation requires stimulation by haemopoietic cells. Bone and mineral. 1992;18(3):199-213.
29. Friedenstein AJ, Chailakhyan RK, Gerasimov UV. Bone marrow osteogenic stem cells: in vitro cultivation and transplantation in diffusion chambers. Cell and tissue kinetics. 1987;20(3):263-72.
30. Lin F. Adipose tissue-derived mesenchymal stem cells: a fat chance of curing kidney disease? Kidney international. 2012;82(7):731-3.
31. Branch MJ, Hashmani K, Dhillon P, Jones DR, Dua HS, Hopkinson A. Mesenchymal stem cells in the human corneal limbal stroma. Investigative ophthalmology & visual science. 2012;53(9):5109-16.
32. Wang HS, Hung SC, Peng ST, Huang CC, Wei HM, Guo YJ, et al. Mesenchymal stem cells in the Wharton's jelly of the human umbilical cord. Stem cells. 2004;22(7):1330-7.
33. Akiyama K, Chen C, Gronthos S, Shi S. Lineage differentiation of mesenchymal stem cells from dental pulp, apical papilla, and periodontal ligament. Methods in molecular biology. 2012;887:111-21.
34. Wouters G, Grossi S, Mesoraca A, Bizzoco D, Mobili L, Cignini P, et al. Isolation of amniotic fluid-derived mesenchymal stem cells. Journal of prenatal medicine. 2007;1(3):39-40.

35. Lindsay SL, Riddell JS, Barnett SC. Olfactory mucosa for transplant-mediated repair: a complex tissue for a complex injury? Glia. 2010;58(2):125-34.
36. Delorme B, Nivet E, Gaillard J, Haupl T, Ringe J, Deveze A, et al. The human nose harbors a niche of olfactory ectomesenchymal stem cells displaying neurogenic and osteogenic properties. Stem cells and development. 2010;19(6):853-66.
37. Hematti P. Mesenchymal stromal cells and fibroblasts: a case of mistaken identity? Cytotherapy. 2012;14(5):516-21.
38. Alt E, Yan Y, Gehmert S, Song YH, Altman A, Gehmert S, et al. Fibroblasts share mesenchymal phenotypes with stem cells, but lack their differentiation and colony-forming potential. Biology of the cell / under the auspices of the European Cell Biology Organization. 2011;103(4):197-208.
39. Pittenger MF, Mackay AM, Beck SC, Jaiswal RK, Douglas R, Mosca JD, et al. Multilineage potential of adult human mesenchymal stem cells. Science. 1999;284(5411):143-7.
40. Dimarino AM, Caplan AI, Bonfield TL. Mesenchymal stem cells in tissue repair. Frontiers in immunology. 2013;4:201.
41. Kawazoe Y, Katoh S, Onodera Y, Kohgo T, Shindoh M, Shiba T. Activation of the FGF signaling pathway and subsequent induction of mesenchymal stem cell differentiation by inorganic polyphosphate. International journal of biological sciences. 2008;4(1):37-47.
42. Cook D, Genever P. Regulation of mesenchymal stem cell differentiation. Advances in experimental medicine and biology. 2013;786:213-29.
43. McMurray RJ, Wann AK, Thompson CL, Connelly JT, Knight MM. Surface topography regulates wnt signaling through control of primary cilia structure in mesenchymal stem cells. Scientific reports. 2013;3:3545.
44. Discher DE, Mooney DJ, Zandstra PW. Growth factors, matrices, and forces combine and control stem cells. Science. 2009;324(5935):1673-7.
45. Engler AJ, Sen S, Sweeney HL, Discher DE. Matrix elasticity directs stem cell lineage specification. Cell. 2006;126(4):677-89.

46. McNamara LE, McMurray RJ, Biggs MJ, Kantawong F, Oreffo RO, Dalby MJ. Nanotopographical control of stem cell differentiation. Journal of tissue engineering. 2010;2010:120623.
47. Augello A, Tasso R, Negrini SM, Amateis A, Indiveri F, Cancedda R, et al. Bone marrow mesenchymal progenitor cells inhibit lymphocyte proliferation by activation of the programmed death 1 pathway. European journal of immunology. 2005;35(5):1482-90.
48. Krampera M, Cosmi L, Angeli R, Pasini A, Liotta F, Andreini A, et al. Role for interferon-gamma in the immunomodulatory activity of human bone marrow mesenchymal stem cells. Stem cells. 2006;24(2):386-98.
49. Spaggiari GM, Capobianco A, Abdelrazik H, Becchetti F, Mingari MC, Moretta L. Mesenchymal stem cells inhibit natural killer-cell proliferation, cytotoxicity, and cytokine production: role of indoleamine 2,3-dioxygenase and prostaglandin E2. Blood. 2008;111(3):1327-33.
50. Uccelli A, Moretta L, Pistoia V. Mesenchymal stem cells in health and disease. Nature reviews Immunology. 2008;8(9):726-36.
51. Ruster B, Gottig S, Ludwig RJ, Bistrian R, Muller S, Seifried E, et al. Mesenchymal stem cells display coordinated rolling and adhesion behavior on endothelial cells. Blood. 2006;108(12):3938-44.
52. Sordi V, Malosio ML, Marchesi F, Mercalli A, Melzi R, Giordano T, et al. Bone marrow mesenchymal stem cells express a restricted set of functionally active chemokine receptors capable of promoting migration to pancreatic islets. Blood. 2005;106(2):419-27.
53. Son BR, Marquez-Curtis LA, Kucia M, Wysoczynski M, Turner AR, Ratajczak J, et al. Migration of bone marrow and cord blood mesenchymal stem cells in vitro is regulated by stromal-derived factor-1-CXCR4 and hepatocyte growth factor-c-met axes and involves matrix metalloproteinases. Stem cells. 2006;24(5):1254-64.
54. Bartholomew A, Sturgeon C, Siatskas M, Ferrer K, McIntosh K, Patil S, et al. Mesenchymal stem cells suppress lymphocyte proliferation in vitro and prolong skin graft survival in vivo. Experimental hematology. 2002;30(1):42-8.

55. Uccelli A, Pistoia V, Moretta L. Mesenchymal stem cells: a new strategy for immunosuppression? Trends in immunology. 2007;28(5):219-26.
56. Li Y, Chen J, Chen XG, Wang L, Gautam SC, Xu YX, et al. Human marrow stromal cell therapy for stroke in rat: neurotrophins and functional recovery. Neurology. 2002;59(4):514-23.
57. Munoz JR, Stoutenger BR, Robinson AP, Spees JL, Prockop DJ. Human stem/progenitor cells from bone marrow promote neurogenesis of endogenous neural stem cells in the hippocampus of mice. Proceedings of the National Academy of Sciences of the United States of America. 2005;102(50):18171-6.
58. Rivera FJ, Couillard-Despres S, Pedre X, Ploetz S, Caioni M, Lois C, et al. Mesenchymal stem cells instruct oligodendrogenic fate decision on adult neural stem cells. Stem cells. 2006;24(10):2209-19.
59. Amamoto R, Arlotta P. Development-inspired reprogramming of the mammalian central nervous system. Science. 2014;343(6170):1239882.
60. Gizurarson S. Anatomical and histological factors affecting intranasal drug and vaccine delivery. Current drug delivery. 2012;9(6):566-82.
61. Kreutzberg GW. Microglia, the first line of defence in brain pathologies. Arzneimittel-Forschung. 1995;45(3A):357-60.
62. Bushong EA, Martone ME, Jones YZ, Ellisman MH. Protoplasmic astrocytes in CA1 stratum radiatum occupy separate anatomical domains. The Journal of neuroscience : the official journal of the Society for Neuroscience. 2002;22(1):183-92.
63. Gehrmann J, Matsumoto Y, Kreutzberg GW. Microglia: intrinsic immuneffector cell of the brain. Brain research Brain research reviews. 1995;20(3):269-87.
64. Ritter MR, Banin E, Moreno SK, Aguilar E, Dorrell MI, Friedlander M. Myeloid progenitors differentiate into microglia and promote vascular repair in a model of ischemic retinopathy. The Journal of clinical investigation. 2006;116(12):3266-76.
65. Ransohoff RM, Cardona AE. The myeloid cells of the central nervous system parenchyma. Nature. 2010;468(7321):253-62.

66. Nash B, Thomson CE, Linington C, Arthur AT, McClure JD, McBride MW, et al. Functional duality of astrocytes in myelination. The Journal of neuroscience : the official journal of the Society for Neuroscience. 2011;31(37):13028-38.
67. Wanner IB, Anderson MA, Song B, Levine J, Fernandez A, Gray-Thompson Z, et al. Glial scar borders are formed by newly proliferated, elongated astrocytes that interact to corral inflammatory and fibrotic cells via STAT3-dependent mechanisms after spinal cord injury. The Journal of neuroscience : the official journal of the Society for Neuroscience. 2013;33(31):12870-86.
68. Yuan YM, He C. The glial scar in spinal cord injury and repair. Neuroscience bulletin. 2013;29(4):421-35.
69. Cregg JM, DePaul MA, Filous AR, Lang BT, Tran A, Silver J. Functional regeneration beyond the glial scar. Experimental neurology. 2014;253:197-207.
70. Nash B, Ioannidou K, Barnett SC. Astrocyte phenotypes and their relationship to myelination. Journal of anatomy. 2011;219(1):44-52.
71. Sofroniew MV. Multiple roles for astrocytes as effectors of cytokines and inflammatory mediators. The Neuroscientist : a review journal bringing neurobiology, neurology and psychiatry. 2014;20(2):160-72.
72. Eng LF, Ghirnikar RS. GFAP and astrogliosis. Brain pathology. 1994;4(3):229-37.
73. Eng LF. Glial fibrillary acidic protein (GFAP): the major protein of glial intermediate filaments in differentiated astrocytes. Journal of neuroimmunology. 1985;8(4-6):203-14.
74. Norenberg MD. Astrocyte responses to CNS injury. Journal of neuropathology and experimental neurology. 1994;53(3):213-20.
75. Sofroniew MV, Vinters HV. Astrocytes: biology and pathology. Acta neuropathologica. 2010;119(1):7-35.
76. Baumann N, Pham-Dinh D. Biology of oligodendrocyte and myelin in the mammalian central nervous system. Physiological reviews. 2001;81(2):871-927.

77. Ishibashi T, Dakin KA, Stevens B, Lee PR, Kozlov SV, Stewart CL, et al. Astrocytes promote myelination in response to electrical impulses. Neuron. 2006;49(6):823-32.
78. Sorensen A, Moffat K, Thomson C, Barnett SC. Astrocytes, but not olfactory ensheathing cells or Schwann cells, promote myelination of CNS axons in vitro. Glia. 2008;56(7):750-63.
79. Ioannidou K, Anderson KI, Strachan D, Edgar JM, Barnett SC. Astroglial-axonal interactions during early stages of myelination in mixed cultures using in vitro and ex vivo imaging techniques. BMC neuroscience. 2014;15:59.
80. Ioannidou K, Anderson KI, Strachan D, Edgar JM, Barnett SC. Time-lapse imaging of the dynamics of CNS glial-axonal interactions in vitro and ex vivo. PloS one. 2012;7(1):e30775.
81. Siyahhan B, Knobloch V, de Zelicourt D, Asgari M, Schmid Daners M, Poulikakos D, et al. Flow induced by ependymal cilia dominates near-wall cerebrospinal fluid dynamics in the lateral ventricles. Journal of the Royal Society, Interface / the Royal Society. 2014;11(94):20131189.
82. Kishimoto N, Sawamoto K. Planar polarity of ependymal cilia. Differentiation; research in biological diversity. 2012;83(2):S86-90.
83. Spassky N, Merkle FT, Flames N, Tramontin AD, Garcia-Verdugo JM, Alvarez-Buylla A. Adult ependymal cells are postmitotic and are derived from radial glial cells during embryogenesis. The Journal of neuroscience : the official journal of the Society for Neuroscience. 2005;25(1):10-8.
84. Malatesta P, Appolloni I, Calzolari F. Radial glia and neural stem cells. Cell and tissue research. 2008;331(1):165-78.
85. Barry DS, Pakan JM, McDermott KW. Radial glial cells: key organisers in CNS development. The international journal of biochemistry & cell biology. 2014;46:76-9.
86. Fields RD. White matter in learning, cognition and psychiatric disorders. Trends in neurosciences. 2008;31(7):361-70.
87. Marner L, Nyengaard JR, Tang Y, Pakkenberg B. Marked loss of myelinated nerve fibers in the human brain with age. The Journal of comparative neurology. 2003;462(2):144-52.

88. Papadopoulou A, Muller-Lenke N, Naegelin Y, Kalt G, Bendfeldt K, Kuster P, et al. Contribution of cortical and white matter lesions to cognitive impairment in multiple sclerosis. Multiple sclerosis. 2013;19(10):1290-6.
89. Benedict RH, Hulst HE, Bergsland N, Schoonheim MM, Dwyer MG, Weinstock-Guttman B, et al. Clinical significance of atrophy and white matter mean diffusivity within the thalamus of multiple sclerosis patients. Multiple sclerosis. 2013;19(11):1478-84.
90. Sun X, Salat D, Upchurch K, Deason R, Kowall N, Budson A. Destruction of White Matter Integrity in Patients With Mild Cognitive Impairment and Alzheimer Disease. Journal of investigative medicine : the official publication of the American Federation for Clinical Research. 2014;62(7):927-33.
91. Barker R, Ashby EL, Wellington D, Barrow VM, Palmer JC, Kehoe PG, et al. Pathophysiology of white matter perfusion in Alzheimer's disease and vascular dementia. Brain : a journal of neurology. 2014;137(Pt 5):1524-32.
92. Mao FX, Li WJ, Chen HJ, Qian LH, Buzby JS. White matter and SVZ serve as endogenous sources of glial progenitor cells for self-repair in neonatal rats with ischemic PVL. Brain research. 2013;1535:38-51.
93. Li WJ, Chen HJ, Qian LH, Mao FX. [Endogenous self-repair in immature white matter induced by ischemia in neonatal rats]. Zhongguo dang dai er ke za zhi = Chinese journal of contemporary pediatrics. 2012;14(7):548-53.
94. Erickson KI, Leckie RL, Weinstein AM. Physical activity, fitness, and gray matter volume. Neurobiology of aging. 2014;35 Suppl 2:S20-8.
95. Thompson PM, Hayashi KM, de Zubicaray G, Janke AL, Rose SE, Semple J, et al. Dynamics of gray matter loss in Alzheimer's disease. The Journal of neuroscience : the official journal of the Society for Neuroscience. 2003;23(3):994-1005.
96. Almeida OP, Garrido GJ, Lautenschlager NT, Hulse GK, Jamrozik K, Flicker L. Smoking is associated with reduced cortical regional gray matter density in brain regions associated with incipient Alzheimer disease. The

American journal of geriatric psychiatry : official journal of the American Association for Geriatric Psychiatry. 2008;16(1):92-8.
97. Xu X, Warrington AE, Bieber AJ, Rodriguez M. Enhancing CNS repair in neurological disease: challenges arising from neurodegeneration and rewiring of the network. CNS drugs. 2011;25(7):555-73.
98. Yiu G, He Z. Glial inhibition of CNS axon regeneration. Nature reviews Neuroscience. 2006;7(8):617-27.
99. Poser CM, Goutieres F, Carpentier MA, Aicardi J. Schilder's myelinoclastic diffuse sclerosis. Pediatrics. 1986;77(1):107-12.
100. Broderick L, Gandhi C, Mueller JL, Putnam CD, Shayan K, Giclas PC, et al. Mutations of complement factor I and potential mechanisms of neuroinflammation in acute hemorrhagic leukoencephalitis. Journal of clinical immunology. 2013;33(1):162-71.
101. West TW. Transverse myelitis--a review of the presentation, diagnosis, and initial management. Discovery medicine. 2013;16(88):167-77.
102. Fragoso YD, Ferreira ML, Oliveira EM, Domingues RB, Ribeiro TA, Brooks JB, et al. Neuromyelitis optica with onset in childhood and adolescence. Pediatric neurology. 2014;50(1):66-8.
103. Erol I, Ozkale Y, Alkan O, Alehan F. Acute disseminated encephalomyelitis in children and adolescents: a single center experience. Pediatric neurology. 2013;49(4):266-73.
104. Alper G. Acute disseminated encephalomyelitis. Journal of child neurology. 2012;27(11):1408-25.
105. Cusick MF, Libbey JE, Fujinami RS. Multiple sclerosis: autoimmunity and viruses. Current opinion in rheumatology. 2013;25(4):496-501.
106. Caucheteux N, Maarouf A, Daelman L, Toupance O, Lavaud S, Tourbah A. Acute disseminated encephalomyelitis in two renal transplant patients: is there a role for Epstein-Barr virus reactivation? Multiple sclerosis. 2013;19(9):1222-5.
107. Pohl-Koppe A, Burchett SK, Thiele EA, Hafler DA. Myelin basic protein reactive Th2 T cells are found in acute disseminated encephalomyelitis. Journal of neuroimmunology. 1998;91(1-2):19-27.

108. Rust RS. Multiple sclerosis, acute disseminated encephalomyelitis, and related conditions. Seminars in pediatric neurology. 2000;7(2):66-90.
109. Poser CM, Brinar VV. Disseminated encephalomyelitis and multiple sclerosis: two different diseases - a critical review. Acta neurologica Scandinavica. 2007;116(4):201-6.
110. Esparza ML, Sasaki S, Kesteloot H. Nutrition, latitude, and multiple sclerosis mortality: an ecologic study. American journal of epidemiology. 1995;142(7):733-7.
111. Ponsonby AL, Lucas RM, van der Mei IA. UVR, vitamin D and three autoimmune diseases--multiple sclerosis, type 1 diabetes, rheumatoid arthritis. Photochemistry and photobiology. 2005;81(6):1267-75.
112. Hayes CE, Cantorna MT, DeLuca HF. Vitamin D and multiple sclerosis. Proceedings of the Society for Experimental Biology and Medicine Society for Experimental Biology and Medicine (New York, NY). 1997;216(1):21-7.
113. Ascherio A, Munger KL, White R, Kochert K, Simon KC, Polman CH, et al. Vitamin D as an early predictor of multiple sclerosis activity and progression. JAMA neurology. 2014;71(3):306-14.
114. Mesliniene S, Ramrattan L, Giddings S, Sheikh-Ali M. Role of vitamin D in the onset, progression, and severity of multiple sclerosis. Endocrine practice : official journal of the American College of Endocrinology and the American Association of Clinical Endocrinologists. 2013;19(1):129-36.
115. Slavov GS, Trenova AG, Manova MG, Kostadinova, II, Vasileva TV, Zahariev ZI. Vitamin D immunomodulatory potential in multiple sclerosis. Folia medica. 2013;55(2):5-9.
116. Mead MN. Benefits of sunlight: a bright spot for human health. Environmental health perspectives. 2008;116(4):A160-7.
117. Newmark HL, Yang K, Kurihara N, Fan K, Augenlicht LH, Lipkin M. Western-style diet-induced colonic tumors and their modulation by calcium and vitamin D in C57Bl/6 mice: a preclinical model for human sporadic colon cancer. Carcinogenesis. 2009;30(1):88-92.
118. Krizova L, Kollar B, Jezova D, Turcani P. Genetic aspects of vitamin D receptor and metabolism in relation to the risk of multiple sclerosis. General physiology and biophysics. 2013;32(4):459-66.

119. Cross AH, Naismith RT. Established and novel disease-modifying treatments in multiple sclerosis. Journal of internal medicine. 2014;275(4):350-63.
120. Compston A, Coles A. Multiple sclerosis. Lancet. 2008;372(9648):1502-17.
121. Hauser SL, Oksenberg JR. The neurobiology of multiple sclerosis: genes, inflammation, and neurodegeneration. Neuron. 2006;52(1):61-76.
122. Milo R, Miller A. Revised diagnostic criteria of multiple sclerosis. Autoimmunity reviews. 2014;13(4-5):518-24.
123. Steinman L, Zamvil S. Transcriptional analysis of targets in multiple sclerosis. Nature reviews Immunology. 2003;3(6):483-92.
124. Steinman L. A molecular trio in relapse and remission in multiple sclerosis. Nature reviews Immunology. 2009;9(6):440-7.
125. Hemmer B, Archelos JJ, Hartung HP. New concepts in the immunopathogenesis of multiple sclerosis. Nature reviews Neuroscience. 2002;3(4):291-301.
126. Lublin FD, Reingold SC. Defining the clinical course of multiple sclerosis: results of an international survey. National Multiple Sclerosis Society (USA) Advisory Committee on Clinical Trials of New Agents in Multiple Sclerosis. Neurology. 1996;46(4):907-11.
127. Zhang Y, Guo TB, Lu H. Promoting remyelination for the treatment of multiple sclerosis: opportunities and challenges. Neuroscience bulletin. 2013;29(2):144-54.
128. Kotsiari A, Voss EV, Pul R, Skripuletz T, Ragancokova D, Trebst C, et al. Interferon-beta treatment normalises the inhibitory effect of serum from multiple sclerosis patients on oligodendrocyte progenitor proliferation. Neuroscience letters. 2010;485(2):107-11.
129. Kennedy P, Chessell ZJ. Traumatic versus non-traumatic spinal cord injuries: are there differential rehabilitation outcomes? Spinal cord. 2013;51(7):579-83.
130. Marino RJ, Barros T, Biering-Sorensen F, Burns SP, Donovan WH, Graves DE, et al. International standards for neurological classification of

spinal cord injury. The journal of spinal cord medicine. 2003;26 Suppl 1:S50-6.
131. Rolls A, Shechter R, Schwartz M. The bright side of the glial scar in CNS repair. Nature reviews Neuroscience. 2009;10(3):235-41.
132. Higginson JR, Thompson SM, Santos-Silva A, Guimond SE, Turnbull JE, Barnett SC. Differential sulfation remodelling of heparan sulfate by extracellular 6-O-sulfatases regulates fibroblast growth factor-induced boundary formation by glial cells: implications for glial cell transplantation. The Journal of neuroscience : the official journal of the Society for Neuroscience. 2012;32(45):15902-12.
133. Faulkner JR, Herrmann JE, Woo MJ, Tansey KE, Doan NB, Sofroniew MV. Reactive astrocytes protect tissue and preserve function after spinal cord injury. The Journal of neuroscience : the official journal of the Society for Neuroscience. 2004;24(9):2143-55.
134. Donoghue PS, Lamond R, Boomkamp SD, Sun T, Gadegaard N, Riehle MO, et al. The development of a epsilon-polycaprolactone scaffold for central nervous system repair. Tissue engineering Part A. 2013;19(3-4):497-507.
135. Boomkamp SD, McGrath MA, Houslay MD, Barnett SC. Epac and the high affinity rolipram binding conformer of PDE4 modulate neurite outgrowth and myelination using an in vitro spinal cord injury model. British journal of pharmacology. 2014;171(9):2385-98.
136. Boomkamp SD, Riehle MO, Wood J, Olson MF, Barnett SC. The development of a rat in vitro model of spinal cord injury demonstrating the additive effects of Rho and ROCK inhibitors on neurite outgrowth and myelination. Glia. 2012;60(3):441-56.
137. Benignus VA, Prah JD. Olfaction: anatomy, physiology and behavior. Environmental health perspectives. 1982;44:15-21.
138. Garcia-Gonzalez D, Murcia-Belmonte V, Clemente D, De Castro F. Olfactory system and demyelination. Anatomical record. 2013;296(9):1424-34.

139. Gallarda BW, Lledo PM. Adult neurogenesis in the olfactory system and neurodegenerative disease. Current molecular medicine. 2012;12(10):1253-60.
140. Mackay-Sim A, St John JA. Olfactory ensheathing cells from the nose: clinical application in human spinal cord injuries. Experimental neurology. 2011;229(1):174-80.
141. Sohur US, Emsley JG, Mitchell BD, Macklis JD. Adult neurogenesis and cellular brain repair with neural progenitors, precursors and stem cells. Philosophical transactions of the Royal Society of London Series B, Biological sciences. 2006;361(1473):1477-97.
142. Murrell W, Feron F, Wetzig A, Cameron N, Splatt K, Bellette B, et al. Multipotent stem cells from adult olfactory mucosa. Developmental dynamics : an official publication of the American Association of Anatomists. 2005;233(2):496-515.
143. Duggan CD, Ngai J. Scent of a stem cell. Nature neuroscience. 2007;10(6):673-4.
144. Murrell W, Wetzig A, Donnellan M, Feron F, Burne T, Meedeniya A, et al. Olfactory mucosa is a potential source for autologous stem cell therapy for Parkinson's disease. Stem cells. 2008;26(8):2183-92.
145. Tome M, Lindsay SL, Riddell JS, Barnett SC. Identification of nonepithelial multipotent cells in the embryonic olfactory mucosa. Stem cells. 2009;27(9):2196-208.
146. Leung CT, Coulombe PA, Reed RR. Contribution of olfactory neural stem cells to tissue maintenance and regeneration. Nature neuroscience. 2007;10(6):720-6.
147. Huard JM, Youngentob SL, Goldstein BJ, Luskin MB, Schwob JE. Adult olfactory epithelium contains multipotent progenitors that give rise to neurons and non-neural cells. The Journal of comparative neurology. 1998;400(4):469-86.
148. Chen X, Fang H, Schwob JE. Multipotency of purified, transplanted globose basal cells in olfactory epithelium. The Journal of comparative neurology. 2004;469(4):457-74.

149. De Feo D, Merlini A, Laterza C, Martino G. Neural stem cell transplantation in central nervous system disorders: from cell replacement to neuroprotection. Current opinion in neurology. 2012;25(3):322-33.
150. Kim H, Cooke MJ, Shoichet MS. Creating permissive microenvironments for stem cell transplantation into the central nervous system. Trends in biotechnology. 2012;30(1):55-63.
151. Muraro PA, Uccelli A. Immuno-therapeutic potential of haematopoietic and mesenchymal stem cell transplantation in MS. Results and problems in cell differentiation. 2010;51:237-57.
152. Neirinckx V, Coste C, Rogister B, Wislet-Gendebien S. Concise review: adult mesenchymal stem cells, adult neural crest stem cells, and therapy of neurological pathologies: a state of play. Stem cells translational medicine. 2013;2(4):284-96.
153. Rivera FJ, Aigner L. Adult mesenchymal stem cell therapy for myelin repair in multiple sclerosis. Biological research. 2012;45(3):257-68.
154. Nandoe Tewarie RD, Hurtado A, Levi AD, Grotenhuis JA, Oudega M. Bone marrow stromal cells for repair of the spinal cord: towards clinical application. Cell transplantation. 2006;15(7):563-77.
155. Bjorklund LM, Sanchez-Pernaute R, Chung S, Andersson T, Chen IY, McNaught KS, et al. Embryonic stem cells develop into functional dopaminergic neurons after transplantation in a Parkinson rat model. Proceedings of the National Academy of Sciences of the United States of America. 2002;99(4):2344-9.
156. Baron-Van Evercooren A, Avellana-Adalid V, Lachapelle F, Liblau R. Schwann cell transplantation and myelin repair of the CNS. Multiple sclerosis. 1997;3(2):157-61.
157. Potts MB, Silvestrini MT, Lim DA. Devices for cell transplantation into the central nervous system: Design considerations and emerging technologies. Surgical neurology international. 2013;4(Suppl 1):S22-30.
158. Tate CC, Shear DA, Tate MC, Archer DR, Stein DG, LaPlaca MC. Laminin and fibronectin scaffolds enhance neural stem cell transplantation into the injured brain. Journal of tissue engineering and regenerative medicine. 2009;3(3):208-17.

159. Setzu A, Lathia JD, Zhao C, Wells K, Rao MS, Ffrench-Constant C, et al. Inflammation stimulates myelination by transplanted oligodendrocyte precursor cells. Glia. 2006;54(4):297-303.
160. Wu B, Sun L, Li P, Tian M, Luo Y, Ren X. Transplantation of oligodendrocyte precursor cells improves myelination and promotes functional recovery after spinal cord injury. Injury. 2012;43(6):794-801.
161. Agudo M, Woodhoo A, Webber D, Mirsky R, Jessen KR, McMahon SB. Schwann cell precursors transplanted into the injured spinal cord multiply, integrate and are permissive for axon growth. Glia. 2008;56(12):1263-70.
162. Lavdas AA, Papastefanaki F, Thomaidou D, Matsas R. Schwann cell transplantation for CNS repair. Current medicinal chemistry. 2008;15(2):151-60.
163. Lamond R, Barnett SC. Schwann cells but not olfactory ensheathing cells inhibit CNS myelination via the secretion of connective tissue growth factor. The Journal of neuroscience : the official journal of the Society for Neuroscience. 2013;33(47):18686-97.
164. Ekberg JA, St John JA. Crucial roles for olfactory ensheathing cells and olfactory mucosal cells in the repair of damaged neural tracts. Anatomical record. 2014;297(1):121-8.
165. Coutts DJ, Humphries CE, Zhao C, Plant GW, Franklin RJ. Embryonic-derived olfactory ensheathing cells remyelinate focal areas of spinal cord demyelination more efficiently than neonatal or adult-derived cells. Cell transplantation. 2013;22(7):1249-61.
166. Franklin RJ, Gilson JM, Franceschini IA, Barnett SC. Schwann cell-like myelination following transplantation of an olfactory bulb-ensheathing cell line into areas of demyelination in the adult CNS. Glia. 1996;17(3):217-24.
167. Barnett SC, Alexander CL, Iwashita Y, Gilson JM, Crowther J, Clark L, et al. Identification of a human olfactory ensheathing cell that can effect transplant-mediated remyelination of demyelinated CNS axons. Brain : a journal of neurology. 2000;123 (Pt 8):1581-8.
168. Toft A, Scott DT, Barnett SC, Riddell JS. Electrophysiological evidence that olfactory cell transplants improve function after spinal cord injury. Brain : a journal of neurology. 2007;130(Pt 4):970-84.

169. Yoo M, Lee GA, Park C, Cohen RI, Schachner M. Analysis of human embryonic stem cells with regulatable expression of the cell adhesion molecule l1 in regeneration after spinal cord injury. Journal of neurotrauma. 2014;31(6):553-64.
170. Erdo F, Buhrle C, Blunk J, Hoehn M, Xia Y, Fleischmann B, et al. Host-dependent tumorigenesis of embryonic stem cell transplantation in experimental stroke. Journal of cerebral blood flow and metabolism : official journal of the International Society of Cerebral Blood Flow and Metabolism. 2003;23(7):780-5.
171. McDonald JW, Liu XZ, Qu Y, Liu S, Mickey SK, Turetsky D, et al. Transplanted embryonic stem cells survive, differentiate and promote recovery in injured rat spinal cord. Nature medicine. 1999;5(12):1410-2.
172. Parsons XH. An Engraftable Human Embryonic Stem Cell Neuronal Lineage-Specific Derivative Retains Embryonic Chromatin Plasticity for Scale-Up CNS Regeneration. Journal of regenerative medicine & tissue engineering. 2012;1(1).
173. Piltti KM, Salazar DL, Uchida N, Cummings BJ, Anderson AJ. Safety of human neural stem cell transplantation in chronic spinal cord injury. Stem cells translational medicine. 2013;2(12):961-74.
174. Grade S, Bernardino L, Malva JO. Oligodendrogenesis from neural stem cells: perspectives for remyelinating strategies. International journal of developmental neuroscience : the official journal of the International Society for Developmental Neuroscience. 2013;31(7):692-700.
175. Mine Y, Tatarishvili J, Oki K, Monni E, Kokaia Z, Lindvall O. Grafted human neural stem cells enhance several steps of endogenous neurogenesis and improve behavioral recovery after middle cerebral artery occlusion in rats. Neurobiology of disease. 2013;52:191-203.
176. Vu Q, Xie K, Eckert M, Zhao W, Cramer SC. Meta-analysis of preclinical studies of mesenchymal stromal cells for ischemic stroke. Neurology. 2014;82(14):1277-86.
177. Bae JS, Jin HK, Lee JK, Richardson JC, Carter JE. Bone marrow-derived mesenchymal stem cells contribute to the reduction of amyloid-beta deposits and the improvement of synaptic transmission in a mouse

model of pre-dementia Alzheimer's disease. Current Alzheimer research. 2013;10(5):524-31.
178. DelaRosa O, Dalemans W, Lombardo E. Mesenchymal stem cells as therapeutic agents of inflammatory and autoimmune diseases. Current opinion in biotechnology. 2012;23(6):978-83.
179. Forostyak S, Homola A, Turnovcova K, Svitil P, Jendelova P, Sykova E. Intrathecal delivery of mesenchymal stromal cells protects the structure of altered perineuronal nets in SOD1 rats and amends the course of ALS. Stem cells. 2014.
180. Forostyak S, Jendelova P, Sykova E. The role of mesenchymal stromal cells in spinal cord injury, regenerative medicine and possible clinical applications. Biochimie. 2013;95(12):2257-70.
181. Caplan AI. Review: mesenchymal stem cells: cell-based reconstructive therapy in orthopedics. Tissue engineering. 2005;11(7-8):1198-211.
182. Freedman MS, Bar-Or A, Atkins HL, Karussis D, Frassoni F, Lazarus H, et al. The therapeutic potential of mesenchymal stem cell transplantation as a treatment for multiple sclerosis: consensus report of the International MSCT Study Group. Multiple sclerosis. 2010;16(4):503-10.
183. Zappia E, Casazza S, Pedemonte E, Benvenuto F, Bonanni I, Gerdoni E, et al. Mesenchymal stem cells ameliorate experimental autoimmune encephalomyelitis inducing T-cell anergy. Blood. 2005;106(5):1755-61.
184. Zhang J, Li Y, Chen J, Cui Y, Lu M, Elias SB, et al. Human bone marrow stromal cell treatment improves neurological functional recovery in EAE mice. Experimental neurology. 2005;195(1):16-26.
185. Gerdoni E, Gallo B, Casazza S, Musio S, Bonanni I, Pedemonte E, et al. Mesenchymal stem cells effectively modulate pathogenic immune response in experimental autoimmune encephalomyelitis. Annals of neurology. 2007;61(3):219-27.
186. Bai L, Lennon DP, Eaton V, Maier K, Caplan AI, Miller SD, et al. Human bone marrow-derived mesenchymal stem cells induce Th2-polarized immune response and promote endogenous repair in animal models of multiple sclerosis. Glia. 2009;57(11):1192-203.

187. Gordon D, Pavlovska G, Glover CP, Uney JB, Wraith D, Scolding NJ. Human mesenchymal stem cells abrogate experimental allergic encephalomyelitis after intraperitoneal injection, and with sparse CNS infiltration. Neuroscience letters. 2008;448(1):71-3.
188. Kassis I, Grigoriadis N, Gowda-Kurkalli B, Mizrachi-Kol R, Ben-Hur T, Slavin S, et al. Neuroprotection and immunomodulation with mesenchymal stem cells in chronic experimental autoimmune encephalomyelitis. Archives of neurology. 2008;65(6):753-61.
189. Rafei M, Campeau PM, Aguilar-Mahecha A, Buchanan M, Williams P, Birman E, et al. Mesenchymal stromal cells ameliorate experimental autoimmune encephalomyelitis by inhibiting CD4 Th17 T cells in a CC chemokine ligand 2-dependent manner. Journal of immunology. 2009;182(10):5994-6002.
190. Akiyama Y, Radtke C, Kocsis JD. Remyelination of the rat spinal cord by transplantation of identified bone marrow stromal cells. The Journal of neuroscience : the official journal of the Society for Neuroscience. 2002;22(15):6623-30.
191. Uccelli A, Laroni A, Freedman MS. Mesenchymal stem cells as treatment for MS - progress to date. Multiple sclerosis. 2013;19(5):515-9.
192. Giovannoni G, Southam E, Waubant E. Systematic review of disease-modifying therapies to assess unmet needs in multiple sclerosis: tolerability and adherence. Multiple sclerosis. 2012;18(7):932-46.
193. Rudick RA, Polman CH. Current approaches to the identification and management of breakthrough disease in patients with multiple sclerosis. The Lancet Neurology. 2009;8(6):545-59.
194. Bloomgren G, Richman S, Hotermans C, Subramanyam M, Goelz S, Natarajan A, et al. Risk of natalizumab-associated progressive multifocal leukoencephalopathy. The New England journal of medicine. 2012;366(20):1870-80.
195. Lindsey JW, Haden-Pinneri K, Memon NB, Buja LM. Sudden unexpected death on fingolimod. Multiple sclerosis. 2012;18(10):1507-8.

196. Martinelli V, Cocco E, Capra R, Salemi G, Gallo P, Capobianco M, et al. Acute myeloid leukemia in Italian patients with multiple sclerosis treated with mitoxantrone. Neurology. 2011;77(21):1887-95.
197. Connick P, Kolappan M, Crawley C, Webber DJ, Patani R, Michell AW, et al. Autologous mesenchymal stem cells for the treatment of secondary progressive multiple sclerosis: an open-label phase 2a proof-of-concept study. The Lancet Neurology. 2012;11(2):150-6.
198. Karussis D, Karageorgiou C, Vaknin-Dembinsky A, Gowda-Kurkalli B, Gomori JM, Kassis I, et al. Safety and immunological effects of mesenchymal stem cell transplantation in patients with multiple sclerosis and amyotrophic lateral sclerosis. Archives of neurology. 2010;67(10):1187-94.
199. Mohyeddin Bonab M, Yazdanbakhsh S, Lotfi J, Alimoghaddom K, Talebian F, Hooshmand F, et al. Does mesenchymal stem cell therapy help multiple sclerosis patients? Report of a pilot study. Iranian journal of immunology : IJI. 2007;4(1):50-7.
200. Yamout B, Hourani R, Salti H, Barada W, El-Hajj T, Al-Kutoubi A, et al. Bone marrow mesenchymal stem cell transplantation in patients with multiple sclerosis: a pilot study. Journal of neuroimmunology. 2010;227(1-2):185-9.
201. Ramon-Cueto A, Cordero MI, Santos-Benito FF, Avila J. Functional recovery of paraplegic rats and motor axon regeneration in their spinal cords by olfactory ensheathing glia. Neuron. 2000;25(2):425-35.
202. Blondheim NR, Levy YS, Ben-Zur T, Burshtein A, Cherlow T, Kan I, et al. Human mesenchymal stem cells express neural genes, suggesting a neural predisposition. Stem cells and development. 2006;15(2):141-64.
203. Zhu Y, Liu T, Song K, Fan X, Ma X, Cui Z. Adipose-derived stem cell: a better stem cell than BMSC. Cell biochemistry and function. 2008;26(6):664-75.
204. Arboleda D, Forostyak S, Jendelova P, Marekova D, Amemori T, Pivonkova H, et al. Transplantation of predifferentiated adipose-derived stromal cells for the treatment of spinal cord injury. Cellular and molecular neurobiology. 2011;31(7):1113-22.

205. Rice CM, Scolding NJ. Autologous bone marrow stem cells--properties and advantages. Journal of the neurological sciences. 2008;265(1-2):59-62.
206. Zhou Z, Chen Y, Zhang H, Min S, Yu B, He B, et al. Comparison of mesenchymal stromal cells from human bone marrow and adipose tissue for the treatment of spinal cord injury. Cytotherapy. 2013;15(4):434-48.
207. Paul G, Anisimov SV. The secretome of mesenchymal stem cells: potential implications for neuroregeneration. Biochimie. 2013;95(12):2246-56.
208. Zhang J, Li Y, Chen J, Yang M, Katakowski M, Lu M, et al. Expression of insulin-like growth factor 1 and receptor in ischemic rats treated with human marrow stromal cells. Brain research. 2004;1030(1):19-27.
209. Vercelli A, Mereuta OM, Garbossa D, Muraca G, Mareschi K, Rustichelli D, et al. Human mesenchymal stem cell transplantation extends survival, improves motor performance and decreases neuroinflammation in mouse model of amyotrophic lateral sclerosis. Neurobiology of disease. 2008;31(3):395-405.
210. Muto T, Miyoshi K, Horiguchi T, Hagita H, Noma T. Novel genetic linkage of rat Sp6 mutation to Amelogenesis imperfecta. Orphanet journal of rare diseases. 2012;7:34.
211. Uccelli A, Benvenuto F, Laroni A, Giunti D. Neuroprotective features of mesenchymal stem cells. Best practice & research Clinical haematology. 2011;24(1):59-64.
212. Wright KT, El Masri W, Osman A, Chowdhury J, Johnson WE. Concise review: Bone marrow for the treatment of spinal cord injury: mechanisms and clinical applications. Stem cells. 2011;29(2):169-78.
213. Hawryluk GW, Mothe A, Wang J, Wang S, Tator C, Fehlings MG. An in vivo characterization of trophic factor production following neural precursor cell or bone marrow stromal cell transplantation for spinal cord injury. Stem cells and development. 2012;21(12):2222-38.
214. Zhukareva V, Obrocka M, Houle JD, Fischer I, Neuhuber B. Secretion profile of human bone marrow stromal cells: donor variability and response to inflammatory stimuli. Cytokine. 2010;50(3):317-21.

215. Kim HS, Choi DY, Yun SJ, Choi SM, Kang JW, Jung JW, et al. Proteomic analysis of microvesicles derived from human mesenchymal stem cells. Journal of proteome research. 2012;11(2):839-49.
216. Chen TS, Lai RC, Lee MM, Choo AB, Lee CN, Lim SK. Mesenchymal stem cell secretes microparticles enriched in pre-microRNAs. Nucleic acids research. 2010;38(1):215-24.
217. Tomasoni S, Longaretti L, Rota C, Morigi M, Conti S, Gotti E, et al. Transfer of growth factor receptor mRNA via exosomes unravels the regenerative effect of mesenchymal stem cells. Stem cells and development. 2013;22(5):772-80.
218. Xin H, Li Y, Liu Z, Wang X, Shang X, Cui Y, et al. MiR-133b promotes neural plasticity and functional recovery after treatment of stroke with multipotent mesenchymal stromal cells in rats via transfer of exosome-enriched extracellular particles. Stem cells. 2013;31(12):2737-46.
219. Budoni M, Fierabracci A, Luciano R, Petrini S, Di Ciommo V, Muraca M. The immunosuppressive effect of mesenchymal stromal cells on B lymphocytes is mediated by membrane vesicles. Cell transplantation. 2013;22(2):369-79.
220. Liao W, Zhong J, Yu J, Xie J, Liu Y, Du L, et al. Therapeutic benefit of human umbilical cord derived mesenchymal stromal cells in intracerebral hemorrhage rat: implications of anti-inflammation and angiogenesis. Cellular physiology and biochemistry : international journal of experimental cellular physiology, biochemistry, and pharmacology. 2009;24(3-4):307-16.
221. Quertainmont R, Cantinieaux D, Botman O, Sid S, Schoenen J, Franzen R. Mesenchymal stem cell graft improves recovery after spinal cord injury in adult rats through neurotrophic and pro-angiogenic actions. PloS one. 2012;7(6):e39500.
222. Aggarwal S, Pittenger MF. Human mesenchymal stem cells modulate allogeneic immune cell responses. Blood. 2005;105(4):1815-22.
223. Le Blanc K. Immunomodulatory effects of fetal and adult mesenchymal stem cells. Cytotherapy. 2003;5(6):485-9.

224. Wang SP, Wang ZH, Peng DY, Li SM, Wang H, Wang XH. Therapeutic effect of mesenchymal stem cells in rats with intracerebral hemorrhage: reduced apoptosis and enhanced neuroprotection. Molecular medicine reports. 2012;6(4):848-54.
225. Oliveri RS, Bello S, Biering-Sorensen F. Mesenchymal stem cells improve locomotor recovery in traumatic spinal cord injury: systematic review with meta-analyses of rat models. Neurobiology of disease. 2014;62:338-53.
226. Dai G, Liu X, Zhang Z, Yang Z, Dai Y, Xu R. Transplantation of autologous bone marrow mesenchymal stem cells in the treatment of complete and chronic cervical spinal cord injury. Brain research. 2013;1533:73-9.
227. Kumagai G, Tsoulfas P, Toh S, McNiece I, Bramlett HM, Dietrich WD. Genetically modified mesenchymal stem cells (MSCs) promote axonal regeneration and prevent hypersensitivity after spinal cord injury. Experimental neurology. 2013;248:369-80.
228. Hodgetts SI, Simmons PJ, Plant GW. Human mesenchymal precursor cells (Stro-1(+)) from spinal cord injury patients improve functional recovery and tissue sparing in an acute spinal cord injury rat model. Cell transplantation. 2013;22(3):393-412.
229. Sykova E, Homola A, Mazanec R, Lachmann H, Konradova SL, Kobylka P, et al. Autologous bone marrow transplantation in patients with subacute and chronic spinal cord injury. Cell transplantation. 2006;15(8-9):675-87.
230. Park HC, Shim YS, Ha Y, Yoon SH, Park SR, Choi BH, et al. Treatment of complete spinal cord injury patients by autologous bone marrow cell transplantation and administration of granulocyte-macrophage colony stimulating factor. Tissue engineering. 2005;11(5-6):913-22.
231. Cristante AF, Barros-Filho TE, Tatsui N, Mendrone A, Caldas JG, Camargo A, et al. Stem cells in the treatment of chronic spinal cord injury: evaluation of somatosensitive evoked potentials in 39 patients. Spinal cord. 2009;47(10):733-8.
232. Amr SM, Gouda A, Koptan WT, Galal AA, Abdel-Fattah DS, Rashed LA, et al. Bridging defects in chronic spinal cord injury using peripheral nerve

grafts combined with a chitosan-laminin scaffold and enhancing regeneration through them by co-transplantation with bone-marrow-derived mesenchymal stem cells: case series of 14 patients. The journal of spinal cord medicine. 2014;37(1):54-71.
233. Caplan AI. Osteogenesis imperfecta, rehabilitation medicine, fundamental research and mesenchymal stem cells. Connective tissue research. 1995;31(4):S9-14.
234. Horwitz EM, Gordon PL, Koo WK, Marx JC, Neel MD, McNall RY, et al. Isolated allogeneic bone marrow-derived mesenchymal cells engraft and stimulate growth in children with osteogenesis imperfecta: Implications for cell therapy of bone. Proceedings of the National Academy of Sciences of the United States of America. 2002;99(13):8932-7.
235. Horwitz EM, Prockop DJ, Fitzpatrick LA, Koo WW, Gordon PL, Neel M, et al. Transplantability and therapeutic effects of bone marrow-derived mesenchymal cells in children with osteogenesis imperfecta. Nature medicine. 1999;5(3):309-13.
236. Bruder SP, Fink DJ, Caplan AI. Mesenchymal stem cells in bone development, bone repair, and skeletal regeneration therapy. Journal of cellular biochemistry. 1994;56(3):283-94.
237. Bruder SP, Kraus KH, Goldberg VM, Kadiyala S. The effect of implants loaded with autologous mesenchymal stem cells on the healing of canine segmental bone defects. The Journal of bone and joint surgery American volume. 1998;80(7):985-96.
238. Caplan AI, Bruder SP. Mesenchymal stem cells: building blocks for molecular medicine in the 21st century. Trends in molecular medicine. 2001;7(6):259-64.
239. Caplan AI, Elyaderani M, Mochizuki Y, Wakitani S, Goldberg VM. Principles of cartilage repair and regeneration. Clinical orthopaedics and related research. 1997(342):254-69.
240. Goldberg VM, Caplan AI. Biological resurfacing: an alternative to total joint arthroplasty. Orthopedics. 1994;17(9):819-21.
241. Wakitani S, Goto T, Pineda SJ, Young RG, Mansour JM, Caplan AI, et al. Mesenchymal cell-based repair of large, full-thickness defects of

articular cartilage. The Journal of bone and joint surgery American volume. 1994;76(4):579-92.
242. Pei M, Solchaga LA, Seidel J, Zeng L, Vunjak-Novakovic G, Caplan AI, et al. Bioreactors mediate the effectiveness of tissue engineering scaffolds. FASEB journal : official publication of the Federation of American Societies for Experimental Biology. 2002;16(12):1691-4.
243. Solchaga LA, Dennis JE, Goldberg VM, Caplan AI. Hyaluronic acid-based polymers as cell carriers for tissue-engineered repair of bone and cartilage. Journal of orthopaedic research : official publication of the Orthopaedic Research Society. 1999;17(2):205-13.
244. Solchaga LA, Yoo JU, Lundberg M, Dennis JE, Huibregtse BA, Goldberg VM, et al. Hyaluronan-based polymers in the treatment of osteochondral defects. Journal of orthopaedic research : official publication of the Orthopaedic Research Society. 2000;18(5):773-80.
245. Solchaga LA, Goldberg VM, Caplan AI. Cartilage regeneration using principles of tissue engineering. Clinical orthopaedics and related research. 2001(391 Suppl):S161-70.
246. Awad HA, Butler DL, Boivin GP, Smith FN, Malaviya P, Huibregtse B, et al. Autologous mesenchymal stem cell-mediated repair of tendon. Tissue engineering. 1999;5(3):267-77.
247. Young RG, Butler DL, Weber W, Caplan AI, Gordon SL, Fink DJ. Use of mesenchymal stem cells in a collagen matrix for Achilles tendon repair. Journal of orthopaedic research : official publication of the Orthopaedic Research Society. 1998;16(4):406-13.
248. Dalby MJ, Gadegaard N, Oreffo RO. Harnessing nanotopography and integrin-matrix interactions to influence stem cell fate. Nature materials. 2014;13(6):558-69.
249. Kim HN, Jiao A, Hwang NS, Kim MS, Kang do H, Kim DH, et al. Nanotopography-guided tissue engineering and regenerative medicine. Advanced drug delivery reviews. 2013;65(4):536-58.
250. Chen G, Lv Y, Guo P, Lin C, Zhang X, Yang L, et al. Matrix mechanics and fluid shear stress control stem cells fate in three dimensional

microenvironment. Current stem cell research & therapy. 2013;8(4):313-23.
251. Chen JC, Jacobs CR. Mechanically induced osteogenic lineage commitment of stem cells. Stem cell research & therapy. 2013;4(5):107.
252. Nava MM, Raimondi MT, Pietrabissa R. Controlling self-renewal and differentiation of stem cells via mechanical cues. Journal of biomedicine & biotechnology. 2012;2012:797410.
253. Rosa AL, Kato RB, Castro Raucci LM, Teixeira LN, de Oliveira FS, Bellesini LS, et al. Nanotopography drives stem cell fate toward osteoblast differentiation through alpha1beta1 integrin signaling pathway. Journal of cellular biochemistry. 2014;115(3):540-8.
254. Kato RB, Roy B, De Oliveira FS, Ferraz EP, De Oliveira PT, Kemper AG, et al. Nanotopography directs mesenchymal stem cells to osteoblast lineage through regulation of microRNA-SMAD-BMP-2 circuit. Journal of cellular physiology. 2014;229(11):1690-6.
255. Kaur G, Wang C, Sun J, Wang Q. The synergistic effects of multivalent ligand display and nanotopography on osteogenic differentiation of rat bone marrow stem cells. Biomaterials. 2010;31(22):5813-24.
256. Dalby MJ, Gadegaard N, Tare R, Andar A, Riehle MO, Herzyk P, et al. The control of human mesenchymal cell differentiation using nanoscale symmetry and disorder. Nature materials. 2007;6(12):997-1003.
257. Maclaine SE, Gadhari N, Pugin R, Meek RM, Liley M, Dalby MJ. Optimizing the osteogenicity of nanotopography using block co-polymer phase separation fabrication techniques. Journal of orthopaedic research : official publication of the Orthopaedic Research Society. 2012;30(8):1190-7.
258. Thomson CE, McCulloch M, Sorenson A, Barnett SC, Seed BV, Griffiths IR, et al. Myelinated, synapsing cultures of murine spinal cord--validation as an in vitro model of the central nervous system. The European journal of neuroscience. 2008;28(8):1518-35.
259. Sorensen A, Alekseeva T, Katechia K, Robertson M, Riehle MO, Barnett SC. Long-term neurite orientation on astrocyte monolayers aligned by microtopography. Biomaterials. 2007;28(36):5498-508.

260. Silajdzic E, Willison HJ, Furukawa K, Barnett SC. In vitro analysis of glial cell function in ganglioside-deficient mice. Journal of neuroscience research. 2009;87(11):2467-83.
261. Elliott C, Lindner M, Arthur A, Brennan K, Jarius S, Hussey J, et al. Functional identification of pathogenic autoantibody responses in patients with multiple sclerosis. Brain : a journal of neurology. 2012;135(Pt 6):1819-33.
262. Ambros V. The functions of animal microRNAs. Nature. 2004;431(7006):350-5.
263. Bartel DP. MicroRNAs: genomics, biogenesis, mechanism, and function. Cell. 2004;116(2):281-97.
264. Wang XJ, Reyes JL, Chua NH, Gaasterland T. Prediction and identification of Arabidopsis thaliana microRNAs and their mRNA targets. Genome biology. 2004;5(9):R65.
265. Jeffrey SS. Cancer biomarker profiling with microRNAs. Nature biotechnology. 2008;26(4):400-1.
266. Son DJ, Kumar S, Takabe W, Kim CW, Ni CW, Alberts-Grill N, et al. The atypical mechanosensitive microRNA-712 derived from pre-ribosomal RNA induces endothelial inflammation and atherosclerosis. Nature communications. 2013;4:3000.
267. Thum T, Galuppo P, Wolf C, Fiedler J, Kneitz S, van Laake LW, et al. MicroRNAs in the human heart: a clue to fetal gene reprogramming in heart failure. Circulation. 2007;116(3):258-67.
268. van Rooij E, Sutherland LB, Liu N, Williams AH, McAnally J, Gerard RD, et al. A signature pattern of stress-responsive microRNAs that can evoke cardiac hypertrophy and heart failure. Proceedings of the National Academy of Sciences of the United States of America. 2006;103(48):18255-60.
269. Tatsuguchi M, Seok HY, Callis TE, Thomson JM, Chen JF, Newman M, et al. Expression of microRNAs is dynamically regulated during cardiomyocyte hypertrophy. Journal of molecular and cellular cardiology. 2007;42(6):1137-41.

270. Romao JM, Jin W, Dodson MV, Hausman GJ, Moore SS, Guan LL. MicroRNA regulation in mammalian adipogenesis. Experimental biology and medicine (Maywood, NJ). 2011;236(9):997-1004.
271. Feng J, Sun G, Yan J, Noltner K, Li W, Buzin CH, et al. Evidence for X-chromosomal schizophrenia associated with microRNA alterations. PloS one. 2009;4(7):e6121.
272. Beveridge NJ, Gardiner E, Carroll AP, Tooney PA, Cairns MJ. Schizophrenia is associated with an increase in cortical microRNA biogenesis. Molecular psychiatry. 2010;15(12):1176-89.
273. Broderick JA, Zamore PD. MicroRNA therapeutics. Gene therapy. 2011;18(12):1104-10.
274. Barker LE, Luman ET, McCauley MM, Chu SY. Assessing equivalence: an alternative to the use of difference tests for measuring disparities in vaccination coverage. American journal of epidemiology. 2002;156(11):1056-61.
275. Tokoyoda K, Egawa T, Sugiyama T, Choi BI, Nagasawa T. Cellular niches controlling B lymphocyte behavior within bone marrow during development. Immunity. 2004;20(6):707-18.
276. Conway A, Schaffer DV. Biophysical regulation of stem cell behavior within the niche. Stem cell research & therapy. 2012;3(6):50.
277. Jones DL, Wagers AJ. No place like home: anatomy and function of the stem cell niche. Nature reviews Molecular cell biology. 2008;9(1):11-21.
278. Drummond-Barbosa D. Stem cells, their niches and the systemic environment: an aging network. Genetics. 2008;180(4):1787-97.
279. Wagers AJ. The stem cell niche in regenerative medicine. Cell stem cell. 2012;10(4):362-9.
280. Lin G, Liu G, Banie L, Wang G, Ning H, Lue TF, et al. Tissue distribution of mesenchymal stem cell marker Stro-1. Stem cells and development. 2011;20(10):1747-52.
281. Ning H, Lin G, Lue TF, Lin CS. Mesenchymal stem cell marker Stro-1 is a 75 kd endothelial antigen. Biochemical and biophysical research communications. 2011;413(2):353-7.

282. Simmons PJ, Torok-Storb B. Identification of stromal cell precursors in human bone marrow by a novel monoclonal antibody, STRO-1. Blood. 1991;78(1):55-62.
283. Gronthos S, Graves SE, Ohta S, Simmons PJ. The STRO-1+ fraction of adult human bone marrow contains the osteogenic precursors. Blood. 1994;84(12):4164-73.
284. Suzuki S, Namiki J, Shibata S, Mastuzaki Y, Okano H. The neural stem/progenitor cell marker nestin is expressed in proliferative endothelial cells, but not in mature vasculature. The journal of histochemistry and cytochemistry : official journal of the Histochemistry Society. 2010;58(8):721-30.
285. Sahlgren CM, Mikhailov A, Vaittinen S, Pallari HM, Kalimo H, Pant HC, et al. Cdk5 regulates the organization of Nestin and its association with p35. Molecular and cellular biology. 2003;23(14):5090-106.
286. Michalczyk K, Ziman M. Nestin structure and predicted function in cellular cytoskeletal organisation. Histology and histopathology. 2005;20(2):665-71.
287. Mendez-Ferrer S, Michurina TV, Ferraro F, Mazloom AR, Macarthur BD, Lira SA, et al. Mesenchymal and haematopoietic stem cells form a unique bone marrow niche. Nature. 2010;466(7308):829-34.
288. Arranz L, Sanchez-Aguilera A, Martin-Perez D, Isern J, Langa X, Tzankov A, et al. Neuropathy of haematopoietic stem cell niche is essential for myeloproliferative neoplasms. Nature. 2014;512(7512):78-81.
289. Farbman AI. Olfactory neurogenesis: genetic or environmental controls? Trends in neurosciences. 1990;13(9):362-5.
290. Derby CD. Why have neurogenesis in adult olfactory systems? The Presidential Symposium at the 2006 AChemS Conference. Chemical senses. 2007;32(4):361-3.
291. Williams SK, Gilbey T, Barnett SC. Immunohistochemical studies of the cellular changes in the peripheral olfactory system after zinc sulfate nasal irrigation. Neurochemical research. 2004;29(5):891-901.
292. Graziadei PP, Graziadei GA. Neurogenesis and neuron regeneration in the olfactory system of mammals. I. Morphological aspects of

differentiation and structural organization of the olfactory sensory neurons. Journal of neurocytology. 1979;8(1):1-18.
293. Carr VM, Farbman AI. The dynamics of cell death in the olfactory epithelium. Experimental neurology. 1993;124(2):308-14.
294. Weiler E, Farbman AI. Proliferation in the rat olfactory epithelium: age-dependent changes. The Journal of neuroscience : the official journal of the Society for Neuroscience. 1997;17(10):3610-22.
295. da Silva Meirelles L, Chagastelles PC, Nardi NB. Mesenchymal stem cells reside in virtually all post-natal organs and tissues. Journal of cell science. 2006;119(Pt 11):2204-13.
296. Brighton CT, Hunt RM. Early histologic and ultrastructural changes in microvessels of periosteal callus. Journal of orthopaedic trauma. 1997;11(4):244-53.
297. Brighton CT, Hunt RM. Early histological and ultrastructural changes in medullary fracture callus. The Journal of bone and joint surgery American volume. 1991;73(6):832-47.
298. Fink T, Zachar V. Adipogenic differentiation of human mesenchymal stem cells. Methods in molecular biology. 2011;698:243-51.
299. Grassel S, Stockl S, Jenei-Lanzl Z. Isolation, culture, and osteogenic/chondrogenic differentiation of bone marrow-derived mesenchymal stem cells. Methods in molecular biology. 2012;879:203-67.
300. Jiang Y, Jahagirdar BN, Reinhardt RL, Schwartz RE, Keene CD, Ortiz-Gonzalez XR, et al. Pluripotency of mesenchymal stem cells derived from adult marrow. Nature. 2002;418(6893):41-9.
301. Franco Lambert AP, Fraga Zandonai A, Bonatto D, Cantarelli Machado D, Pegas Henriques JA. Differentiation of human adipose-derived adult stem cells into neuronal tissue: does it work? Differentiation; research in biological diversity. 2009;77(3):221-8.
302. Rose RA, Keating A, Backx PH. Do mesenchymal stromal cells transdifferentiate into functional cardiomyocytes? Circulation research. 2008;103(9):e120.
303. Yeh ET, Zhang S, Wu HD, Korbling M, Willerson JT, Estrov Z. Transdifferentiation of human peripheral blood CD34+-enriched cell

population into cardiomyocytes, endothelial cells, and smooth muscle cells in vivo. Circulation. 2003;108(17):2070-3.
304. Caddick J, Kingham PJ, Gardiner NJ, Wiberg M, Terenghi G. Phenotypic and functional characteristics of mesenchymal stem cells differentiated along a Schwann cell lineage. Glia. 2006;54(8):840-9.
305. Qian SW, Li X, Zhang YY, Huang HY, Liu Y, Sun X, et al. Characterization of adipocyte differentiation from human mesenchymal stem cells in bone marrow. BMC developmental biology. 2010;10:47.
306. Weir C, Morel-Kopp MC, Gill A, Tinworth K, Ladd L, Hunyor SN, et al. Mesenchymal stem cells: isolation, characterisation and in vivo fluorescent dye tracking. Heart, lung & circulation. 2008;17(5):395-403.
307. Vellasamy S, Sandrasaigaran P, Vidyadaran S, George E, Ramasamy R. Isolation and characterisation of mesenchymal stem cells derived from human placenta tissue. World journal of stem cells. 2012;4(6):53-61.
308. Lu LL, Liu YJ, Yang SG, Zhao QJ, Wang X, Gong W, et al. Isolation and characterization of human umbilical cord mesenchymal stem cells with hematopoiesis-supportive function and other potentials. Haematologica. 2006;91(8):1017-26.
309. Banas A. Purification of adipose tissue mesenchymal stem cells and differentiation toward hepatic-like cells. Methods in molecular biology. 2012;826:61-72.
310. Hung CN, Mar K, Chang HC, Chiang YL, Hu HY, Lai CC, et al. A comparison between adipose tissue and dental pulp as sources of MSCs for tooth regeneration. Biomaterials. 2011;32(29):6995-7005.
311. Fei X, Jiang S, Zhang S, Li Y, Ge J, He B, et al. Isolation, culture, and identification of amniotic fluid-derived mesenchymal stem cells. Cell biochemistry and biophysics. 2013;67(2):689-94.
312. Gnecchi M, Melo LG. Bone marrow-derived mesenchymal stem cells: isolation, expansion, characterization, viral transduction, and production of conditioned medium. Methods in molecular biology. 2009;482:281-94.
313. Pontikoglou C, Deschaseaux F, Sensebe L, Papadaki HA. Bone marrow mesenchymal stem cells: biological properties and their role in

hematopoiesis and hematopoietic stem cell transplantation. Stem cell reviews. 2011;7(3):569-89.
314. Bara JJ, McCarthy HE, Humphrey E, Johnson WE, Roberts S. Bone marrow-derived mesenchymal stem cells become antiangiogenic when chondrogenically or osteogenically differentiated: implications for bone and cartilage tissue engineering. Tissue engineering Part A. 2014;20(1-2):147-59.
315. Gimble JM, Katz AJ, Bunnell BA. Adipose-derived stem cells for regenerative medicine. Circulation research. 2007;100(9):1249-60.
316. Huang GT, Gronthos S, Shi S. Mesenchymal stem cells derived from dental tissues vs. those from other sources: their biology and role in regenerative medicine. Journal of dental research. 2009;88(9):792-806.
317. Hartmann K, Raabe O, Wenisch S, Arnhold S. Amniotic fluid derived stem cells give rise to neuron-like cells without a further differentiation potential into retina-like cells. American journal of stem cells. 2013;2(2):108-18.
318. Jones EA, Kinsey SE, English A, Jones RA, Straszynski L, Meredith DM, et al. Isolation and characterization of bone marrow multipotential mesenchymal progenitor cells. Arthritis and rheumatism. 2002;46(12):3349-60.
319. Jones EA, English A, Kinsey SE, Straszynski L, Emery P, Ponchel F, et al. Optimization of a flow cytometry-based protocol for detection and phenotypic characterization of multipotent mesenchymal stromal cells from human bone marrow. Cytometry Part B, Clinical cytometry. 2006;70(6):391-9.
320. Giancotti FG, Ruoslahti E. Integrin signaling. Science. 1999;285(5430):1028-32.
321. Gospodarowicz D, Ferrara N, Schweigerer L, Neufeld G. Structural characterization and biological functions of fibroblast growth factor. Endocrine reviews. 1987;8(2):95-114.
322. Cadigan KM, Nusse R. Wnt signaling: a common theme in animal development. Genes & development. 1997;11(24):3286-305.

323. Komiya Y, Habas R. Wnt signal transduction pathways. Organogenesis. 2008;4(2):68-75.
324. Geiger B, Spatz JP, Bershadsky AD. Environmental sensing through focal adhesions. Nature reviews Molecular cell biology. 2009;10(1):21-33.
325. Yim EK, Darling EM, Kulangara K, Guilak F, Leong KW. Nanotopography-induced changes in focal adhesions, cytoskeletal organization, and mechanical properties of human mesenchymal stem cells. Biomaterials. 2010;31(6):1299-306.
326. Rowlands AS, George PA, Cooper-White JJ. Directing osteogenic and myogenic differentiation of MSCs: interplay of stiffness and adhesive ligand presentation. American journal of physiology Cell physiology. 2008;295(4):C1037-44.
327. Trappmann B, Gautrot JE, Connelly JT, Strange DG, Li Y, Oyen ML, et al. Extracellular-matrix tethering regulates stem-cell fate. Nature materials. 2012;11(7):642-9.
328. Guilak F, Cohen DM, Estes BT, Gimble JM, Liedtke W, Chen CS. Control of stem cell fate by physical interactions with the extracellular matrix. Cell stem cell. 2009;5(1):17-26.
329. Tse JR, Engler AJ. Stiffness gradients mimicking in vivo tissue variation regulate mesenchymal stem cell fate. PloS one. 2011;6(1):e15978.
330. Skardal A, Mack D, Atala A, Soker S. Substrate elasticity controls cell proliferation, surface marker expression and motile phenotype in amniotic fluid-derived stem cells. Journal of the mechanical behavior of biomedical materials. 2013;17:307-16.
331. von der Mark K, Park J, Bauer S, Schmuki P. Nanoscale engineering of biomimetic surfaces: cues from the extracellular matrix. Cell and tissue research. 2010;339(1):131-53.
332. Bettinger CJ, Langer R, Borenstein JT. Engineering substrate topography at the micro- and nanoscale to control cell function. Angewandte Chemie. 2009;48(30):5406-15.

333. Huang J, Grater SV, Corbellini F, Rinck S, Bock E, Kemkemer R, et al. Impact of order and disorder in RGD nanopatterns on cell adhesion. Nano letters. 2009;9(3):1111-6.
334. Kulangara K, Yang Y, Yang J, Leong KW. Nanotopography as modulator of human mesenchymal stem cell function. Biomaterials. 2012;33(20):4998-5003.
335. Kolf CM, Cho E, Tuan RS. Mesenchymal stromal cells. Biology of adult mesenchymal stem cells: regulation of niche, self-renewal and differentiation. Arthritis research & therapy. 2007;9(1):204.
336. Steward AJ, Wagner DR, Kelly DJ. The pericellular environment regulates cytoskeletal development and the differentiation of mesenchymal stem cells and determines their response to hydrostatic pressure. European cells & materials. 2013;25:167-78.
337. Zou C, Luo Q, Qin J, Shi Y, Yang L, Ju B, et al. Osteopontin promotes mesenchymal stem cell migration and lessens cell stiffness via integrin beta1, FAK, and ERK pathways. Cell biochemistry and biophysics. 2013;65(3):455-62.
338. Sykova E, Jendelova P, Urdzikova L, Lesny P, Hejcl A. Bone marrow stem cells and polymer hydrogels--two strategies for spinal cord injury repair. Cellular and molecular neurobiology. 2006;26(7-8):1113-29.
339. Jayawarna V, Richardson SM, Hirst AR, Hodson NW, Saiani A, Gough JE, et al. Introducing chemical functionality in Fmoc-peptide gels for cell culture. Acta biomaterialia. 2009;5(3):934-43.
340. Zhou M, Smith AM, Das AK, Hodson NW, Collins RF, Ulijn RV, et al. Self-assembled peptide-based hydrogels as scaffolds for anchorage-dependent cells. Biomaterials. 2009;30(13):2523-30.
341. Li Z, Guo X, Guan J. A thermosensitive hydrogel capable of releasing bFGF for enhanced differentiation of mesenchymal stem cell into cardiomyocyte-like cells under ischemic conditions. Biomacromolecules. 2012;13(6):1956-64.
342. Merceron C, Portron S, Masson M, Fellah BH, Gauthier O, Lesoeur J, et al. Cartilage tissue engineering: From hydrogel to mesenchymal stem cells. Bio-medical materials and engineering. 2010;20(3):159-66.

343. Kim IL, Khetan S, Baker BM, Chen CS, Burdick JA. Fibrous hyaluronic acid hydrogels that direct MSC chondrogenesis through mechanical and adhesive cues. Biomaterials. 2013;34(22):5571-80.
344. Hu J, Feng K, Liu X, Ma PX. Chondrogenic and osteogenic differentiations of human bone marrow-derived mesenchymal stem cells on a nanofibrous scaffold with designed pore network. Biomaterials. 2009;30(28):5061-7.
345. Janeczek Portalska K, Leferink A, Groen N, Fernandes H, Moroni L, van Blitterswijk C, et al. Endothelial differentiation of mesenchymal stromal cells. PloS one. 2012;7(10):e46842.
346. Dalby MJ, Gadegaard N, Curtis AS, Oreffo RO. Nanotopographical control of human osteoprogenitor differentiation. Current stem cell research & therapy. 2007;2(2):129-38.
347. Pensabene V, Taccola S, Ricotti L, Ciofani G, Menciassi A, Perut F, et al. Flexible polymeric ultrathin film for mesenchymal stem cell differentiation. Acta biomaterialia. 2011;7(7):2883-91.
348. Matsumoto T, Hattori K, Matsushima A, Tadokoro M, Yagyuu T, Kodama M, et al. Osteogenic potential of mesenchymal stem cells on expanded polytetrafluoroethylene coated with both a poly-amino-Acid urethane copolymer and collagen. Tissue engineering Part A. 2011;17(1-2):171-80.
349. Yu HS, Won JE, Jin GZ, Kim HW. Construction of mesenchymal stem cell-containing collagen gel with a macrochanneled polycaprolactone scaffold and the flow perfusion culturing for bone tissue engineering. Biores Open Access. 2012;1(3):124-36.
350. Reichert JC, Heymer A, Berner A, Eulert J, Noth U. Fabrication of polycaprolactone collagen hydrogel constructs seeded with mesenchymal stem cells for bone regeneration. Biomedical materials. 2009;4(6):065001.
351. Wiesmann A, Buhring HJ, Mentrup C, Wiesmann HP. Decreased CD90 expression in human mesenchymal stem cells by applying mechanical stimulation. Head & face medicine. 2006;2:8.

352. Halfon S, Abramov N, Grinblat B, Ginis I. Markers distinguishing mesenchymal stem cells from fibroblasts are downregulated with passaging. Stem cells and development. 2011;20(1):53-66.
353. Lee HJ, Choi BH, Min BH, Park SR. Changes in surface markers of human mesenchymal stem cells during the chondrogenic differentiation and dedifferentiation processes in vitro. Arthritis and rheumatism. 2009;60(8):2325-32.
354. Kantawong F, Burchmore R, Gadegaard N, Oreffo RO, Dalby MJ. Proteomic analysis of human osteoprogenitor response to disordered nanotopography. Journal of the Royal Society, Interface / the Royal Society. 2009;6(40):1075-86.
355. Dalby MJ, McCloy D, Robertson M, Agheli H, Sutherland D, Affrossman S, et al. Osteoprogenitor response to semi-ordered and random nanotopographies. Biomaterials. 2006;27(15):2980-7.
356. Arnsdorf EJ, Tummala P, Castillo AB, Zhang F, Jacobs CR. The epigenetic mechanism of mechanically induced osteogenic differentiation. Journal of biomechanics. 2010;43(15):2881-6.
357. Huang S, Wang S, Bian C, Yang Z, Zhou H, Zeng Y, et al. Upregulation of miR-22 promotes osteogenic differentiation and inhibits adipogenic differentiation of human adipose tissue-derived mesenchymal stem cells by repressing HDAC6 protein expression. Stem cells and development. 2012;21(13):2531-40.
358. Zhang Y, Khan D, Delling J, Tobiasch E. Mechanisms underlying the osteo- and adipo-differentiation of human mesenchymal stem cells. TheScientificWorldJournal. 2012;2012:793823.
359. Bakhshandeh B, Hafizi M, Ghaemi N, Soleimani M. Down-regulation of miRNA-221 triggers osteogenic differentiation in human stem cells. Biotechnology letters. 2012;34(8):1579-87.
360. Darby I, Skalli O, Gabbiani G. Alpha-smooth muscle actin is transiently expressed by myofibroblasts during experimental wound healing. Laboratory investigation; a journal of technical methods and pathology. 1990;63(1):21-9.

361. Skalli O, Ropraz P, Trzeciak A, Benzonana G, Gillessen D, Gabbiani G. A monoclonal antibody against alpha-smooth muscle actin: a new probe for smooth muscle differentiation. The Journal of cell biology. 1986;103(6 Pt 2):2787-96.
362. Desmouliere A, Geinoz A, Gabbiani F, Gabbiani G. Transforming growth factor-beta 1 induces alpha-smooth muscle actin expression in granulation tissue myofibroblasts and in quiescent and growing cultured fibroblasts. The Journal of cell biology. 1993;122(1):103-11.
363. Roskams AJ, Cai X, Ronnett GV. Expression of neuron-specific beta-III tubulin during olfactory neurogenesis in the embryonic and adult rat. Neuroscience. 1998;83(1):191-200.
364. Calof AL, Chikaraishi DM. Analysis of neurogenesis in a mammalian neuroepithelium: proliferation and differentiation of an olfactory neuron precursor in vitro. Neuron. 1989;3(1):115-27.
365. Foudah D, Monfrini M, Donzelli E, Niada S, Brini AT, Orciani M, et al. Expression of neural markers by undifferentiated mesenchymal-like stem cells from different sources. Journal of immunology research. 2014;2014:987678.
366. Saura C, Tseng LM, Chan S, Chacko RT, Campone M, Manikhas A, et al. Neoadjuvant doxorubicin/cyclophosphamide followed by ixabepilone or paclitaxel in early stage breast cancer and evaluation of betaIII-tubulin expression as a predictive marker. The oncologist. 2013;18(7):787-94.
367. Locher H, de Rooij KE, de Groot JC, van Doorn R, Gruis NA, Lowik CW, et al. Class III beta-tubulin, a novel biomarker in the human melanocyte lineage. Differentiation; research in biological diversity. 2013;85(4-5):173-81.
368. Wang Y, Sparano JA, Fineberg S, Stead L, Sunkara J, Horwitz SB, et al. High expression of class III beta-tubulin predicts good response to neoadjuvant taxane and doxorubicin/cyclophosphamide-based chemotherapy in estrogen receptor-negative breast cancer. Clinical breast cancer. 2013;13(2):103-8.
369. Skalli O, Pelte MF, Peclet MC, Gabbiani G, Gugliotta P, Bussolati G, et al. Alpha-smooth muscle actin, a differentiation marker of smooth muscle

cells, is present in microfilamentous bundles of pericytes. The journal of histochemistry and cytochemistry : official journal of the Histochemistry Society. 1989;37(3):315-21.
370. Hinz B, Celetta G, Tomasek JJ, Gabbiani G, Chaponnier C. Alpha-smooth muscle actin expression upregulates fibroblast contractile activity. Molecular biology of the cell. 2001;12(9):2730-41.
371. Ludin A, Itkin T, Gur-Cohen S, Mildner A, Shezen E, Golan K, et al. Monocytes-macrophages that express alpha-smooth muscle actin preserve primitive hematopoietic cells in the bone marrow. Nature immunology. 2012;13(11):1072-82.
372. Chatakun P, Nunez-Toldra R, Diaz Lopez EJ, Gil-Recio C, Martinez-Sarra E, Hernandez-Alfaro F, et al. The effect of five proteins on stem cells used for osteoblast differentiation and proliferation: a current review of the literature. Cellular and molecular life sciences : CMLS. 2014;71(1):113-42.
373. Bignami A, Eng LF, Dahl D, Uyeda CT. Localization of the glial fibrillary acidic protein in astrocytes by immunofluorescence. Brain research. 1972;43(2):429-35.
374. Kasantikul V, Shuangshoti S. Positivity to glial fibrillary acidic protein in bone, cartilage, and chordoma. Journal of surgical oncology. 1989;41(1):22-6.
375. Tsimbouri PM, Murawski K, Hamilton G, Herzyk P, Oreffo RO, Gadegaard N, et al. A genomics approach in determining nanotopographical effects on MSC phenotype. Biomaterials. 2013;34(9):2177-84.
376. McMurray RJ, Gadegaard N, Tsimbouri PM, Burgess KV, McNamara LE, Tare R, et al. Nanoscale surfaces for the long-term maintenance of mesenchymal stem cell phenotype and multipotency. Nature materials. 2011;10(8):637-44.
377. Chen W, Villa-Diaz LG, Sun Y, Weng S, Kim JK, Lam RH, et al. Nanotopography influences adhesion, spreading, and self-renewal of human embryonic stem cells. ACS nano. 2012;6(5):4094-103.

378. McNamara LE, Sjostrom T, Seunarine K, Meek RD, Su B, Dalby MJ. Investigation of the limits of nanoscale filopodial interactions. Journal of tissue engineering. 2014;5:2041731414536177.
379. Nicolas FE, Pais H, Schwach F, Lindow M, Kauppinen S, Moulton V, et al. Experimental identification of microRNA-140 targets by silencing and overexpressing miR-140. RNA (New York, NY). 2008;14(12):2513-20.
380. Suzuki Y, Kim HW, Ashraf M, Haider H. Diazoxide potentiates mesenchymal stem cell survival via NF-kappaB-dependent miR-146a expression by targeting Fas. American journal of physiology Heart and circulatory physiology. 2010;299(4):H1077-82.
381. Tome M, Lopez-Romero P, Albo C, Sepulveda JC, Fernandez-Gutierrez B, Dopazo A, et al. miR-335 orchestrates cell proliferation, migration and differentiation in human mesenchymal stem cells. Cell death and differentiation. 2011;18(6):985-95.
382. Guo L, Zhao RC, Wu Y. The role of microRNAs in self-renewal and differentiation of mesenchymal stem cells. Experimental hematology. 2011;39(6):608-16.
383. Gao J, Yang T, Han J, Yan K, Qiu X, Zhou Y, et al. MicroRNA expression during osteogenic differentiation of human multipotent mesenchymal stromal cells from bone marrow. Journal of cellular biochemistry. 2011;112(7):1844-56.
384. Uccelli A, Moretta L, Pistoia V. Immunoregulatory function of mesenchymal stem cells. European journal of immunology. 2006;36(10):2566-73.
385. Chen X, Armstrong MA, Li G. Mesenchymal stem cells in immunoregulation. Immunology and cell biology. 2006;84(5):413-21.
386. Ma S, Xie N, Li W, Yuan B, Shi Y, Wang Y. Immunobiology of mesenchymal stem cells. Cell death and differentiation. 2014;21(2):216-25.
387. Schinkothe T, Bloch W, Schmidt A. In vitro secreting profile of human mesenchymal stem cells. Stem cells and development. 2008;17(1):199-206.

388. Park CW, Kim KS, Bae S, Son HK, Myung PK, Hong HJ, et al. Cytokine secretion profiling of human mesenchymal stem cells by antibody array. International journal of stem cells. 2009;2(1):59-68.
389. Blaber SP, Webster RA, Hill CJ, Breen EJ, Kuah D, Vesey G, et al. Analysis of in vitro secretion profiles from adipose-derived cell populations. Journal of translational medicine. 2012;10:172.
390. Hsieh JY, Wang HW, Chang SJ, Liao KH, Lee IH, Lin WS, et al. Mesenchymal stem cells from human umbilical cord express preferentially secreted factors related to neuroprotection, neurogenesis, and angiogenesis. PloS one. 2013;8(8):e72604.
391. Zagoura DS, Roubelakis MG, Bitsika V, Trohatou O, Pappa KI, Kapelouzou A, et al. Therapeutic potential of a distinct population of human amniotic fluid mesenchymal stem cells and their secreted molecules in mice with acute hepatic failure. Gut. 2012;61(6):894-906.
392. Yoon BS, Moon JH, Jun EK, Kim J, Maeng I, Kim JS, et al. Secretory profiles and wound healing effects of human amniotic fluid-derived mesenchymal stem cells. Stem cells and development. 2010;19(6):887-902.
393. Melief SM, Zwaginga JJ, Fibbe WE, Roelofs H. Adipose tissue-derived multipotent stromal cells have a higher immunomodulatory capacity than their bone marrow-derived counterparts. Stem cells translational medicine. 2013;2(6):455-63.
394. Amable PR, Teixeira MV, Carias RB, Granjeiro JM, Borojevic R. Protein synthesis and secretion in human mesenchymal cells derived from bone marrow, adipose tissue and Wharton's jelly. Stem cell research & therapy. 2014;5(2):53.
395. Timotijevic G, Mostarica Stojkovic M, Miljkovic D. CXCL12: role in neuroinflammation. The international journal of biochemistry & cell biology. 2012;44(6):838-41.
396. Jaerve A, Muller HW. Chemokines in CNS injury and repair. Cell and tissue research. 2012;349(1):229-48.
397. Heskamp A, Leibinger M, Andreadaki A, Gobrecht P, Diekmann H, Fischer D. CXCL12/SDF-1 facilitates optic nerve regeneration. Neurobiology of disease. 2013;55:76-86.

398. Patel JR, McCandless EE, Dorsey D, Klein RS. CXCR4 promotes differentiation of oligodendrocyte progenitors and remyelination. Proceedings of the National Academy of Sciences of the United States of America. 2010;107(24):11062-7.
399. Maysami S, Nguyen D, Zobel F, Pitz C, Heine S, Hopfner M, et al. Modulation of rat oligodendrocyte precursor cells by the chemokine CXCL12. Neuroreport. 2006;17(11):1187-90.
400. Vazirinejad R, Ahmadi Z, Kazemi Arababadi M, Hassanshahi G, Kennedy D. The biological functions, structure and sources of CXCL10 and its outstanding part in the pathophysiology of multiple sclerosis. Neuroimmunomodulation. 2014;21(6):322-30.
401. Antonelli A, Ferrari SM, Fallahi P, Piaggi S, Paolicchi A, Franceschini SS, et al. Cytokines (interferon-gamma and tumor necrosis factor-alpha)-induced nuclear factor-kappaB activation and chemokine (C-X-C motif) ligand 10 release in Graves disease and ophthalmopathy are modulated by pioglitazone. Metabolism: clinical and experimental. 2011;60(2):277-83.
402. Antonelli A, Ferrari SM, Giuggioli D, Ferrannini E, Ferri C, Fallahi P. Chemokine (C-X-C motif) ligand (CXCL)10 in autoimmune diseases. Autoimmunity reviews. 2014;13(3):272-80.
403. Lee EY, Lee ZH, Song YW. CXCL10 and autoimmune diseases. Autoimmunity reviews. 2009;8(5):379-83.
404. Mithal DS, Banisadr G, Miller RJ. CXCL12 signaling in the development of the nervous system. Journal of neuroimmune pharmacology : the official journal of the Society on NeuroImmune Pharmacology. 2012;7(4):820-34.
405. Mithal DS, Ren D, Miller RJ. CXCR4 signaling regulates radial glial morphology and cell fate during embryonic spinal cord development. Glia. 2013;61(8):1288-305.
406. Ardelt AA, Bhattacharyya BJ, Belmadani A, Ren D, Miller RJ. Stromal derived growth factor-1 (CXCL12) modulates synaptic transmission to immature neurons during post-ischemic cerebral repair. Experimental neurology. 2013;248:246-53.
407. Patel JR, Williams JL, Muccigrosso MM, Liu L, Sun T, Rubin JB, et al. Astrocyte TNFR2 is required for CXCL12-mediated regulation of

oligodendrocyte progenitor proliferation and differentiation within the adult CNS. Acta neuropathologica. 2012;124(6):847-60.
408. Zheng H, Fu G, Dai T, Huang H. Migration of endothelial progenitor cells mediated by stromal cell-derived factor-1alpha/CXCR4 via PI3K/Akt/eNOS signal transduction pathway. Journal of cardiovascular pharmacology. 2007;50(3):274-80.
409. Welford AF, Biziato D, Coffelt SB, Nucera S, Fisher M, Pucci F, et al. TIE2-expressing macrophages limit the therapeutic efficacy of the vascular-disrupting agent combretastatin A4 phosphate in mice. The Journal of clinical investigation. 2011;121(5):1969-73.
410. Bleul CC, Farzan M, Choe H, Parolin C, Clark-Lewis I, Sodroski J, et al. The lymphocyte chemoattractant SDF-1 is a ligand for LESTR/fusin and blocks HIV-1 entry. Nature. 1996;382(6594):829-33.
411. Balabanian K, Lagane B, Infantino S, Chow KY, Harriague J, Moepps B, et al. The chemokine SDF-1/CXCL12 binds to and signals through the orphan receptor RDC1 in T lymphocytes. The Journal of biological chemistry. 2005;280(42):35760-6.
412. Burns JM, Summers BC, Wang Y, Melikian A, Berahovich R, Miao Z, et al. A novel chemokine receptor for SDF-1 and I-TAC involved in cell survival, cell adhesion, and tumor development. The Journal of experimental medicine. 2006;203(9):2201-13.
413. Cruz-Orengo L, Holman DW, Dorsey D, Zhou L, Zhang P, Wright M, et al. CXCR7 influences leukocyte entry into the CNS parenchyma by controlling abluminal CXCL12 abundance during autoimmunity. The Journal of experimental medicine. 2011;208(2):327-39.
414. Thelen M, Thelen S. CXCR7, CXCR4 and CXCL12: an eccentric trio? Journal of neuroimmunology. 2008;198(1-2):9-13.
415. Cashen AF. Plerixafor hydrochloride: a novel agent for the mobilization of peripheral blood stem cells. Drugs of today (Barcelona, Spain : 1998). 2009;45(7):497-505.
416. Cashen AF, Nervi B, DiPersio J. AMD3100: CXCR4 antagonist and rapid stem cell-mobilizing agent. Future oncology (London, England). 2007;3(1):19-27.

417. To LB, Levesque JP, Herbert KE. How I treat patients who mobilize hematopoietic stem cells poorly. Blood. 2011;118(17):4530-40.
418. Kalatskaya I, Berchiche YA, Gravel S, Limberg BJ, Rosenbaum JS, Heveker N. AMD3100 is a CXCR7 ligand with allosteric agonist properties. Molecular pharmacology. 2009;75(5):1240-7.
419. Gottle P, Kremer D, Jander S, Odemis V, Engele J, Hartung HP, et al. Activation of CXCR7 receptor promotes oligodendroglial cell maturation. Annals of neurology. 2010;68(6):915-24.
420. Goswami R, Kaplan MH. A brief history of IL-9. Journal of immunology. 2011;186(6):3283-8.
421. Wang XY, Gelfanov V, Sun HB, Tsai S, Yang YC. Distinct actions of interleukin-9 and interleukin-4 on a hematopoietic stem cell line, EMLC1. Experimental hematology. 1999;27(1):139-46.
422. Metcalf D. The granulocyte-macrophage colony-stimulating factors. Science. 1985;229(4708):16-22.
423. Thomas J, Liu F, Link DC. Mechanisms of mobilization of hematopoietic progenitors with granulocyte colony-stimulating factor. Current opinion in hematology. 2002;9(3):183-9.
424. Jose PJ, Griffiths-Johnson DA, Collins PD, Walsh DT, Moqbel R, Totty NF, et al. Eotaxin: a potent eosinophil chemoattractant cytokine detected in a guinea pig model of allergic airways inflammation. The Journal of experimental medicine. 1994;179(3):881-7.
425. Ponath PD, Qin S, Ringler DJ, Clark-Lewis I, Wang J, Kassam N, et al. Cloning of the human eosinophil chemoattractant, eotaxin. Expression, receptor binding, and functional properties suggest a mechanism for the selective recruitment of eosinophils. The Journal of clinical investigation. 1996;97(3):604-12.
426. Garcia-Zepeda EA, Rothenberg ME, Ownbey RT, Celestin J, Leder P, Luster AD. Human eotaxin is a specific chemoattractant for eosinophil cells and provides a new mechanism to explain tissue eosinophilia. Nature medicine. 1996;2(4):449-56.

427. Villeda SA, Luo J, Mosher KI, Zou B, Britschgi M, Bieri G, et al. The ageing systemic milieu negatively regulates neurogenesis and cognitive function. Nature. 2011;477(7362):90-4.
428. Maysami S, Nguyen D, Zobel F, Heine S, Hopfner M, Stangel M. Oligodendrocyte precursor cells express a functional chemokine receptor CCR3: implications for myelination. Journal of neuroimmunology. 2006;178(1-2):17-23.
429. Adzemovic MZ, Ockinger J, Zeitelhofer M, Hochmeister S, Beyeen AD, Paulson A, et al. Expression of Ccl11 associates with immune response modulation and protection against neuroinflammation in rats. PloS one. 2012;7(7):e39794.
430. De La Luz Sierra M, Yang F, Narazaki M, Salvucci O, Davis D, Yarchoan R, et al. Differential processing of stromal-derived factor-1alpha and stromal-derived factor-1beta explains functional diversity. Blood. 2004;103(7):2452-9.
431. Li M, Ransohoff RM. Multiple roles of chemokine CXCL12 in the central nervous system: a migration from immunology to neurobiology. Progress in neurobiology. 2008;84(2):116-31.
432. Mendez-Ferrer S, Lucas D, Battista M, Frenette PS. Haematopoietic stem cell release is regulated by circadian oscillations. Nature. 2008;452(7186):442-7.
433. Tiveron MC, Cremer H. CXCL12/CXCR4 signalling in neuronal cell migration. Current opinion in neurobiology. 2008;18(3):237-44.
434. Moreno M, Bannerman P, Ma J, Guo F, Miers L. Conditional ablation of astroglial CCL2 suppresses CNS accumulation of M1 macrophages and preserves axons in mice with MOG peptide EAE. 2014;34(24):8175-85.
435. Di Prisco S, Merega E, Milanese M, Summa M, Casazza S, Raffaghello L, et al. CCL5-glutamate interaction in central nervous system: Early and acute presynaptic defects in EAE mice. Neuropharmacology. 2013;75:337-46.
436. Zhu W, Acosta C, MacNeil B, Cortes C, Intrater H, Gong Y, et al. Elevated expression of fractalkine (CX3CL1) and fractalkine receptor (CX3CR1) in the dorsal root ganglia and spinal cord in experimental

autoimmune encephalomyelitis: implications in multiple sclerosis-induced neuropathic pain. BioMed research international. 2013;2013:480702.
437. Dawes JM, Calvo M, Perkins JR, Paterson KJ, Kiesewetter H, Hobbs C, et al. CXCL5 mediates UVB irradiation-induced pain. Science translational medicine. 2011;3(90):90ra60.
438. Sheridan GK, Dev KK. S1P1 receptor subtype inhibits demyelination and regulates chemokine release in cerebellar slice cultures. Glia. 2012;60(3):382-92.
439. Carr MW, Roth SJ, Luther E, Rose SS, Springer TA. Monocyte chemoattractant protein 1 acts as a T-lymphocyte chemoattractant. Proceedings of the National Academy of Sciences of the United States of America. 1994;91(9):3652-6.
440. Xu LL, Warren MK, Rose WL, Gong W, Wang JM. Human recombinant monocyte chemotactic protein and other C-C chemokines bind and induce directional migration of dendritic cells in vitro. Journal of leukocyte biology. 1996;60(3):365-71.
441. Gerard C, Rollins BJ. Chemokines and disease. Nature immunology. 2001;2(2):108-15.
442. Foresti ML, Arisi GM, Katki K, Montanez A, Sanchez RM, Shapiro LA. Chemokine CCL2 and its receptor CCR2 are increased in the hippocampus following pilocarpine-induced status epilepticus. Journal of neuroinflammation. 2009;6:40.
443. Fabene PF, Bramanti P, Constantin G. The emerging role for chemokines in epilepsy. Journal of neuroimmunology. 2010;224(1-2):22-7.
444. Kim JS, Gautam SC, Chopp M, Zaloga C, Jones ML, Ward PA, et al. Expression of monocyte chemoattractant protein-1 and macrophage inflammatory protein-1 after focal cerebral ischemia in the rat. Journal of neuroimmunology. 1995;56(2):127-34.
445. Hickman SE, El Khoury J. Mechanisms of mononuclear phagocyte recruitment in Alzheimer's disease. CNS & neurological disorders drug targets. 2010;9(2):168-73.
446. Ransohoff RM, Hamilton TA, Tani M, Stoler MH, Shick HE, Major JA, et al. Astrocyte expression of mRNA encoding cytokines IP-10 and JE/MCP-1 in

experimental autoimmune encephalomyelitis. FASEB journal : official publication of the Federation of American Societies for Experimental Biology. 1993;7(6):592-600.
447. Semple BD, Bye N, Rancan M, Ziebell JM, Morganti-Kossmann MC. Role of CCL2 (MCP-1) in traumatic brain injury (TBI): evidence from severe TBI patients and CCL2-/- mice. Journal of cerebral blood flow and metabolism : official journal of the International Society of Cerebral Blood Flow and Metabolism. 2010;30(4):769-82.
448. Dubinski A, Zdrojewicz Z. [The role of interleukin-6 in development and progression of atherosclerosis]. Polski merkuriusz lekarski : organ Polskiego Towarzystwa Lekarskiego. 2007;22(130):291-4.
449. Swardfager W, Lanctot K, Rothenburg L, Wong A, Cappell J, Herrmann N. A meta-analysis of cytokines in Alzheimer's disease. Biological psychiatry. 2010;68(10):930-41.
450. Tackey E, Lipsky PE, Illei GG. Rationale for interleukin-6 blockade in systemic lupus erythematosus. Lupus. 2004;13(5):339-43.
451. Nishimoto N. Interleukin-6 in rheumatoid arthritis. Current opinion in rheumatology. 2006;18(3):277-81.
452. Ishimi Y, Miyaura C, Jin CH, Akatsu T, Abe E, Nakamura Y, et al. IL-6 is produced by osteoblasts and induces bone resorption. Journal of immunology. 1990;145(10):3297-303.
453. Vlahopoulos S, Boldogh I, Casola A, Brasier AR. Nuclear factor-kappaB-dependent induction of interleukin-8 gene expression by tumor necrosis factor alpha: evidence for an antioxidant sensitive activating pathway distinct from nuclear translocation. Blood. 1999;94(6):1878-89.
454. Yan Z, Zhuansun Y, Chen R, Li J, Ran P. Immunomodulation of mesenchymal stromal cells on regulatory T cells and its possible mechanism. Experimental cell research. 2014;324(1):65-74.
455. Mohammadzadeh A, Pourfathollah AA, Shahrokhi S, Hashemi SM, Moradi SL, Soleimani M. Immunomodulatory effects of adipose-derived mesenchymal stem cells on the gene expression of major transcription factors of T cell subsets. International immunopharmacology. 2014;20(2):316-21.

456. Monteleone G, Caruso R, Pallone F. Targets for new immunomodulation strategies in inflammatory bowel disease. Autoimmunity reviews. 2014;13(1):11-4.
457. Singh B, Nikoopour E, Huszarik K, Elliott JF, Jevnikar AM. Immunomodulation and regeneration of islet Beta cells by cytokines in autoimmune type 1 diabetes. Journal of interferon & cytokine research : the official journal of the International Society for Interferon and Cytokine Research. 2011;31(10):711-9.
458. Casado JG, Tarazona R, Sanchez-Margallo FM. NK and MSCs crosstalk: the sense of immunomodulation and their sensitivity. Stem cell reviews. 2013;9(2):184-9.
459. Ohishi K, Katayama N, Shiku H, Varnum-Finney B, Bernstein ID. Notch signalling in hematopoiesis. Seminars in cell & developmental biology. 2003;14(2):143-50.
460. Tarasova A, Haylock D, Winkler D. Principal signalling complexes in haematopoiesis: structural aspects and mimetic discovery. Cytokine & growth factor reviews. 2011;22(4):231-53.
461. Mercer EM, Lin YC, Murre C. Factors and networks that underpin early hematopoiesis. Seminars in immunology. 2011;23(5):317-25.
462. Nishida C, Kusubata K, Tashiro Y, Gritli I, Sato A, Ohki-Koizumi M, et al. MT1-MMP plays a critical role in hematopoiesis by regulating HIF-mediated chemokine/cytokine gene transcription within niche cells. Blood. 2012;119(23):5405-16.
463. Yamane T, Kunisada T, Tsukamoto H, Yamazaki H, Niwa H, Takada S, et al. Wnt signaling regulates hemopoiesis through stromal cells. Journal of immunology. 2001;167(2):765-72.
464. Van Den Berg DJ, Sharma AK, Bruno E, Hoffman R. Role of members of the Wnt gene family in human hematopoiesis. Blood. 1998;92(9):3189-202.
465. Calvi LM, Adams GB, Weibrecht KW, Weber JM, Olson DP, Knight MC, et al. Osteoblastic cells regulate the haematopoietic stem cell niche. Nature. 2003;425(6960):841-6.

466. Karanu FN, Murdoch B, Gallacher L, Wu DM, Koremoto M, Sakano S, et al. The notch ligand jagged-1 represents a novel growth factor of human hematopoietic stem cells. The Journal of experimental medicine. 2000;192(9):1365-72.
467. Selvamani SP, Mishra R, Singh SK. Chikungunya virus exploits miR-146a to regulate NF-kappaB pathway in human synovial fibroblasts. PloS one. 2014;9(8):e103624.
468. Rathnasamy G, Sivakumar V, Rangarajan P, Foulds WS, Ling EA, Kaur C. NF-kappaB-Mediated Nitric Oxide Production and Activation of Caspase-3 Cause Retinal Ganglion Cell Death in the Hypoxic Neonatal Retina. Investigative ophthalmology & visual science. 2014;55(9):5878-89.
469. Duan H, Chen L, Qu L, Yang H, Song SW, Han Y, et al. Mycoplasma hyorhinis infection promotes NF-kappaB dependent migration of gastric cancer cells. Cancer research. 2014.
470. Luo Y, Wang SX, Zhou ZQ, Wang Z, Zhang YG, Zhang Y, et al. Apoptotic effect of genistein on human colon cancer cells via inhibiting the nuclear factor-kappa B (NF-kappaB) pathway. Tumour biology : the journal of the International Society for Oncodevelopmental Biology and Medicine. 2014.
471. Frederiksen K, McKay RD. Proliferation and differentiation of rat neuroepithelial precursor cells in vivo. The Journal of neuroscience : the official journal of the Society for Neuroscience. 1988;8(4):1144-51.
472. Dahlstrand J, Lardelli M, Lendahl U. Nestin mRNA expression correlates with the central nervous system progenitor cell state in many, but not all, regions of developing central nervous system. Brain research Developmental brain research. 1995;84(1):109-29.
473. Kuhn NZ, Tuan RS. Regulation of stemness and stem cell niche of mesenchymal stem cells: implications in tumorigenesis and metastasis. Journal of cellular physiology. 2010;222(2):268-77.
474. Chitteti BR, Cheng YH, Poteat B, Rodriguez-Rodriguez S, Goebel WS, Carlesso N, et al. Impact of interactions of cellular components of the bone marrow microenvironment on hematopoietic stem and progenitor cell function. Blood. 2010;115(16):3239-48.

475. Nemeth CL, Janebodin K, Yuan AE, Dennis JE, Reyes M, Kim DH. Enhanced Chondrogenic Differentiation of Dental Pulp Stem Cells Using Nanopatterned PEG-GelMA-HA Hydrogels. Tissue engineering Part A. 2014.
476. Shi Z, Neoh KG, Kang ET, Poh CK, Wang W. Enhanced endothelial differentiation of adipose-derived stem cells by substrate nanotopography. Journal of tissue engineering and regenerative medicine. 2014;8(1):50-8.
477. Teo BK, Wong ST, Lim CK, Kung TY, Yap CH, Ramagopal Y, et al. Nanotopography modulates mechanotransduction of stem cells and induces differentiation through focal adhesion kinase. ACS nano. 2013;7(6):4785-98.
478. Neirinckx V, Cantinieaux D, Coste C, Rogister B, Franzen R, Wislet-Gendebien S. Concise review: Spinal cord injuries: how could adult mesenchymal and neural crest stem cells take up the challenge? Stem cells. 2014;32(4):829-43.
479. Neirinckx V, Marquet A, Coste C, Rogister B, Wislet-Gendebien S. Adult bone marrow neural crest stem cells and mesenchymal stem cells are not able to replace lost neurons in acute MPTP-lesioned mice. PloS one. 2013;8(5):e64723.
480. Achilleos A, Trainor PA. Neural crest stem cells: discovery, properties and potential for therapy. Cell research. 2012;22(2):288-304.
481. Liu C, Ding H, Zhu W, Jiang S, Xu J, Zou GM. LIGHT regulates the adipogenic differentiation of mesenchymal stem cells. Journal of cellular biochemistry. 2013;114(2):346-53.
482. Naruse K, Urabe K, Mukaida T, Ueno T, Migishima F, Oikawa A, et al. Spontaneous differentiation of mesenchymal stem cells obtained from fetal rat circulation. Bone. 2004;35(4):850-8.
483. Li Z, Liu C, Xie Z, Song P, Zhao RC, Guo L, et al. Epigenetic dysregulation in mesenchymal stem cell aging and spontaneous differentiation. PloS one. 2011;6(6):e20526.
484. Wegner SA, Ehrenberg PK, Chang G, Dayhoff DE, Sleeker AL, Michael NL. Genomic organization and functional characterization of the chemokine receptor CXCR4, a major entry co-receptor for human

immunodeficiency virus type 1. The Journal of biological chemistry. 1998;273(8):4754-60.
485. Moriuchi M, Moriuchi H, Margolis DM, Fauci AS. USF/c-Myc enhances, while Yin-Yang 1 suppresses, the promoter activity of CXCR4, a coreceptor for HIV-1 entry. Journal of immunology. 1999;162(10):5986-92.
486. Cristillo AD, Highbarger HC, Dewar RL, Dimitrov DS, Golding H, Bierer BE. Up-regulation of HIV coreceptor CXCR4 expression in human T lymphocytes is mediated in part by a cAMP-responsive element. FASEB journal : official publication of the Federation of American Societies for Experimental Biology. 2002;16(3):354-64.
487. Jourdan P, Vendrell JP, Huguet MF, Segondy M, Bousquet J, Pene J, et al. Cytokines and cell surface molecules independently induce CXCR4 expression on CD4+ CCR7+ human memory T cells. Journal of immunology. 2000;165(2):716-24.
488. Wang J, Guan E, Roderiquez G, Calvert V, Alvarez R, Norcross MA. Role of tyrosine phosphorylation in ligand-independent sequestration of CXCR4 in human primary monocytes-macrophages. The Journal of biological chemistry. 2001;276(52):49236-43.
489. Feil C, Augustin HG. Endothelial cells differentially express functional CXC-chemokine receptor-4 (CXCR-4/fusin) under the control of autocrine activity and exogenous cytokines. Biochemical and biophysical research communications. 1998;247(1):38-45.
490. Salcedo R, Wasserman K, Young HA, Grimm MC, Howard OM, Anver MR, et al. Vascular endothelial growth factor and basic fibroblast growth factor induce expression of CXCR4 on human endothelial cells: In vivo neovascularization induced by stromal-derived factor-1alpha. The American journal of pathology. 1999;154(4):1125-35.
491. Phillips RJ, Mestas J, Gharaee-Kermani M, Burdick MD, Sica A, Belperio JA, et al. Epidermal growth factor and hypoxia-induced expression of CXC chemokine receptor 4 on non-small cell lung cancer cells is regulated by the phosphatidylinositol 3-kinase/PTEN/AKT/mammalian target of rapamycin signaling pathway and activation of hypoxia inducible factor-1alpha. The Journal of biological chemistry. 2005;280(23):22473-81.

492. Gupta SK, Lysko PG, Pillarisetti K, Ohlstein E, Stadel JM. Chemokine receptors in human endothelial cells. Functional expression of CXCR4 and its transcriptional regulation by inflammatory cytokines. The Journal of biological chemistry. 1998;273(7):4282-7.
493. Han Y, Wang J, He T, Ransohoff RM. TNF-alpha down-regulates CXCR4 expression in primary murine astrocytes. Brain research. 2001;888(1):1-10.
494. http://www.anthonynolan.org/media/facts-and-stats
495. http://clinicaltrials.gov/ct2/show/NCT00874783?term=embryonic+stem+cells+parkinson%27s&rank=1
496. http://www.clinicaltrials.gov/ct2/show/NCT01345006?term=ACT+and+human+embryonic&rank=1
497. http://www.clinicaltrials.gov/ct2/show/NCT01344993?term=ACT+and+human+embryonic&rank=2
498. Wozniak MA, Chen CS. Mechanotransduction in development: A growing role for contractility. Nat Rev Mol Cell Biol. 2009 Jan;10(1):34-43.
499. Developmental Biology. 6th edition. Gilbert SF. Sunderland (MA): Sinauer Associates; 2000.
500. Gammill LS, Bronner-Fraser M. Neural crest specification: Migrating into genomics. Nat Rev Neurosci. 2003 Oct;4(10):795-805.
501. http://www.rndsystems.com/molecule_group.aspx?g=811&r=7&g2=819
502. http://en.wikipedia.org/wiki/Neuron#mediaviewer/File:Blausen_0657_MultipolarNeuron.png
503. http://commons.wikimedia.org/wiki/File:Synapse_Illustration2_tweaked.svg
504. http://commons.wikimedia.org/wiki/Category:Spinal_cord#mediaviewer/File:Medulaespinal.GIF
505. http://www.nlm.nih.gov/medlineplus/ency/imagepages/18117.htm
506. http://multiplesclerosis.net/what-is-ms/statistics/
507. http://www.who.int/mediacentre/factsheets/fs384/en/
508. http://www.christopherreeve.org/site/c.mtKZKgMWKwG/b.5184189/k.5587/Paralysis_Facts__Figures.htm

509. Thuret S, Moon LD, Gage FH. Therapeutic interventions after spinal cord injury. Nat Rev Neurosci. 2006 Aug;7(8):628-43.
510. http://www.lifetechnologies.com/content/dam/LifeTech/migration/en/images/ics-organized/applications/cell-tissue-analysis/data-diagram/560-wide.par.47851.image.-1.-1.1.gif
511. Jackson JE. (1991). A User's Guide to Principal Components, New York: John Wiley & Sons.
512. Grubbs, F (1969). Procedures for Detecting Outlying Observations in Samples, Technometrics, 11:1-21.
513. Benjamini Y and Hochberg Y (1995). Controlling the false discovery rate: a practical and powerful approach to multiple testing. J Royal Stat Soc B, 57:289–300.
514. Xu J, Wang W, Kapila Y, Lotz J, Kapila S. Multiple Differentiation Capacity of STRO-1+/CD146+ PDL Mesenchymal Progenitor Cells. Stem Cells Dev. 2009 Apr;18(3):487-96.
515. Truzzi F, Saltari A, Palazzo E, Lotti R, Petrachi T, Dallaglio K, Gemelli C, Grisendi G, Dominici M, Pincelli C, Marconi A. CD271 Mediates Stem Cells to Early Progeny Transition in Human Epidermis. J Invest Dermatol. 2015 Mar;135(3):786-95.
516. Klinkhammer BM, Kramann R, Mallau M, Makowska A, van Roeyen CR, Rong S, Buecher EB, Boor P, Kovacova K, Zok S, Denecke B, Stuettgen E, Otten S, Floege J, Kunter U. Mesenchymal Stem Cells from Rats with Chronic Kidney Disease Exhibit Premature Senescence and Loss of Regenerative Potential. PLoS One. 2014 Mar 25;9(3):e92115.